A study on metabolic rewiring in cancer cell plasticity

Sissel Elisabeth Dyrstad

Thesis for the degree of Philosophiae Doctor (PhD)
University of Bergen, Norway
2020

UNIVERSITY OF BERGEN

A study on metabolic rewiring in cancer cell plasticity

Sissel Elisabeth Dyrstad

Thesis for the degree of Philosophiae Doctor (PhD)
at the University of Bergen

Date of defense: 21.08.2020

Year: 2020

Title: A study on metabolic rewiring in cancer cell plasticity

Name: Sissel Elisabeth Dyrstad

Print: Skipnes Kommunikasjon / University of Bergen

Scientific environment

The presented work has been carried out at the Department of Biomedicine, University of Bergen, during 2016-2020. It was supervised by Professor Karl Johan Tronstad, and co-supervised by Gro Vatne Røsland and James Bradley Lorens. Funding was provided by the University of Bergen.

UNIVERSITY OF BERGEN
Faculty of Medicine

Acknowledgements

First and foremost, I would like to thank my supervisor Karl Johan Tronstad for the countless of hours he has used reading my mails, helping me interpret data and answering all my questions. Thank you for allowing me to be a part of your group for such a long time. My sincere gratitude also goes to my co-supervisor Gro Vatne Røsland. Not all supervisors would reply to my emails during holidays or answer so promptly. I would also like to show my appreciation to co-supervisor James Lorens. Having great supervisors is easily taken for granted and is something that I am very grateful for.

To all my colleagues in the cellular networks group, you are a great gang. Just like a mitochondrion, a PhD student is not as efficient alone, but when multiplying and forming networks, they are the powerhouse of the lab. To Sissel Berge, the nucleus of the group, without you we would be a highly unorganized bunch of primitive prokaryotes. You are great, not only when it comes to organization, but your positive spirit is something I truly admire. I am also grateful for Ingrid Strand, Ingrid Gavlen and Endre Stigen who kept the lab in order for all of us. Further, I would like to thank the people at the technical support division for helping with all the laboratory equipment, and always doing so with a smile. I would like to especially thank Bård Sværi for help with access and other practical stuff, when it comes to finishing this thesis during the period of lock-down due to the Covid-19 pandemic.

I also want to thank my present (Stacey) and spare (Maria and Ina) office mates, you can only be described as a pocketful of sunshine. Thank you for keeping up with my singing and endless interruptions. Without you, life would contain a lot less laughter.

Last, but not least, I would like to thank my family and friends for your support, and for keeping up with my long work hours with little complaint. I'm sincerely grateful for my parents for giving me a great childhood and always believing in me. Thank you Silje and Bjørn, for being family as well as friends. Thank you, Andreas, Christine and Balder who have been the most important people (and dog) throughout

the last few months. Thank you for reminding me that there are more important things that require my attention. I would never have made this without *any* of you.

Thank you!

Bergen, May, 2020.

Sissel Elisabeth Dyrstad

Contents

Abbreviations

2-DG	2-deoxy glucose
Acetyl-CoA	Acetyl coenzyme A
ADP	Adenosine diphosphate
AMP	Adenosine monophosphate
AMPK	Adenosine monophosphate (AMP) - activated protein kinase
ATP	Adenosine triphosphate
BLBC	Basal-like breast cancer
BNIP3	Bcl-2/adenovirus E1B 19kDa-interacting protein 3
^{14}C	Carbon 14
CCCP	Carbonyl cyanide m-chlorophenylhydrazone
c-MET	Tyrosine-protein kinase MET
CoA	Coenzyme A
CPT	Carnitine palmitoyl transferase
DCA	Dichloroacetic acid or dichloroacetate
DNA	Deoxyribonucleic acid
Drp1	Dynamin-related protein 1
e-	Electron
ECAR	Extracellular flux analysis
ECM	Extracellular matrix
EGF	Epidermal growth factor
EGFR	Epidermal growth factor receptor
EGFR TKI	Epidermal growth factor receptor tyrosine kinase inhibitor
EMP	Epithelial to mesenchymal plasticity
EMT	Epithelial to mesenchymal transition
ER	Estrogen receptor
ETC	Electron transport chain
FAD	Oxidized flavin adenine dinucleotide
$FADH_2$	Reduced flavin adenine dinucleotide
FAO	Fatty acid oxidation
FATP	Fatty acid transport proteins
FIS1	Human fission protein 1
FFA	Free fatty acids
FH	Fumarate dehydrogenase
GDP	Guanosine diphosphate
GLOBOCAN	Global cancer observatory
GLUT	Glucose transporter
GPX	Glutathione peroxidase
GTP	Guanosine triphosphate
H+	Proton
H_2O_2	Hydrogen peroxide
$HCO3^-$	Bicarbonate
HIF	Hypoxia inducible factor
HK	Hexokinase
HR	Hormone receptor
IDH	Isocitrate dehydrogenase
IF1	Inhibitory factor 1
IMM	Inner mitochondrial membrane
IMS	Intermembrane space
LCFA	Long chain fatty acids
LDH	Lactate dehydrogenase
MCT	Monocarboxylate transporters
MELAS	Mitochondrial myopathy, encephalopathy, lactic acidosis and stroke-like episodes
MET	Mesenchymal to epithelial transition

Mfn	Mitofusins
MMP	Matrix metalloproteinase
MPC	Mitochondrial pyruvate carrier
mRNA	messenger RNA
mtDNA	Mitochondrial DNA
mTOR	Mammalian target of rapamycin / mechanistic target of rapamycin
NAD+	Oxidized nicotinamide adenine dinucleotide
NADH	Reduced nicotinamide adenine dinucleotide
NADP+	Oxidized nicotinamide adenine dinucleotide phosphate
NADPH	Reduced nicotinamide adenine dinucleotide phosphate
nDNA	Nuclear DNA
NF-KB	Nuclear factor kappa-light-chain-enhancer of activated B cells
NRF	Nuclear respiratory factor
NSCLC	Non-small cell lung cancer
OCR	Oxygen consumption rate
OH-	Hydroxyl radical
OMM	Outer mitochondrial membrane
Opa1	Optic atrophy 1
OXHPOS	Oxidative phosphorylation
PARK2	Parkin
PDH	Pyruvate dehydrogenase
PDK	Pyruvate dehydrogenase kinase
PFK	Phosphofructokinase
PGC1α	Peroxisome proliferator-activated receptor gamma coactivator 1 alpha
PHD	Prolyl hydroxylases
Pi	Inorganic phosphate
PINK1	PTEN-induced putative kinase 1
PKL	Pyruvate kinase liver isoform
PKM	Pyruvate kinase muscle isoform
PKR	Pyruvate kinase red blood cell isoform
PMP	Plasma membrane permeabilizer
PPAR	Peroxisome proliferator-activated receptor
PPP	Pentose phosphate pathway
Q	Ubiquinone, Coenzyme Q10
QH2	Ubiquinol
RET	Reverse electron flow
RNA	Ribonucleic acid
ROS	Reactive oxygen species
SCLC	Small cell lung cancer
SDH	Succinate dehydrogenase
Seahorse	Seahorse XFe96 Analyzer
SOD1	Cytoplasmic superoxide dismutase
SOD2	Mitochondrial superoxide dismutase (mnSOD)
TCA	Tricarboxylic acid
TFAM	Mitochondrial transcription factor A
TGFβ	Transforming growth factor beta
TNBC	Triple negative breast cancer
TPP	Thiamine pyrophosphate
UCP	Uncoupling protein
VEGF	Vascular endothelial growth factor
VLCFA	Very long chain fatty acids
WAT	White adipose tissue
WY 14,643	4-chloro-6-(2,3-xylidino)-2-pirymidinylthioacteic acid
ΔΨm	Mitochondrial membrane potential

Abstract

Adaptation of cellular energetics is an important feature of tumorigenesis as a vast supply of nutrients is needed to accommodate increased growth. Essential energy pathways includes glucose, fatty acid and amino acid metabolism, where mitochondria function as key orchestrators. The main aim of this thesis was to investigate metabolic rewiring during cancer cell plasticity. Providing knowledge on central metabolic regulators and markers of metabolic reprogramming may present new therapeutic strategies to overcome development of resistance to cancer therapy.

In order to identify metabolic rewiring associated with cancer cell plasticity we focused especially on cellular energetics in epithelial to mesenchymal transition (EMT) and drug resistance, which are both well-documented examples of cancer cell plasticity. EMT is important in cellular functions such as wound healing and embryonal development. However, this process is hijacked in cancer development and is known to be an important mediator of invasion and metastasis, and associated with poor overall survival. We found that altered mitochondrial function contributed to development of EMT in breast cancer. This included reduced mitochondrial size and network, and reduced mitochondrial Complex II succinate dehydrogenase (SDH) activity, which resulted in reduced mitochondrial respiration. Upon analyzing gene expression data in breast tumors, we found the SDH subunit C and EMT to be inversely correlated, especially in basal-like breast cancer.

Upon investigating markers of altered response to starvation and fatty acid oxidation, we found pyruvate dehydrogenase kinase 4 (PDK4), a central regulator of pyruvate metabolism, to be upregulated. We found that PDK4 was a sensitive hallmark of cellular plasticity as upregulation of PDK4 marked the metabolic shift from glucose to fatty acid oxidation (FAO). This was evident both upon overexpression of central FAO regulators and pharmacological FAO inducers.

Altered PDK expression was also evident in non-small cell lung cancer (NSCLC), with PDK1 being upregulated in tissue from NSCLC patients compared to healthy tissue. Acquired drug resistance to epidermal growth factor receptor tyrosine kinase inhibitors

(EGFR TKIs) in NSCLC remain one of the major contributors to the high mortality rate of lung cancer, and is an example of cancer cell plasticity. Therefore, we developed cell lines resistant EGFR TKIs to mimic acquired drug resistance. We also found evidence of deregulated pyruvate metabolism upon drug resistance through upregulation of PDK2. As PDKs was identified as a common denominator both in NSCLC patient cohorts and upon acquired drug resistance, we tested the sensitivity and effect of the PDK inhibitor dichloroacetate (DCA) with the aim to increase therapeutic efficacy. Upon DCA treatment, we found increased pyruvate and lactate oxidation, while reducing glucose oxidation and lactate production. We further found that DCA reduced growth alone or in synergy with EGFR TKIs in both sensitive and resistant cell lines.

To conclude, we show that metabolic rewiring is an important feature of cancer cell plasticity, both through dysregulation of mitochondrial function and altered pyruvate metabolism. We found that metabolic rewiring mediates the process of EMT and drug resistance. Rewiring of cellular energetics is a common feature in cancer cell plasticity, and we show that inducing metabolic stress through targeting pyruvate metabolism, may represent a promising therapeutic strategy.

List of Publications

Paper I

Røsland, G. V*., **S. E. Dyrstad***, D. Tusubira, R. Helwa, T. Z. Tan, M. L. Lotsberg, I. K. N. Pettersen, A. Berg, C. Kindt, F. Hoel, K. Jacobsen, A. J. Arason, A. S. T. Engelsen, H. J. Ditzel, P. E. Lønning, C. Krakstad, J. P. Thiery, J. B. Lorens, S. Knappskog and K. J. Tronstad (2019). *"Epithelial to mesenchymal transition (EMT) is associated with attenuation of succinate dehydrogenase (SDH) in breast cancer through reduced expression of SDHC."* Cancer & Metabolism 7(1): 6.

*equal contributions

Paper II

Pettersen, I. K. N*., D. Tusubira*, H. Ashrafi, **S. E. Dyrstad**, L. Hansen, X.-Z. Liu, L. I. H. Nilsson, N. G. Løvsletten, K. Berge, H. Wergedahl, B. Bjørndal, Ø. Fluge, O. Bruland, A. C. Rustan, N. Halberg, G. V. Røsland, R. K. Berge and K. J. Tronstad (2019). *"Upregulated PDK4 expression is a sensitive marker of increased fatty acid oxidation."* Mitochondrion 49: 97-110.

*equal contributions

Paper III

Dyrstad S. E., M. L. Lotsberg, T. Z. Tan, S. Hjellbrekke, I.K.N Pettersen, D. Tusubira., A. S. T. Engelsen, T. Daubon, A. Mourier, O. Dahl, J. P. Thiery, J. Lorens, K. J. Tronstad and G.V. Røsland *"Inhibition of pyruvate dehydrogenase kinase redirects NSCLC cell metabolism and counteracts development of resistance to epidermal growth factor receptor tyrosine kinase inhibitors."* Manuscript.

Additional work not included this thesis:

Dyrstad, S.E., D, Tusubira., S, Knappskog., K. J. Tronstad and G. V. Røsland (2018). “Introducing Nano-Scale Quantitative Polymerase Chain Reaction.” Biochemical and Biophysical Research Communications 506(4): 923-926.

Fluge, Ø., O. Mella, O. Bruland, K. Risa**, S. E. Dyrstad**, K. Alme, I. G. Rekeland, D. Sapkota, G. V. Røsland, A. Fosså, I. Ktoridou-Valen, S. Lunde, K. Sørland, K. Lien, I. Herder, H. Thürmer, M. E. Gotaas, K. A. Baranowska, L. M. L. J. Bohnen, C. Schäfer, A. McCann, K. Sommerfelt, L. Helgeland, P. M. Ueland, O. Dahl and K. J. Tronstad (2016). "Metabolic profiling indicates impaired pyruvate dehydrogenase function in myalgic encephalopathy/chronic fatigue syndrome." JCI insight 1(21): e89376-e89376.

VanLinden, M. R., C. Dölle, I. K. N. Pettersen, V. A. Kulikova, M. Niere, G. Agrimi, **S. E. Dyrstad**, F. Palmieri, A. A. Nikiforov, K. J. Tronstad and M. Ziegler (2015). "Subcellular Distribution of NAD+ between Cytosol and Mitochondria Determines the Metabolic Profile of Human Cells." Journal of Biological Chemistry 290(46): 27644-27659.

Tronstad, K., M. Nooteboom, L. Nilsson, J. Nikolaisen, M. Sokolewicz, S. Grefte, I. Pettersen, **S. Dyrstad**, F. Hoel, P. Willems and W. Koopman (2014). "Regulation and Quantification of Cellular Mitochondrial Morphology and Content." Current Pharmaceutical Design 20(35): 5634-5652.

Lotsberg M. L., **S. E. Dyrstad,** G. V. Røsland, S. D. Peters, K. Jackobsen, H. J. Ditzel, K. J. Tronstad, L. A. Akslen, J. B. Lorens and A. S. T. Engelsen “A heterotypic 3D model to study microenvironmental influence on acquired drug resistance and invasiveness in NSCLC.“ Manuscript.

1. Introduction

Cellular metabolic pathways involve anabolic and catabolic processes that are regulated to support energy homeostasis. Anabolism includes processes where precursors from the food we eat are converted into proteins, lipids and nucleic acids, which are the essential building blocks of life. Anabolic processes require energy produced from catabolism of the energy rich nutrients we eat. In catabolic processes, sugar (glucose), fat (fatty acids) and proteins (amino acids) are broken down to fuel production of adenosine triphosphate (ATP). When ATP is hydrolyzed it releases energy which is rapidly consumed to meet the energy demand of cellular functions and processes. The daily turnover of ATP is estimated to be equivalent to our own body weight [1, 2]. ATP is mainly produced via oxidative and oxygen dependent (aerobic) pathways in the mitochondria or through glycolysis, which occur independently of oxygen (anaerobic).

Cellular energetics is often deregulated in tumorigenesis as cancer cells are highly dependent on catabolic and anabolic processes to sustain growth. One of the main contributors to why cancer has such a high death toll, is cancer cell plasticity. Cancer cell plasticity is defined by the ability of cancerous cells to invade and metastasize to form secondary tumors, as well as tolerate therapeutic pressure and develop drug resistance [3, 4]. The evolution of drug resistance represents a case of natural selection. Within a heterogeneous population such as cancer, there is a lot of genetic and epigenetic variation, and this variance is inherited by cell division [5, 6]. As with organisms, only the “fittest” cell with the most favorable variation will tolerate therapy. The role of energy metabolism in cancer cell plasticity is a reoccurring focus throughout this thesis.

1.1 The mitochondrion

A crucial component in the ATP producing machinery is the mitochondrion. In popular science, the mitochondria are often called “the powerhouse of the cell” as they are the main producers of the energy currency ATP. However, these thread-like structures are important for other cellular processes such as cell death (apoptosis), aging (senescence) and cell signaling (e.g. reactive oxygen species (ROS) production) [7-9].

1.1.1 Mitochondrial history

Cellular organelles later known to be mitochondrial structures were reported as early as the 1840s. Richard Altman named them "bioblasts" [10] and proposed that they were organisms living inside cells, which were essential for cellular function. The first time the term "mitochondrion" was used was in 1898 by Carl Brenda. In Greek mitochondrion translates to thread (mitos) little granule (khondrion) [10]. In 1948, Friedkin and Lehninger reported that the mitochondria indeed were important for cellular function through the discovery that they harbored the process of oxidative phosphorylation (OXPHOS) [10, 11].

Supporting Altman's theory, the term endosymbiosis was first made known in the 1960s by Lynn Sagan [12-14]. Sagan proposed that the mitochondria were aerobic prokaryotes ingested into a heterotrophic anaerobe. We now know, through the work of genome sequencing done by Andersson et al., that an obligate intracellular endoparasite belonging to the Alphaproteobacteria class, namely *Rickettsia prowazekii,* is the closest relative to the mitochondria [15]. This indicates that the mitochondria most likely were an Alphaproteobacteria engulfed within an early relative of a eukaryotic cell [15]. Further evidence supporting the endosymbiosis theory is the fact that the mitochondria have their own mitochondrial DNA (mtDNA), which was first described by Nass and Nass in 1963 [16].

1.1.2 Mitochondrial structure

In addition to mtDNA, a mitochondrion consists of two membranes, an inner membrane and an outer membrane. The inner membrane is densely folded, and this structural invagination is referred to as cristae (**Figure 1**). The space between the inner and outer membrane is called the intermembrane space whereas the space inside the cristae is named the matrix [1, 9, 10]. The matrix is central for the metabolic machinery as it harbors enzymes required for the TCA-cycle (Chapter 1.2.3) and fatty acid oxidation (Chapter 1.2.4). The folding of the inner membrane into cristae is important for generation of the proton gradient and OXPHOS, as the protein complexes necessary for electron transport chain (ETC) reside within (See more on OXPHOS in Chapter 1.2.5) [9].

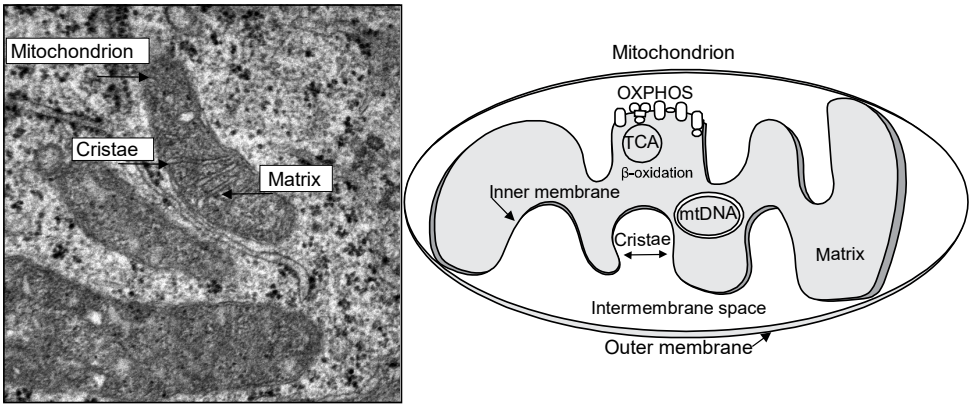

Figure 1: The mitochondrion. Left: showing a representative transmission electron microscopy image of a mitochondrion in HCC827 cells (Image taken by Endy Spriet (MIC, University of Bergen) of HCC827 cells) showing the folding of the inner membrane to form cristae and the matrix. Right: a simplified cartoon of a mitochondrion with its most important features: outer membrane, inner membrane, intermembrane space, matrix, oxidative phosphorylation (OXPHOS), mtDNA, β-oxidation and TCA cycle. *Abbreviations are listed in the beginning of the thesis.*

Despite having several copies of their own mtDNA, the mammalian mitochondria do not function independently of the rest of the cellular machinery as the majority of the mitochondrial proteins are encoded by genes residing within the nucleus [17, 18]. The mtDNA harbors 16,569 base pairs encoding 13 of the 83 respiratory chain proteins, along with 2 ribosomal RNA and 22 transfer RNA [17, 18]. During the course of evolution, the mtDNA size has decreased and mitochondrial genes have been transferred to nuclear DNA (nDNA) [19]. Interestingly, mtDNA is normally only maternally inherited as the mitochondria in the sperm are targeted for degradation after fertilization, although exceptions do occur [18, 20].

1.1.3 Mitochondrial dynamics and morphofunction

The mitochondria are not always single structures. They often form complex networks and are motile organelles through microtubule transport [21, 22], and can be transferred between cells via nanotubes [22, 23]. The amount and size of the mitochondria is dynamic, and dependent on cellular energy state, cell type, disease and stress. Regulating metabolic adaptations in response to starvation, physical activity or stress

is a highly controlled process. Important mitochondrial regulatory pathways in that respect are mitophagy and mitochondrial biogenesis, which, when combined with fission and fusion, are essential for mitochondrial quality control. Together they are often referred to as “mitochondrial dynamics” or the mitochondrial life cycle **(Figure 2)** [9, 24, 25].

Mitochondrial activity and function is highly dependent on their structure, networks and shape (morphofunction) [22]. As mentioned above, the inner membrane folding into cristae is essential for maintaining mitochondrial OXPHOS rates [9]. Fission and fusion are major governing pathways regulating mitochondrial structure, function and numbers. Fission is important when cells divide, but it may also trigger apoptosis through release of apoptotic proteins and initiate mitophagy [26, 27]. Fusion is important for compensation for damaged mitochondria, for example in heteroplasmy where cells contain both wild type and mutant mtDNA. Mitochondrial fusion allows for transfer of proteins and organelle compartments to adjust for stress and increase mitochondrial efficiency [22, 26]. Examples of proteins regulating fission are dynamin-related protein 1 (Drp1) and human fission protein 1 (Fis1), whereas fusion regulators are mitofusins (Mfn1 and Mfn2) and optic atrophy 1 (Opa1) [22, 24, 28].

Mitophagy describes the process where dysfunctional or otherwise damaged mitochondria are engulfed and degraded in lysosomes through autophagosome delivery [25, 29]. Essential proteins regulating mitophagy include PTEN-induced kinase 1 (PINK1) and parkin (PARK2) [22, 30]. In healthy mitochondria, PINK1 is transported through the inner membrane, before it is cleaved by presenilin-associated rhomboid-like protein and thus targeted for degradation within the mitochondrion [22, 25]. In dysfunctional mitochondria, especially uncoupled or otherwise membrane compromised mitochondria, PINK1 is not able to cross the inner membrane and accumulates in its un-cleaved form. PINK1 accumulation activates PARK2 via phosphorylation. PARK2 targets the mitochondria for degradation by ubiquitination of mitochondrial membrane proteins like Mfn1 and Mfn2 [25, 29, 31]. Evidence suggest that fission is an important regulator of mitophagy, as inhibition of fission through Drp1 mutation results in a decrease in mitophagy [27, 30].

As mitochondria are broken down, new ones must be formed to sustain metabolic capacity, a process which is termed mitochondrial biogenesis. Mitochondrial biogenesis is complementary linked to mitophagy and involve the cellular transcriptional and translational machinery [25, 31]. A master regulator in that respect is peroxisome proliferator-activated receptor gamma co-activator 1-alpha (PGC1α) which activates many downstream regulators of biogenesis. Examples include nuclear respiratory factors (NRFs) and peroxisome proliferator-activated receptor gamma (PPARγ) [25, 29]. NRF1 and 2 are known to activate transcription of mitochondrial encoding nuclear DNA in addition to mtDNA regulating mitochondrial transcription factor A (TFAM) expression [24]. However, the numerous processes involved in mitochondrial morphofunction and dynamics is still not fully understood. Disruption in this complex machinery is known to be involved in a range of diseases such as neurodegeneration, aging, cardiovascular disease, muscle atrophy and cancer [22, 25, 28, 32].

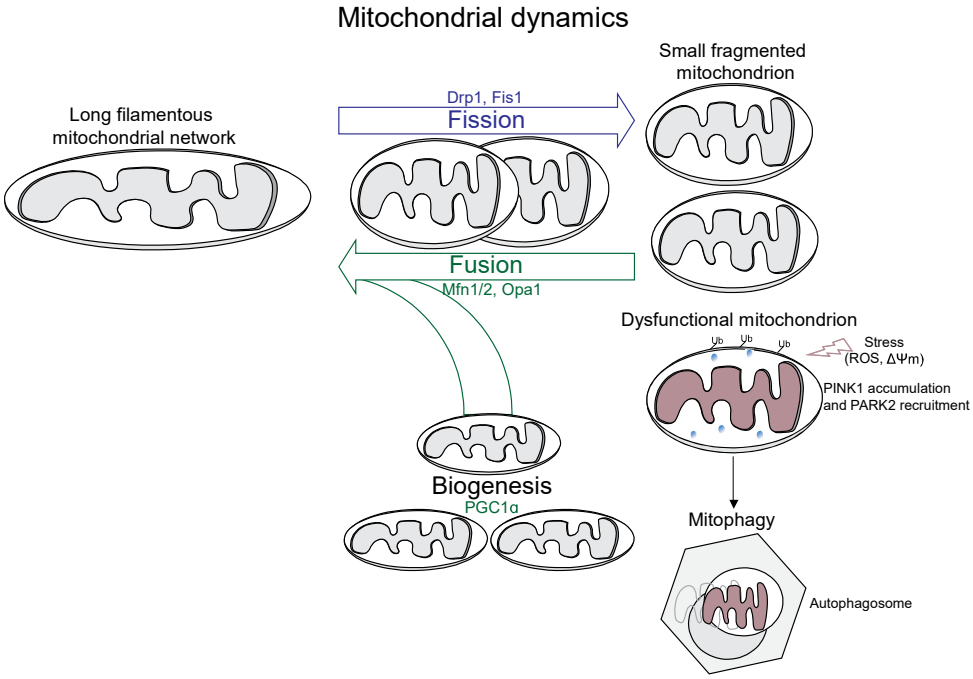

Figure 2: Mitochondrial dynamics. Mitochondrial quality control is a highly regulated process which involves fission, fusion, biogenesis and mitophagy. Master regulators of fission include: Drp1 and Fis1, and the fusion proteins: Mfn1 and Mfn2, and Opa1. PGC1α is a master regulator of

biogenesis. Upon stress induced by ROS or altered membrane potential (ΔΨm), PINK1 accumulates in the mitochondria leading to PARK2 recruitment which ubiquitinates the mitochondria and leads to mitophagy. *Abbreviations are listed in the beginning of the thesis.* Figure based on [26].

1.2 Cellular energy metabolism

Mitochondria are the headquarters of cellular energy metabolism, however, mitochondrial function depends on a range of different cellular processes which takes place both in the cytoplasm and within the mitochondrial organelles. The metabolic pathways associated with maintaining cellular homeostasis consists of a vast network of biochemical processes, where most are crucial for survival. Essential parts in this respect are glycolysis, the TCA-cycle, fatty acid and amino acid oxidation, and the OXPHOS.

1.2.1 Glucose uptake and glycolysis

Glucose transport into the cytoplasm is dependent on glucose transporters (GLUTs). There are 14 GLUT isoforms known to date, which are categorized into classes depending on their gene sequences. Class I consists of GLUT 1 to 4 and 14, class II 5, 7, 9 and 11, and finally class III 6, 8, 1, 12 and 13 [33, 34]. As an example of the complexity and importance of these transporters, muscle cells contain as many as six different GLUT isoforms (GLUT 3-5, GLUT 10-11) to facilitate their high energy demand [33]. Brain cells display high levels of GLUT1 and GLUT3, which is orchestrated by the glucose dependence of the brain, as GLUT1–3 are reported to be the isoforms with the highest affinity for glucose [33, 34]. The GLUT expression profile is an important determinant of contextual glucose uptake in the cell. For example, GLUT4 is known as the major insulin-regulated GLUT and is central in facilitating glucose uptake in muscle and adipose tissue [35]. GLUT3 and GLUT4 are both reported to be translocated to the plasma membrane upon insulin stimulation in white blood cells [34, 36]. Further, GLUT4 is also a marker of insulin sensitivity, as GLUT4 reduction is found in insulin resistance, pre-diabetes and type 2 diabetes [35, 37]. Upregulation of GLUT has been linked to many different cancer types such as lung, breast and ovarian cancers to name a few [34, 38, 39].

A central pathway in the breakdown of glucose to form ATP is the glycolysis, which has a net gain of 2 ATP. This ten-step enzymatic process converts glucose to its end product, pyruvate (**Figure 3**). The two pyruvate molecules produced from one glucose molecule in glycolysis can be converted to lactate via lactate dehydrogenase (LDH) or transported into the mitochondria where it is converted into acetyl coenzyme A (acetyl-CoA) via the pyruvate dehydrogenase complex (PDH) (See more in Chapter 1.2.2) [40, 41]. Master regulators of glycolysis include hexokinase (HK), phosphofructokinase (PFK) and pyruvate kinase (PK). In essence, these enzymes regulates glycolysis through allosteric mechanisms, when the energy charge of the cell, i.e. ATP level, is high. HK consists of four isoforms (HK1–4) and is responsible for phosphorylating glucose to glucose-6-phosphate thereby using ATP. PFK is dependent on ATP to phosphorylate fructose-6-phosphate, which forms fructose 1.6-bisphosphate. This step is irreversible, and is inhibited by decreased pH, and elevated cellular ATP and citrate levels [42, 43]. PK includes four isoenzymes namely PK muscle (PKM1 and 2), PK liver (PKL) and PK red blood cells (PKR) [44]. PK completes the glycolysis through the irreversible conversion of phosphoenol pyruvate to pyruvate, a process which generates ATP [44].

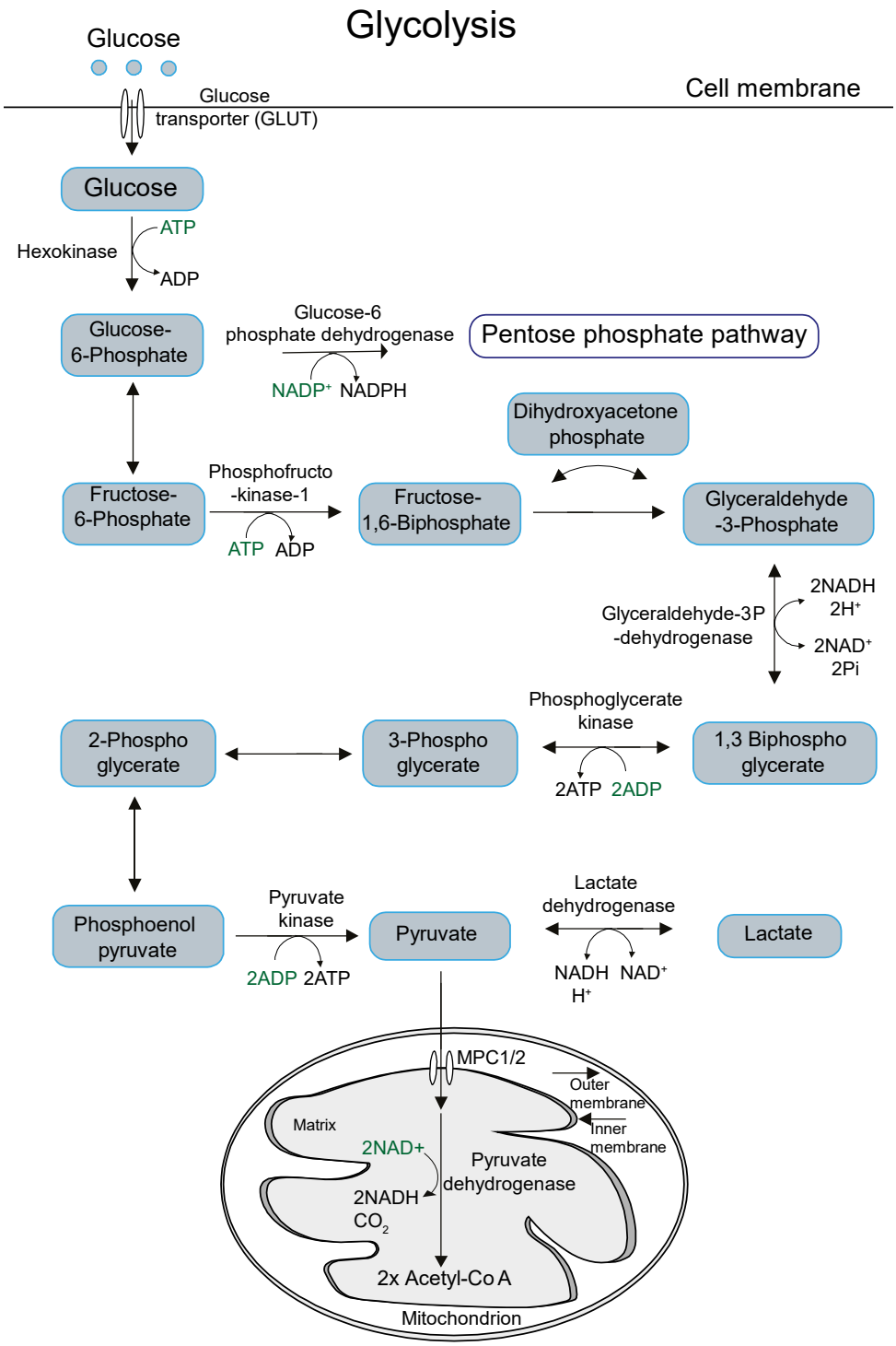

Figure text on next page

Figure 3: Glycolysis. Glucose is taken up through the plasma membrane by glucose transporters (GLUTs). In total, two ATP molecules are used, the first where hexokinase phosphorylate glucose and the second where phosphofructokinase-1 forms fructose 1.6-bisphosphate from fructose 6-phosphate. The net production is two NADH generated from the conversion of glyceraldehyde-3-phosphate to 1,3 biphosphoglycerate. Two ATP are formed from the subsequent phosphoglycerate kinase step. The pyruvate kinase completes the glycolysis by converting phosphoenol pyruvate to pyruvate, while generating two ATP. In the pentose phosphate pathway, NADPH is generated through glucose-6 phosphate dehydrogenase and 6-Phosphogluco-natedehydrogenase dependent steps. *Abbreviations are listed in the beginning of the thesis*. Figure based on [2, 45].

Glucose can also fuel the pentose phosphate pathway (PPP) by glucose-6-phosphate conversion to 6-phosphogluconolactone by glucose-6-phosphate dehydrogenase. The PPP pathway is mainly anabolic and yields NADPH and ribulose-5-phosophate which is a precursor for nucleotide production. Ribulose-5-phosphate can also enter the glycolytic pathway through fructose-1,6-biphosphate or glyceraldehyde-3-phosphate [1, 46].

Depending on the cellular need, pyruvate can either be transferred to the mitochondria and be broken down to acetyl-CoA, or it can be converted to lactate in a fermentative process generating NAD^+. The conversion of pyruvate to lactate is not irreversible, as lactate can also be reconverted into pyruvate via LDH, which facilitates the use of lactate as an energy substrate. LDH is built up of four subunits, thus forming a tetramer, and may include a varying composition of LDHA, LDHB or LDHC [47, 48]. The most common complex consists of LDHA and/or LDHB subunits which either alone or combined form the tetramer [49]. The subunit composition influences the enzyme functions of the complex. For example, a tetramer consisting of a majority of LDHA subunits ($LDHA_4$ or $LDHA_3B_1$) is associated with lactate production whereas the LDHB dominated tetramer ($LDHB_4$ or $LDHA_1B_3$) is associated with pyruvate production from lactate [49].

Monocarboxylate transporters (MCT1–4) are proteins facilitating pyruvate and lactate transport across membranes [50]. They are mainly located in the plasma membrane, however they have also been found in the peroxisomal and mitochondrial membrane

[51-53]. Thus, MCT is hypothesized to be important for pyruvate transport into the mitochondria [52, 53]. Lactate and pyruvate flux is largely dependent on pH and tissue specific settings. For instance, MCT2 reduction in brain is known to lead to brain impairment, and MCT11 reduction in liver is a causal factor in type 2 diabetes [54, 55]. MCT1 and MCT4 upregulation is found to be important for adipocyte differentiation [56]. Further, MCT1 is known to be involved in increased migration and invasion in cancer through activation of nuclear factor kappa-light-chain-enhancer of activated B cells (NF-KB) [57], and has been proposed as a possible prognostic marker in NSCLC [52, 53].

1.2.2 Acetyl-CoA production via pyruvate dehydrogenase

The pyruvate produced in the cytoplasm by glycolysis diffuses through the mitochondrial outer membrane via porins to the intermembrane space, before it is transported through the inner membrane to the matrix via mitochondrial pyruvate carriers (MPCs) [40, 58, 59]. In the mitochondrial matrix, pyruvate is converted into acetyl-CoA, CO_2 and NADH by the pyruvate dehydrogenase (PDH) complex. The complex consists of several copies of pyruvate dehydrogenase (E1), dihydrolopoyl transacetylase (E2) and E3 binding protein (E3BP), and dihydrolipoyl dehydrogenase (E3) (**Figure 4**) [40, 41, 46]. The reaction requires five cofactors which are bound to the enzyme complex, these include thiamine pyrophosphate (TPP), flavin adenine dinucleotide (FAD), coenzyme A (CoA), nicotinamide adenine dinucleotide (NAD^+) and lipoate [46, 60, 61].

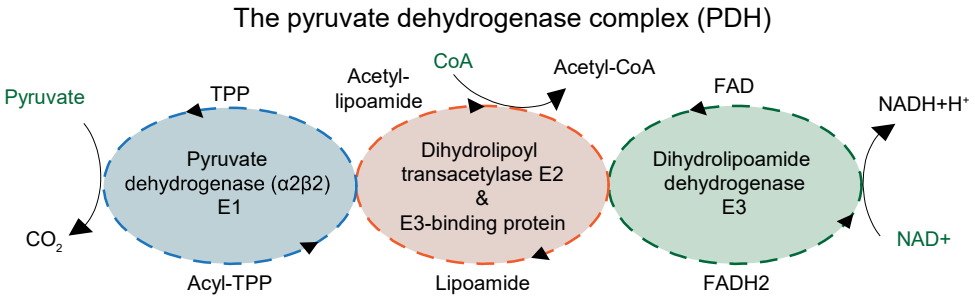

Figure 4. The pyruvate dehydrogenase (PDH) complex. A cartoon of the PDH complex consisting of pyruvate dehydrogenase (α2β2) E1, dihydrolipoyl transacetylase E2 and E3-binding protein, and dihydrolipoamide dehydrogenase E3. Pyruvate is decarboxylated into acetyl-CoA, CO_2, NADH and H^+. First, E1 decarboxylases pyruvate to form a hydroxyetyl-TPP group and oxidizes it to an acyl group, with the release of a CO_2 molecule. The acyl group is reached by the lipoamide arm from E2, forming acyl lipoamide. In E2, acetyl-CoA is formed by transfer of acetyl to coenzyme A (COA). The E3 complex aids in the regeneration of the oxidized lipoamide, which fuels electron to FAD and NAD^+ which generates $FADH_2$ and NADH and H^+. *Abbreviations can be found in the beginning of the thesis*. Based on [1, 46, 60, 61].

During fasting when blood glucose is low, in resting states with low energy charge or when ATP, NADH and/or acetyl-CoA levels are high, PDH is inactivated via phosphorylation of the alpha-E1 subunit by serine specific pyruvate dehydrogenase kinases (PDKs) (**Figure 5**) [60-62]. Dysregulation of PDH through either mutations or phosphorylation by PDKs can lead to quite severe metabolic dysfunctions like diabetes and insulin resistance, lactic acidosis and late-onset neurodegenerative disease [40, 61, 63]. Moreover, changes in PDH activity has also been linked to myalgic encephalomyelitis (ME) / chronic fatigue syndrome (CFS) [64].

There are four PDK isoforms known to date (PDK1–4), all of which are commonly found highly expressed in heart, pancreatic islet and skeletal muscle. PDK2 and PDK4 are the most ubiquitously expressed as they additionally can be found in tissue such as liver, kidney and brain [40, 65, 66]. The PDKs have differing responses to NADH and acetyl-CoA levels as PDK1 and PDK2 were found to increase activity both upon stimulation by NADH alone, and an NADH and acetyl-CoA combination, whereas PDK4 was stimulated by NADH alone and PDK3 remained unresponsive to both treatments [67]. During fasting both PDK2 and PDK4 are found to be upregulated [68,

69], and PDK4 upregulation is associated with increased mitochondrial fatty acid oxidation [65, 70, 71]. Although starvation increases both PDK2 and PDK4, they appear to be regulated in different manners [72, 73]. Insulin is found to decrease both expression of PDK2 and PDK4, however, insulin has a stronger effect on PDK4 expression [72-74]. Further, PPARα expression was found to increase PDK4 levels as opposed to PDK2 in hepatic cells [72]. PPARα, which is a part of a family of PPARs consisting of PPARα, PPARβ/δ, and PPARγ, has been found to be essential in PDK4 upregulation in starvation and diabetes [65, 73, 75]. PPARs are known to be regulated in diabetes, lipid metabolism, inflammation, proliferation and cancer to name a few [76], and long chain fatty acids (LCFA) are known to act as PPAR agonistic ligands [77]

The inactivating phosphorylation of PDH can be removed by pyruvate dehydrogenase phosphatases (PDP) (**Figure 5**). The activity of PDPs can be increased through Ca^{2+} signaling (PDP1) and insulin, and decreased by starving (PDP2) [40, 69, 78]. Moreover, increased PDK4 expression is associated with a decrease in PDP2 expression [66, 69].

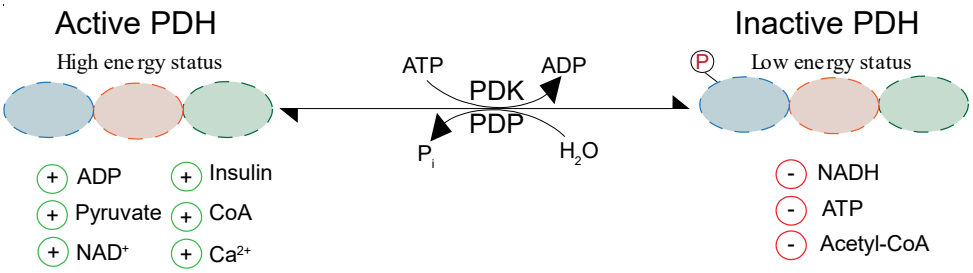

Figure 5: Pyruvate dehydrogenase regulation. PDH activity is induced by high levels of ADP, pyruvate, NAD^+, insulin, COA and Ca^{2+} when energy levels are high. During fasting or heavy exercise, PDH is inhibited by PDKs via phosphorylation of the E1 subunit. PDH activity can be restored through de-phosphorylation by PDPs. *Abbreviations are listed in the beginning of the thesis*. Based on [1, 60, 62].

An example of a PDH inducing chemical is dichloroacetic acid (dichloroacetate or DCA), which inhibits PDKs. It is a pyruvate analogue found to reduce plasma glucose and lactate levels in humans, and increase cellular lactate oxidation [63, 66, 79-81]. Research suggest that DCA treatment reduce fatty acid oxidation, increase ROS

production (Chapter 1.2.6) and induce mitochondrial calcium signaling [61, 79, 81, 82]. Interestingly, according to Bowker et al., [67] DCA appears to be more efficient decreasing PDK2 levels than the other isoenzymes (DCA effect: PDK2<PDK4<PDK1<PDK3) [66, 67]. Due to the effect of DCA on glucose metabolism, DCA has been suggested and used as a therapy in diabetes type 2, lactic acidosis (lactate build up) and cancer (DCA is further discussed in Chapter 5.2) [61, 79, 82, 83].

1.2.3 Tricarboxylic acid cycle

The acetyl-CoA derived from glycolysis, β-oxidation of fatty acids or amino acid oxidation enters the tricarboxylic acid cycle (TCA-cycle) which is also known as the citric acid cycle or Krebs cycle [84]. It is normally presented as an eight-step process (**Figure 6**). The NADH and $FADH_2$ produced from the acetyl-CoA, are essential electron donors which fuel the mitochondrial ETC.

The TCA-cycle is initiated by the conversion of acetyl-CoA and oxaloacetate into citrate by citrate synthase, and comes full cycle by the conversion of malate into oxaloacetate by malate dehydrogenase [46, 85]. It is considered an open-ended pathway as compounds such as anaplerotic amino acids and odd chained fatty acids may re-fuel the cycle (anaplerosis), whereas some intermediates may exit the cycle and supply biosynthetic pathways such as gluconeogenesis and fatty acid synthesis (cataplerosis) [2, 17, 86, 87]. Cataplerosis and anaplerosis are equally as important to maintain carbon flux [86]. An example of an anaplerotic enzyme is pyruvate carboxylase which converts pyruvate to oxaloacetate and thereby fuel the TCA-cycle. Glutamate dehydrogenase (GLDH) is mainly considered a cataplerotic enzyme although it also functions as an anaplerotic enzyme through its involvement in glutamate metabolism [86]. Glutamate can be converted from glutamine by glutaminase before glutamate is converted into α-ketoglutaric acid via GLDH (anaplerotic). However, the α-ketoglutaric can also be converted back to glutamate aided by the same enzyme (cataplerotic). Thus, glutamate is an amino acid that can be both anaplerotic and cataplerotic [86, 87].

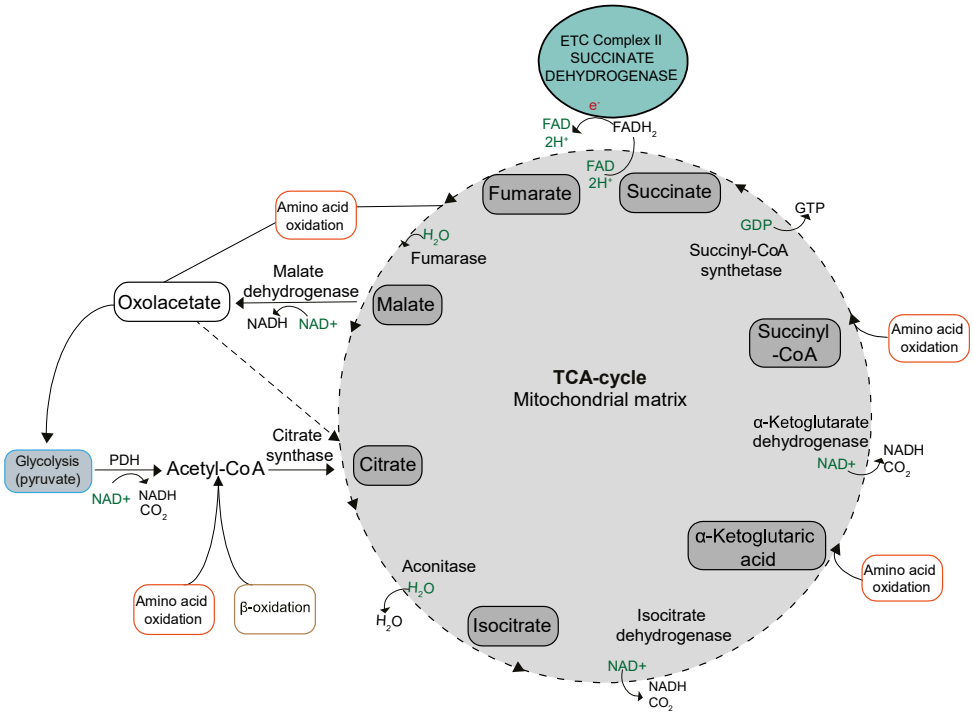

Figure 6: The TCA-cycle. The TCA-cycle initiates with the formation of citrate from acetyl-CoA and oxaloacetate, which is driven by citrate synthase. The citrate is thereby converted to isocitrate by aconitase. NADH and CO_2 is produced in the two following steps: isocitrate formation to α-ketoglutaric acid by isocitrate dehydrogenase, and its α-ketoglutarate dehydrogenase driven conversion to form succinyl-CoA. Succinyl-CoA is thereby converted into succinate by succinyl-CoA synthetase, releasing GTP, before the succinate dehydrogenase converts succinate to fumarate while creating $FADH_2$. Fumarate is from there converted into malate by fumarase. In the final step, NADH is created from the conversion of malate to oxaloacetate by malate dehydrogenase. Oxaloacetate may re-enter the cycle or be used in a range of processes such as gluconeogenesis and as a precursor for amino acid synthesis. Anaplerotic amino acids (orange boxes) are able to replenish the intermediates in the TCA-cycle. *Abbreviations are listed in the beginning of the thesis*. Based on [2, 64, 88].

1.2.4 Acetyl-CoA production via β-oxidation of fatty acids

Acetyl-CoA can also be produced via β-oxidation (fatty acid oxidation, FAO) of free-fatty acids (FFA). Upon lipolysis FFAs are hydrolyzed from triacylglycerols in white adipose tissue (WAT), and released into circulation [2, 89].

If we are to follow palmitate through the oxidation process as an example, it is first transported into the cytosol via fatty acid transport proteins (FATPs) and converted into palmitoyl-CoA by acyl-CoA synthase **(Figure 7**) [89-91]. From there it is transported through the mitochondrial membranes via the carnitine shuttle. Two important enzymes which facilitate the transport of palmitoyl-CoA are the carnitine palmitoyltransferases (CPTs) [91]. CPT1 sits in the outer mitochondrial membrane and converts the acyl-CoA to acylcarnitine. Carnitine acylcarnitine translocase (CACT) transports the carnitine linked fatty acid from the intermembrane space to the inner membrane, and translocates carnitine between the outer membrane to the inner membrane [92]. CPT2 localized in the inner membrane, transports acylcarnitine into the matrix, removes the carnitine and re-forms the acyl-CoA [91-93]. Carnitine reenters the intermembrane space whereas palmitoyl-CoA is further broken down in the matrix through β-oxidation where four enzyme reactions breaks down the acyl-CoAs to acetyl-CoA, producing NADH, $FADH_2$, acetyl-CoA and an acyl-CoA (now with two carbons lost). The shortened acyl-chain can re-enter the cycle for further oxidation [46, 91, 93].

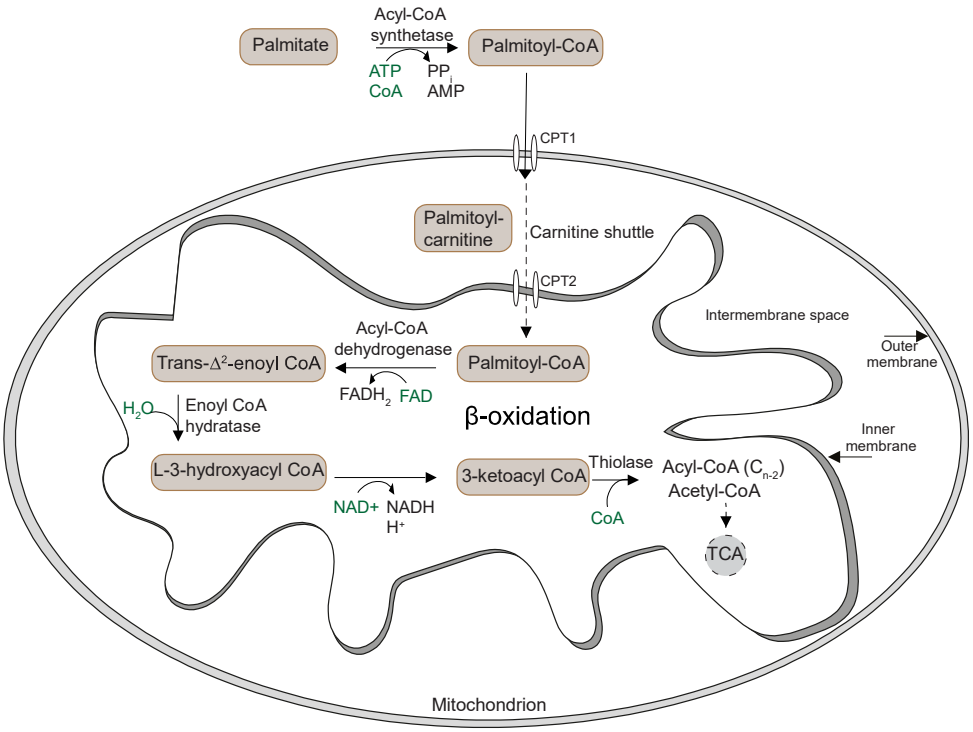

Figure 7: β-oxidation of palmitate. Palmitate is converted into palmitoyl-CoA by acyl-CoA synthetase, before it enters the mitochondria through the carnitine shuttle. Inside the matrix it is converted into acetyl-CoA and acyl-CoA with $FADH_2$ and NADH being formed in the process. Acetyl-CoA enter the TCA-cycle whereas the acyl-CoA re-enter the pathway. *Abbreviations are listed in the beginning of the thesis*. Based on [2, 91].

The mitochondria oxidize both short and long chain fatty acids for energy production when glucose is limiting. For example during fasting, there is a switch towards FAO [89]. This switch is also named "the Randle cycle" after Philip Randle who first described the "glucose fatty-acid cycle" [94]. Most tissues can use FFA for acetyl-CoA production, but FAO is especially important in the heart whereas the brain mostly relies on glucose and ketone bodies for energy production. Whether the brain can use FFAs or not is debated, but research suggest the brain use FFAs and ketone bodies during fasting and diabetes [95, 96]. Although albumin bound FFAs are able to diffuse through the cell membrane, FATPs are important enablers of long chain and very long chain fatty acid (VLCFA) transport [90, 91, 97, 98]. There are several associated proteins discovered so far which supports FFA transport, like plasma membrane fatty acid

binding proteins, cytoplasmic fatty acid binding proteins and fatty acid translocases [90, 91, 97, 98].

The mitochondria are not the only organelle able to oxidize fatty acids. The peroxisomes are structures which play additional roles in amino acid catabolism, ROS production and inflammation to name a few [99]. Research suggest that the two organelles complement each other as the mitochondria oxide the short and long chained fatty acids whereas the peroxisomes oxidize VLCFAs and branched chain fatty acids [99, 100]. However, peroxisomes have been observed to be able to oxidize smaller chained fatty acids during mitochondrial FAO dysfunction [100]. While the mitochondria can utilize the products of FAO for energy production, the peroxisomes reduce the carbon chain to six to eight carbons before it is exported and taken up by the mitochondria for further oxidation to acetyl-CoA [91, 100].

1.2.4.1 Ketone bodies

The low carb diet and the ketogenic diet are currently popular dieting trends. Here, people restrict their diet avoiding carbohydrates and mainly rely on foods high in fat and moderate levels of protein [101]. Altering carbohydrate metabolism through either diet, endurance exercise or starvation results in increased production of ketone bodies [101-104]. When glucose levels are low, increased gluconeogenesis results in reduced oxaloacetate levels [2, 101, 102, 104]. As acetyl-CoA is dependent on oxaloacetate to enter the TCA-cycle, the excess acetyl-CoA is converted into acetoacetate or β-hydroxybuturate, which along with acetone are named ketone bodies [2, 101]. Even though the brain is largely dependent on glucose, ketone bodies have been shown to be an important alternate fuel, especially when glucose is scarce [96]. The ketogenic diet is relatively safe in controlled environments, however, in uncontrolled diabetes, high blood levels of glucose and ketone bodies may result in reduced blood pH resulting in diabetic ketoacidosis, a condition which may be fatal if not addressed properly [101].

1.2.5 Mitochondrial oxidative phosphorylation

During aerobic conditions, the NADH and $FADH_2$ produced in catabolic oxidation reactions acts as electron donors, which fuel the mitochondrial electron transport chain. The electron transport, and subsequent proton pumping through the complexes located in the mitochondrial inner membrane, is what drives the ATP production, a process named oxidative phosphorylation or OXPHOS (**Figure 8**) [1, 105-107].

The OXPHOS system is comprised of five different multi-subunit complexes located in the inner mitochondrial membrane (IMM). The NADH ubiquinone oxidoreductase (Complex I) is a proton pump which oxidizes NADH and pumps protons across the membrane to the intermembrane space [106]. Succinate ubiquinone oxidoreductase (Complex II), also named succinate dehydrogenase, consists of four subunits SDHA, SDHB, SDHC and SDHD. SDHC and SDHD are anchored to the membrane, whereas SDHB and SDHA are the catalytic subunits which links the SDH to the mitochondrial matrix [108]. It is, as the only complex in the ETC, a part of the TCA cycle where it oxidizes succinate and FAD (SDHA bound) to fumarate and $FADH_2$, however without any proton pumping involved [1, 107, 109]. Both Complex I and II transfer electrons, which reduces ubiquinone (Q) to ubiquinol (QH_2). QH2 then delivers electrons to ubiqinol cytochrome c oxidoreductase (Complex III). Complex III transports electrons to cytochrome c while pumping protons to the intermembrane space. Cytochrome c shuttles electrons to cytochrome c oxidase (Complex IV) where O_2 acts as the terminal electron acceptor to form H_2O, all while protons are translocated to the intermebrane space [22, 107]. The proton pumping in Complex I, III and IV generates a proton gradient that creates the electrochemical membrane potential. The membrane potential represents a proton motive force which drives the ATP synthase (Complex V) [22]. Complex V acts like a membrane-bound rotor that generates ATP from ADP and phosphate (Pi) [107, 110]. The theoretical combined amount of ATP produced from the conversion of one glucose molecule to ATP in aerobic conditions is reported to be 38 ATP. However the exact amount depends on many interacting processes and is estimated to range somewhere around 30 – 36 ATP [2, 46, 106].

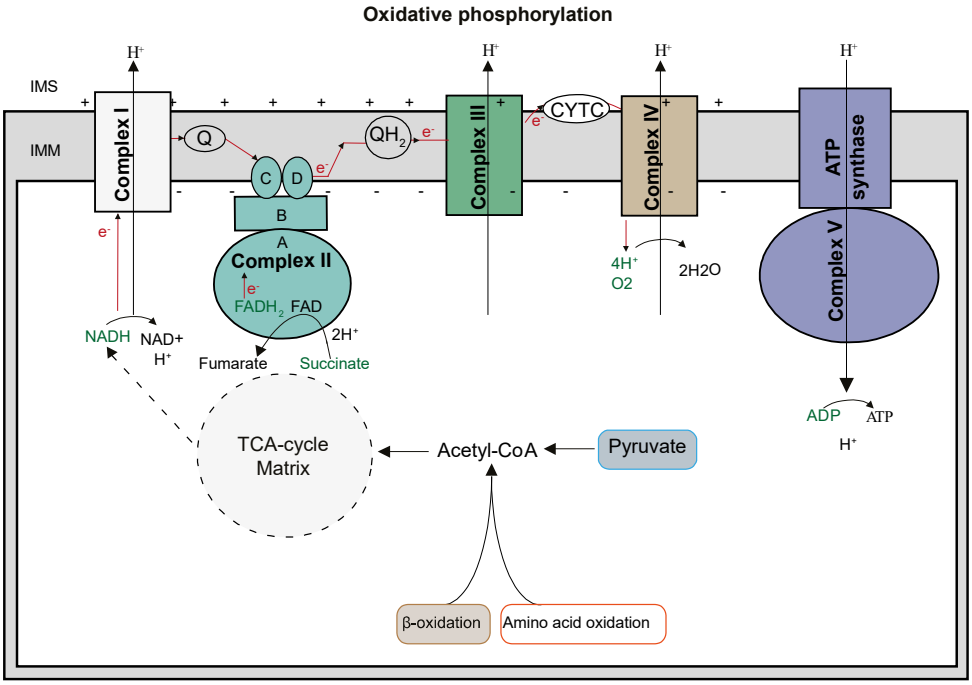

Figure 8: Mitochondrial oxidative phosphorylation. Electrons (e^-) donated by NADH or $FADH_2$ enter the electron transport chain via Complex I and Complex II. O_2 acts as an electron acceptor in Complex IV which results in the production of H_2O. Q, QH_2 and cytochrome c all participates in electron shuttling to the respective complexes. Complex I, III and IV driven proton pumping create the proton motive force which drives the ATP synthase and produces ATP from ADP and Pi. *Abbreviations are listed in the beginning of the thesis*. Figure based on [46, 105, 107].

Examples of proteins regulating mitochondrial OXPHOS function are uncoupling proteins (UCP), which influence the mitochondrial membrane potential as they facilitate proton re-entry to the inner membrane [111, 112]. UCPs are known as proton channels that induce energy release as heat due to mitochondrial uncoupling [112]. Upon compromised membrane potential induced by UCPs, mitochondrial damage or mutations, Complex V may act in reverse and aid in proton translocation by the use of ATP to sustain mitochondrial membrane potential [22, 113]. Inhibitory factor 1 (IF1) has been shown to be an important regulator of both forward and reverse ATP synthase activity [113]. Moreover, IF1 expression has been shown to promote coupling, and to protect against cell death in relation to hypoxia and glucose depriving states [113, 114]. Whereas IF1 knockdown reduce mitochondrial mass and alter cristae formation [113,

114]. Furthermore, increased mitochondrial uncoupling and reduced IF1 activity has been linked to reduced ROS production, as a reduced membrane potential results in a decrease in ROS formation [111, 112, 114].

1.2.6 Mitochondrial reactive oxygen species

Although ROS are also produced in peroxisomes [99], the mitochondrial Complex I-III are considered the main producers of ROS in cells [110, 115]. The formation of ROS is normally a highly regulated process and important in cellular signaling processes, but disturbances in this machinery may lead to various diseases as oxidative damage accumulate. When the antioxidant defense system is saturated, the excess ROS may induce mtDNA mutations, lipid peroxidation and mitochondrial oxidative damage [116]. Superoxide (O_2^-) is a ROS that is spontaneously produced when the mitochondria utilize O_2 as the main electron acceptor in the ETC [110, 117]. Superoxide can be converted into hydrogen peroxide (H_2O_2) and hydroxyl radical (OH^-), which are considered the three main forms of ROS. Reverse electron transport (RET) in Complex I is also shown to be an important driver of ROS production, which is mediated by a highly reduced Q pool along with increased membrane potential [115, 118, 119]. Succinate and FAO have been shown to be important drivers of RET [115, 119, 120], for example isolated mitochondria have been found to produce ROS through RET when respiring on succinate and fatty acids [120].

Important mediators combating ROS are antioxidants such as superoxide dismutases (SODs) which are found in the cytoplasm (SOD1) and mitochondria (SOD2). These are crucial enzymes as they turn superoxide to hydrogen peroxide. Other important regulators are glutathione peroxidase (GPX) and catalase which reduces hydrogen peroxide to water [110]. Disturbances in the equilibrium between ROS production and antioxidant defense may lead to apoptosis, through opening of mitochondrial pores and release of cytochrome c [110]. Furthermore, increasing antioxidant levels may reduce neuronal damage in Alzheimer's and Parkinson's disease as reducing ROS production has been known to have a neuroprotective effect [117]. As antioxidants have a protective function on mitochondrial function and cellular homeostasis, they were hypothesized to be protective against tumorigenesis. To study the effect of antioxidants

in cancer, the Alpha-Tocopherol Beta Carotene Cancer Prevention Study Group performed a study where over 29 000 male smokers participated. The results were surprising, as smokers taking beta carotene (antioxidant) supplements had a higher risk of developing lung cancer [121]. A follow-up study published in 2003 confirmed this observation stating that beta carotene supplements increased both risk and mortality rate [122].

1.3 Cancer

Cancer is most commonly described as an increase in cell proliferation, accompanied increased invasion of surrounding tissue and metastasis from tumor origin to a secondary site [123, 124]. Thus, cancer is rather a generic description of a disease that differs greatly within and between specific tissues [123, 125, 126]. According to the global cancer observatory (GLOBCAN 2018), there were over 18 million cancer cases diagnosed and over 9.5 million cancer related deaths worldwide in 2018 [127-129]. Lung cancer was ranged as the cancer type with the highest number of incidences and deaths (**Figure 9**). If separated by sex, lung cancer incidence and death was ranked highest in men, whereas breast cancer was ranked highest in women.

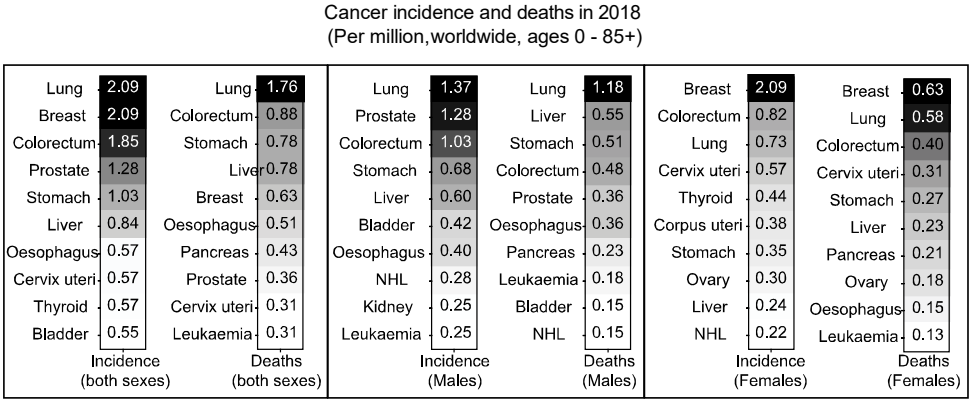

Figure 9: Top 10 cancer incidence and death rates in 2018. Top 10 cancer incidence and death rates in both sexes combined and separately (Numbers displayed per 10^6). NHL = Non-Hodgkin's lymphoma. Numbers from [127].

1.3.1 Lung cancer classification and treatment

At the time of diagnosis, lung cancer is most often classified into stages according to size (T), lymph node status (N) and metastatic status (M) (TNM status) [130]. Lung cancer is further divided into two main sub types based on histology: small cell lung cancer (SCLC) and non-small cell lung cancer (NSCLC), where NSCLC attributes to over three quarters of all lung cancer cases [131]. The most common subtypes of NSCLC are adenocarcinoma, squamous cell carcinoma and large cell carcinomas. In NSCLC, surgical resection is the most effective treatment option; however, it is not feasible in over 70 % of the cases as many tumors have metastasized or advanced locally [131]. Therefore, treatment options vary and may include immunotherapy, radiation, surgery and chemotherapy [131-133]. Targeted therapy has also proven to be beneficial for NSCLC patients and is based on tumor biomarkers such as oncogenic mutations [132, 134, 135]. The most common include epidermal growth factor receptor tyrosine kinase inhibitors (EGFR TKI), anaplastic lymphoma kinase inhibitors or Kras protein inhibitors [132, 134, 136].

Mutations in the EGFR has been found to exist in over 10 % of NSCLC cases reported in the U.S, with even higher percentages found in Asia [137]. These mutations sensitize the tumor to EGFR inhibitors. EGFR activation is known to occur by extracellular ligand binding which activate signaling pathways associated with phosphatidylinositol 3-kinase (PI3K)/AKT and mTOR regulation, along with the STAT and MAPK/ERK pathways, leading to increased survival, proliferation, angiogenesis, invasion and metastasis [132, 138, 139]. There have been numerous EGFR TKI inhibitors developed, including first-generation inhibitors such as erlotinib and gefitinib that binds reversibly to the mutated EGFR. However, they may also cause off target effects as they may interact with wild type EGFR. Moreover, acquired resistance usually develops within a year of treatment [133]. To overcome this, second generation inhibitors (afatinib and dacotinib) were developed. These inhibitors bind irreversible to EGFR; however, side effects are evident as they also may target wild type EGFR. Recently, third generation EGFR inhibitors targeting the specific T790M mutation (rociletinib and osimertinib) to relieve wild type EGFR binding, have been developed

[133, 140]. Despite efforts in improvement of EGFR inhibitors, development of resistance still is a devastating fact for most patients [140].

1.3.2 Breast cancer classification and treatment

Other than TNM status, breast cancer sub-classification provides a useful strategic implementation for breast cancer treatment [141-145]. Recent advances has been made in classifying breast cancer the last decade, which started twenty years ago when Perou et al., were able to classify breast cancer subtypes into estrogen receptor positive (ER+) and negative (ER-) based on gene expression analysis [142]. A short time later they expanded the classification to include five intrinsic sub types [142, 145]. Sub-classification include hormone receptor (HR) status such as ER and progesterone receptor (PR), and human epidermal growth factor receptor 2 (HER2) [146-148]. The underlying subtypes include HR+ *luminal A*, *luminal B* and *normal-breast like* which are ER+, and/or PR+, but are otherwise separated by differing gene signatures. The HR- sub types include *HER2 enriched* (HER2+) and triple negative breast cancer (TNBC). As TNBC have very heterogeneous gene profiles, the amount of subtypes is rapidly increasing, examples being *basal like 1* and *2*, *claudin high* and *low*, *mesenchymal, mesenchymal stem like, immunomodulatory* and *luminal androgen receptor* [143, 144, 148, 149]. The most common type is HR+, which attribute to ~70 % of all cases, whereas 15 – 20 % are diagnosed with HER2+ and ~15 % with TNBC [150].

Due to the heterogeneity within breast cancer, treatment options vary according to TNM status and sub classification. For example, stage I HR+ tumors benefit from targeted therapy, which results in good overall prognosis with a five-year overall survival of ~85% [143]. However, in TNBC, the treatment options reflect the diversity within the subclass as there is no clear treatment option. Although TNBC initially appear to be highly sensitive to chemotherapy, the limited therapeutic options and the aggressive nature of TNBC makes the overall prognosis poor [143, 149].

A common denominator in treatment of both NSCLC and breast cancer is development of drug resistance [136, 151, 152]. Acquired EGFR TKI resistance is for example

reported to develop within 9–13 months in NSCLC [153]. Thus, the major contributor to a high mortality rate in lung cancer and breast cancer is often not the primary tumor itself, but invasion, metastasis and drug resistance, which are all features characterizing cancer cell plasticity [154, 155].

1.4 Cancer cell plasticity

Cellular plasticity encompasses the ability of cells to adapt to changes in terms of stress, injury, altered nutrient supply or drug exposure. In adult tissue, plasticity is needed when the stem cells in the intestines regenerate tissue in order to absorb nutrients or in wound healing [154]. However, the term plasticity is also used to describe the genotypic and phenotypic heterogeneity within a tumor. The plastic nature of tumors may be driven by mutations, microenvironmental signals, therapeutic treatment or epigenetic changes [156]. What characterizes the plasticity of cancer cells is increased inflammation and expression of proliferation related growth factors and cytokines epidermal growth factor (EGF), vascular endothelial growth factor (VEGF), transforming growth factor beta (TGFβ) and tumor necrosis factor alpha [155, 157].

A well described example of cellular plasticity induced by some of these factors is epithelial to mesenchymal transition (EMT), a process where epithelial cells loose cell-cell contacts and cell polarity, thus becoming more migratory (**Figure 10**). EMT is commonly defined by loss of the associated epithelial marker E-cadherin, and gain of mesenchymal markers like N-cadherin, Axl and vimentin, although several other factors are involved (markers of EMT is further discussed Chapter 3.2) [136, 158, 159]. EMT is crucial for embryonic development and wound healing. Research by Chen and Behringer showed that knock-out of the EMT related transcription factor TWIST in mice resulted in failure in the formation of the cranial neural tube resulting in embryonal death at day 11 [160, 161].

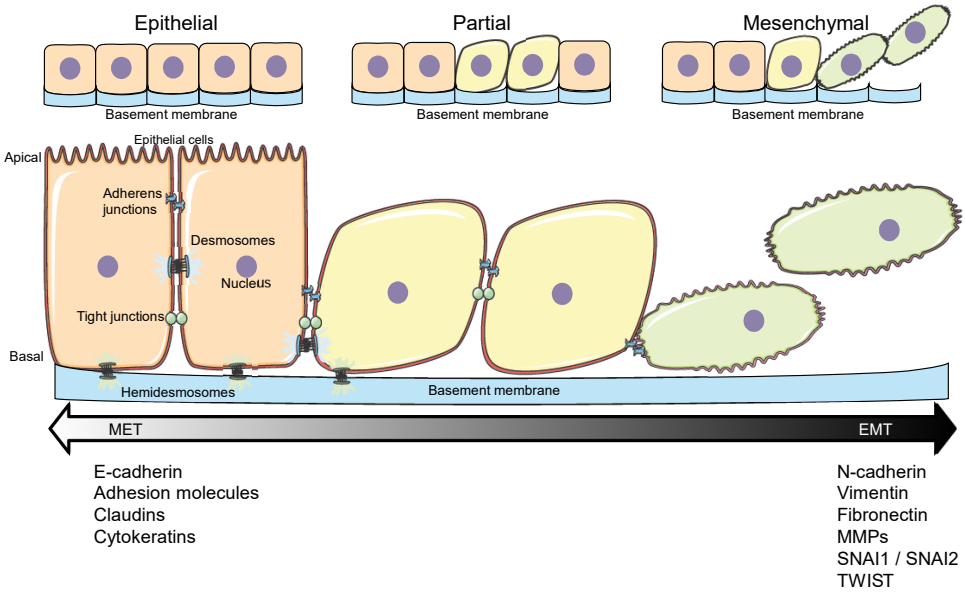

Figure 10: Epithelial to mesenchymal transition.

Epithelial cells in light orange are held together by adherens junctions, tight junctions and desmosomes, and retain an apical-basal polarity. As the cells acquire more mesenchymal properties they lose cell-cell contacts, polarity and become more migratory (yellow and green). Key characteristics of epithelial cells is expression of E-cadherin, the mentioned adhesion molecules, claudins and cytokeratins. As the cells undergo EMT, they increase expression of N-cadherin, vimentin, fibronectin, in addition MMPs and transcription factors SNAI1, SNAI2 and TWIST. It is of importance to note that the cartoon only shows a few of the related EMT-MET markers and that EMT is a reversible plastic process meaning cells can fluctuate between the different EMT-MET states. *Abbreviations are listed in the beginning of the thesis.* Illustration composed of smart medical art [162] and is adapted from [163].

The process of EMT is reversible, meaning that cells can undergo mesenchymal to epithelial transition (MET), and many have suggested that cells display a various degree of EMT within a tumor, with hybrid and multiple intermediate stages [157, 158]. In recent years, it has become clear that EMT is a transient process, where the cells fluctuate between the different epithelial and mesenchymal states [163, 164]. The transient characteristics of EMT-MET has made the term epithelial to mesenchymal plasticity (EMP) increasingly popular. EMT has been shown to be induced by microenvironmental growth factors like TGFβ and EGF. Hypoxia mediated signaling via hypoxia inducible factors (HIF) is also known to induce EMT by activation of EMT

associated factors like vimentin, SNAIL and ZEB [165-167]. Moreover, EMT and hypoxia is also associated with mutations in the TCA-cycle linked enzymes SDH, fumarate hydratase (FH) and isocitrate dehydrogenase (IDH) (Chapter 1.5.2) [168, 169]. EMT is known to alter metabolism through increased glycolysis and glutamine metabolism, and to reduce fatty acid metabolism [166].

1.4.1 Drug resistance

Apart from being an important step in invasion and metastasis, EMT and cancer cell plasticity has been linked to development of drug resistance [136, 161, 170]. Drug resistance is often defined by intrinsic or acquired resistance, which involve cells already harboring or developing tolerance to chemotherapeutics during the course of treatment [132]. Intrinsic resistance includes innate factors such as already present mutations, altered drug transport or drug metabolism. Acquired drug resistance may include secondary mutations in the direct target of the drug (like the EGF receptor (EGFR)) or amplification of possible compensatory receptors like tyrosine-protein kinase MET (c-MET). Induction of the EMT machinery may also result in altered drug response [132]. As most tumor cells have a high mutational load, providing variance and possible survival benefits, drug resistance can be described as a way of evolution by natural selection. Only the “fittest” cell with the most favorable variation enabling intrinsic resistance or otherwise is able to acquire increased tolerance, will sustain prolonged drug treatment [5, 126].

The major mechanisms of EGFR resistance include secondary mutations like the Thr790Met (T790M), c-MET amplification which activates the PI3K/AKT signaling pathways, and phenotypical changes like EMT [133, 171]. How EMT induces drug resistance is complex, but upregulation of associated EMT-linked markers including TWIST, is found to increase expression of ATP binding cassette (ABC) transporters, which are important for drug influx and efflux [172]. Furthermore, tumors that display high levels of mesenchymal markers appear to have a negative response to drugs targeting the EGF receptor (EGFR) in NSCLC [136].

1.5 Cancer cell metabolism

Twenty years ago, Hanahan and Weinberg described six “Hallmarks of Cancer” [173], which later were updated to ten in the publication “Hallmarks of Cancer: The Next Generation” [124]. One of the added hallmarks was deregulating cellular energetics, which highlighted the fact that cellular energy metabolism needs to be further investigated in respect to cancer initiation and development.

1.5.1 Rewiring cellular energetics

Metabolic reprogramming is a critical part of cancer development as increased biosynthesis and ATP production is a necessity to fuel tumor growth. In fact, the altered tumor energetics like increased glucose uptake has been advantageous in cancer diagnostics by the use of 18F-fluorodeoxyglucose (18F-FDG). 18F-FDG is a radioactively labeled glucose analogue that can be imaged using positron emission tomography [124, 174, 175]. Otto Warburg described the increased preference of aerobic glycolysis in cancer cells almost a hundred years ago, a characteristic which has been termed “the Warburg effect” [125, 176, 177]. In 1956 Warburg followed up the observation with a study where he concluded that the glucose preference was due to faulty mitochondria [178]. The Warburg effect, which is described to be a dysregulation of the ratio of glycolysis to oxidative phosphorylation, is to date the most recognized metabolic alteration observed in cancer. Normally, during aerobic conditions, the mitochondria are the main producers of ATP through OXPHOS (net: 30 - 36 ATP). However, cancer cells are described to have a preference towards aerobic glycolysis (net: 2 ATP), meaning that the theoretical ATP yield from glucose is more than 15 times higher if oxidized completely to CO_2 [106, 124].

A range of different studies on the different glucose transporters and glycolytic enzymes has been performed to understand the altered glucose transport. As an example GLUT1 upregulation has been linked to oncogenic PI3K/AKT and Ras signaling [34, 179]. Furthermore, upregulation of GLUT1, GLUT3 or GLUT4 has been linked to reduced survival in numerous cancer types [33, 34, 38, 179]. Glycolytic enzymes, such as HK and PKM, are also found to be involved in regulation of apoptosis, aerobic glycolysis and to fuel tumor growth [180-184]. Why cancer cells for

the most part rely on aerobic glycolysis for ATP production is not fully understood, but it is believed that reducing mitochondrial OXPHOS results in protection against cell death and damage via mitochondrial induced ROS and apoptosis [124, 176, 185]. Other advantages of increased glucose uptake and lactate production includes rapid ATP generation, sustained glycolysis branched biosynthesis (e.g. pentose phosphate pathway (PPP)) and increased acidification of the microenvironment [176]. For instance, the PPP is important for nucleotide synthesis and generation of the ROS scavenger NADPH [186, 187]. Moreover, lactate has been shown to be involved in invasion and migration through increasing cancer cell motility, while reducing immune cell function [188, 189].

1.5.1.1 Nutrient scavenging

A central part of the metabolic plasticity of cancer cells is the ability to scavenge nutrients. Continuous nutrient supply is of essential importance in order to sustain proliferation, however, within a tumor nutrient levels are highly variable and sometimes limiting, [190]. For example, amino acid and glucose concentrations have been found to be low in pancreatic, colon and breast tumors compared to normal tissue [190, 191]. In addition, intratumoral location, such as distance to blood vessels in the growing tumor is essential for nutrient availability. Therefore, in order to gain sufficient nutrient supply, tumor cells exhibit increased nutrient scavenging through upregulated amino acid uptake, substrate recycling and macropinocytosis.

Some tumor cells have been shown to recycle lactate which fuel the TCA cycle [174], while some have increased glutamine dependence or altered amino acid uptake [125, 185, 192]. The theory behind lactate recycling is that hypoxic cells within the tumor convert pyruvate to lactate. The lactate is secreted before it is taken up and oxidized by the cells in the oxygenated part of the tumor [53, 124, 174]. Lactate recycling is only one example energy supply to fuel tumor growth when nutrients are limiting. Macropinocytosis is important in growing cells, and is an example of a non-specific scavenging pathway where extracellular nutrients and solutes are taken up through an endocytic process [193]. It is an evolutionary conserved form of endocytosis, which allows for catabolism of amino acids which may in turn be used for anaplerosis of the

TCA-cycle and fuel cellular energetics [194]. It is found to be important in cancer as well as neurodegenerative diseases, atherosclerosis and kidney disorders [193].

Kim et al., has reported that adenosine monophosphate activated protein kinase (AMPK) activation is necessary for macropinocytosis in prostate cancer [195]. AMPK is known to be a master regulator of cellular energetics through its activation of β-oxidation, mitochondrial biogenesis and glucose uptake [195-197]. Macropinocytosis may also be induced by cytokines and growth factors like EGF, and has been reported to be triggered by Ras mutation [193, 198]. Qian and colleagues (2014) proposed that extracellular uptake of ATP through macropinocytosis is necessary to maintain growth, increase survival and development of drug resistance in the NSCLC cell line A549 [199]. Furthermore, in a study by Colin et al., 60% of genes associated with macropinocytosis was deregulated in glioblastoma, suggesting that macropinocytosis may be a promising target to diminish tumor cell nutrient supply and drug resistance [198]. As some cancer cells appear to some extent to be relatively dependent on macropinocytosis for nutrient scavenging, it has been suggested as a useful tool for drug delivery [198].

Nutrient scavenging can also occur through autophagy, where cytoplasmic organelles and molecules are degraded in lysosomes, which may provide amino acids, glucose and fatty acids for ATP production [200]. Autophagy may also be used to maintain cellular homeostasis, through the removal of dysfunctional mitochondria through mitophagy. As mitophagy is important for handling dysfunctional mitochondria it is believed to be important in tumorigenesis. Deletions in BCL2-interacting protein 3 (BNIP3) or PARK2 has been linked to multiple cancer types, such as pancreas, ovarian, breast and liver cancer [30, 201]. BNIP3, which is also known for harboring tumor suppressive functions such as induction of apoptosis, is a regulator of hypoxia-induced mitophagy [30, 202]. Furthermore, Zhang et al., found increased PARK2 expression mediated by p53 both *in vitro* and *in vivo* [201]. p53 is one of the most described tumor suppressor genes and is, amongst other things, important in glucose metabolism. PARK2 has been found to be important for p53 mediated glucose regulation and antioxidant defense [201].

A major regulator of both autophagy and macropinocytosis is mammalian target of rapamycin (mTOR). mTOR, which is known to be suppressed by AMPK activation, acts as a nutrient sensor which increase cell growth when cellular amino acids levels are high [194, 203, 204]. Moreover, mTOR expression is induced by intracellular amino acid levels, and has been found to inhibit autophagy and macropinocytosis [194, 205]. mTOR is also believed to be important in EMT induction, as inhibition of the PI3K/mTOR pathway has been found to prevent E-cadherin downregulation and induction of EMT [206]. mTOR is also involved in hypoxic response as HIF stabilizers. Moreover, mTOR is known to be regulated by hypoxia, although the mechanism is still relatively unclear [203, 204].

1.5.1.2 Hypoxia

A major contributor to metabolic reprogramming in tumor cells other than nutrient availability and scavenging is the amount of oxygen present. Healthy cells located more than 200 micrometers (oxygen diffusion limit) from the nearest blood vessel die unless new vasculature is formed [207]. As the oxygen levels within the tissue decrease (hypoxia), growth factors inducing blood vessel formation (angiogenesis) may increase. Hypoxic conditions have been found to drive tumorigenesis and effectuate drug resistance and metastasis [208]. Master regulators of the cellular response to hypoxia are hypoxia inducible factors (HIFs). HIFs is a heterodimer consisting of two subunits, α and β, with three known α and two known β subunits [85]. The α subunit is oxygen sensitive whereas the β is constitutively expressed [209]. HIFs are normally degraded when oxygen is present, a process which is enabled by α-ketoglutarate dependent prolyl hydroxylases (PHD) [85, 183, 210]. An E3-ubiquitin ligase recognizes the hydroxylated group of the α subunit, and targets it for proteasome degradation [85, 209]. HIFs are known to activate genes involved in survival, angiogenesis, growth, invasion, metastasis and EMT [165, 211]. They are also found to be important regulators of metabolic reprogramming through their regulation of major glycolytic enzymes like GLUTs and HK [165, 183, 211]. Further, PKM2 is reported to both regulate and be regulated by HIF, and to be upregulated in cancer [42, 183]. Mitochondrial respiration is also shown to be disturbed by HIF activation through

upregulation of PDKs, as HIF directly targets PDK1, thus disrupting pyruvate oxidation [165, 211, 212].

1.5.2 Mitochondrial tumor suppressor genes and oncometabolites

Mitochondrial metabolites such as fumarate and succinate are found to act as signaling molecules driving oncogenesis upon accumulation, and are therefore considered to be oncometabolites [210]. Mutations in TCA-cycle associated enzymes like SDH, FH and IDH are known to prompt oncometabolite accumulation and drive tumorigenesis.

Mutations in either of the genes encoding Complex II subunits SDHA–D, and SDH assembly factor 2 (SDHAF2) are known to be related to benign tumors such as paraganglioma and pheochromocytomas [108, 213-215]. Mutations associated with SDH are also connected to gastrointestinal tumors and paragangliomas in Carney-Stratakis syndrome (mutations in SDHB, C and D), Leigh syndrome (SHDA) and neoplasms in Carney triad (diseased SDH, not mutational). Thus, highlighting the importance of a functional SDH and its role as a tumor suppressor gene [7, 108, 210, 214].

Mutations in other TCA-related enzymes such as IDH and FH has also been associated with a range of different tumors, as well as induction of EMT [85, 168, 169, 213, 216, 217]. Wild type IDH normally convert isocitrate to α-ketoglutarate (as shown in **Figure 6**). However, mutations in IDH induce a loss of function and is found to instead drive conversion of α-ketoglutarate to 2-hydroxyglutarate (2-HG), which also is considered an oncometabolite [166, 210, 218]. FH converts fumarate to malate and is considered a tumor suppressor gene as mutational inactivation is known to drive tumorigenesis [85, 168, 210, 219]. FH is also believed to be involved in DNA damage response and the antioxidant defense system [85, 219]. Moreover, mutations in SDH, IDH and FH are all known to induce “pseudohypoxia” which means activation of hypoxic responses during normoxic conditions [85, 220]. A pseudohypoxic response occur when mutations or a dysfunction in TCA-cycle related enzymes efficiently stifle mitochondrial electron donor supply, or otherwise initiate an hypoxic response through HIF activation [210, 220, 221]. Accumulation of TCA-cycle oncometabolites such as

fumarate, succinate and oxaloacetate, and depletion of α-ketoglutarate, has been linked to pseudohypoxia through PHD inhibition, resulting in increased HIF levels. [85, 219, 222].

2. Aim of study

The aim of the presented work was to characterize metabolic rewiring mechanisms controlling cancer cell plasticity, and thereby crucial features of tumor malignancy. The presented project focused especially on cellular energetics in epithelial to mesenchymal transition (EMT) and drug resistance, which represent well-documented examples of cancer cell plasticity. The purpose was to provide knowledge that may lead to identification of new therapeutic targets and enable development of new treatments.

Specific aims:

1) To explore regulatory and functional associations between succinate dehydrogenase (SDH) and EMT in breast cancer in order to uncover new mechanisms underlying malignant development.
2) To characterize the role of pyruvate dehydrogenase kinase 4 (PDK4) in regulation of cellular energy fuel utilization.
3) To identify metabolic signatures in non-small cell lung cancer (NSCLC) and investigate their possible impact on acquired resistance to epidermal growth factor receptor tyrosine kinase inhibitors.

3. Methods and methodological considerations

As the choice of advanced methodologies and optimal cell models have been recurrent topics throughout this project (Paper I-III), I will here consider some methodological experimental aspects that has emerged during the course of the work included in this thesis.

3.1 Cells and cell culture

Upon investigating mitochondrial function and dynamics, there are numerous laboratory methods available, most of them being applied *in vitro* on cultured cells, harvested muscle fibers or isolated mitochondria. We chose to mostly rely on immortalized cell lines as they are easier to work with in terms of gene editing and stable doubling time [223-226]. The use of immortalized cells in cancer research remains a discussed topic in laboratories today. The advantages of using immortalized cells are unlimited replicative potential and a relatively homogenous population. However, the genetic and epigenetic drift during culture time, as well as the risk of contamination of other cells or microorganisms, remains challenging [224, 227].

To ensure experimental consistency and check for contaminations, we regularly sent our cell lines to ATCC for cell line authentication through short tandem repeat (STR) profiling and tested cells for *Mycoplasma, Acholeplasma, Entomoplasma* and *Spiroplasma* by using the MyCoAlert kit from Lonza. *Mycoplasma* is a relatively common infection in cell culture and is often ignored, as it is hard to detect in routine culturing conditions and believed not to influence experimental results. However, *Mycoplasma* has been shown to alter the metabolism of infected cells. A microarray expression analysis has shown that an mycoplasma infection affect genes involved in metabolic processes and stress response, as well as genes encoding cytokine and oncogenes to name a few [228]. Moreover, a study performed by [229] showed that a variety of different metabolic pathways and metabolites were changed in mycoplasma infected PNAC-1 cells compared to controls. Further, gentamicin, a common antibiotic used to treat mycoplasma, is also known to alter metabolism and cellular function [230].

3.2 Relevancy of cell models

The EGFR pathway is an important driver in a major subgroup of non-small cell lung cancer (NSCLC) (Chapter 1.4.1) and EGFR TKIs are widely used in clinics today [231]. Acquired resistance to EGFR TKIs in the patient is normally developed within the course of treatment and is one of the many contributors to the high mortality rate in NSCLC [127, 129]. To investigate possible therapeutic strategies to overcome acquired resistance, we chose to develop our own drug resistant clones *in vitro* in the NSCLC cell line HCC827 and HCC4006 (ATCC) that have a Thr790Met (T790M) mutation in the EGFR receptor making it constitutively active. This mutation makes them sensitive to first generation EGFR inhibitors, and resistant clones were established through continuous growth in 1 μM erlotinib as described in Paper III. The main difference between the two cell lines is that the HCC827 cells are harvested from the lung of a 39-year-old female whereas the HCC4006 is harvested from a metastatic site (pleural effusion) in a > 50-year-old male. To verify our findings in HCC827 and HCC4006, we used the H1975 cell line, which have an additional EGFR Leu858Arg/Thr790Met (L858R/T790M) mutation in the EGFR, and are resistant to erlotinib [140, 152]. However, they are sensitive to third-generation inhibitors like rociletinib (co-1686). A resistant H1975 clone were provided by Clovis Oncology and prepared as described in Walter et al., [140].

Further, for Paper I we chose cell lines that have an epithelial phenotype (MCF10A and MCF7) to study possible alterations in metabolism during *in vitro* induced EMT. As EMT is a plastic process, consisting of several phenotypic shifts, there is no specific biomarker for EMT [157, 158, 164, 232]. Therefore, a combination of markers associated with either epithelial phenotype or mesenchymal phenotypes were investigated in order to define the process of EMT. Examples being the EMT related transcription factors TWIST, SNAI1 (SNAIL), SNAI2 (SLUG), ZEB1 and ZEB2, Axl, and/or cytoskeleton markers such as cell adhesion molecules E-Cadherin (CDH1), N-cadherin (CDH2) or the intermediate filament marker vimentin (VIM) [164, 232-234]. Regulation of these markers is widely dependent on tissue and setting, which is why a combination of these markers is used to ensure consistency in experimental procedures

performed [164]. Two distinct EMT signatures, including one "global" signature as well as one less comprehensive signature was used to analyze the breast cancer cohorts in Paper I, and a wide range of different markers of EMT was used in qPCR and western blot throughout this thesis.

3.3 Data normalization

Data normalization is a necessity in order to acquire consistent and trustworthy quantitative data. Normalization serves to neutralize potential differences due to variation in sample mass or cell number between groups. In cell culture experiments, we chose to normalize to µg protein as described in Paper I–III. In quantitative PCR (qPCR) and western blot, reference markers that are stable between samples, are needed. Commonly used reference markers for both qPCR and western blot include glyceraldehyde 3-phosphate dehydrogenase (GAPDH), cytoskeleton markers such as actin and alpha tubulin, and the ribosomal RNA marker 18s for qPCR. However, the expression levels of these markers are dependent on tissues and setting. For example, 18s RNA and GAPDH were found to be the most reliable in lamb lung tissue [235]. However, Glare et al., found that GAPDH along with β-actin are not suitable references when looking at lung tissue harvested from asthmatic patients [236]. We also found differences in GAPDH expression in normal vs NSCLC tumor samples (Paper III, **Figure 1**). This highlights the need to test the references best suited for each experimental and tissue setting. As a way of minimizing the discrepancy between different references in western blot analyses, we chose to display the total amount of protein loaded using image analysis (Paper I) in order to get an overview over the total protein loaded [237, 238].

3.4 Investigating metabolic adaptations

Measuring metabolic function was performed using two distinct methods, the Seahorse XFe96 Analyzer (Seahorse) and by measuring oxidation through carbon-14 (^{14}C) labeled substrates, which is hereby referred to as substrate oxidation. These two methods may complement each other as the Seahorse methodology provides a general insight into mitochondrial respiration and glycolysis, whereas $^{14}CO2$ trapping

following substrate oxidation provides a more detailed description of cellular substrate preference (Further discussed in Chapter 5.3).

3.4.1 Measuring mitochondrial oxygen consumption and glycolysis

The Seahorse methodology was extensively used in this thesis as it can measure the oxygen consumption rate (OCR), and glycolysis indirectly through the extracellular acidification rate (ECAR) in real time **(Figure 11A-B**). As the Seahorse is limited to addition of up to four modulators, careful titration of the stocks and cell number used prior to each experiment is required **(Figure 11C-D).**

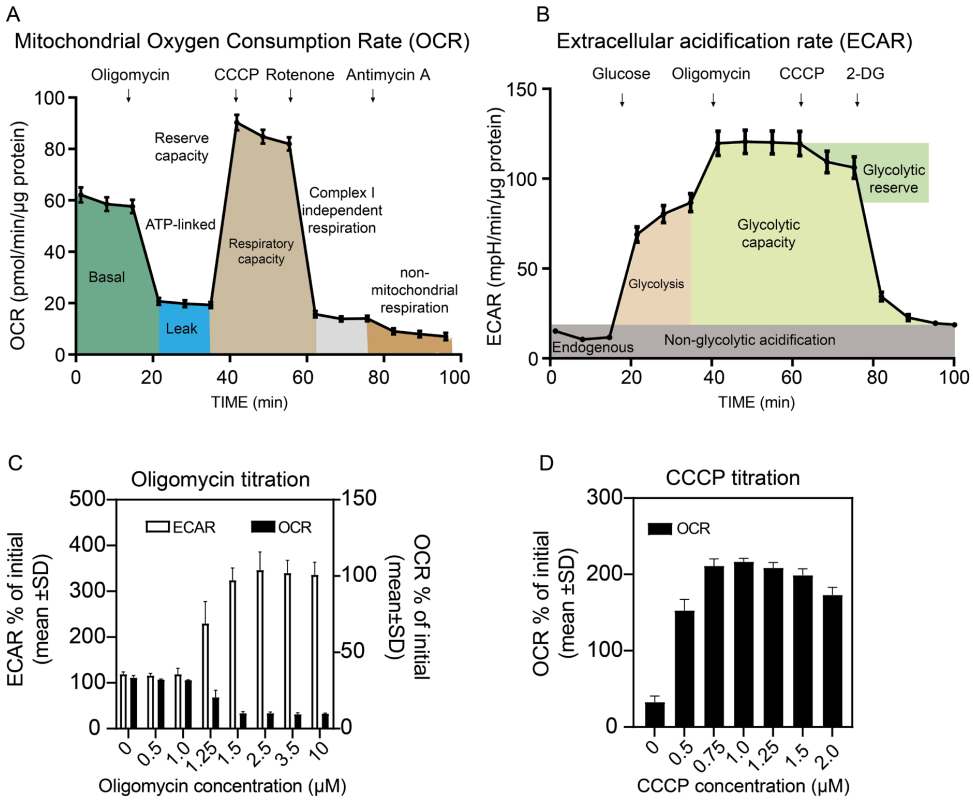

Figure 11: Measuring oxygen consumption rate (OCR) and glycolysis (ECAR) by the Seahorse XFe Analyzer. A and B) is adapted from Paper I and III and [239], and explains what information is gained in a standard Seahorse mitostress and glycostress test run. C-D) highlights the need to titrate each individual compound with C) oligomycin titration in MCF10A cells and D) CCCP in MCF7 cells. Please refer to Paper I-III for more detailed information regarding each specific experiment. *Abbreviations are listed in the beginning of the thesis*

Upon measuring *basal* OCR one gets information on the mitochondrial activity during basal culture conditions (**Figure 11A)**. Through addition of the ATP synthase (Complex V) inhibitor oligomycin, one gets information about the integrity of the mitochondria as it gives indications of proton *leak* across the mitochondrial membrane and the amount of oxygen which was used to produce ATP (*ATP-linked*) [240, 241]. Upon oligomycin titration (**Figure 11C**), we found that in order to fully inhibit ATP synthase, a concentration over 1.5 µM was needed in MCF10A cells, and that concentrations as high as 10 µM gave similar results as 1.5 µM. Further, upon adding carbonyl cyanide m-chlorophenylhydrazone (CCCP), which acts as an uncoupler, one gets information on the *respiratory capacity* of the cell as well as the *reserve capacity*. CCCP is a protonophore which alters the ETC proton gradient, consequently resulting in collapsed mitochondrial membrane potential [240, 241]. The protons can thereby freely cross the mitochondrial membrane which results in a rapid consumption of oxygen, though, without ATP production. CCCP needs to be carefully titrated, as lower concentrations will not provide a true maximal respiratory rate and higher concentrations will result in a collapse of the mitochondrial membrane potential (**Figure 11C)** [240-242]. Addition of rotenone, a Complex I inhibitor, gives indication of C*omplex I independent respiration*. Upon antimycin A stimulation, the mitochondrial Complex I, V and III are all inhibited, which provides information on *non-mitochondrial respiration* [240, 241].

When investigating the glycolytic activity by measuring (ECAR) some of the same metabolic modulators are used (**Figure 11B**). First, the ECAR is measured without glucose added in order to get insight into the *endogenous* levels of glycolysis. When adding glucose, it fuels the *glycolysis* and the ECAR rises. As oligomycin inhibits ATP synthase, it efficiently blocs mitochondrial ATP production, meaning that the metabolism is further shifted towards glycolysis, which is further fueled by CCCP stimulation [240]. This may also provide information on the *glycolytic reserve.* The addition of 2-dexy glucose (2-DG), is an important control as it acts as a glucose analogue that inhibits glycolysis, which gives information on *non-glycolytic acidification* [240, 243]. A factor to consider when measuring glycolysis (ECAR) is that mitochondrial activity may influence the acidification of the medium. When

glucose is broken down to lactate$^-$ through glycolysis, H^+ protons are produced. The lactate and protons H^+ are secreted, and the H^+ is what dictates the ECAR. However, as the cells respire, the CO_2 produced is converted into $HCO3^-$ and H^+, meaning mitochondrial respiration also influence the ECAR [244].

A limitation of the standard methods measuring the OCR and ECAR in real time is that one does not get direct insight into substrate preference nor the molecular mechanisms causing subsequent changes in the metabolic rate. However, one can look at function directly related to the mitochondrial compartments by using isolated mitochondria or permeabilized cells. In permeabilized cells the importance of keeping a balanced environment is more profound, therefore we used a buffered mannitol and sucrose based medium with added fatty acid free BSA (MAS medium) [245]. In Paper I, as we wanted to specifically investigate SDH, and as succinate is unable to cross the mitochondrial membrane, we permeabilized the cells using a plasma membrane permeabilizer (PMP). An advantage when it comes to using permeabilized cells as opposed to isolated mitochondria is the reduction in the number of cells needed. Moreover, many of the cellular compartments remains relatively intact and the mitochondria retain their network [245]. Other important additions used except PMP and succinate, was rotenone, oligomycin and ADP. Rotenone was added to inhibit Complex I dependent respiration. Further, ADP was added to assay the succinate driven OXPHOS, and oligomycin and antimycin A was added to control for mitochondrial integrity and non-mitochondrial respiration [238, 245]. A more detailed description of the concentration of compounds and assay medium used can be found in the respective papers.

3.4.2 Substrate oxidation

In order to measure the dependency and oxidation of each substrate, we used ^{14}C labeled pyruvate, glucose, lactate or palmitic acid as described in Paper II and III. The principle behind the method is that the ^{14}C labeled substrates is taken up by the cells and oxidized, releasing ^{14}C labeled CO_2. The CO_2 released through cellular respiration is absorbed by a filter plate immersed with NaOH, creating HCO_3. After trapping the CO_2, the amount of radioactivity absorbed by the filter plate can be counted using a

scintillation counter, and provides information on the substrate oxidation activity (**Figure 12A**) [246]. The amount of µCi used was carefully optimized prior to each experiment in order to reduce the amount of exposure to ionizing radiation in accordance to health and safety regulation. Also, in regards to minimizing the amount of ^{14}C, non-labeled (referred to as cold) substrate was added in combination with radioactive (referred to as hot) substrate, as described in Paper II and Paper III. A full description of the assay medium composition can be found in the respective articles. In most of the substrates used, the ^{14}C label was uniformly distributed on all carbon atoms. However, in order to get a better insight into PDH function, we used pyruvate labeled only in the first carbon atom (**Figure 12B-E**). Labeling only the first carbon atom, enables the detection of the CO_2 which is released from the PDH dependent step of turning pyruvate into acetyl CoA, and thereby gives an indication of the efficiency and functionality of the PDH enzyme.

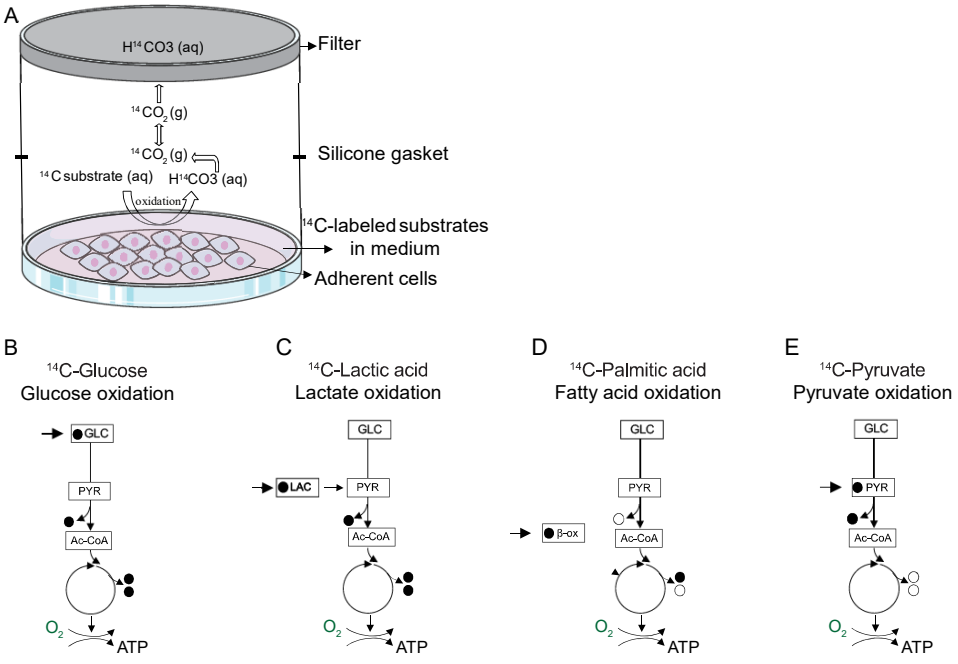

Figure 12: Substrate oxidation: trapping of radioactively labeled $^{14}CO_2$. A) Adherent cells in blue grown in a monolayer, with ^{14}C -labeled substrate. The filter plate is attached on top of the culture plate, with a silicone gasket seal. As the cells respire, the $^{14}CO_2$ released from oxidation is trapped in the NaOH soaked filterplate on top. B-D) The black circle displaying the ^{14}C -labeled

carbons released as CO2 molecules in A) glucose, B) lactic acid, C) palmitic acid and finally D) pyruvate oxidation [65]. Figure A) was adapted form [246] by using illustrations from smart medical art [162] and B-E is adapted from [65].

3.4.3 Metabolic modulators

The following metabolic modulators were used in this thesis (Table 1).

Table 1: ***Metabolic modulators.*** *Cell number and concentrations of compound added was titrated and optimized prior to running all assays. Abbreviations are listed in the beginning of the thesis.*

Name	Assay	Effect	Reference
2-DG	Seahorse, trapping	Inhibits glycolysis competitively. Induce oxidative stress, autophagy and AMPK pathway	[247]
AICAR	Seahorse, trapping and cell culture	AMPK activator and triggers mitochondrial biogenesis	[197]
ADP	Seahorse,	Increases oxidative phosphorylation.	[245, 248]
Antimycin A	Seahorse	Inhibits Complex III	[241, 249]
Carnitine	Trapping	Aids in LCFA transport	[248]
CCCP	Seahorse, trapping	Uncoupler	[241, 250]
Dichloroacetic acid	Seahorse, trapping, resazurin, incucyte	Inhibits pyruvate dehydrogenase kinase	[63, 251]
Oligomycin	Seahorse	Inhibits ATP synthase	[241, 249]
Malonate	Seahorse	Inhibits succinate competitively	[249]
PMP	Seahorse	Permeabilizes cells	[245, 252]
Rotenone	Seahorse	Inhibits Complex I	[241, 249]
Succinate	Seahorse	Fuel for CII (succinate dehydrogenase)	[248]

TTA	Seahorse, trapping and cell culture	Induces mitochondrial fatty acid oxidation	[65]
WY 14,643,	Seahorse, trapping and cell culture	PPARα-agonists	[65]

4. Summary of Papers

4.1 Paper I

Title: *Epithelial to mesenchymal transition (EMT) is associated with attenuation of succinate dehydrogenase (SDH) in breast cancer through reduced expression of SDHC*

Here we investigated the role of the mitochondrial Complex II succinate dehydrogenase (SDH) subunit C in EMT. In two breast cancer patient cohorts we found an inverse relationship between EMT associated markers and SHDC. The reduced expression of SDHC was more profound in basal-like molecular subtypes than non-basal subtypes. Upon CRISPR heterozygous knockdown of the SDHC subunit in epithelial MCF7 cells (MCF7 SDHC +/- cells), we found EMT related markers and characteristics such as increased wound healing and reduced abilities to form spheroids. These properties were also evident when using the SDH enzymatic inhibitor malonate on the non-tumorigenic cell line MCF10A. Interestingly, when we overexpressed the EMT inducing transcription factors TWIST and SNAI2 independently in MCF10A cells we found a reduction in both the SDHB and SDHC subunit. The MCF7 SDHC +/- cells showed reduced respiratory capacity, whereas both MCF10A malonate, MCF10A/TWIST and MCF10A/SNAI2 cell lines showed reduced mitochondrial basal respiration and respiratory capacity compared to parental controls.

Upon measuring oxygen consumption rate in permeabilized cells, we found a common characteristic in both MCF10A/TWIST, MCF10A malonate treated and MCF7/SDHC+/-, namely reduced succinate dehydrogenase activity. When assaying mitochondrial mass and morphology in the MCF10A/TWIST overexpressing cells, we found a higher fraction of smaller and fragmented mitochondria in the TWIST overexpressing cell lines compared to the control. This was supported by a reduction in the fission related protein Drp1. Furthermore, we found that the TWIST overexpressing cells had a larger proportion of small mitochondria, lower expression of the mitochondrial fusion protein Opa1 and thinner tubular mitochondrial structures compared to the parental control.

In conclusion, we found a link between SDHC expression and EMT, through remodeling of mitochondrial dynamics. This was followed by reduced mitochondrial activity, suggesting that mitochondrial remodeling play an important role in cancer cell plasticity. The altered mitochondrial activity may provide tolerance to hypoxia and nutrient deprivation, however, it may also imply reduced tolerance to metabolic modulators targeting glucose metabolism. As the mitochondrial structure and volume is altered in EMT, and EMT is induced upon SDH knockdown, we propose further research into the use of mitochondrial specific drugs alongside conventional cancer therapy.

4.2 Paper II

Title: *Upregulated PDK4 expression is a sensitive marker of increased fatty acid oxidation*

In this study, we set out to investigate the role of pyruvate dehydrogenase kinase 4 (PDK4) in cellular regulation of fuel utilization. We specifically looked at the role of PDK4 in mitochondrial fatty acid oxidation (FAO), and whether PDK4 could be an associated marker of metabolic adaptation through a substrate switch from glucose to fatty acid oxidation. Measuring fatty acid oxidation in the laboratory is difficult, as it usually involves measuring radioactively labeled derivatives of FAO and not FAO directly, a process which often require fresh sample material like intact cells or tissue homogenates.

We found the PDK4 expression, along with other associated markers such as Cpt, Acox and Me-1, to be upregulated in tissue harvested from rats treated with tetradecylthioacetic acid (TTA). Furthermore, after upregulating PPARα in MDA-MB-231 cells and inducing PDK4 upregulation, we used ^{14}C-labeled substrates and discovered an increase in palmitic acid oxidation; conversely, the glucose oxidation was significantly reduced.

Treatment with AICAR, WY 14,643 and ranging concentrations of TTA in MDA-MB-231 cells revealed an increase in CPT1A and PDK4, along with an increase in palmitic acid oxidation in the TTA treated cells. However, only WY 14,643 and the higher concentrations of TTA showed increased basal oxygen consumption rate compared to

controls. Furthermore, TTA was found to cause acute uncoupling effects when added to cultured cells.

To conclude, PDK4 upregulation was found to be a marker of metabolic adaptations as it was consistently upregulated upon increased fatty acid oxidation. PDK4 expression analysis can be used to evaluate changes in fatty acid oxidation as a component of metabolic adaptation, and provide a useful implementation when investigating FAO in the laboratory.

4.3 Paper III

Title: *Inhibition of pyruvate dehydrogenase kinase redirects NSCLC cell metabolism and counteracts development of resistance to epidermal growth factor receptor tyrosine kinase inhibitors.*

In 2018, over 2 million new lung cancer cases were diagnosed. A common feature of lung cancer is drug resistance, which represents one of the major contributors to lung cancer mortality. Here we aimed to identify metabolic targets in non-small cell lung cancer (NSCLC), and upon acquired epidermal growth factor tyrosine kinase inhibitor (EGFR TKI) resistance.

We found increased PDK1 expression in two NSCLC cohorts, and increased expression of glycolytic and antioxidant related markers, which paralleled a decrease in fatty acid oxidation markers and mitochondrial biogenesis. We used three NSCLC cell lines harboring EGFR activating mutations. These included the EGFR TKI sensitive HCC827 and HCC4006 cell lines with a T790M mutation. In addition, we used the L858R/T790M mutated H1975 cell line, which are resistant to first generation EGFR TKIs such as erlotinib. Upon targeting pyruvate metabolism using dichloroacetate (DCA), we found glycolysis to be reduced in an acute manner, and that DCA alone or in combination with EGFR TKIs inhibited cell growth. Further, treatment of NSCLC with DCA increased pyruvate and lactate oxidation, in addition to reducing glucose oxidation. DCA treatment further increased markers of mitochondrial biogenesis and reduced lactate dehydrogenase expression (LDH).

In order to further investigate pyruvate metabolism and the effects of DCA treatment in resistant NSCLC clones, we developed subtypes resistant to erlotinib, and acquired a rociletinib H1975 resistant clone from Clovis Oncology. Upon acquired drug resistance, we found increased expression of EMT related markers, which was followed by altered expression of PDKs, mitochondrial superoxide dismutase, glucose transporters, mitochondrial pyruvate carrier and monocarboxylate transporters. The dysregulated glucose, pyruvate and lactate transporters indicated metabolic rewiring in EGFR TKI resistance. Although the metabolic phenotype varied between the resistant cell lines upon investigating mitochondrial oxygen consumption rate and glycolysis, they responded to DCA treatment by reducing glycolysis. The reduction in glycolysis was followed by a trending or decreased glucose oxidation, and increased lactate and pyruvate oxidation. Further, when investigating cell growth upon EGFR TKI and DCA alone or in combination, we found that DCA further mediated the effects of EGFR TKIs.

Based on our findings in the two patient cohorts and resistant models, we propose that DCA treatment result in increased energetic stress which further sensitizes cells to the additional therapeutic effect of EGFR TKIs. DCA treatment may results in reduced acidification of the extracellular environment due to decreased lactate production in addition to increased lactate and pyruvate oxidation. We hypothesize that targeting cellular pyruvate metabolism by the use of DCA will increase therapeutic efficacy of EGFR TKIs and prolong overall survival in patients with NSCLC.

5. Discussion

One of the leading causes of mortality in cancer is cell plasticity through invasion, metastasis and drug resistance [124, 185, 208]. The development of these characteristics, enables the cancer cells to evolve and change according to the microenvironment, and can be viewed as a way of evolution [6, 126]. The term evolution by natural selection is often associated with Charles Darwin [253]. Interestingly, in a similar manner as animals adapt to environmental changes, cancerous cells do the same within the body [5]. For cancer cells, such environmental changes include hypoxia, nutrient availability, pH and cancer therapy [6, 126, 165, 208]. As an example, upon drug exposure, cancer cells harboring or acquiring mutations overcoming treatment are able to survive and sustain proliferation. Due to the uncontrolled growth rate in cancer cells compared to normal tissue, they are prone to a rapid turnover of genetic mutations. In my opinion, which is shared by others, cancer development may be described as rapid evolution [254]. The adaptive capabilities of cancer cells are underlined through tumor heterogeneity, as a tumor may contain a variety of cells harboring different epigenetic and genetic properties. Tumorigenic cells face trade-offs between proliferation, evading immune suppression, invasion and metastasis [126, 155, 255]. As an example, slow proliferating cells harboring metastatic properties often reside on the edges of tumors [6]. Within the growing tumor there are highly proliferating cells, however, as oxygen and nutrient levels become limiting, the core often contain glycolytic cells more resistant to hypoxia [6, 255]. An essential part of the “survival of the fittest cancer cell” is adaptation of metabolic pathways, which are important suppliers of precursors for biosynthesis and sustained survival.

In the present study, we identified pathways and regulators crucial for metabolic rewiring in processes of cell plasticity. In Paper I we found EMT associated transcription factors to induce changes in mitochondrial structure and function, and that the process of EMT is associated with altered mitochondrial Complex II function. We further observed that low levels of Complex II subunit SDHC was associated with the development of EMT in breast cancer. In Paper II, we identified PDK4 as a sensitive

marker of FAO both in cells and rats. In the third paper we further investigated how metabolism is influenced by EMT and drug resistance, and how targeting specific metabolic pathways may aid in combating cancer therapy resistance. Pinpointing areas of metabolic flexibility in cancer, through discovering markers or regulators of metabolic changes and cancer cell plasticity, may assist in identify pathways inducing energy stress which can act as possible therapeutic targets.

5.1 Is metabolic deregulation involved in cancer cell plasticity and drug resistance?

EMT is an acknowledged example of cellular plasticity as it is associated with wound healing and embryonal development. It also remains an important feature of cancer cell plasticity through facilitating drug resistance, invasion and metastasis. [155, 158, 159, 166]. Metabolic reprogramming has been linked to EMT, as it has been shown that dysregulation and dysfunction of key metabolic enzymes, including FH, SDH and IDH, can drive EMT and tumorigenesis [168, 169, 210, 213]. As mentioned in the introduction, dysfunction in either of these enzymes is associated with pseudohypoxia, meaning that the hypoxic response is initiated even in aerobic conditions, for example through HIF stabilization [85, 210, 220-222]. HIF1α is known to regulate cancer cell plasticity through activation of genes that are associated with angiogenesis, invasion and metastasis [157, 166, 208]. Research done by Zhang et al., has linked SDH to osimertinib (EGFR TKI) resistance and pseudohypoxia via miR-147b SDH targeting in NSCLC [256]. However, how these metabolic alterations are driving cellular plasticity is relatively unexplored. In Paper I, we identified the mitochondrial Complex II SDHC subunit to be negatively associated with EMT in a breast cancer cohort. Moreover, overexpression of EMT related transcription factors TWIST and SNAI2, resulted in reduced mitochondrial respiration and altered the intrinsic mitochondrial networks, which resulted in more fragmented mitochondria (Paper I, **figure 6**). Overexpression of TWIST in MCF10A cells also lead to reduced SDH driven respiration (Paper I, **figure 5**) in a similar manner as by treatment of the known SDH inhibitor malonate (Paper I, **figure 4**), indicating that deregulation of Complex II is an important step in EMT. We saw the same trend in a breast cancer cohort, i.e. that EMT

and SDH were found to have an inverse relationship. The inverse relation between EMT and SDHC was shown to be particularly strong in the basal-like breast cancer (BLBC) subgroup. In addition, we found that BLBC with low SDHC had a trend ($P < 0.1$) towards reduced survival compared to high SDHC (Paper I, **figure 2**), indicating decreased SDHC as a possible prognostic marker. Although, BLBC is considered highly aggressive, it appears that it can be divided into two sub-groups. One with poor five-year survival rate, and the other with increased long-term survival [257, 258]. Even if the differences between these subtypes remains elusive, it is tempting to speculate that metabolic markers and markers of EMT can be important prognostic factors to consider.

Research on the link between EMT and drug resistance has been increasing during the last 20 years. Li and colleagues showed *in vitro* that Adriamycin treatment induced EMT in MCF7 cells [259]. The cells that displayed characteristics of EMT, developed multidrug resistance and increased invasion. Furthermore, knock out of TWIST resulted in a reduction of invasion and resistance upon Adriamycin treatment *in vitro,* and increased efficacy of the drug *in vivo* [259]. The link between metabolic dysregulation, EMT and drug resistance remain unclear, though it has been speculated that suppressing mitochondrial function is a way to avoid apoptosis and decrease ROS production [260, 261]. Furthermore, as increased lactate secretion is known to contribute to ECM degradation, the switch to aerobic glycolysis may further aid in invasion [181, 262]. As we found that mitochondrial dysfunction and altered metabolic pathways are important in EMT, and that EMT is linked to drug resistance and poor prognosis [136, 161, 170], we chose to investigate how metabolism may be targeted to increase drug sensitivity in NSCLC in Paper III.

In order to fully explore the metabolic changes upon drug resistance, we developed *in vitro* models of acquired erlotinib resistance in two different NSCLC cell lines and obtained a cell line resistant to rociletinib from Clovis Oncology. We observed, in concordance with other findings, that EMT was induced upon drug resistance (Paper III, **figure** 4) [136, 161, 170]. Moreover, we found that the induction of EMT in our cell models were related to reduced respiration rate and/or reduced respiratory capacity

in the EGFR TKI resistant clones, resembling the results found upon EMT induction in Paper I. Interestingly, one of the three NSCLC cell lines had a different metabolic phenotype compared to the others. The HCC4006/BERL, except from reduced respiratory capacity, displayed higher OCR rates, and higher pyruvate and lactate oxidation compared to control. The main difference between the cells according to ATCC is that HCC4006 is harvested from a metastatic site, which may be a factor influencing their metabolic signature.

Changes in metabolism of fatty acids is linked to a wide range of metabolically linked diseases such as diabetes, cancer and ME/CFS to name a few [65, 263, 264]. In Paper II we found that increased PDK4 expression is associated with increased FAO, which is in accordance with other studies [70, 71, 265, 266]. According to Bowker et al., PDK1 and PDK2 are important for short-term PDH regulation, whereas PDK4 is more involved during starvation [67]. Throughout Paper II we investigated gene regulation upon increased FAO. Either though overexpression of relevant FAO regulators, by adding pharmacological inducers of FAO to cell culture medium *in vitro* or through a TTA supplemented diet in rats *in vivo.* Overexpression in cell culture experiments included PPARα, as PPARs are known regulators of PDK4 expression and FAO. PPAR expression is induced as a consequence of starving and can be activated by LCFA which acts as agonistic ligands [77]. As expected, upon PPARα overexpression, we found increased FAO at the expense of glucose oxidation (Paper II, **figure 2**), along with increased expression of PDK4, CPT1A, ACOX in cell culture. Pdk4, along with other markers of FAO such as Cpt1a, Cpt1b, Cpt2 and Acox, were upregulated in the liver of TTA treated rats.

Although the role of FAO in cancer remains elusive, changes in CPTs and other FAO associated markers have been reported [264]. Upon looking at FAO related genes in NSCLC such as CPT1A, ACOX, PDK4 and PPARG (Paper III, **figure 1**) we found a decreased expression in two distinct NSCLC cohorts. In Paper III, (**Figure 1** and **figure 4**), we found PDK1 upregulation in the patient cohorts compared to healthy tissue, and PDK2 upregulation upon acquired drug resistance in NSCLC. PDK3 and/or PDK2 upregulation has previously been associated with poor survival in AML and lung

cancer patients [267, 268] and PDK2 to confer drug resistance *in vitro* in lung, head and neck cancer [82, 268].

An emerging theory suggests that reduced rates of mitochondrial respiration and/or increased antioxidant activity in tumorigenesis is a way to reduce ROS production, and increase cancer cell survival [260, 269, 270]. Recent research has shown that many tumors have reduced levels of the antioxidant SOD2, and that a reduction in ROS production drive tumorigenesis and drug resistance [7, 260, 269, 270]. In Paper III we found upregulation of a range of different genes associated with antioxidant defense in NSCLC, in addition to SOD1 and SOD2 upregulation in EGFR TKI resistant NSCLC cells compared to parental cells (Paper III, **figure 1**). In Paper I, upon investigating SDHC levels in breast cancer cohorts, we found decreased levels of SDHC to be associated with increased expression of genes involved in ROS defense mechanisms (Paper I, **figure 7**).

5.2 Targeting cancer metabolism

As tumorigenesis involves dysregulation and deregulation of a network of pathways associated with metabolism, targeting cellular energetics represents a promising therapeutic option. There are numerous drugs that may target cancer metabolism directly or indirectly, many of which are already used or are in clinical trials (**Figure 13**).

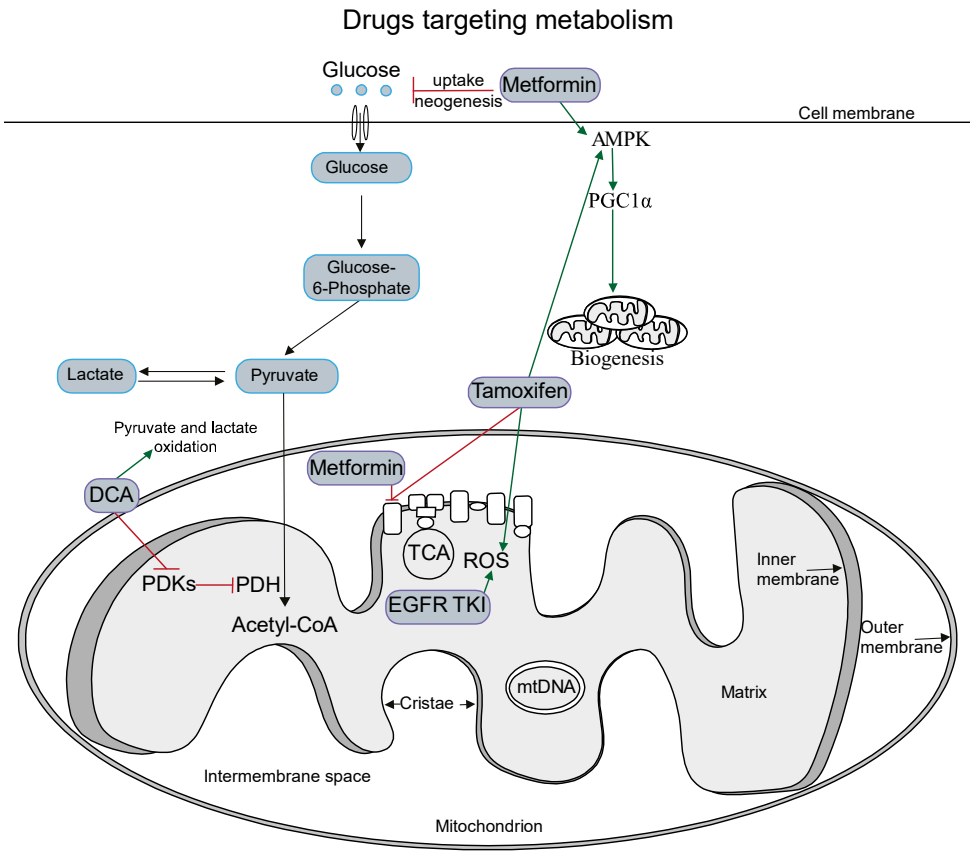

Figure 13: Drugs targeting metabolism. Displaying a selection of drugs and how they target metabolism. In short, DCA targets PDKs thus increasing PDH activity and pyruvate and lactate oxidation. EGFR TKIs are found to induce ROS production and to reduce mitochondrial respiration. Tamoxifen inhibits Complex I, induce ROS and AMPK activation. Metformin inhibits Complex I, glucose uptake and gluconeogenesis. In addition, metformin induces AMPK and PGC1α. *Abbreviations are listed in the beginning of the thesis.* Figure based on [185].

DCA is known to rewire metabolism through PDK inhibition, thus increasing the activity of the PDH complex [271]. Increased PDH activation fuels mitochondrial respiration through increased acetyl-CoA production. As mentioned in the introduction, DCA inhibits PDK expression and increase oxidation of pyruvate and lactate, and reduce plasma lactate and glucose concentrations [63, 80]. As expected, we found increased pyruvate oxidation, lactate oxidation and altered glycolysis in both

sensitive and resistant NSCLC cells upon DCA treatment. Furthermore, DCA treatment reduced LDHA mRNA in the three EGFR TKI sensitive NSCLC cell lines.

The altered lactate flux upon DCA treatment could be one of the main reasons to why DCA show promising clinical results, as lactate is known to increase invasion and metastasis, and to disturb immune cell mobility, T-cell and NK cell function [188, 189, 272-274]. Further, increased LDH expression is linked to decreased progression free survival and overall survival [275]. We found evidence of altered lactate metabolism in our NSCLC cohorts compared to normal tissue through LDHA upregulation. However, as we only investigated LDH levels through RNA sequencing cohorts, we cannot conclude. Though, the increased mRNA LDHA/LDHB ratio may indicate increased lactate production in NSCLC. LDH is important for the reversible conversion of pyruvate to lactate, where a LDHA dominated tetramer will aid in lactate formation [49]. Therefore, targeting LDHA has become a promising therapeutic option. Inhibiting LDHA along with PD-1 has for instance been shown to improve PD-1 efficacy through increased inflammation, NK cell and CD8+ T-cell activity [274]. Moreover, targeting LDHA in T790M, K-RAS and/or EGFR L858R mutated tumors resulted in reduced tumorigenesis in lung cancer and reduced growth of pre-existing tumors [276].

Clinical trials elucidating the effect of DCA and conventional cancer therapy are already in progress [271, 277, 278]. DCA is suggested to be more potent in synergy with already established treatment such as cisplatin, tamoxifen and radiotherapy [278]. In order to improve DCA efficacy and reduce side effects, advances has been made into DCA design and engineering [279, 280]. As DCA has an anionic charge, it has low permeability due to difficulty crossing the plasma membrane via diffusion. Furthermore, solute carriers such as SLC5A8, which is able to mediate DCA transport, is often downregulated in cancer [279, 280]. Trapella and colleagues, reported that they were able to design a multiple DCA loaded compound (compound 10), which sustained the same effects as DCA with over a 30 fold lower concentration [279]. Moreover, Pathak et al., has shown that by using a DCA analogue targeted to mitochondria (mito-DCA), they reduced the toxicity in normal tissue, whereas they retained the efficacy in cancer cells [280].

In Paper III, we show that the combination of EGFR TKIs and DCA show promising results to counteract acquired resistance in NSCLC. EGFR inhibitors are common drugs used to treat NSCLC and other EGF dependent cancers. Gefitinib has been known to induce ROS along with reduced mitochondrial respiration in resistant clones [261]. Furthermore, De Rosa et al., observed reduced lactate production and glucose uptake, increased OXPHOS in NSCLC cells treated with EGFR inhibitors. Based on their findings, they conclude that a combination of agents targeting oncogenic drivers (such as EGFR mutation), along with glucose metabolism, may increase therapeutic efficacy [175]. A drug, which has already been tried out in NSCLC and breast cancer, is metformin. Metabolic rewiring upon metformin treatment includes AMPK activation which is followed by PGC1α activation and mTOR inhibition [281, 282], and restoration of mitochondrial networks [281]. As to how metformin induces these master regulators is unknown, although many have proposed it is linked to ETC Complex I targeting [282]. It is commonly used to target diabetes through its reduction of blood glucose levels and gluconeogenesis, and induction of insulin sensitivity [283, 284]. As it is commonly used in diabetic treatment, possible side effects are known, and it is well-tolerated in most patients. Diabetes type 2 has been linked to cancer development, which is likely to be caused by decreased insulin sensitivity and high glucose blood levels [283, 284].

Fifteen years ago, Evans et al., hypothesized that metformin is a promising cancer preventing drug [285], which fueled further research on the topic. Several studies have now shown that diabetic patients treated with metformin have reduced cancer incidence rate and better overall survival compared to diabetic patients receiving different treatment [283, 284, 286, 287]. Moreover, metformin has also been shown to be preventative towards NSCLC development in patients with diabetes in the U.S military [287]. Research done on NSCLC and breast cancer has shown that metformin use increase survival, [185, 284, 286, 287]. Further, metformin is known to act synergistically with doxorubicin, 2-deoxy glucose and DCA [243, 283, 288, 289]. Though, the exact mechanism to how remains relatively unclear. The promising results on metformin use has led to numerous clinical trials which are currently in progress [282].

PPARs as targets in anti-cancer therapeutics has proven to be a double-edged sword. For example, PPARγ ligands has been shown to induce apoptosis and reduce lung cancer growth [290], whereas prolonged treatment with PPARα ligands such as WY-14,643 has shown increased hepatocellular neoplasia in rodents [291]. The PPARδ agonist GW501516 is known to be involved in tumor growth of both breast and lung cancer [292]. Further, PPARδ activation was shown to increase mTOR expression [292]. The important role of mTOR as a nutrient sensor has made the use of mTOR inhibitors in cancer research another promising therapeutic option [206, 293]. However, the effects of mTOR inhibitors also appear challenging, due to the many roles of mTOR signaling [194, 294]. For example, mTOR has a dual role as both a nutrient sensor modulating cell growth, and as an inhibitor of macropinocytosis and autophagy [194]. Although, mTOR targeting has been hypothesized to be an important target in combating EMT induction [206], inhibiting mTOR may increase cellular energetic plasticity as the cancer cells are increasingly able to absorb extracellular proteins to be used for catabolic and anabolic processes [194]. The inconsistent efficacy of targeting master metabolic regulators such as PPARs and mTOR may explained by their numerous roles in cellular energetics. For instance, along with their role in metabolism, they are also known to be involved in inflammation, angiogenesis, insulin resistance, adipocyte differentiation, apoptosis, EMT, hypoxia and proliferation [76, 194, 203, 290, 292].

A promising therapeutic option in cancer treatment is targeting solute carriers such as GLUTs and MCTs [295]. Since these are essential for cellular substrate transport, they are important for contextual substrate uptake in the cell. Also, as the level of these carriers often are increased in cancer, they serve as promising drug delivery options [296]. In Paper I, we found saw upregulation of GLUT1 and/or GLUT2 in NSCLC cohorts and upon development of EGFR TKI resistance in our cell models, in accordance with other findings [34, 38, 53]. GLUT1 is also associated with hypoxic response, as its expression has been shown to be increased by HIF in glioblastoma [209]. GLUTs are essential for glucose transport and their upregulation is found to be associated with poor overall survival [38, 39].

MCTs are essential for import and export of both pyruvate and lactate, and we found MCT1 and/or MCT2 to be upregulated in both the NSCLC patient cohorts as well as upon development of drug resistance *in vitro*. MCTs are often found to be upregulated in tumors compared to healthy tissue, and is associated with a poor patient outcome in numerous cancer types, including breast and lung cancer [295]. MCT is known to support invasion and migration, highlighting the possible therapeutic implications of MCT inhibitors [57, 295]. MCT inhibitors in synergy with chemotherapy has already proven to be beneficial, and there are currently clinical trials in progress evaluating the effects of MCT1 inhibitors [51, 52, 295, 297]. Confirming altered pyruvate metabolism and transport, the MPC1/2 ratio was reduced. MPCs are multisubunit complexes consisting of MPC1, MPC2 and MPC3 (yeast) [58, 59]. MPC1 downregulation is known to induce EMT and resistance to ionizing radiation [298]. Further, MPC suppression is believed to be a mediator of aerobic glycolysis (the Warburg effect) [59, 298, 299].

5.3 Current prospects in metabolic phenotyping

Tracking metabolic changes in cultured cells was relevant for all three papers in this thesis, which included both state-of-the art technology such as the Seahorse technology and well established methods such as substrate oxidation. During standard cell culture conditions, where cells have an abundance of substrates available, the energy metabolism often remain unchallenged and metabolic weaknesses remain undiscovered. Examples of such effects are shown both in Paper I and II, where modulation of metabolism through SDHC knockdown, AICAR (AMPK stimulator), and PPAR overexpression or activation by WY-14,643 resulted in modest effects on cellular metabolism (Paper I, **figure 3** and Paper II, **figure 5**). This might be reflected by an unchanged mitochondrial respiration and glycolytic balance, as metabolic rewiring enables acetyl-CoA production via alternate metabolic pathways. In order to gain more insight into these metabolic adaptations, reducing glucose concentrations or replacing glucose with galactose, which promotes OXPHOS, may provide a useful strategy [299].

Implementing substrate oxidation in parallel to measuring OCR is another strategy to measure altered substrate preference in cultured cells and tissue homogenate. As seen in Paper III, the NSCLC EGFR TKI resistant subtypes had differing metabolic phenotypes when measuring mitochondrial respiration (OCR) and glycolysis (ECAR). These phenotypes were reflected by the detected substrate oxidation of pyruvate, lactate and glucose (Paper III, **figure 5**). The use of radioactively labeled substrates is not only useful *in vitro*. 18F-FDG is commonly used in cancer diagnostics as a measure to gain insight into cancer therapy response as it gives high contrast resolution of tumors compared to healthy tissue [174, 300]. However, 18F-FDG use is not as effective in cancer types with inflamed tissue, a high FDG uptake in surrounding tissue or in cancer types with low FDG uptake and low metabolic rates [300, 301]. Witney et al., has provided insight into ^{13}C labeled pyruvate as a means of detecting therapeutic response [300], and suggests that measuring ^{13}C labeled lactate and pyruvate flux by using magnetic resonance imaging (MRI) is a promising alternative to using 18F-FDG. Along with limiting patient exposure to ionizing radiation, the use of ^{13}C pyruvate can be implemented in tumor tissue with limited FDG imaging quality such as the brain and prostate [300, 301].

Further advances into implementing cellular energetics in tumor imaging has been made by Momcilovic and colleagues. They have recently developed a membrane potential sensitive radiotraceable probe (4-[^{18}F] fluorobenzyl-triphenylphosphonium), which can be imaged by the use of positron emission tomography [302]. By the use of this radiotracer, they show that it is feasible to phenotype solid tumors based on metabolic activity, including glycolytic- and mitochondrial activity. They could further predict the effect of inhibitors of Complex I in the electron transport chain, as cancer cells with high mitochondrial activity showed an increased sensitivity towards these inhibitors [302]. Thus, by including this method, there might be a robust clinical experimental approach that enables the inclusion of mitochondrial activity.

The metabolism of cancer cells includes dysregulation of a wide network of pathways supporting energy homeostasis. With increased metabolic requirements, comes the need to increase ATP production and biomolecule synthesis through alternate

pathways. In the present thesis I aimed to gain a deeper insight into the role of metabolic rewiring in cancer cell plasticity and progression. We found examples of metabolic reprogramming through deregulation of mitochondrial function and pyruvate metabolism in the processes of EMT and drug resistance. Redirection and targeting of cell metabolism represents a promising therapeutic strategies as cancer cells are highly dependent on metabolic adaptations to maintain the vast energy requirement in an ever-changing microenvironment.

6. Concluding remarks

The main aim of this thesis was to investigate metabolic rewiring in cancer cell plasticity and drug resistance, and how altered cellular energetics may represent a therapeutic target. Three different approaches were used to address aspects of metabolic rewiring in this context, and the following conclusions were obtained:

In breast cancer, EMT has shown to be associated with attenuated SDH activity and altered mitochondrial dynamics through regulation of mitochondrial fission and fusion. Further, we found that upon SDH inhibition or SDHC knockdown, the cells increased their invasive properties through induction of EMT. Likewise, overexpression of the EMT-linked transcription factor TWIST resulted in changed mitochondrial morphofunction through reduced SDH activity, increased mitochondrial fragmentation and reduced mitochondrial size, resulting in reduced mitochondrial respiration.

PDK4 expression was found to be a marker of metabolic rewiring involving increased FAO *in vitro* and *in vivo*. In cultured cells, pharmacological and genetic strategies to activate the PPARα transcription factor caused increased FAO and reduced glucose oxidation. Thus, increased PDK4 expression signals a shift from glucose to fatty acids as energy fuels, and can therefore be a useful marker for altered substrate utilization for energy metabolism.

In NSCLC patients, increased expression of genes involved in glucose metabolism and ROS defense was found in tumor tissue compared to normal tissue. These effects were correlated with increased PDK1 expression. Moreover, altered glucose, pyruvate and lactate transport was indicated by differential expression of solute carriers upon development of drug resistance. Data from cultured NSCLC cells indicated that the PDK inhibitor DCA may counteract features of EGFR TKI resistance, potentially by mediating an influential shift in energy metabolism towards pyruvate oxidation. The data support further evaluation of targeting PDKs to obtain beneficial effects against EGFR TKI resistant cancer.

To summarize, our data points to specific molecular mechanisms of metabolic rewiring associated with key malignant phenotypes involving cancer cell plasticity. The finding warrants further exploration of targeted strategies to modulate metabolism to counteract malignant features of cancer cell plasticity.

7. Future perspectives

As metabolic rewiring in cancer cell plasticity is a vast and uncharted field, many questions remain unanswered. Therefore, there are numerous studies which would have been interesting to further elucidate in this thesis, some which are highlighted below.

One of the major questions I would have preferred to further address, is whether induction of EMT or acquired drug resistance regulate ROS production. ROS production, in addition to being important in cell signaling, is reported to be deregulated in tumorigenesis and drug resistance [261, 269]. However, measuring ROS is difficult to do as they have a short half-life, are spontaneously produced as cells respire and are regulated by the antioxidant defense system [115, 117].

In Paper I, it would be of interesting to further investigate the role of SDHA-D knockdown on cellular energetics, especially since SDHD was positively associated with EMT. As both SDHC and SDHD are mitochondrial anchor proteins, it would be interesting to further elucidate the differences between the subunits in regard to both cellular plasticity, ROS production through reverse electron flow and mitochondrial OXPHOS.

In Paper II and III, it would be of interest to quantify mitochondrial mass and morphology as performed in Paper I, **figure 6**. This includes investigating mitochondrial networks and volume in PDK4 overexpressing cells, and in NSCLC sensitive and resistant cells before and after DCA treatment. Gaining such insight into mitochondrial structure and network would provide useful information on mitochondrial morphofunction.

Moreover, would be interesting to verify the DCA effect other EGFR mutated cancers, or in different cancer treatments associated with a high rate of drug resistance. In addition, it would be useful to implement the already redesigned DCA (compound 10 or mito-DCA), in order reduce concentration and increase DCA cellular uptake [279, 280]. As immune cells are influenced by the acidity of the tumor microenvironment, it would also be interesting to investigate how DCA, or other relevant drugs modulating

lactate oxidation, influences inflammation, T-cell infiltration and NK cell activity upon cancer treatment.

Metformin, which is thoroughly described in Chapter 5.2, is a highly promising drug when it comes to synergy with already approved therapeutic options [283, 286, 288]. It would therefore be of interest to see whether metformin could aid in combating drug resistance, and how it alters substrate oxidation. Further, as there seem to be a link between type 2 diabetes and cancer, and that certain antioxidant supplements have been shown to increase mortality in lung cancer [122, 284], it would be of interest to further elucidate if diet could be an important adjuvant prior to chemotherapy.

Source of data

1. Berg, J.M., et al., *Biochemistry*. 9th edition ed. 2019: W. H. Freeman and Company.
2. Salway, J.G., *Metabolism at a Glance*. Third ed. 2004, Oxford, U.K: Blackwell Publishing.
3. Vander Heiden, M.G., *Targeting cancer metabolism: a therapeutic window opens.* Nature Reviews Drug Discovery, 2011. **10**(9): p. 671-684.
4. Du, B. and J.S. Shim, *Targeting Epithelial-Mesenchymal Transition (EMT) to Overcome Drug Resistance in Cancer.* Molecules, 2016. **21**(7).
5. Crespi, B. and K. Summers, *Evolutionary biology of cancer.* Trends in Ecology & Evolution, 2005. **20**(10): p. 545-552.
6. Gallaher, J.A., J.S. Brown, and A.R.A. Anderson, *The impact of proliferation-migration tradeoffs on phenotypic evolution in cancer.* Scientific Reports, 2019. **9**(1): p. 2425.
7. Wallace, D.C., *A Mitochondrial Paradigm of Metabolic and Degenerative Diseases, Aging, and Cancer: A Dawn for Evolutionary Medicine.* Annual Review of Genetics, 2005. **39**(1): p. 359-407.
8. Quinlan, C.L., et al., *Mitochondrial complex II can generate reactive oxygen species at high rates in both the forward and reverse reactions.* The Journal of biological chemistry, 2012. **287**(32): p. 27255-27264.
9. Cogliati, S., J.A. Enriquez, and L. Scorrano, *Mitochondrial Cristae: Where Beauty Meets Functionality.* Trends in Biochemical Sciences, 2016. **41**(3): p. 261-273.
10. Ernster, L. and G. Schatz, *Mitochondria: a historical review.* The Journal of Cell Biology, 1981. **91**(3): p. 227s-255s.
11. Friedkin, M. and A.L. Lehninger, *Phosphorylation coupled to electron transport between dihydrodiphosphopyridine nucleotide and oxygen* Journal of Biological Chemistry, 1948. **174**(2): p. 757-758.
12. Sagan, L., *On the origin of mitosing cells.* Journal of Theoretical Biology, 1967. **14**(3): p. 225-IN6.
13. Lane, N., *Serial endosymbiosis or singular event at the origin of eukaryotes?* Journal of Theoretical Biology, 2017. **434**: p. 58-67.
14. Roger, A.J., S.A. Muñoz-Gómez, and R. Kamikawa, *The Origin and Diversification of Mitochondria.* Current Biology, 2017. **27**(21): p. R1177-R1192.
15. Andersson, S.G.E., et al., *The genome sequence of Rickettsia prowazekii and the origin of mitochondria.* Nature, 1998. **396**(6707): p. 133-140.
16. Nass, M.M. and S. Nass, *Intramitochondrial fibers with DNA characteristics. I. Fixation and electron staining reactions.* The Journal of cell biology, 1963. **19**(3): p. 593-611.
17. Zong, W.-X., J.D. Rabinowitz, and E. White, *Mitochondria and Cancer.* Molecular Cell, 2016. **61**(5): p. 667-676.
18. Rusecka, J., et al., *Nuclear genes involved in mitochondrial diseases caused by instability of mitochondrial DNA.* Journal of applied genetics, 2018. **59**(1): p. 43-57.

19. Ju, Y.S., et al., *Frequent somatic transfer of mitochondrial DNA into the nuclear genome of human cancer cells.* Genome research, 2015. **25**(6): p. 814-824.
20. Luo, S., et al., *Biparental Inheritance of Mitochondrial DNA in Humans.* Proceedings of the National Academy of Sciences, 2018. **115**(51): p. 13039-13044.
21. Tronstad, K., et al., *Regulation and Quantification of Cellular Mitochondrial Morphology and Content.* Current Pharmaceutical Design, 2014. **20**(35): p. 5634-5652.
22. Elianne P. Bulthuis, M.J.W.A.-H., Peter H.G.M. Willems, and Werner J.H. Koopma, *Mitochondrial Morphofunction in Mammalian Cells.* Antioxidants & Redox Signaling, 2019. **30**(18): p. 2066-2109.
23. Tan, A.S., et al., *Mitochondrial genome acquisition restores respiratory function and tumorigenic potential of cancer cells without mitochondrial DNA.* Cell Metab, 2015. **21**(1): p. 81-94.
24. Singh, B.K., et al., *Thyroid hormone receptor and ERRα coordinately regulate mitochondrial fission, mitophagy, biogenesis, and function.* Science Signaling, 2018. **11**(536): p. eaam5855.
25. Vásquez-Trincado, C., et al., *Mitochondrial dynamics, mitophagy and cardiovascular disease.* The Journal of Physiology, 2016. **594**(3): p. 509-525.
26. Youle, R.J. and A.M. van der Bliek, *Mitochondrial fission, fusion, and stress.* Science (New York, N.Y.), 2012. **337**(6098): p. 1062-1065.
27. Twig, G., et al., *Fission and selective fusion govern mitochondrial segregation and elimination by autophagy.* The EMBO journal, 2008. **27**(2): p. 433-446.
28. Giacomello, M., et al., *The cell biology of mitochondrial membrane dynamics.* Nature Reviews Molecular Cell Biology, 2020.
29. Palikaras, K., E. Lionaki, and N. Tavernarakis, *Balancing mitochondrial biogenesis and mitophagy to maintain energy metabolism homeostasis.* Cell death and differentiation, 2015. **22**(9): p. 1399-1401.
30. Chourasia, A.H., M.L. Boland, and K.F. Macleod, *Mitophagy and cancer.* Cancer & Metabolism, 2015. **3**(1): p. 4.
31. Kane, L.A., et al., *PINK1 phosphorylates ubiquitin to activate Parkin E3 ubiquitin ligase activity.* The Journal of cell biology, 2014. **205**(2): p. 143-153.
32. Horan, M.P., N. Pichaud, and J.W.O. Ballard, *Review: Quantifying Mitochondrial Dysfunction in Complex Diseases of Aging.* The Journals of Gerontology: Series A, 2012. **67**(10): p. 1022-1035.
33. Thorens, B. and M. Mueckler, *Glucose transporters in the 21st Century.* American journal of physiology. Endocrinology and metabolism, 2010. **298**(2): p. E141-E145.
34. Ancey, P.-B., C. Contat, and E. Meylan, *Glucose transporters in cancer – from tumor cells to the tumor microenvironment.* The FEBS Journal, 2018. **285**(16): p. 2926-2943.
35. Abel, E.D., et al., *Adipose-selective targeting of the GLUT4 gene impairs insulin action in muscle and liver.* Nature, 2001. **409**(6821): p. 729-733.

36. Maratou, E., et al., *Glucose transporter expression on the plasma membrane of resting and activated white blood cells.* European Journal of Clinical Investigation, 2007. **37**(4): p. 282-290.
37. Carvalho, E., et al., *Insulin resistance with low cellular IRS-1 expression is also associated with low GLUT4 expression and impaired insulin-stimulated glucose transport.* The FASEB journal, 2001. **15**(6): p. 1101-3.
38. Chai, Y.J., et al., *Upregulation of SLC2 (GLUT) family genes is related to poor survival outcomes in papillary thyroid carcinoma: Analysis of data from The Cancer Genome Atlas.* Surgery, 2017. **161**(1): p. 188-194.
39. Kim, E., et al., *Upregulation of SLC2A3 gene and prognosis in colorectal carcinoma: analysis of TCGA data.* BMC Cancer, 2019. **19**(1): p. 302.
40. Gray, L.R., S.C. Tompkins, and E.B. Taylor, *Regulation of pyruvate metabolism and human disease.* Cellular and Molecular Life Sciences, 2014. **71**(14): p. 2577-2604.
41. Ciszak, E.M., et al., *How Dihydrolipoamide Dehydrogenase-binding Protein Binds Dihydrolipoamide Dehydrogenase in the Human Pyruvate Dehydrogenase Complex.* Journal of Biological Chemistry, 2006. **281**(1): p. 648-655.
42. Gill, K.S., et al., *Glycolysis inhibition as a cancer treatment and its role in an anti-tumour immune response.* Biochimica et Biophysica Acta (BBA) - Reviews on Cancer, 2016. **1866**(1): p. 87-105.
43. Lu, J., M. Tan, and Q. Cai, *The Warburg effect in tumor progression: Mitochondrial oxidative metabolism as an anti-metastasis mechanism.* Cancer Letters, 2015. **356**(2, Part A): p. 156-164.
44. Takenaka, M., et al., *Rat pyruvate kinase M gene. Its complete structure and characterization of the 5'-flanking region.* J Biol Chem, 1989. **264**(4): p. 2363-7.
45. Kanehisa, M. and S. Goto, *KEGG: kyoto encyclopedia of genes and genomes.* Nucleic acids research, 2000. **28**(1): p. 27-30.
46. David Nelson, M.C., *LEHNINGER PRINCIPLES OF BIOCHEMISTRY*. Fifth edition ed. 2008: W.H. Freeman and Company.
47. Edwards, Y., et al., *Regional localization of the sperm-specific lactate dehydrogenase, LDHC, gene on human chromosome 11.* Annals of Human Genetics, 1989. **53**(3): p. 215-219.
48. Adeva, M., et al., *Enzymes involved in l-lactate metabolism in humans.* Mitochondrion, 2013. **13**(6): p. 615-629.
49. Echigoya, Y., et al., *Molecular characterization and expression pattern of the equine lactate dehydrogenase A and B genes.* Gene, 2009. **447**(1): p. 40-50.
50. Price, N.T., V.N. Jackson, and A.P. Halestrap, *Cloning and sequencing of four new mammalian monocarboxylate transporter (MCT) homologues confirms the existence of a transporter family with an ancient past.* The Biochemical journal, 1998. **329 (Pt 2)**(Pt 2): p. 321-328.
51. Hussien, R. and G.A. Brooks, *Mitochondrial and plasma membrane lactate transporter and lactate dehydrogenase isoform expression in breast cancer cell lines.* Physiological genomics, 2011. **43**(5): p. 255-264.

52. Eilertsen, M., et al., *Monocarboxylate Transporters 1–4 in NSCLC: MCT1 Is an Independent Prognostic Marker for Survival.* PLOS ONE, 2014. **9**(9): p. e105038.
53. Koukourakis, M.I., et al., *Comparison of Metabolic Pathways between Cancer Cells and Stromal Cells in Colorectal Carcinomas: a Metabolic Survival Role for Tumor-Associated Stroma.* Cancer Research, 2006. **66**(2): p. 632-637.
54. Shima, T., et al., *Differential effects of type 2 diabetes on brain glycometabolism in rats: focus on glycogen and monocarboxylate transporter 2.* The Journal of Physiological Sciences, 2018. **68**(1): p. 69-75.
55. Rusu, V., et al., *Type 2 Diabetes Variants Disrupt Function of SLC16A11 through Two Distinct Mechanisms.* Cell, 2017. **170**(1): p. 199-212.e20.
56. Petersen, C., et al., *MCT1 and MCT4 Expression and Lactate Flux Activity Increase During White and Brown Adipogenesis and Impact Adipocyte Metabolism.* Scientific Reports, 2017. **7**(1): p. 13101.
57. Payen, V.L., et al., *Monocarboxylate Transporter MCT1 Promotes Tumor Metastasis Independently of Its Activity as a Lactate Transporter.* Cancer Research, 2017. **77**(20): p. 5591-5601.
58. Herzig, S., et al., *Identification and Functional Expression of the Mitochondrial Pyruvate Carrier.* Science, 2012. **337**(6090): p. 93-96.
59. Bricker, D.K., et al., *A Mitochondrial Pyruvate Carrier Required for Pyruvate Uptake in Yeast, Drosophila, and Humans.* Science, 2012. **337**(6090): p. 96-100.
60. Patel, M.S., et al., *The Pyruvate Dehydrogenase Complexes: Structure-based Function and Regulation.* Journal of Biological Chemistry, 2014. **289**(24): p. 16615-16623.
61. Stacpoole, P.W., *Therapeutic Targeting of the Pyruvate Dehydrogenase Complex/Pyruvate Dehydrogenase Kinase (PDC/PDK) Axis in Cancer.* JNCI: Journal of the National Cancer Institute, 2017. **109**(11).
62. Sugden, M.C. and M.J. Holness, *Interactive regulation of the pyruvate dehydrogenase complex and the carnitine palmitoyltransferase system.* The FASEB Journal, 1994. **8**(1): p. 54-61.
63. Stacpoole, P.W. and Y.J. Greene, *Dichloroacetate.* Diabetes Care, 1992. **15**(6): p. 785-791.
64. Fluge, Ø., et al., *Metabolic profiling indicates impaired pyruvate dehydrogenase function in myalgic encephalopathy/chronic fatigue syndrome.* JCI insight, 2016. **1**(21): p. e89376-e89376.
65. Pettersen, I.K.N., et al., *Upregulated PDK4 expression is a sensitive marker of increased fatty acid oxidation.* Mitochondrion, 2019. **49**: p. 97-110.
66. Holness, M.J. and M.C. Sugden, *Regulation of pyruvate dehydrogenase complex activity by reversible phosphorylation.* Biochemical Society Transactions, 2003. **31**(6): p. 1143-1151.
67. Bowker-Kinley, M.M., et al., *Evidence for existence of tissue-specific regulation of the mammalian pyruvate dehydrogenase complex.* Biochem J, 1998. **329 (Pt 1)**(Pt 1): p. 191-6.

68. Wu, P., et al., *Starvation Increases the Amount of Pyruvate Dehydrogenase Kinase in Several Mammalian Tissues.* Archives of Biochemistry and Biophysics, 2000. **381**(1): p. 1-7.
69. Huang, B., et al., *Starvation and Diabetes Reduce the Amount of Pyruvate Dehydrogenase Phosphatase in Rat Heart and Kidney.* Diabetes, 2003. **52**(6): p. 1371-1376.
70. Chambers, K.T., et al., *Chronic Inhibition of Pyruvate Dehydrogenase in Heart Triggers an Adaptive Metabolic Response.* Journal of Biological Chemistry, 2011. **286**(13): p. 11155-11162.
71. Sugden, M.C., *PDK4: A Factor in Fatness?* Obesity Research, 2003. **11**(2): p. 167-169.
72. Holness, M.J., et al., *Investigation of potential mechanisms regulating protein expression of hepatic pyruvate dehydrogenase kinase isoforms 2 and 4 by fatty acids and thyroid hormone.* The Biochemical journal, 2003. **369**(Pt 3): p. 687-695.
73. Huang, B., et al., *Regulation of Pyruvate Dehydrogenase Kinase Expression by Peroxisome Proliferator–Activated Receptor-α Ligands, Glucocorticoids, and Insulin.* Diabetes, 2002. **51**(2): p. 276-283.
74. Chokkalingam, K., et al., *High-Fat/Low-Carbohydrate Diet Reduces Insulin-Stimulated Carbohydrate Oxidation but Stimulates Nonoxidative Glucose Disposal in Humans: An Important Role for Skeletal Muscle Pyruvate Dehydrogenase Kinase 4.* The Journal of Clinical Endocrinology & Metabolism, 2007. **92**(1): p. 284-292.
75. Sugden, M.C., et al., *Peroxisome-proliferator-activated receptor-alpha (PPARalpha) deficiency leads to dysregulation of hepatic lipid and carbohydrate metabolism by fatty acids and insulin.* The Biochemical journal, 2002. **364**(Pt 2): p. 361-368.
76. Mirza, A.Z., I.I. Althagafi, and H. Shamshad, *Role of PPAR receptor in different diseases and their ligands: Physiological importance and clinical implications.* European Journal of Medicinal Chemistry, 2019. **166**: p. 502-513.
77. Nakamura, M.T., B.E. Yudell, and J.J. Loor, *Regulation of energy metabolism by long-chain fatty acids.* Progress in Lipid Research, 2014. **53**: p. 124-144.
78. Park, S., et al., *Role of the Pyruvate Dehydrogenase Complex in Metabolic Remodeling: Differential Pyruvate Dehydrogenase Complex Functions in Metabolism.* Diabetes & metabolism journal, 2018. **42**(4): p. 270-281.
79. Stacpoole, P.W., et al., *Dichloroacetate-induced peripheral neuropathy.* International review of neurobiology, 2019. **145**: p. 211-238.
80. Brown, J.A. and D.C. Gore, *In VivoMetabolic Response of Glucose to Dichloroacetate in Humans.* Journal of Surgical Research, 1996. **61**(2): p. 391-394.
81. Stockwin, L.H., et al., *Sodium dichloroacetate selectively targets cells with defects in the mitochondrial ETC.* International Journal of Cancer, 2010. **127**(11): p. 2510-2519.

82. Roh, J.-L., et al., *Activation of mitochondrial oxidation by PDK2 inhibition reverses cisplatin resistance in head and neck cancer.* Cancer Letters, 2016. **371**(1): p. 20-29.
83. James, M.O., et al., *Therapeutic applications of dichloroacetate and the role of glutathione transferase zeta-1.* Pharmacology & Therapeutics, 2017. **170**: p. 166-180.
84. Krebs, H.A., *Rate control of the tricarboxylic acid cycle.* Advances in Enzyme Regulation, 1970. **8**: p. 335-353.
85. Raimundo, N., B.E. Baysal, and G.S. Shadel, *Revisiting the TCA cycle: signaling to tumor formation.* Trends in Molecular Medicine, 2011. **17**(11): p. 641-649.
86. Owen, O.E., S.C. Kalhan, and R.W. Hanson, *The Key Role of Anaplerosis and Cataplerosis for Citric Acid Cycle Function.* Journal of Biological Chemistry, 2002. **277**(34): p. 30409-30412.
87. Brunengraber, H. and C.R. Roe, *Anaplerotic molecules: Current and future.* Journal of Inherited Metabolic Disease, 2006. **29**(2-3): p. 327-331.
88. Nelson, D.L., A.L. Lehninger, and M.M. Cox, *Lehninger Principles of Biochemistry*. 2008: W. H. Freeman.
89. Alves-Bezerra, M. and D.E. Cohen, *Triglyceride Metabolism in the Liver.* Comprehensive Physiology, 2017. **8**(1): p. 1-8.
90. Nickerson, J.G., et al., *Greater Transport Efficiencies of the Membrane Fatty Acid Transporters FAT/CD36 and FATP4 Compared with FABPpm and FATP1 and Differential Effects on Fatty Acid Esterification and Oxidation in Rat Skeletal Muscle.* Journal of Biological Chemistry, 2009. **284**(24): p. 16522-16530.
91. Houten, S.M. and R.J.A. Wanders, *A general introduction to the biochemistry of mitochondrial fatty acid β-oxidation.* Journal of inherited metabolic disease, 2010. **33**(5): p. 469-477.
92. Qu, Q., et al., *Fatty acid oxidation and carnitine palmitoyltransferase I: emerging therapeutic targets in cancer.* Cell Death & Disease, 2016. **7**(5): p. e2226-e2226.
93. Murgasova, R., E. Tor Carreras, and J. Bourgailh, *In Vitro Monitoring of the Mitochondrial Beta-Oxidation Flux of Palmitic Acid and Investigation of Its Pharmacological Alteration by Therapeutics.* European Journal of Drug Metabolism and Pharmacokinetics, 2018. **43**(6): p. 675-684.
94. Randle, P.J., et al., *The glucose fatty-acid cycle. Its role in insulin sensitivity and the metabolic disturbances of diabetes mellitus.* Lancet (London, England), 1963. **1**(7285): p. 785-789.
95. Romano, A., et al., *Fats for thoughts: An update on brain fatty acid metabolism.* The International Journal of Biochemistry & Cell Biology, 2017. **84**: p. 40-45.
96. Owen, O.E., et al., *Brain metabolism during fasting.* The Journal of clinical investigation, 1967. **46**(10): p. 1589-1595.
97. Anderson, C.M. and A. Stahl, *SLC27 fatty acid transport proteins.* Molecular Aspects of Medicine, 2013. **34**(2): p. 516-528.

98. Schwenk, R.W., et al., *Fatty acid transport across the cell membrane: Regulation by fatty acid transporters.* Prostaglandins, Leukotrienes and Essential Fatty Acids (PLEFA), 2010. **82**(4): p. 149-154.
99. Fransen, M., C. Lismont, and P. Walton, *The Peroxisome-Mitochondria Connection: How and Why?* International Journal of Molecular Sciences, 2017. **18**(6): p. 1126.
100. Violante, S., et al., *Peroxisomes contribute to the acylcarnitine production when the carnitine shuttle is deficient.* Biochimica et Biophysica Acta (BBA) - Molecular and Cell Biology of Lipids, 2013. **1831**(9): p. 1467-1474.
101. Allen, B.G., et al., *Ketogenic diets as an adjuvant cancer therapy: History and potential mechanism.* Redox Biology, 2014. **2**: p. 963-970.
102. Garber, A.J., et al., *Hepatic Ketogenesis and Gluconeogenesis in Humans.* The Journal of Clinical Investigation, 1974. **54**(4): p. 981-989.
103. Reichard, G.A., Jr., et al., *Ketone-body production and oxidation in fasting obese humans.* The Journal of Clinical Investigation, 1974. **53**(2): p. 508-515.
104. Klein, S. and R.R. Wolfe, *Carbohydrate restriction regulates the adaptive response to fasting.* American Journal of Physiology-Endocrinology and Metabolism, 1992. **262**(5): p. E631-E636.
105. Tretter, L., A. Patocs, and C. Chinopoulos, *Succinate, an intermediate in metabolism, signal transduction, ROS, hypoxia, and tumorigenesis.* Biochimica et Biophysica Acta (BBA) - Bioenergetics, 2016. **1857**(8): p. 1086-1101.
106. Rich, P.R., *The molecular machinery of Keilin's respiratory chain.* Biochemical Society Transactions, 2003. **31**(6): p. 1095-1105.
107. Harris, R.J. and E.J. Boekema, *Membrane Protein Complexes: Structure and Function*. 2018: Springer, Singapore.
108. Settas, N., F.R. Faucz, and C.A. Stratakis, *Succinate dehydrogenase (SDH) deficiency, Carney triad and the epigenome.* Molecular and Cellular Endocrinology, 2018. **469**: p. 107-111.
109. Yankovskaya, V., et al., *Architecture of Succinate Dehydrogenase and Reactive Oxygen Species Generation.* Science, 2003. **299**(5607): p. 700-704.
110. Turrens, J.F., *Mitochondrial formation of reactive oxygen species.* The Journal of physiology, 2003. **552**(Pt 2): p. 335-344.
111. Bouillaud, F., M.-C. Alves-Guerra, and D. Ricquier, *UCPs, at the interface between bioenergetics and metabolism.* Biochimica et Biophysica Acta (BBA) - Molecular Cell Research, 2016. **1863**(10): p. 2443-2456.
112. Lopaschuk, G.D., et al., *Myocardial Fatty Acid Metabolism in Health and Disease.* Physiological Reviews, 2010. **90**(1): p. 207-258.
113. Campanella, M., et al., *Regulation of Mitochondrial Structure and Function by the F1Fo-ATPase Inhibitor Protein, IF1.* Cell Metabolism, 2008. **8**(1): p. 13-25.
114. Faccenda, D., et al., *Control of Mitochondrial Remodeling by the ATPase Inhibitory Factor 1 Unveils a Pro-survival Relay via OPA1.* Cell Reports, 2017. **18**(8): p. 1869-1883.

115. Scialò, F., D.J. Fernández-Ayala, and A. Sanz, *Role of Mitochondrial Reverse Electron Transport in ROS Signaling: Potential Roles in Health and Disease.* Frontiers in physiology, 2017. **8**: p. 428-428.
116. Nissanka, N. and C.T. Moraes, *Mitochondrial DNA damage and reactive oxygen species in neurodegenerative disease.* FEBS letters, 2018. **592**(5): p. 728-742.
117. Yamada, Y., et al., *Therapeutic Strategies for Regulating Mitochondrial Oxidative Stress.* Biomolecules, 2020. **10**(1): p. 83.
118. Hinkle, P.C., et al., *Partial Resolution of the Enzymes Catalyzing Oxidative Phosphorylation: XV. Reverse electron transfer in the flavin-cytochrome b region of the respiratory chain of beef heart submitochondrial particles.* Journal of Biological Chemistry, 1967. **242**(22): p. 5169-5173.
119. Mills, E.L., et al., *Succinate Dehydrogenase Supports Metabolic Repurposing of Mitochondria to Drive Inflammatory Macrophages.* Cell, 2016. **167**(2): p. 457-470.e13.
120. Murphy, M.P., *How mitochondria produce reactive oxygen species.* The Biochemical journal, 2009. **417**(1): p. 1-13.
121. The Alpha-Tocopherol Beta Carotene Cancer Prevention Study Group., *The Effect of Vitamin E and Beta Carotene on the Incidence of Lung Cancer and Other Cancers in Male Smokers.* New England Journal of Medicine, 1994. **330**(15): p. 1029-1035.
122. Virtamo, J., et al., *Incidence of cancer and mortality following alpha-tocopherol and beta-carotene supplementation: a postintervention follow-up.* JAMA, 2003. **290**(4): p. 476-485.
123. Pecorino, L., *Molecular Biology of Cancer: Mechanisms, Targets, and Therapeutics*. Second edition ed. 2008: Oxford University Press.
124. Hanahan, D. and Robert A. Weinberg, *Hallmarks of Cancer: The Next Generation.* Cell, 2011. **144**(5): p. 646-674.
125. Pavlova, Natalya N. and Craig B. Thompson, *The Emerging Hallmarks of Cancer Metabolism.* Cell Metabolism, 2016. **23**(1): p. 27-47.
126. Hausser, J. and U. Alon, *Tumour heterogeneity and the evolutionary trade-offs of cancer.* Nature Reviews Cancer, 2020.
127. Ferlay J, et al. *Global Cancer Observatory: Cancer Today.* . 2018 [cited 2019 29.12.2019]; Available from: Available from: https://gco.iarc.fr/today.
128. Bray, F., et al., *Global cancer statistics 2018: GLOBOCAN estimates of incidence and mortality worldwide for 36 cancers in 185 countries.* CA: A Cancer Journal for Clinicians, 2018. **68**(6): p. 394-424.
129. Ferlay, J., et al., *Estimating the global cancer incidence and mortality in 2018: GLOBOCAN sources and methods.* International Journal of Cancer, 2019. **144**(8): p. 1941-1953.
130. Brustugun, O.T. *Stadier ved lungekreft*. 2014; Available from: http://oncolex.no/Lunge/Bakgrunn/Stadier.
131. Santos, G.d.C., F.A. Shepherd, and M.S. Tsao, *EGFR Mutations and Lung Cancer.* Annual Review of Pathology: Mechanisms of Disease, 2011. **6**(1): p. 49-69.

132. Asao, T., F. Takahashi, and K. Takahashi, *Resistance to molecularly targeted therapy in non-small-cell lung cancer.* Respiratory Investigation, 2019. **57**(1): p. 20-26.
133. Tan, C.-S., D. Gilligan, and S. Pacey, *Treatment approaches for EGFR-inhibitor-resistant patients with non-small-cell lung cancer.* The Lancet Oncology, 2015. **16**(9): p. e447-e459.
134. Mendes, C. and J. Serpa, *Metabolic Remodelling: An Accomplice for New Therapeutic Strategies to Fight Lung Cancer.* Antioxidants (Basel, Switzerland), 2019. **8**(12): p. 603.
135. Kobayashi, S., et al., *EGFR mutation and resistance of non-small-cell lung cancer to gefitinib.* N Engl J Med, 2005. **352**(8): p. 786-92.
136. Byers, L.A., et al., *An Epithelial–Mesenchymal Transition Gene Signature Predicts Resistance to EGFR and PI3K Inhibitors and Identifies Axl as a Therapeutic Target for Overcoming EGFR Inhibitor Resistance.* Clinical Cancer Research, 2013. **19**(1): p. 279.
137. Pao, W., et al., *Acquired resistance of lung adenocarcinomas to gefitinib or erlotinib is associated with a second mutation in the EGFR kinase domain.* PLoS Med, 2005. **2**(3): p. e73.
138. Weng, M.-S., et al., *The interplay of reactive oxygen species and the epidermal growth factor receptor in tumor progression and drug resistance.* Journal of experimental & clinical cancer research : CR, 2018. **37**(1): p. 61-61.
139. Yang, Z., et al., *Inhibition of pyruvate dehydrogenase kinase 1 enhances the anti-cancer effect of EGFR tyrosine kinase inhibitors in non-small cell lung cancer.* Eur J Pharmacol, 2018. **838**: p. 41-52.
140. Walter, A.O., et al., *Discovery of a Mutant-Selective Covalent Inhibitor of EGFR that Overcomes T790M-Mediated Resistance in NSCLC.* Cancer Discovery, 2013. **3**(12): p. 1404-1415.
141. Naume, B. *Stadier ved brystkreft*. Brystkreft 2015 [cited 2020 11.04.2020]; Available from: http://oncolex.no/Bryst/Bakgrunn/Stadier.
142. Perou, C.M., et al., *Molecular portraits of human breast tumours.* Nature, 2000. **406**(6797): p. 747-752.
143. Tang, Y., et al., *Classification, Treatment Strategy, and Associated Drug Resistance in Breast Cancer.* Clinical Breast Cancer, 2016. **16**(5): p. 335-343.
144. Wang, D.-Y., et al., *Molecular stratification within triple-negative breast cancer subtypes.* Scientific Reports, 2019. **9**(1): p. 19107.
145. Sørlie, T., et al., *Gene expression patterns of breast carcinomas distinguish tumor subclasses with clinical implications.* Proceedings of the National Academy of Sciences, 2001. **98**(19): p. 10869-10874.
146. Koboldt, D.C., et al., *Comprehensive molecular portraits of human breast tumours.* Nature, 2012. **490**(7418): p. 61-70.
147. Prat, A. and C.M. Perou, *Deconstructing the molecular portraits of breast cancer.* Mol Oncol, 2011. **5**(1): p. 5-23.
148. Rossing, M., et al., *Whole genome sequencing of breast cancer.* APMIS, 2019. **127**(5): p. 303-315.
149. Podo, F., et al., *Triple-negative breast cancer: present challenges and new perspectives.* Molecular oncology, 2010. **4**(3): p. 209-229.

150. Waks, A.G. and E.P. Winer, *Breast Cancer Treatment: A Review.* Jama, 2019. **321**(3): p. 288-300.
151. Tang, J., et al., *Erlotinib resistance in lung cancer: current progress and future perspectives.* Frontiers in pharmacology, 2013. **4**: p. 15-15.
152. Lotsberg, M.L., et al., *AXL targeting abrogates autophagic flux and induces immunogenic cell death in drug resistant cancer cells.* Journal of Thoracic Oncology, 2020.
153. Lee, D.H., *Treatments for EGFR-mutant non-small cell lung cancer (NSCLC): The road to a success, paved with failures.* Pharmacology & Therapeutics, 2017. **174**: p. 1-21.
154. Varga, J. and F.R. Greten, *Cell plasticity in epithelial homeostasis and tumorigenesis.* Nature Cell Biology, 2017. **19**(10): p. 1133-1141.
155. Meacham, C.E. and S.J. Morrison, *Tumour heterogeneity and cancer cell plasticity.* Nature, 2013. **501**(7467): p. 328-337.
156. Yuan, S., R.J. Norgard, and B.Z. Stanger, *Cellular Plasticity in Cancer.* Cancer Discovery, 2019. **9**(7): p. 837-851.
157. da Silva-Diz, V., et al., *Cancer cell plasticity: Impact on tumor progression and therapy response.* Seminars in Cancer Biology, 2018. **53**: p. 48-58.
158. Nieto, M.A., et al., *EMT: 2016*, in *Cell*. 2016, Elsevier. p. 21-45.
159. Thiery, J.P., et al., *Epithelial-Mesenchymal Transitions in Development and Disease.* Cell, 2009. **139**(5): p. 871-890.
160. Chen, Z.F. and R.R. Behringer, *twist is required in head mesenchyme for cranial neural tube morphogenesis.* Genes & Development, 1995. **9**(6): p. 686-699.
161. Zhang, Y. and R.A. Weinberg, *Epithelial-to-mesenchymal transition in cancer: complexity and opportunities.* Frontiers of medicine, 2018. **12**(4): p. 361-373.
162. Servier, L.L. *smart SERVIER MEDICAL ART*. [cited 2020 19.04.2020]; Available from: https://smart.servier.com/.
163. Dongre, A. and R.A. Weinberg, *New insights into the mechanisms of epithelial–mesenchymal transition and implications for cancer.* Nature Reviews Molecular Cell Biology, 2019. **20**(2): p. 69-84.
164. Tan, T.Z., et al., *Epithelial-mesenchymal transition spectrum quantification and its efficacy in deciphering survival and drug responses of cancer patients.* EMBO Molecular Medicine, 2014. **6**(10): p. 1279-1293.
165. Semenza, G.L., *Hypoxia-inducible factors: mediators of cancer progression and targets for cancer therapy.* Trends in Pharmacological Sciences, 2012. **33**(4): p. 207-214.
166. Sciacovelli, M. and C. Frezza, *Metabolic reprogramming and epithelial-to-mesenchymal transition in cancer.* The FEBS Journal, 2017. **284**(19): p. 3132-3144.
167. Chaffer, C.L., et al., *EMT, cell plasticity and metastasis.* Cancer and Metastasis Reviews, 2016. **35**(4): p. 645-654.
168. Sciacovelli, M., et al., *Fumarate is an epigenetic modifier that elicits epithelial-to-mesenchymal transition.* Nature, 2016. **537**(7621): p. 544-547.

169. Grassian, A.R., et al., *Isocitrate Dehydrogenase (IDH) Mutations Promote a Reversible ZEB1/MicroRNA (miR)-200-dependent Epithelial-Mesenchymal Transition (EMT).* Journal of Biological Chemistry, 2012. **287**(50): p. 42180-42194.
170. Shibue, T. and R.A. Weinberg, *EMT, CSCs, and drug resistance: the mechanistic link and clinical implications.* Nature reviews. Clinical oncology, 2017. **14**(10): p. 611-629.
171. Rotow, J. and T.G. Bivona, *Understanding and targeting resistance mechanisms in NSCLC.* Nature Reviews Cancer, 2017. **17**(11): p. 637-658.
172. Saxena, M., et al., *Transcription factors that mediate epithelial–mesenchymal transition lead to multidrug resistance by upregulating ABC transporters.* Cell Death & Disease, 2011. **2**(7): p. e179-e179.
173. Hanahan, D. and R.A. Weinberg, *The hallmarks of cancer.* Cell, 2000. **100**(1): p. 57-70.
174. Faubert, B., et al., *Lactate Metabolism in Human Lung Tumors.* Cell, 2017. **171**(2): p. 358-371.e9.
175. De Rosa, V., et al., *Reversal of Warburg Effect and Reactivation of Oxidative Phosphorylation by Differential Inhibition of EGFR Signaling Pathways in Non–Small Cell Lung Cancer.* Clinical Cancer Research, 2015. **21**(22): p. 5110-5120.
176. DeBerardinis, R.J. and N.S. Chandel, *We need to talk about the Warburg effect.* Nature Metabolism, 2020. **2**(2): p. 127-129.
177. Warburg , O., F. Wind , and E. Negelein *THE METABOLISM OF TUMORS IN THE BODY.* Journal of General Physiology, 1927. **8**(6): p. 519-530.
178. Warburg, O., *On the Origin of Cancer Cells.* Science, 1956. **123**(3191): p. 309-314.
179. Sasaki, H., et al., *Overexpression of GLUT1 correlates with Kras mutations in lung carcinomas.* Mol Med Rep, 2012. **5**(3): p. 599-602.
180. Kim, J.-w. and C.V. Dang, *Multifaceted roles of glycolytic enzymes.* Trends in Biochemical Sciences, 2005. **30**(3): p. 142-150.
181. Bonnet, S., et al., *A Mitochondria-K+ Channel Axis Is Suppressed in Cancer and Its Normalization Promotes Apoptosis and Inhibits Cancer Growth.* Cancer Cell, 2007. **11**(1): p. 37-51.
182. Dayton, T.L., T. Jacks, and M.G. Vander Heiden, *PKM2, cancer metabolism, and the road ahead.* EMBO reports, 2016. **17**(12): p. 1721-1730.
183. Luo, W., et al., *Pyruvate kinase M2 is a PHD3-stimulated coactivator for hypoxia-inducible factor 1.* Cell, 2011. **145**(5): p. 732-744.
184. Liang, J., et al., *Mitochondrial PKM2 regulates oxidative stress-induced apoptosis by stabilizing Bcl2.* Cell research, 2017. **27**(3): p. 329-351.
185. Luengo, A., D.Y. Gui, and M.G. Vander Heiden, *Targeting Metabolism for Cancer Therapy.* Cell Chemical Biology, 2017. **24**(9): p. 1161-1180.
186. Cho, E.S., et al., *The Pentose Phosphate Pathway as a Potential Target for Cancer Therapy.* Biomolecules & Therapeutics, 2018. **26**(1): p. 29-38.
187. Chen, Y., et al. *Multiple myeloma acquires resistance to EGFR inhibitor via induction of pentose phosphate pathway*. Scientific reports, 2015. **5**, 9925 DOI: 10.1038/srep09925.

188. Zhao, J., Huang, X., Xu, Z., Dai, J., He, H., Zhu, Y., Wang, H., *LDHA promotes tumor metastasis by facilitating epithelial-mesenchymal transition in renal cell carcinoma.* Molecular Medicine Reports, 2017. **16**(6): p. 8335-8344.
189. Goetze, K., Walenta, S., Ksiazkiewicz, M., Kunz-Schughart, L.A., & Mueller-Klieser, W., *Lactate enhances motility of tumor cells and inhibits monocyte migration and cytokine release.* International Journal of Oncology, 2011. **39**(2): p. 453-463.
190. Finicle, B.T., V. Jayashankar, and A.L. Edinger, *Nutrient scavenging in cancer.* Nat Rev Cancer, 2018. **18**(10): p. 619-633.
191. Kamphorst, J.J., et al., *Human pancreatic cancer tumors are nutrient poor and tumor cells actively scavenge extracellular protein.* Cancer Res, 2015. **75**(3): p. 544-53.
192. Altman, B.J., Z.E. Stine, and C.V. Dang, *From Krebs to clinic: glutamine metabolism to cancer therapy.* Nat Rev Cancer, 2016. **16**(10): p. 619-34.
193. Yoshida, S., et al., *Macropinocytosis, mTORC1 and cellular growth control.* Cellular and Molecular Life Sciences, 2018. **75**(7): p. 1227-1239.
194. Palm, W., et al., *The Utilization of Extracellular Proteins as Nutrients Is Suppressed by mTORC1.* Cell, 2015. **162**(2): p. 259-270.
195. Kim, S.M., et al., *PTEN Deficiency and AMPK Activation Promote Nutrient Scavenging and Anabolism in Prostate Cancer Cells.* Cancer Discovery, 2018. **8**(7): p. 866-883.
196. Hardie, D.G., *AMP-activated protein kinase—an energy sensor that regulates all aspects of cell function.* Genes & Development, 2011. **25**(18): p. 1895-1908.
197. Hodneland Nilsson, L.I., et al., *A new live-cell reporter strategy to simultaneously monitor mitochondrial biogenesis and morphology.* Scientific Reports, 2015. **5**(1): p. 17217.
198. Colin, M., et al., *Dysregulation of Macropinocytosis Processes in Glioblastomas May Be Exploited to Increase Intracellular Anti-Cancer Drug Levels: The Example of Temozolomide.* Cancers, 2019. **11**(3): p. 411.
199. Qian, Y., et al., *Extracellular ATP is internalized by macropinocytosis and induces intracellular ATP increase and drug resistance in cancer cells.* Cancer Letters, 2014. **351**(2): p. 242-251.
200. Kaur, J. and J. Debnath, *Autophagy at the crossroads of catabolism and anabolism.* Nat Rev Mol Cell Biol, 2015. **16**(8): p. 461-72.
201. Zhang, C., et al., *Parkin, a p53 target gene, mediates the role of p53 in glucose metabolism and the Warburg effect.* Proceedings of the National Academy of Sciences of the United States of America, 2011. **108**(39): p. 16259-16264.
202. Tang, C., et al., *Activation of BNIP3-mediated mitophagy protects against renal ischemia–reperfusion injury.* Cell Death & Disease, 2019. **10**(9): p. 677.
203. Brugarolas, J., et al., *Regulation of mTOR function in response to hypoxia by REDD1 and the TSC1/TSC2 tumor suppressor complex.* Genes & development, 2004. **18**(23): p. 2893-2904.
204. Arsham, A.M., J.J. Howell, and M.C. Simon, *A Novel Hypoxia-inducible Factor-independent Hypoxic Response Regulating Mammalian Target of*

Rapamycin and Its Targets. Journal of Biological Chemistry, 2003. **278**(32): p. 29655-29660.
205. Nicklin, P., et al., *Bidirectional Transport of Amino Acids Regulates mTOR and Autophagy.* Cell, 2009. **136**(3): p. 521-534.
206. Lin, G., et al., *The dual PI3K/mTOR inhibitor NVP-BEZ235 prevents epithelial–mesenchymal transition induced by hypoxia and TGF-β1.* European Journal of Pharmacology, 2014. **729**: p. 45-53.
207. Carmeliet, P. and R.K. Jain, *Angiogenesis in cancer and other diseases.* Nature, 2000. **407**(6801): p. 249-257.
208. Luo, W. and Y. Wang, *Hypoxia Mediates Tumor Malignancy and Therapy Resistance*, in *Hypoxia and Cancer Metastasis*, D.M. Gilkes, Editor. 2019, Springer International Publishing: Cham. p. 1-18.
209. Li, Z., et al., *Hypoxia-inducible factors regulate tumorigenic capacity of glioma stem cells.* Cancer Cell, 2009. **15**(6): p. 501-13.
210. Sciacovelli, M. and C. Frezza, *Oncometabolites: Unconventional triggers of oncogenic signalling cascades.* Free Radical Biology and Medicine, 2016. **100**: p. 175-181.
211. Semenza, G.L., *Hypoxia-inducible factor 1: master regulator of O2 homeostasis.* Current Opinion in Genetics & Development, 1998. **8**(5): p. 588-594.
212. Kim, J.-w., et al., *HIF-1-mediated expression of pyruvate dehydrogenase kinase: A metabolic switch required for cellular adaptation to hypoxia.* Cell Metabolism, 2006. **3**(3): p. 177-185.
213. Loriot, C., et al., *Epithelial to Mesenchymal Transition Is Activated in Metastatic Pheochromocytomas and Paragangliomas Caused by SDHB Gene Mutations.* The Journal of Clinical Endocrinology & Metabolism, 2012. **97**(6): p. E954-E962.
214. Brandon, M., P. Baldi, and D.C. Wallace, *Mitochondrial mutations in cancer.* Oncogene, 2006. **25**(34): p. 4647-4662.
215. Burnichon, N., et al., *SDHA is a tumor suppressor gene causing paraganglioma.* Human molecular genetics, 2010. **19**(15): p. 3011-3020.
216. Saxena, N., et al., *SDHB-Deficient Cancers: The Role of Mutations That Impair Iron Sulfur Cluster Delivery.* J Natl Cancer Inst, 2016. **108**(1).
217. Ricketts, C.J., et al., *Tumor risks and genotype-phenotype-proteotype analysis in 358 patients with germline mutations in SDHB and SDHD.* Hum Mutat, 2010. **31**(1): p. 41-51.
218. Dang, L., et al., *Cancer-associated IDH1 mutations produce 2-hydroxyglutarate.* Nature, 2009. **462**(7274): p. 739-744.
219. Yogev, O., et al., *Fumarase: A Mitochondrial Metabolic Enzyme and a Cytosolic/Nuclear Component of the DNA Damage Response.* PLOS Biology, 2010. **8**(3): p. e1000328.
220. Zecchini, V., et al., *Nuclear ARRB1 induces pseudohypoxia and cellular metabolism reprogramming in prostate cancer.* The EMBO Journal, 2014. **33**(12): p. 1365-1382.
221. Selak, M.A., et al., *Succinate links TCA cycle dysfunction to oncogenesis by inhibiting HIF-α prolyl hydroxylase.* Cancer Cell, 2005. **7**(1): p. 77-85.

222. Shanmugasundaram, K., et al., *The Oncometabolite Fumarate Promotes Pseudohypoxia Through Noncanonical Activation of NF-κB Signaling.* Journal of Biological Chemistry, 2014. **289**(35): p. 24691-24699.
223. Burdall, S.E., et al., *Breast cancer cell lines: friend or foe?* Breast cancer research : BCR, 2003. **5**(2): p. 89-95.
224. Brekke, T.D., K.A. Steele, and J.F. Mulley, *Inbred or Outbred? Genetic Diversity in Laboratory Rodent Colonies.* G3: Genes|Genomes|Genetics, 2018. **8**(2): p. 679-686.
225. Geraghty, R.J., et al., *Guidelines for the use of cell lines in biomedical research.* British journal of cancer, 2014. **111**(6): p. 1021-1046.
226. Hynds, R.E., E. Vladimirou, and S.M. Janes, *The secret lives of cancer cell lines.* Disease Models & Mechanisms, 2018. **11**(11): p. dmm037366.
227. Lucey, B.P., W.A. Nelson-Rees, and G.M. Hutchins, *Henrietta Lacks, HeLa Cells, and Cell Culture Contamination.* Archives of Pathology & Laboratory Medicine, 2009. **133**(9): p. 1463-1467.
228. Miller, C.J., et al., *Mycoplasma infection significantly alters microarray gene expression profiles.* BioTechniques, 2003. **35**(4): p. 812-814.
229. Yu, T., et al., *Metabolomics reveals mycoplasma contamination interferes with the metabolism of PANC-1 cells.* Analytical and Bioanalytical Chemistry, 2016. **408**(16): p. 4267-4273.
230. Elliott, R.L. and X.-P. Jiang, *The adverse effect of gentamicin on cell metabolism in three cultured mammary cell lines: "Are cell culture data skewed?".* PLOS ONE, 2019. **14**(4): p. e0214586.
231. Wang, Y., G. Schmid-Bindert, and C. Zhou, *Erlotinib in the treatment of advanced non-small cell lung cancer: an update for clinicians.* Therapeutic advances in medical oncology, 2012. **4**(1): p. 19-29.
232. Stemmler, M.P., et al., *Non-redundant functions of EMT transcription factors.* Nature Cell Biology, 2019. **21**(1): p. 102-112.
233. Zeisberg, M. and E.G. Neilson, *Biomarkers for epithelial-mesenchymal transitions.* The Journal of Clinical Investigation, 2009. **119**(6): p. 1429-1437.
234. Bae, Y.K., et al., *Epithelial-Mesenchymal Transition Phenotype Is Associated with Clinicopathological Factors That Indicate Aggressive Biological Behavior and Poor Clinical Outcomes in Invasive Breast Cancer.* Journal of breast cancer, 2015. **18**(3): p. 256-263.
235. Pereira-Fantini, P.M., et al., *Selection of Reference Genes for Gene Expression Studies related to lung injury in a preterm lamb model.* Scientific reports, 2016. **6**: p. 26476-26476.
236. Glare, E.M., et al., *β-Actin and GAPDH housekeeping gene expression in asthmatic airways is variable and not suitable for normalising mRNA levels.* Thorax, 2002. **57**(9): p. 765-770.
237. Gilda, J.E. and A.V. Gomes, *Stain-Free total protein staining is a superior loading control to β-actin for Western blots.* Analytical Biochemistry, 2013. **440**(2): p. 186-188.
238. Røsland, G.V., et al., *Epithelial to mesenchymal transition (EMT) is associated with attenuation of succinate dehydrogenase (SDH) in breast*

cancer through reduced expression of SDHC. Cancer & Metabolism, 2019. **7**(1): p. 6.
239. Agilent Technologies, I. *Agilent Seahorse XF Live-Cell Metabolism Solutions for Cancer Research*. 2019 14.04.2020]; Available from: https://www.agilent.com/cs/library/brochures/brochure-live-cell-metabolism-solutions-for-cancer-research-cell-analysis-5994-0741en-agilent.pdf.
240. VanLinden, M.R., et al., *Subcellular Distribution of NAD+ between Cytosol and Mitochondria Determines the Metabolic Profile of Human Cells.* Journal of Biological Chemistry, 2015. **290**(46): p. 27644-27659.
241. Agilent Technologies, I. *Agilent Seahorse XF Cell Mito Stress Test Kit*. [cited 2020 27.04.2020]; Available from: https://www.agilent.com/cs/library/usermanuals/public/XF_Cell_Mito_Stress_Test_Kit_User_Guide.pdf.
242. Brennan, J.P., et al., *FCCP is cardioprotective at concentrations that cause mitochondrial oxidation without detectable depolarisation.* Cardiovascular Research, 2006. **72**(2): p. 322-330.
243. Hou, X.-b., et al., *Combination of 2-deoxy d-glucose and metformin for synergistic inhibition of non-small cell lung cancer: A reactive oxygen species and P-p38 mediated mechanism.* Biomedicine & Pharmacotherapy, 2016. **84**: p. 1575-1584.
244. Mookerjee, S.A., D.G. Nicholls, and M.D. Brand, *Determining Maximum Glycolytic Capacity Using Extracellular Flux Measurements.* PLOS ONE, 2016. **11**(3): p. e0152016.
245. Salabei, J.K., A.A. Gibb, and B.G. Hill, *Comprehensive measurement of respiratory activity in permeabilized cells using extracellular flux analysis.* Nature protocols, 2014. **9**(2): p. 421-438.
246. Wensaas, A.J., et al., *Cell-based multiwell assays for the detection of substrate accumulation and oxidation.* Journal of Lipid Research, 2007. **48**(4): p. 961-967.
247. Zhang, D., et al., *2-Deoxy-D-glucose targeting of glucose metabolism in cancer cells as a potential therapy.* Cancer Letters, 2014. **355**(2): p. 176-183.
248. Gnaiger, E. *MitoPedia: Substrates and metabolites*. 2019 [cited 2019; Available from: https://www.bioblast.at/index.php/MitoPedia:_Substrates_and_metabolites.
249. Gnaiger, E. *MitoPedia: Inhibitors*. 2019 [cited 2019; Available from: https://www.bioblast.at/index.php/MitoPedia:_Inhibitors.
250. Gnaiger, E. *MitoPedia: Uncouplers*. 2019 [cited 2019; Available from: https://www.bioblast.at/index.php/MitoPedia:_Uncouplers.
251. Ma, W., et al., *Dichloroacetic acid (DCA) synergizes with the SIRT2 inhibitor Sirtinol and AGK2 to enhance anti-tumor efficacy in non-small cell lung cancer.* Cancer Biology & Therapy, 2018. **19**(9): p. 835-846.
252. Agilent Technologies, I. *Seahorse XF Plasma Membrane Permeabilizer*. 14.04.2020]; Available from: https://www.agilent.com/en/products/cell-analysis/seahorse-xfe-consumables/kits-reagents-media/seahorse-xf-plasma-membrane-permeabilizer#howitworks.

253. Darwin, C., *On the Origin of Species by Means of Natural Selection or the Preservation of Favoured Races in the Struggle for Life*. 1859, John Murray.
254. Hairston Jr, N.G., et al., *Rapid evolution and the convergence of ecological and evolutionary time.* Ecology Letters, 2005. **8**(10): p. 1114-1127.
255. McGranahan, N. and C. Swanton, *Biological and Therapeutic Impact of Intratumor Heterogeneity in Cancer Evolution.* Cancer Cell, 2015. **27**(1): p. 15-26.
256. Zhang, W.C., et al., *miR-147b-mediated TCA cycle dysfunction and pseudohypoxia initiate drug tolerance to EGFR inhibitors in lung adenocarcinoma.* Nature metabolism, 2019. **1**(4): p. 460-474.
257. Hallett, R.M., et al., *A Gene Signature for Predicting Outcome in Patients with Basal-like Breast Cancer.* Scientific Reports, 2012. **2**(1): p. 227.
258. Milioli, H.H., et al., *Basal-like breast cancer: molecular profiles, clinical features and survival outcomes.* BMC Medical Genomics, 2017. **10**(1): p. 19.
259. Li, Q.-Q., et al., *Twist1-Mediated Adriamycin-Induced Epithelial-Mesenchymal Transition Relates to Multidrug Resistance and Invasive Potential in Breast Cancer Cells.* Clinical Cancer Research, 2009. **15**(8): p. 2657.
260. An, B.C., et al., *GPx3-mediated redox signaling arrests the cell cycle and acts as a tumor suppressor in lung cancer cell lines.* PLOS ONE, 2018. **13**(9): p. e0204170.
261. Okon, I.S., et al., *Gefitinib-mediated Reactive Oxygen Specie (ROS) Instigates Mitochondrial Dysfunction and Drug Resistance in Lung Cancer Cells.* Journal of Biological Chemistry, 2015. **290**(14): p. 9101-9110.
262. Zhao, H., et al., *Up-regulation of glycolysis promotes the stemness and EMT phenotypes in gemcitabine-resistant pancreatic cancer cells.* Journal of cellular and molecular medicine, 2017. **21**(9): p. 2055-2067.
263. Naviaux, R.K., et al., *Metabolic features of chronic fatigue syndrome.* Proceedings of the National Academy of Sciences of the United States of America, 2016. **113**(37): p. E5472-E5480.
264. Ma, Y., et al., *Fatty acid oxidation: An emerging facet of metabolic transformation in cancer.* Cancer letters, 2018. **435**: p. 92-100.
265. Tsintzas, K., et al., *Elevated Free Fatty Acids Attenuate the Insulin-Induced Suppression of PDK4 Gene Expression in Human Skeletal Muscle: Potential Role of Intramuscular Long-Chain Acyl-Coenzyme A.* The Journal of Clinical Endocrinology & Metabolism, 2007. **92**(10): p. 3967-3972.
266. Øie, E., et al., *Tetradecylthioacetic Acid Increases Fat Metabolism and Improves Cardiac Function in Experimental Heart Failure.* Lipids, 2013. **48**(2): p. 139-154.
267. Cui, L., et al., *Overexpression of PDK2 and PDK3 reflects poor prognosis in acute myeloid leukemia.* Cancer Gene Therapy, 2018.
268. Hu, T., et al., *PDK2 induces cisplatin-resistance in lung adenocarcinoma via transcriptional regulation of CNNM3.* Journal of Drug Targeting, 2019. **27**(4): p. 460-465.

269. Avolio, R., et al., *Modulation of Mitochondrial Metabolic Reprogramming and Oxidative Stress to Overcome Chemoresistance in Cancer.* Biomolecules, 2020. **10**(1): p. 135.
270. Bu, L., et al., *Inhibition of TrxR2 suppressed NSCLC cell proliferation, metabolism and induced cell apoptosis through decreasing antioxidant activity.* Life Sciences, 2017. **178**: p. 35-41.
271. Tataranni, T. and C. Piccoli, *Dichloroacetate (DCA) and Cancer: An Overview towards Clinical Applications.* Oxidative medicine and cellular longevity, 2019. **2019**: p. 8201079-8201079.
272. Fischer, K., et al., *Inhibitory effect of tumor cell–derived lactic acid on human T cells.* Blood, 2007. **109**(9): p. 3812-3819.
273. Brand, A., et al., *LDHA-Associated Lactic Acid Production Blunts Tumor Immunosurveillance by T and NK Cells.* Cell Metabolism, 2016. **24**(5): p. 657-671.
274. Daneshmandi, S., B. Wegiel, and P. Seth, *Blockade of Lactate Dehydrogenase-A (LDH-A) Improves Efficacy of Anti-Programmed Cell Death-1 (PD-1) Therapy in Melanoma.* Cancers, 2019. **11**(4): p. 450.
275. Zhang, Z., et al., *Pretreatment lactate dehydrogenase may predict outcome of advanced non small-cell lung cancer patients treated with immune checkpoint inhibitors: A meta-analysis.* Cancer Medicine, 2019. **8**(4): p. 1467-1473.
276. Xie, H., et al., *Targeting lactate dehydrogenase--a inhibits tumorigenesis and tumor progression in mouse models of lung cancer and impacts tumor-initiating cells.* Cell Metab, 2014. **19**(5): p. 795-809.
277. Dunbar, E.M., et al., *Phase 1 trial of dichloroacetate (DCA) in adults with recurrent malignant brain tumors.* Investigational New Drugs, 2014. **32**(3): p. 452-464.
278. Chu, Q.S.-C., et al., *A phase I open-labeled, single-arm, dose-escalation, study of dichloroacetate (DCA) in patients with advanced solid tumors.* Investigational New Drugs, 2015. **33**(3): p. 603-610.
279. Trapella, C., et al., *Design, Synthesis, and Biological Characterization of Novel Mitochondria Targeted Dichloroacetate-Loaded Compounds with Antileukemic Activity.* J Med Chem, 2016. **59**(1): p. 147-56.
280. Pathak, R.K., et al., *Mito-DCA: a mitochondria targeted molecular scaffold for efficacious delivery of metabolic modulator dichloroacetate.* ACS chemical biology, 2014. **9**(5): p. 1178-1187.
281. Izzo, A., et al., *Metformin restores the mitochondrial network and reverses mitochondrial dysfunction in Down syndrome cells.* Human Molecular Genetics, 2017. **26**(6): p. 1056-1069.
282. Mallik, R. and T.A. Chowdhury, *Metformin in cancer.* Diabetes Research and Clinical Practice, 2018. **143**: p. 409-419.
283. Hirsch, H.A., et al., *Metformin selectively targets cancer stem cells, and acts together with chemotherapy to block tumor growth and prolong remission.* Cancer research, 2009. **69**(19): p. 7507-7511.
284. Bowker, S.L., et al., *Increased Cancer-Related Mortality for Patients With Type 2 Diabetes Who Use Sulfonylureas or Insulin.* Diabetes Care, 2006. **29**(2): p. 254-258.

285. Evans, J.M.M., et al., *Metformin and reduced risk of cancer in diabetic patients.* BMJ, 2005. **330**(7503): p. 1304-1305.
286. Chuang, M.-C., et al., *Survival benefit associated with metformin use in inoperable non-small cell lung cancer patients with diabetes: A population-based retrospective cohort study.* PLOS ONE, 2018. **13**(1): p. e0191129.
287. Lin, J., et al., *Metformin use and survival after non-small cell lung cancer: A cohort study in the US Military health system.* International Journal of Cancer, 2017. **141**(2): p. 254-263.
288. Wen-Xiu, X., et al., *Impact of metformin use on survival outcomes in non-small cell lung cancer treated with platinum.* Medicine, 2018. **97**(51): p. e13652.
289. Haugrud, A.B., et al., *Dichloroacetate enhances apoptotic cell death via oxidative damage and attenuates lactate production in metformin-treated breast cancer cells.* Breast Cancer Research and Treatment, 2014. **147**(3): p. 539-550.
290. Han, S., et al., *Up-regulation of p21 Gene Expression by Peroxisome Proliferator-Activated Receptor γ in Human Lung Carcinoma Cells.* Clinical Cancer Research, 2004. **10**(6): p. 1911-1919.
291. Peters, J.M., R.C. Cattley, and F.J. Gonzalez, *Role of PPAR alpha in the mechanism of action of the nongenotoxic carcinogen and peroxisome proliferator Wy-14,643.* Carcinogenesis, 1997. **18**(11): p. 2029-2033.
292. Yuan, H., et al., *PPARδ Induces Estrogen Receptor-Positive Mammary Neoplasia through an Inflammatory and Metabolic Phenotype Linked to mTOR Activation.* Cancer Research, 2013. **73**(14): p. 4349-4361.
293. Zhang, Q., et al., *A Novel mTORC1/2 Inhibitor (MTI-31) Inhibits Tumor Growth, Epithelial–Mesenchymal Transition, Metastases, and Improves Antitumor Immunity in Preclinical Models of Lung Cancer.* Clinical Cancer Research, 2019. **25**(12): p. 3630-3642.
294. Xie, J., X. Wang, and C.G. Proud, *mTOR inhibitors in cancer therapy.* F1000Research, 2016. **5**: p. F1000 Faculty Rev-2078.
295. Payen, V.L., et al., *Monocarboxylate transporters in cancer.* Molecular metabolism, 2020. **33**: p. 48-66.
296. Nyquist, M.D., B. Prasad, and E.A. Mostaghel, *Harnessing Solute Carrier Transporters for Precision Oncology.* Molecules (Basel, Switzerland), 2017. **22**(4): p. 539.
297. Cancer Research, U.K. *A Phase I Trial of AZD3965 in Patients With Advanced Cancer*. [cited 2020 30.05.2020]; Available from: https://clinicaltrials.gov/ct2/show/NCT01791595.
298. Takaoka, Y., et al., *Mitochondrial pyruvate carrier 1 expression controls cancer epithelial-mesenchymal transition and radioresistance.* Cancer Science, 2019. **110**(4): p. 1331-1339.
299. Schell, John C., et al., *A Role for the Mitochondrial Pyruvate Carrier as a Repressor of the Warburg Effect and Colon Cancer Cell Growth.* Molecular Cell, 2014. **56**(3): p. 400-413.
300. Witney, T.H., et al., *A comparison between radiolabeled fluorodeoxyglucose uptake and hyperpolarized (13)C-labeled pyruvate utilization as methods for*

detecting tumor response to treatment. Neoplasia (New York, N.Y.), 2009. **11**(6): p. 574-582.
301. Kurhanewicz, J., et al., *Hyperpolarized (13)C MRI: Path to Clinical Translation in Oncology.* Neoplasia (New York, N.Y.), 2019. **21**(1): p. 1-16.
302. Momcilovic, M., et al., *Targeted Inhibition of EGFR and Glutaminase Induces Metabolic Crisis in EGFR Mutant Lung Cancer.* Cell Reports, 2017. **18**(3): p. 601-610.

I

Røsland et al. Cancer & Metabolism (2019) 7:6
https://doi.org/10.1186/s40170-019-0197-8

Cancer & Metabolism

RESEARCH Open Access

Epithelial to mesenchymal transition (EMT) is associated with attenuation of succinate dehydrogenase (SDH) in breast cancer through reduced expression of *SDHC*

Gro V. Røsland[1,2†], Sissel E. Dyrstad[1†], Deusdedit Tusubira[1], Reham Helwa[2,3], Tuan Zea Tan[4], Maria L. Lotsberg[1,5], Ina K. N. Pettersen[1], Anna Berg[2,6], Charlotte Kindt[7], Fredrik Hoel[1], Kirstine Jacobsen[7], Ari J. Arason[8], Agnete S. T. Engelsen[1,9], Henrik J. Ditzel[7,10], Per E. Lønning[2,11], Camilla Krakstad[2,6], Jean P. Thiery[1,9,12,13,14], James B. Lorens[1,9], Stian Knappskog[2,11] and Karl J. Tronstad[1*]

Abstract

Background: Epithelial to mesenchymal transition (EMT) is a well-characterized process of cell plasticity that may involve metabolic rewiring. In cancer, EMT is associated with malignant progression, tumor heterogeneity, and therapy resistance. In this study, we investigated the role of succinate dehydrogenase (SDH) as a potential key regulator of EMT.

Methods: Associations between SDH subunits and EMT were explored in gene expression data from breast cancer patient cohorts, followed by in-depth studies of SDH suppression as a potential mediator of EMT in cultured cells.

Results: We found an overall inverse association between EMT and the SDH subunit C (SDHC) when analyzing gene expression in breast tumors. This was particularly evident in carcinomas of basal-like molecular subtype compared to non-basal-like tumors, and a low *SDHC* expression level tended to have a prognostic impact in those patients. Studies in cultured cells revealed that EMT was induced by SDH inhibition through SDHC CRISPR/Cas9 knockdown or by the enzymatic inhibitor malonate. Conversely, overexpression of EMT-promoting transcription factors TWIST and SNAI2 caused decreased levels of SDHB and C and reduced rates of SDH-linked mitochondrial respiration. Cells overexpressing TWIST had reduced mitochondrial mass, and the organelles were thinner and more fragmented compared to controls.

Conclusions: Our findings suggest that downregulation of SDHC promotes EMT and that this is accompanied by structural remodeling of the mitochondrial organelles. This may confer survival benefits upon exposure to hostile microenvironment including oxidative stress and hypoxia during cancer progression.

Keywords: Cell plasticity, Cell metabolism, Mitochondria, SDH, Breast cancer

* Correspondence: karl.tronstad@uib.no
†Gro V. Røsland and Sissel E. Dyrstad contributed equally to this work.
[1]Department of Biomedicine, University of Bergen, Bergen, Norway
Full list of author information is available at the end of the article

Introduction

Epithelial to mesenchymal transition (EMT) provides a useful mechanistic framework for studying the regulation and dynamics of cell fate transitions (i.e., cell plasticity) central to developmental and cancer cell biology [1–3]. Events involving downregulation or dysfunction of mitochondrial enzymes have been linked to EMT, but the potential role of mitochondrial remodeling as part of the EMT program has not yet been evaluated through systematic studies of mitochondrial physiology [4].

EMT is a reversible transdifferentiation program whereby epithelial cells convert into migratory mesenchymal cells with enhanced cell survival attributes [1, 2]. EMT is recognized by a loss of epithelial markers such as cytokeratins and E-cadherin, followed by a concomitant increase in mesenchymal markers such as N-cadherin and vimentin [5]. In cancer development, this is associated with therapy resistance and poor clinical outcome [6]. The cellular processes of EMT are orchestrated by several key transcription factors (e.g., TWIST, SNAI1, SNAI2, ZEB1/2) that act in concert with epigenetic mechanisms and post-translational protein modifications to coordinate the cellular alterations [1]. Application of gene expression signatures combining multiple EMT-linked genes has proven useful to evaluate EMT as a contributing factor in tumor development in human cancers [7].

Cellular metabolism provides the energy and building blocks required for cell function and growth and is regulated in close relation to changes in the physiological state of the cell and in the microenvironment [8]. To this end, mitochondrial reprogramming has been shown to be of significance in oncogenic events [9, 10]. Several oncometabolites recognized as drivers of tumor development and progression have been identified, including fumarate, D-2-hydroxyglutarate (D-2HG), and succinate [11]. Such metabolites have been found to have causative influence in cancers with genetic deficiencies in associated enzymes, including fumarate hydratase (FH) [12], isocitrate dehydrogenase 1 (IDH1) [8], and succinate dehydrogenase (SDH) [13]. Mutations (germline) in SDH subunits have been linked to familial paraganglioma syndromes, pheochromocytomas (PGL/PCC), renal cell carcinomas (RCC), and gastrointestinal stromal tumors (GISTs) [14], both as predisposing and prognostic factors [13]. Thus, in PGL/PCC, GIST, and RCC, SDH is classified as a tumor suppressor [13, 15–18].

The SDH complex, also referred to as respiratory complex II in the mitochondrial electron transport chain, is composed of four subunits (SDHA, SDHB, SDHC, and SDHD). It has a central role in energy metabolism, as it directly links the tricarboxylic acid cycle (TCA-cycle) to the respiratory machinery [19]. SDHA and SDHB are hydrophilic subunits and form the catalytic unit of the complex, whereas SDHC and SDHD represent the hydrophobic membrane-bound part of the complex. SDH genes can act as classic tumor suppressor genes, as the mutated alleles often are inherited in a heterozygous manner, and the respective wild-type allele is lost in tumors [9]. Mutations in or downregulation of the SDHB subunit have previously been associated with TGFβ-induced EMT in cancer cells [20–22]. In a previous study investigating breast cancer, the protein expression level of SDHA and B was lost in 3% of the samples [23]. Such effects may indicate that metabolic rewiring could be a facilitating feature for cell plasticity, as it also has been linked to cell state transitions such as differentiation, senescence, and oncogenic transformation [4, 24–27]. In summary, there are several observations supporting that genetic defects in mitochondrial enzymes may affect features of EMT [4, 13, 28, 29]. However, the potential role of metabolic rewiring as a more general driving force of cellular plasticity in human tumors remains poorly explored.

In this study, we present gene expression analysis of human breast cancer samples, correlating the level of SDH subunits to the levels of EMT-related genes. We show that reduced expression of *SDHC* was particularly associated with EMT in the breast cancer cohorts of this study, especially the ductal- and basal-like subgroups. In subsequent cell studies, we found a bilateral causative relationship between SDH attenuation and EMT induction, which involved significant changes in mitochondrial morphofunctional properties.

Methods

Gene expression analysis of human breast cancer samples

We investigated the association between EMT and SDH genes in a breast cancer patient cohort obtained from the Haukeland University Hospital ($n = 204$) [30], as well as an Affymetrix breast cancer meta-cohort ($n = 3992$) [7]. In this study, we used two distinct signatures, one generic comprising 315 genes related to EMT in various tissues (EMT315 signature) [7], and the other consisting of 8 genes of particular relevance for EMT in breast cancer (EMT8 signature). The EMT8 signature was designed based on a previously described 5-gene signature (*CDH1*, *CTNNB1*, *CTNNA2*, *CDH2*, *CDH3*) [31], which we extended with *KRT19*, an established marker for breast cancer cells, and *SNAI2* and *TWIST* due to their role as determinants of EMT in breast cancer metastasis and invasion. The correlation between the two different EMT signature scores was strong in our study cohorts (for the meta-cohort $Rho = 0.674$, $p < 0.0001$ and for the $n = 204$ cohort $Rho = 0.6651$, $p < 0.0001$). Further details about the gene expression analysis (GEA) are provided in Additional file 1: Supplemental methods.

Cell models

The breast epithelial cell line MCF10A and the breast cancer cell line MCF7 (both from ATCC, Manassas, VA) were cultured according to conventional procedures (further described in Additional file 1: Supplemental methods).

Overexpression of EMT-linked transcription factors

Stable modified MCF10A subclones overexpressing *TWIST* or *SNAI2* were established by retroviral transduction, as described previously [32], and termed MCF10A/TWIST and MCF10/SNAI2, respectively. The plasmid constructs used are previously described [33]. The cells were exposed to the virus for 2 × 8 h, interrupted by 8-h incubation in standard medium. In addition, a control subclone was prepared by insertion of the empty vector, which contained the gene for GFP (MCF10A/GFP). Transduction positive cells were sorted by FACS using the GFP marker.

CRISPR/Cas9 in vitro gene editing of *SDHC* and *SDHD*

MCF7 cells with heterozygous knockdown of *SDHC* (MCF7 $SDHC^{+/-}$) was obtained by introducing a frameshift deletion within the coding region (exon 3) of the gene. Twenty nucleotides gRNA targeting *SDHC* were designed (ATAGTAATGTGGGGAGACAG) using the Benchling online tool (www.benchling.com). The oligo-nucleotide sequences were synthesized with the suitable overhangs for plasmid insertion (CACCGATAGTAATGTGGGGAGACAG and AAACCTGTCTCCCCACATTACTATC), before insertion into the pX458SpCas9 plasmid (Addgene, Waltertown, MA, USA), which had been modified to increase the fidelity of Cas9, (according to [34], kindly provided by Ole M. Seternes). The primers were phosphorylated and annealed using T4 PNK (NEB), followed by digestion/ligation into the plasmid, utilizing Golden Gate reaction using BbsI enzyme (NEB) and T7 ligase (NEB). The gRNA inserts were further sequenced to confirm the correct insertion using the U6 primer (GATACAAGGCTGTTAGAGAGATAATT). The cells were transfected with the gRNA containing construct using Lipofectamine LTX (Invitrogen, Carlsbad, CA, USA) for 5 days. Subsequently, cells were sorted into a 96-well plate (one cell per well) based on GFP expression from the vector, using Sony SH800S cell sorter. Upon colony formation in the wells, DNA was purified from each clonal colony and the targeted region was amplified by PCR and sequenced using forward primer CTCG GCCTCCCAAAGAGCTGAGATTA and reverse primer CTCATCTACATAGCAGTATTTTGGTTGAGTAA. The PCR products revealing deletion(s) were further inserted into (vector) by TOPO TA cloning and subject to re-sequencing, in order to confirm that mutation was introduced.

mRNA expression analysis by quantitative polymerase chain reaction

Total RNA was isolated from cell pellets using the RNeasy MINI KIT (74104, Qiagen, Venlo, Netherlands). cDNA was synthesized using the High-Capacity cDNA Reverse Transcription Kit (4368813, Thermo Fisher Scientific, Waltham, MA) and Biorad MJ Mini Thermal Cycler (Hercules, CA, USA). The quantitative polymerase chain reaction (qPCR) was performed using the Light Cycler 480 system (Roche, Basel, Germany) and the Light Cycler 480 Probes Master reaction mix (Cat# 04887301001, Roche). The gene-specific probes used are listed in Additional file 2: Table S3. The ΔΔct method was used for calculating fold change in gene expression relative to the control sample.

Mitochondrial DNA quantification

Total DNA was purified from cell pellets using the DNeasy blood and tissue kit from Qiagen (69504, DNeasy Blood and tissue kit, Qiagen). Taqman probe/primer mixtures for mitochondrial NADH dehydrogenase 1 (mitochondrial DNA (mtDNA) gene; Hs02596873_s1 MTND1) and eukaryotic 18 s rRNA (nuclear gene; 4333760F, Applied Biosystems, CA, USA) were used. Following quantification by qPCR, the amount of mtDNA relative to nuclear DNA was calculated as the ratio between the levels of MTND1 and 18 s RNA using the ΔΔct method [32].

Western blot analysis

Cells were scraped and lysed in RIPA lysis buffer (sc24948, Santa Cruz Biotechnology, Dallas, TX). Protein concentration of the lysed samples were measured by the Pierce® BCA Protein Assay Kit (Thermo Fisher Scientific). Electrophoresis was done using premade Biorad stain-free gels (Biorad Mini-PROTEAN 3 Cell), and the protein was transferred to polyvinylidene fluoride PVDF membranes (GE Healthcare, Little Chalfont, U.K) by BioradTurbo Transfer System. Before stained with respective antibodies (Additional file 2: Table S3), total protein was assessed by imaging on ChemiDocTM XRS+ with Image Lab Software (Biorad).

Spheroid and scratch-wound assays

For measurement of spheroid formation capacity, Geltrex LDEV-free (Thermo Fisher Scientific) was used as a gel matrix. In a 12-well plate, 350 μl/well of Geltrex was casted and solidified at 37 °C for 30 min. Twenty-five thousand cells were suspended in 500 μl of assay medium (2% of geltrex in medium) and added to the solidified matrix. Cells were incubated at 37 °C and cell growth and colonies were observed for 3–7 days. For analysis of spheroid stability and growth, centrifugation-assisted spheroid formation was performed by transferring the cells (5000 cells/well) to a 96-well u-bottom ultralow attachment

plate (Corning, Thermo Fisher Scientific), followed by centrifugation for 15 min at 300 rcf (room temperature). The Incucyte ZOOM 2016B (EssenBioscience Ltd., UK) was used for time-lapse imaging of the spheroids and for scratch-wound assay. For MCF7 spheroids, the area was calculated from the average radius retrieved from measuring two perpendicular diameters (Image Pro Software version 7.0, Media Cybernetics, Inc., Washington, USA). Ten spheroids were measured in each group. For the scratch-wound assay, cells were plated at 45 k cells/well (IncuCyte ImageLock Plates cat #4397) for an optimal 80–90% confluency and incubated over-night. Just prior to the time-lapse imaging sequence, scratch wound was made to the monolayer using the wound maker (IncuCyte Cell Migration Kit, cat# 4493). The cultures were imaged using the Incucyte ZOOM 2016B or by phase contrast microscopy of monolayers fixed in methanol with crystal violet. The percent wound closing after 24 h relative to start was measured using the IncuCyte scratch-wound cell migration software module (Cat# 9600-0012), or by phase contrast microscopy with ocular micrometer, measuring the gap distance at a fixed location.

Mitochondrial respiration

Oxygen consumption rate (OCR) was measured using the Seahorse XFe96 Analyzer (Agilent, Santa Clara, CA), according to the manufacturer's protocols and previous descriptions [32, 35]. All materials were from Sigma-Aldrich (St. Louis, MO) unless otherwise stated. For analysis of SDH-linked activity, the cells were permeabilized to facilitate cellular uptake of succinate and ADP, by adding the Seahorse XF plasma membrane permeabilizer (PMP) (Agilent), as indicated. The concentration of PMP and metabolic modulators (uncoupler, inhibitors) were optimized for each cell type. The data were normalized to cell number using Hoechst 33342 (Thermo Fisher Scientific) or protein content (Pierce® BCA Protein Assay Kit, Thermo Fisher Scientific). Further details are provided in Additional file 1: Supplemental methods.

Flow cytometric G0–G1 separation by Pyronin Y and Hoechst 33258 staining

Cell pellets (1 mill cells) were treated with 50 μg/ml Hoechst 33342 (Thermo Fisher Scientific) for 1 h in 37 °C. After washing, the cells were stained with 1 μg/ml Pyronin Y (Sigma-Aldrich) for 30 min in 37 °C. Cells were washed and filtered before flow cytometric analysis. Pyronin Y was detected at ca 570 nM and Hoechst was detected at 405 nm at the Fortessa LSR (BD Biosciences, San Jose, CA). Analysis was performed in FlowJo software.

Immunocytochemistry

Cells were plated on cover slips in 24-well culture plates (10,000 cells/well) and left until they reached 70% confluency. The cells were then fixed in 3.7% PFA, permeabilized with TBS-T, and stained with primary antibodies for E-cadherin (cat # 14472, Cell Signaling, Leiden, Netherlands) and vimentin (AB92547, Abcam, UK), and diluted 1:100 in TBS-T with 0.5% BSA. Alexa 594 anti-mouse and Alexa-647 anti-rabbit were used as secondary antibodies. The cells were thereafter stained with 1:40 Phalloidin AF555 (a34055, Thermo Fisher Scientific) according to the manufacturer's instruction, before mounting with Prolong Dimond with Dapi (Thermo Fisher Scientific). Images were acquired on a Leica TC2 SP8 STED 3X with HC PL APO CS2 lasers using the 100 × 1.4 NA oil objective.

Confocal microscopy and three-dimensional image analysis of mitochondria

Mitochondria were stained using immunocytochemistry (ICC) (as described above) with primary antibodies against TOM20 (FL145 Santa Cruz Biotech, Dallas, Texas; 1:100); and ATPB (AB5452 Abcam, Cambridge, UK; 1:500). Imaging was performed by confocal microscopy (Leica TCS S5 microscope, Leica microsystems, Wetzlar, Germany). Image processing, three-dimensional (3D)-modeling and quantitative analysis of mitochondrial structures were performed using the Image-Pro Plus software (version 7.0) (Media Cybernetics), as described previously [32, 36]. Further details are provided in Additional file 1: Supplemental methods.

Results

Association between EMT and reduced *SDHC* expression in human breast cancer

We investigated the association between EMT and the different SDH subunits in human breast tumors, based on gene expression in a patient cohort obtained from the Haukeland University Hospital ($n = 204$) [30] and an Affymetrix breast cancer meta-cohort ($n = 3992$) [7]. Using both a breast cancer-directed 8-gene signature (EMT8) and a generic 315-gene signature (EMT315), EMT was found to be particularly associated with reduced *SDHC* expression in the $n = 204$ cohort, with a *Rho* value of − 0.422 ($p < 0.0001$) using the EMT8 signature (Fig. 1a) and *Rho* value of − 0.55 ($p < 0.0001$) using the EMT315 signature (Fig. 1b). *SDHA* and *SDHB* expression were not associated with EMT, whereas *SDHD* demonstrated a positive relationship upon using the EMT315 signature (*Rho* = 0.303, $p < 0.0001$) (Fig. 1b). We also investigated if the expression of the SDH subunits was specifically associated with the central EMT-linked transcription factors TWIST and SNAI2. The analysis indicated that *SDHC* was inversely correlated to both *TWIST1* (*Rho* = − 0.337,

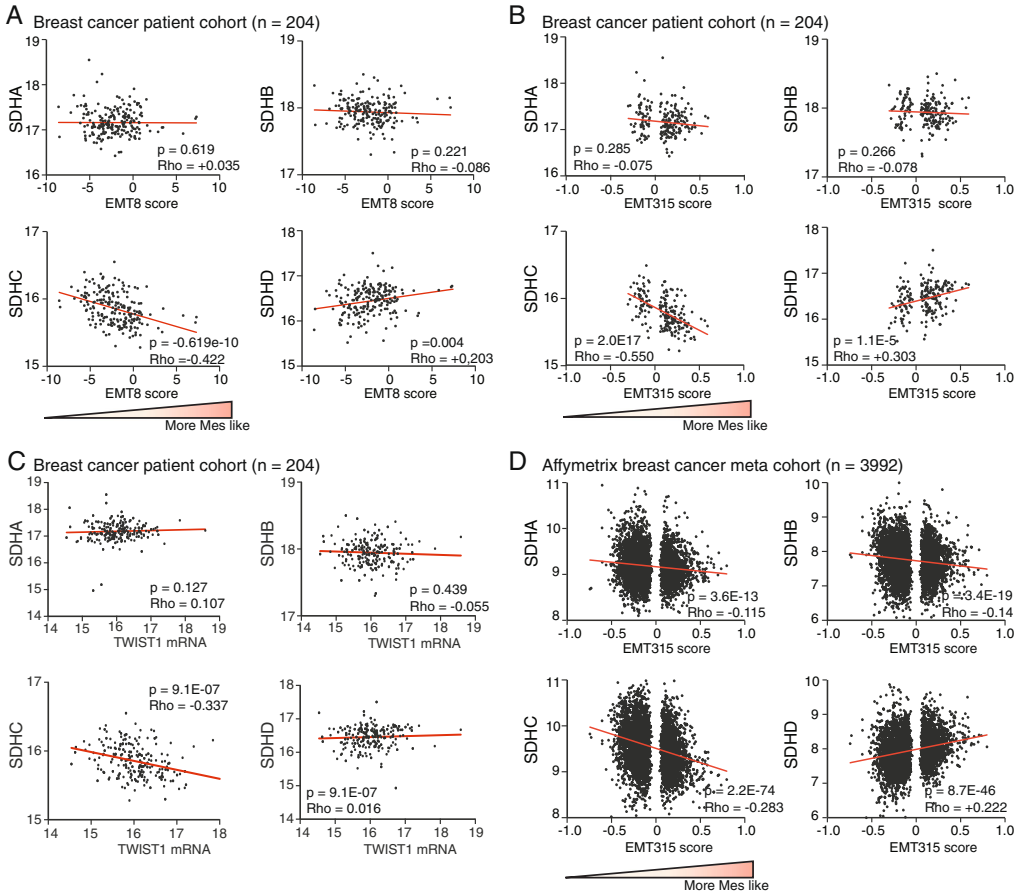

Fig. 1 Association between SDH and EMT in gene expression data from breast cancer patient cohorts. Gene expression (mRNA) correlation analysis (Spearman) between SDH subunits and EMT signature in datasets from breast cancer patients. **a** Breast cancer patient cohort ($n = 204$), using the EMT8 signature (8 genes). **b** Breast cancer patient cohort ($n = 204$), using the EMT315 signature (315 genes). **c** Breast cancer patient cohort ($n = 204$), correlation with TWIST1 expression. **d** Affymetrix breast cancer patient meta cohort ($n = 3992$), relative to the EMT315 signature. The gene expression data are displayed with relative arbitrary units

$p < 0.0001$) (Fig. 1c) and *SNAI2* (*Rho* = 0.27, $p < 0.0001$), whereas *SDHD* showed a positive correlation to *SNAI2* (*Rho* = 0.328, $p < 0.0001$) (Additional file 2: Figure S1A). Neither *SDHA*, *SDHB*, nor *SDHD* showed associations to *TWIST1*. To verify these results, we applied the EMT315 signature on the Affymetrix breast cancer patient meta-cohort ($n = 3992$). In concordance with our previous observations in the $n = 204$ cohort, there was an inverse association between EMT and *SDHC* (*Rho* = − 0.283, $p < 0.0001$) (Fig. 1d). In support, we found a similar inverse correlation between EMT315 and *SDHC* gene expression in a breast invasive carcinoma cohort (*Rho* = − 0.337, $p < 0.0001$) as well as in breast cancer cell lines (*Rho* = − 0.517, $p < 0.0001$) in TCGA RNA-seq data (Additional file 2: Table S1). Correlation analysis between the individual SDH subunits in the $n = 204$ cohort generally returned statistically significant associations between subunit pairs, although with relatively low *Rho*-value (Additional file 2: Figure S1B). This suggests some level of co-regulation of the expression of the individual subunits, as would be expected since the resulting proteins belong to the same enzyme complex. In summary, these data linked EMT to *SDHC* suppression in breast cancer and suggested that TWIST and SNAI2, two of the master promoters of EMT, could be involved.

Low *SDHC* expression is associated with a poor prognosis in basal-like tumors

Next, we investigated the relationship between EMT and *SDHC* when the cohort was divided into molecular subgroups. When we looked at the relative levels of SDHC mRNA, we found no difference between the $n = 204$ cohort tumors classified as either ER+ and ER−, or as ductal and lobular carcinoma (Fig. 2a). Noteworthy, we found significantly lower *SDHC* expression in basal-like compared to non-basal tumors, and this coincided with significantly higher EMT8 score (Fig. 2b). A higher EMT8 score was seen in ER− tumors compared to ER+, but there was no difference between the histological ductal and lobular types. This is in agreement with the known phenotypic differences between basal-like and other breast tumor subtypes. The higher EMT status in ER− vs ER+ tumors and basal-like vs non-basal-like tumors were further supported in the Affymetrix meta-cohort, using either of the EMT signatures (Fig. 2d); however, the overall *SDHC* expression did not differ between the subgroups of this cohort (Fig. 2c). Histological subclassification (i.e., ductal vs lobular carcinoma) was not available for the Affymetrix meta-cohort. Correlation analysis was performed to evaluate the relationship between *SDHC* expression and EMT status within each breast cancer subgroup. The SDHC mRNA level was inversely associated with the EMT8 score in each subgroup of the $n = 204$ cohort (with *Rho* between − 0.431 and − 0.373), except for lobular breast cancer (Fig. 2e). In support, we found an inverse association between *SDHC* expression and EMT315 score in the subgroups of the Affymetrix meta-cohort, somehow stronger in basal-like tumors (*Rho* = − 0.361, $p < 0.0001$) compared to the non-basal-like tumors (with *Rho* between − 0.292 and − 0.256) (Fig. 2f). Interestingly, low *SDHC* expression tended to be associated with poorer survival in patients with basal-like tumors, compared to patients with a high level of *SDHC* (chi-square = 2.821, $p = 0.093$) (Fig. 2g). This trend was not seen in patients with non-basal like tumors.

SDH attenuation by *SDHC* knockdown induces EMT in breast cancer cells (MCF7)

The initial gene expression analysis in human breast tumors and cell lines convincingly suggested that EMT is associated with reduced *SDHC* expression. To explore the impact of reduced *SDHC* expression on EMT-related features, we knocked down this gene in MCF7 breast cancer cells, using the CRISPR/Cas9 system. Successful heterozygous CRISPR/Cas9 editing of *SDHC* (MCF7 $SDHC^{+/-}$) was confirmed by sequencing (Additional file 2: Figure S2), and the resulting reduction in SDHC mRNA and protein was verified (Fig. 3a and b). Immunostaining and fluorescence microscopy indicated reduced protein levels of E-cadherin in MCF7 $SDHC^{+/-}$ compared to MCF7 $SDHC^{+/+}$cells, and F-actin staining with phalloidin revealed a concordant transition from epithelial to mesenchymal-like cell morphology (Fig. 3c). The knockdown of *SDHC* was also accompanied by marker expression consistent with induction of EMT, i.e, E-cadherin (*CDH1*) was downregulated and vimentin (*VIM*), *SNAI2*, *TWIST*, and *AXL* [33] were upregulated (Fig. 3d). The level of N-cadherin (*CDH2*) mRNA was undetectable in both MCF7 $SDHC^{+/+}$ and MCF7 $SDHC^{+/-}$ cells. Consistent alterations in morphological phenotype were also visualized by contrast enhancement microscopy during the course of these experiments. The MCF7 $SDHC^{+/-}$ cells demonstrated reduced capacity to form spheroids in plates with low surface adherence when compared to MCF7 $SDHC^{+/+}$ cells (Fig. 3e). Further, following centrifugation-aided spheroid formation, the MCF7 $SDHC^{+/-}$ spheroids decreased in size, whereas the MCF7 $SDHC^{+/+}$ spheroids grew significantly (Fig. 3f and g). This reduced growth and stability of the multicellular spheroids are consistent with a mesenchymal phenotype, as is the loss of cell-cell adherence observed near the periphery of the MCF7 $SDHC^{+/-}$ spheroids.

In order to study effects of *SDHC* knockdown on mitochondrial respiration, we measured the oxygen consumption rate (OCR) under normal cell culture conditions (DMEM medium) with glucose, pyruvate, and glutamine as the major fuels and then under conditions specifically composed to access changes in SDH function. In the presence of glucose, pyruvate, and glutamine as the major oxidative substrates, the MCF7 $SDHC^{+/-}$ cells demonstrated normal basal respiratory rate; however, they had significantly reduced uncoupled respiratory capacity after addition of oligomycin and CCCP (Fig. 3h). To investigate succinate-dependent mitochondrial respiration, OCR was measured in permeabilized cells, in the presence of the complex I inhibitor, rotenone, and with succinate as the only oxidation fuel (Fig. 3i). After adding succinate, the OCR increased immediately and continued to rise in the MCF7 $SDHC^{+/+}$ cultures. In contrast, succinate caused only a transient OCR induction in the MCF7 $SDHC^{+/-}$ cultures. Furthermore, while OCR increased after addition of ADP in MCF7 $SDHC^{+/+}$ cultures, there was no effect of ADP for MCF7 $SDHC^{+/-}$. The increased OCR after addition of ADP, and the subsequent inhibition by the ATP synthase inhibitor oligomycin, confirms that this SDH-linked respiration was coupled to ATP production through oxidative phosphorylation (OXHOS) in the MCF7 $SDHC^{+/+}$ cells. The absence of such ADP-linked effects in the MCF7 $SDHC^{+/-}$ cells indicates that these cells were unable to utilize succinate to fuel ATP production. In summary, the MCF7 $SDHC^{+/-}$ cells were incapable of maintaining succinate-driven mitochondrial respiration and OXPHOS under these conditions, consistent with an attenuation of SDH activity.

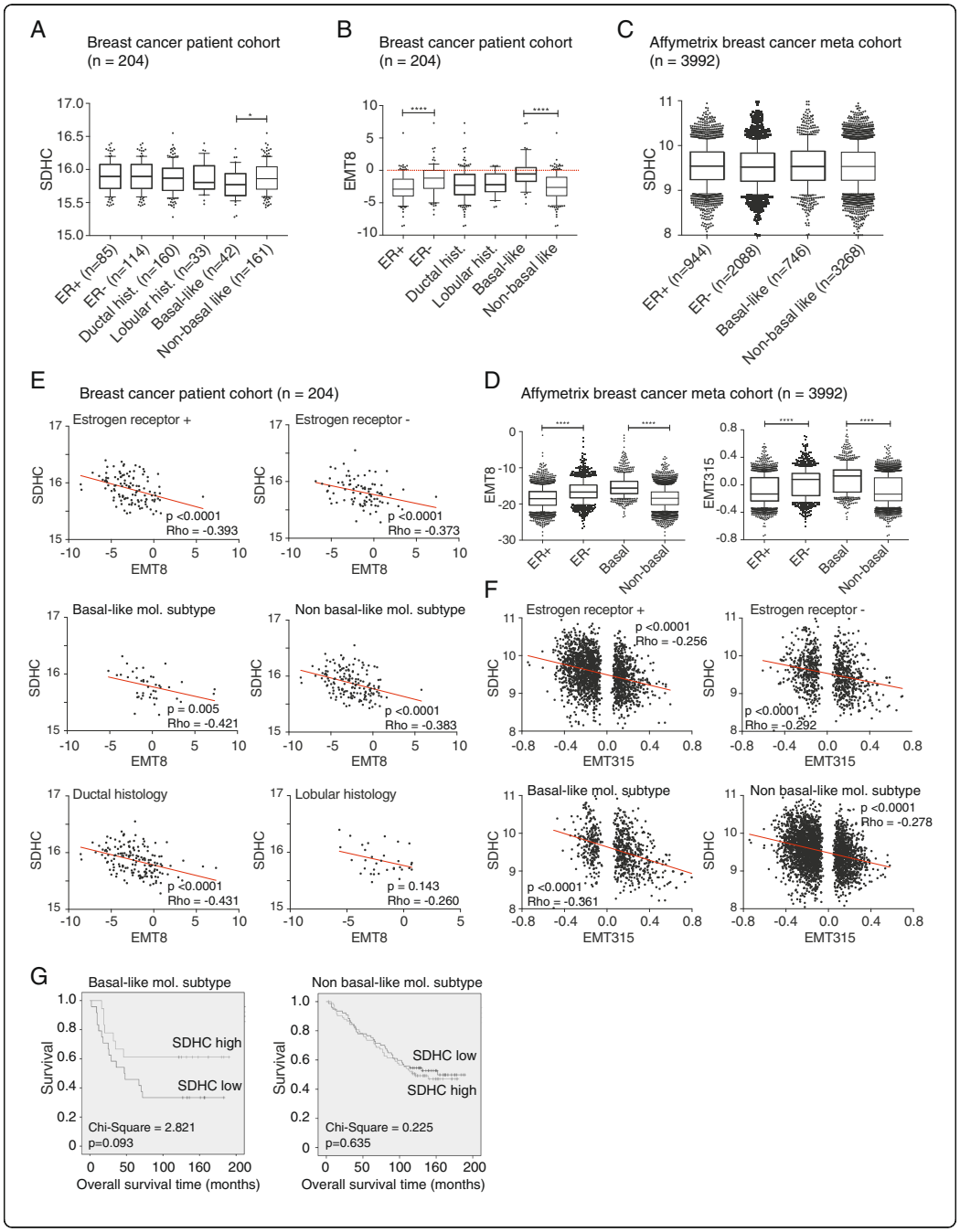
A
Breast cancer patient cohort
(n = 204)
SDHC
ER+ (n=85)
ER- (n=114)
Ductal hist. (n=160)
Lobular hist. (n=33)
Basal-like (n=42)
Non-basal like (n=161)
B
Breast cancer patient cohort
(n = 204)
EMT8
ER+
ER-
Ductal hist.
Lobular hist.
Basal-like
Non-basal like
C
Affymetrix breast cancer meta cohort
(n = 3992)
SDHC
ER+ (n=944)
ER- (n=2088)
Basal-like (n=746)
Non-basal like (n=3268)
E
Breast cancer patient cohort (n = 204)
Estrogen receptor +
p <0.0001
Rho = -0.393
Estrogen receptor -
p <0.0001
Rho = -0.373
Basal-like mol. subtype
p = 0.005
Rho = -0.421
Non basal-like mol. subtype
p <0.0001
Rho = -0.383
Ductal histology
p <0.0001
Rho = -0.431
Lobular histology
p = 0.143
Rho = -0.260
SDHC
EMT8
D
Affymetrix breast cancer meta cohort (n = 3992)
EMT8
EMT315
ER+
ER-
Basal
Non-basal
F
Estrogen receptor +
p <0.0001
Rho = -0.256
Estrogen receptor -
p <0.0001
Rho = -0.292
Basal-like mol. subtype
p <0.0001
Rho = -0.361
Non basal-like mol. subtype
p <0.0001
Rho = -0.278
SDHC
EMT315
G
Basal-like mol. subtype
SDHC high
SDHC low
Chi-Square = 2.821
p=0.093
Non basal-like mol. subtype
SDHC low
SDHC high
Chi-Square = 0.225
p=0.635
Survival
Overall survival time (months)

(See figure on previous page.)**Fig. 2** *SDHC* gene expression in subgroups of breast cancer. The two cohorts included in the study was subdivided based on molecular characteristics such as estrogen receptor positive and negative (ER+ and ER–) and basal- and non-basal phenotype. Claudin-low and triple negative subgroups were included in the basal category. In addition, the breast cancer patient cohort ($n = 204$) was subgrouped based on histology, i.e., into ducal and lobular characteristics. **a** mRNA expression of *SDHC* and **b** EMT8 signature were assessed for the distinct subgroups in the $n = 204$ cohort. **c** mRNA expression of *SDHC* and **d** EMT8 and EMT315 signatures were determined for the subgroups in the $n = 3992$ Affymetrix meta cohort. **e** Spearman correlation analysis for *SDHC* expression relative to EMT8 signature for subgroups of the breast cancer cohort ($n = 204$) and **f** the Affymetrix meta cohort. **g** Kaplan-Meier survival plots for basal- ($n = 42$) and non-basal-like ($n = 161$) breast carcinoma of the breast cancer cohort. The gene expression data are displayed with relative arbitrary units

Further, properties of migration were investigated in a scratch wound experiment, where we also included MCF7 $SDHD^{+/-}$ cells (sequencing data in Additional file 2: Figure S2B), as SDHD demonstrated a different relationship with EMT compared to SDHC in the previous tumor gene expression analysis. Similar to the control MCF7 $SDHC/D^{+/+}$ cells (parental), and in contrast to the mesenchymal-like MCF7 $SDHC^{+/-}$ cells, the MCF7 $SDHD^{+/-}$ cells had an epithelial morphology (Fig. 3j). The scratch-wound study clearly showed that MCF7 $SDHC^{+/-}$ cells had significantly higher wound healing capacity compared to MCF7 $SDHC/D^{+/+}$ and MCF7 $SDHD^{+/-}$ cells, as evident by a significantly smaller gap distance 24 h after the wound was made (Fig. 3k and l).

SDH enzyme inhibition triggers EMT

The results so far suggested that EMT is associated with downregulation of SDH and that defective function of this enzyme may be a causative factor for EMT in tumors. To investigate if this link between EMT and SDH has a general relevance also in non-tumorigenic cells, we studied the effects of the competitive succinate dehydrogenase enzymatic inhibitor malonate in the human mammary epithelial cell line MCF10A. Treatment with malonate for 3 days significantly reduced basal respiration and uncoupled respiratory capacity (Fig. 4a and b). Further, malonate treatment was confirmed to inhibit SDH by reducing SDH-linked respiration measured in permeabilized cells in the presence of succinate and ADP (Fig. 4c and d). In both of these experiments, the normal response to the addition of oligomycin, and subsequently ADP or uncoupler, confirmed that the integrity of the OXPHOS system remained intact upon malonate treatment. Importantly, the malonate treatment caused increased expression of vimentin and N-cadherin and reduced expression of E-cadherin, both on the level of mRNA (Fig. 4e) and on protein (Fig. 4f). This typical marker profile of EMT was consistent with the consequent change in cellular morphology (Fig. 4g). These data support that inhibition of SDH enzyme activity may constitute an inherent trigger of the EMT program.

Overexpression of EMT-linked transcription factors leads to attenuation of SDH

Gene expression analysis suggested that there is a regulatory relationship between EMT-related genes and SDH subunits, especially regarding SDHC, in the breast cancer cohorts of this study. To determine if EMT-linked transcription factors could be involved in SDH downregulation, we overexpressed TWIST and SNAI2 in MCF10A cells (MCF10A/TWIST and MCF10A/SNAI2, respectively). Both the modified cell types presented a switch from epithelial to mesenchymal phenotype, as seen by confocal imaging showing characteristic changes in cell morphology, remodeling of the cytoskeleton, increased level of vimentin, and a reduced level of E-cadherin (Fig. 5a). Induction of EMT was further verified by increased expression levels of vimentin, N-cadherin, Axl, PRXX1, and downregulated E-cadherin, as well as reduced cell proliferation (Additional file 2: Figure S3). In a centrifugation-aided spheroid formation experiment, the parental MCF10A cells formed dense spheroid structures, whereas the MCF10A/TWIST and MCF10A/SNAI2 cells formed less compact structures with loosened cell-cell contact, as expected upon EMT (Fig. 5b). Moreover, a congruent reduction in total RNA level was measured in MCF10A/TWIST cells (Fig. 5c), reflecting a higher content of cells in the state of quiescence due to EMT. Following the verification of EMT in the modified cells, we investigated the effects on SDH. Reduced protein expression of both SDHB and SDHC was detected in the MCF10A/TWIST cells (Fig. 5d). Analysis of oxygen consumption demonstrated that the rates of mitochondrial respiration were lower in MCF10A/TWIST and MCF10A/SNAI2 cells, compared to controls (Fig. 5e–g). The lower rates of leak respiration in the overexpressing cells contradict the possibility that the integrity of mitochondrial inner membrane could be compromised, as this would lead to increased leak respiration due to uncoupling effects. Rather, the lower leak respiration may be explained by a general decrease in mitochondrial respiration. Similar to the previous studies, we then measured SDH-linked respiration in permeabilized cells, in the presence of rotenone, succinate, and ADP (Fig. 5h and i). We found that the activity of SDH was significantly reduced in the MCF10A/TWIST cells, compared to control. Also in these cells, mitochondrial integrity remained intact despite the loss of SDH activity,

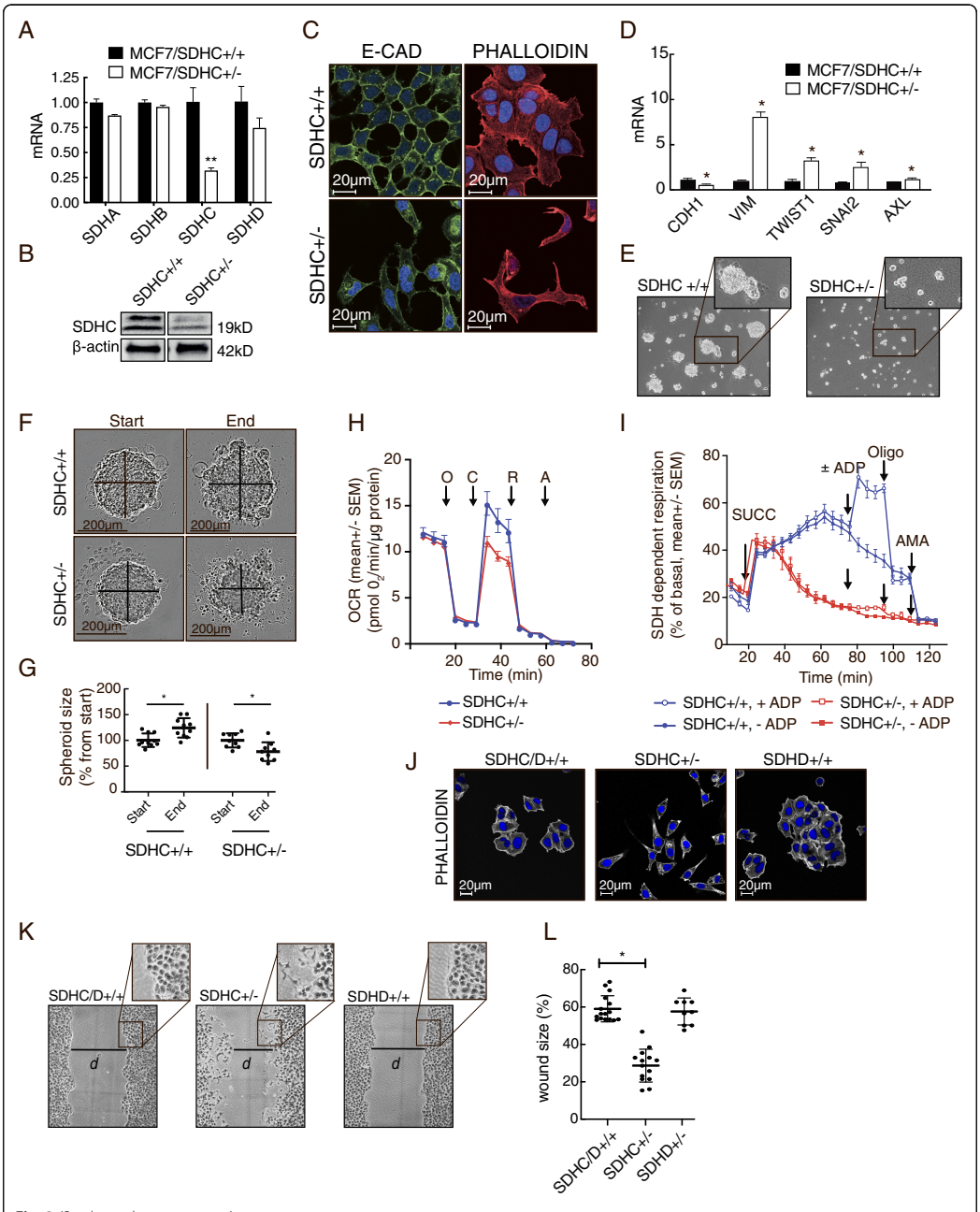

Fig. 3 (See legend on next page.)

(See figure on previous page.)
Fig. 3 Induction of EMT in MCF7 upon *SDHC* knockdown. Parental MCF7 cells (MCF7 $SDHC^{+/+}$) were modified by CRISPR/Cas9 editing to knock down the expression of SDHC (MCF7 $SDHC^{+/-}$). **a** *SDHA-D* mRNA was analyzed by qPCR. **b** SDHC protein expression was analyzed by western blotting. **c** Confocal microscopy was performed to evaluate E-cad (immuno-stained, green) expression level and cell morphology (F-actin stained by phalloidin, red). **d** mRNA expression of the EMT markers E-cad (CDH1), vimentin (VIM), TWIST1, SNAI2, and Axl. **e** Spheroid formation (anchorage-independent) was evaluated after seeding the cells in wells with low surface adherence. **f** Spheroid growth and stability was assessed after centrifugation-aided spheroid formation. The spheroid size was measured after 48 h in culture. **g** The diagram shows statistical data from the experiment described in (**f**). **h** Mitochondrial respiratory rates were measured in MCF7 $SDHC^{+/+}$ and MCF7 $SDHC^{+/-}$ cultures, with glucose, pyruvate, and glutamine provided as the major fuels. Oxygen consumption rate (OCR) was monitored upon sequential additions of oligomycin (O, 3 μM), CCCP (C, 0.75 μM), rotenone (R, 1 μM), and antimycin A (A, 1 μM) as indicated, to assess specific properties of mitochondrial respiration. **i** For measurement of SDH-dependent mitochondrial respiration, the cells were permeabilized (with PMP) and rotenone was added prior to analysis in restricted assay medium (MAS). Succinate (SUCC, 10 mM), ADP (4 mM), oligomycin (OLIGO, 3 μM), and antimycin A (AMA, 1 μM) were added sequentially as indicated. **j** Fluorescence microscopy was performed to compare cell morphology (F-actin stained by phalloidin, white) in MCF7 $SDHD/C^{+/+}$, MCF7 $SDHC^{+/-}$, and MCF7 $SDHD^{+/-}$ cultures. **k** Scratch-wound assay comparing MCF7 $SDHD/C^{+/+}$, MCF7 $SDHC^{+/-}$, and MCF7 $SDHD^{+/-}$ cells. The images were taken 24 h after the scratch was made. **l** In the experiment described in (**k**), we measured scratch size as gap distance (*d*) at a fixed position, after 24 h, and calculated the results relative to the initial scratch size. Each dot represents separate wells. Data are shown as mean ± SD for (**a**), (**d**), (**g**), and (**l**) and mean ± SEM for (**h**) and (**i**). Student's *t* test was used for statistical analysis. *$p < 0.01$; ns, not significant

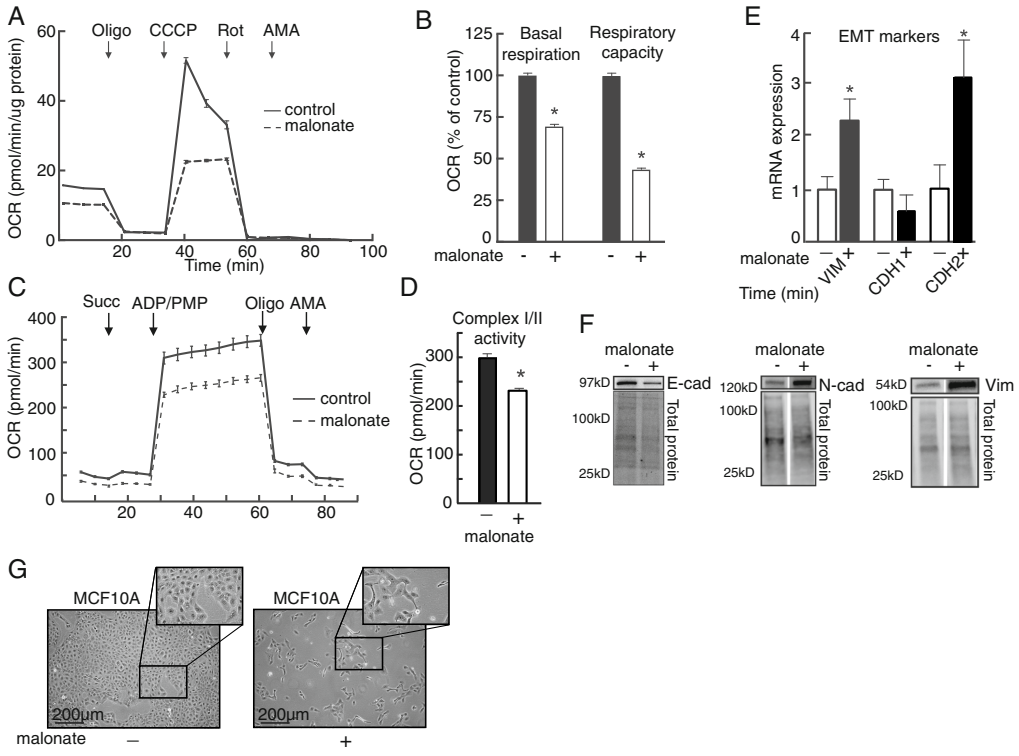

Fig. 4 SDH enzyme inhibition causes induction of EMT. We investigated if SDH enzyme inhibition causes induction of EMT by treating MCF10A cells with the SDH inhibitor malonate (25 mM) for 3 days. **a** Conventional analysis of mitochondrial respiratory function by measuring oxygen consumption rate (OCR) in DMEM medium in malonate treated MCF10A cells. **b** The diagram shows statistical data from the experiment described in (**a**). **c** SDH-linked respiration was assessed with succinate (Succ) as the only provided substrate, following the addition of cell permeabilizing agent (PMP) and ADP. Oligomycin (Oligo) and antimycin A (AMA) was added to control mitochondrial integrity and background activity, respectively. **d** The diagram shows statistical data from the experiment described in (**c**). **e** mRNA and **f** protein expression of epithelial (E-cadherin (*CDH1*)) and mesenchymal (N-cadherin, (*CDH2*); vimentin, (*VIM*)) markers. **g** Phase contrast microscopy. Student's *t* test was used for statistical analysis. Data are shown as mean ± SEM for (**a**)–(**d**) and mean ± SD for (**e**). *$p < 0.01$

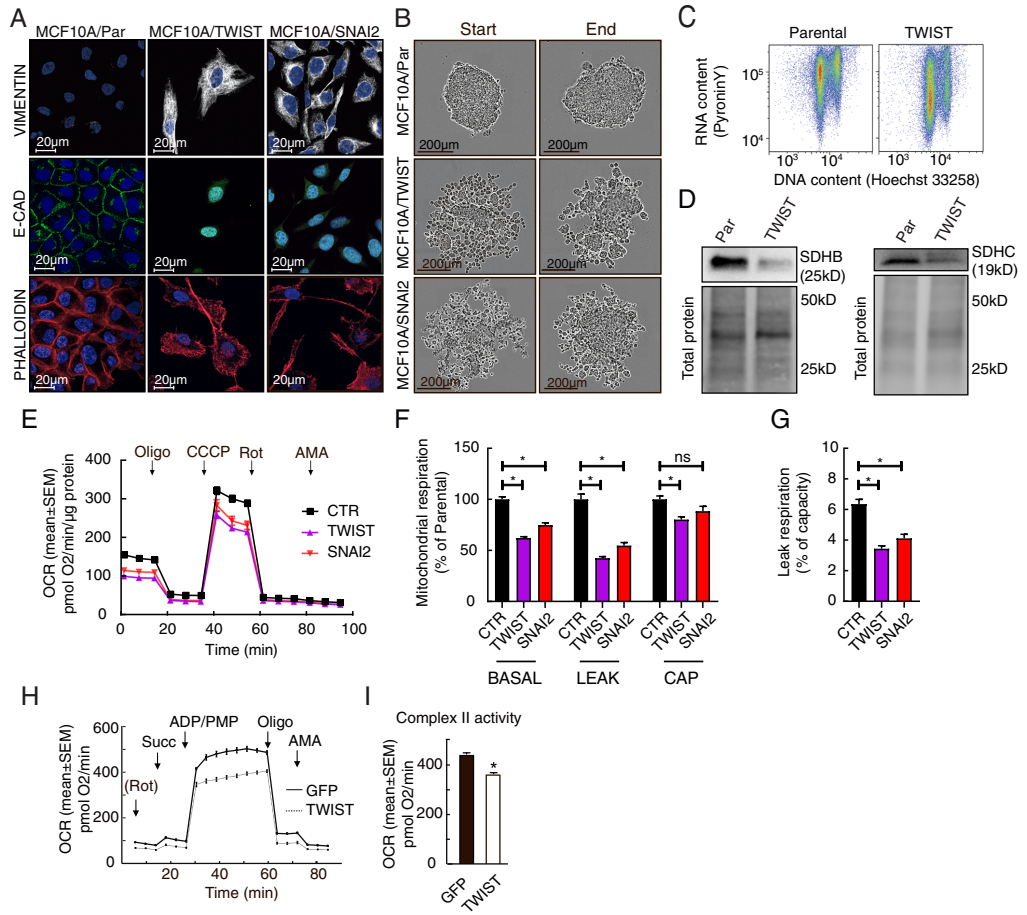

Fig. 5 Induction of EMT in MCF10A cells overexpressing TWIST or SNAI2. The EMT-linked transcription factors TWIST and SNAI2 were overexpressed in epithelial MCF10A cells. EMT was manifested by acquisition of mesenchymal traits. **a** Fluorescence microscopy for detection of vimentin and E-cadherin, and cell morphology (using phalloidin to stain F-actin), in the parental cells (MCF10A/Par), and cells overexpressing TWIST (MCF10A/TWIST) and SNAI2 (MCF10A/SNAI2). **b** Images (phase-contrast microscopy) showing spheroid formation capacity. **c** Total cellular RNA versus DNA content (Hoechst 33258) in MCF10A/TWIST, compared to MCF10A/Par (flow cytometry). **d** Protein expression of subunit SDHB and SDHC in MCF10A/Par and MCF10A/TWIST cells. **e** Mitochondrial respiration after overexpression of EMT-linked transcription factors. Oxygen consumption rate (OCR) was measured after sequential additions of oligomycin (Oligo), CCCP, rotenone (Rot), and antimycin A (AMA), in DMEM medium. **f** Extracted data from the experiment in (**e**), showing rates of basal and leak (with oligomycin) respiration and respiratory capacity (uncoupled, with CCCP), in the MCF10A/TWIST and MCF10A/SNAI2 cells relative to parental cells (CTR). **g** Leak respiration (with oligomycin) as the percentage of respiratory capacity (uncoupled, with CCCP), from the experiment in (**e**). **h** SDH activity measured in restricted medium (MAS) after the supply of rotenone (Rot), succinate (Succ), ADP, and permabilizing agent (PMP). Oligomycin (Oligo) and antimycin A (AMA) were then added to control mitochondrial integrity and background activity. **i** The diagram shows statistical data from the experiment described in (**h**). Data are shown as mean ± SD (column plots) or mean ± SEM (OCR traces). Student's *t* test was used for statistical analysis. *$p < 0.01$

supported by the normal response to oligomycin in the presence of ADP. In summary, these data suggest that initiation of the EMT program leads to attenuation of SDH.

TWIST overexpression leads to reduced mitochondrial biomass and changed organelle morphology

Based on the findings suggesting that EMT involves a change in the mitochondrial functional state partly

through SDH downregulation, we investigated mitochondrial morphology in MCF10A/TWIST compared to parental MCF10A cells using confocal microscopy and quantitative 3D-image analysis. The mitochondria in MCF10A cells were tubular and formed a compact and continuous reticulum throughout the cytoplasm (Fig. 6a). Mitochondria in MCF10A/TWIST cells were also tubular, but the structures were thinner and there was a fraction of relatively small peripheral organelles dissociated from the major mitochondrial assembly. Quantitative analysis revealed that the number of organelles was significantly higher in MCF10A/TWIST cells, compared to parental cells (Fig. 6b). However, the total mitochondrial volume was smaller (Fig. 6c), though the total mitochondrial tubule length was unchanged (Fig. 6d). Frequency distribution analysis of single mitochondria showed increased proportion of smaller organelles in the MCF10A/TWIST cells (Fig. 6e). Consequently, small- and medium-size mitochondria were found to constitute a larger fraction of the total mitochondrial volume, compared to epithelial MCF10A cells (Fig. 6f). Increased surface-to-volume ratio in MCF10A/TWIST mitochondria further supported a change towards thinner tubular structures compared to the parental phenotype (Fig. 6g). Taken together, these imaging data show that EMT in this model is accompanied by a pronounced decrease in

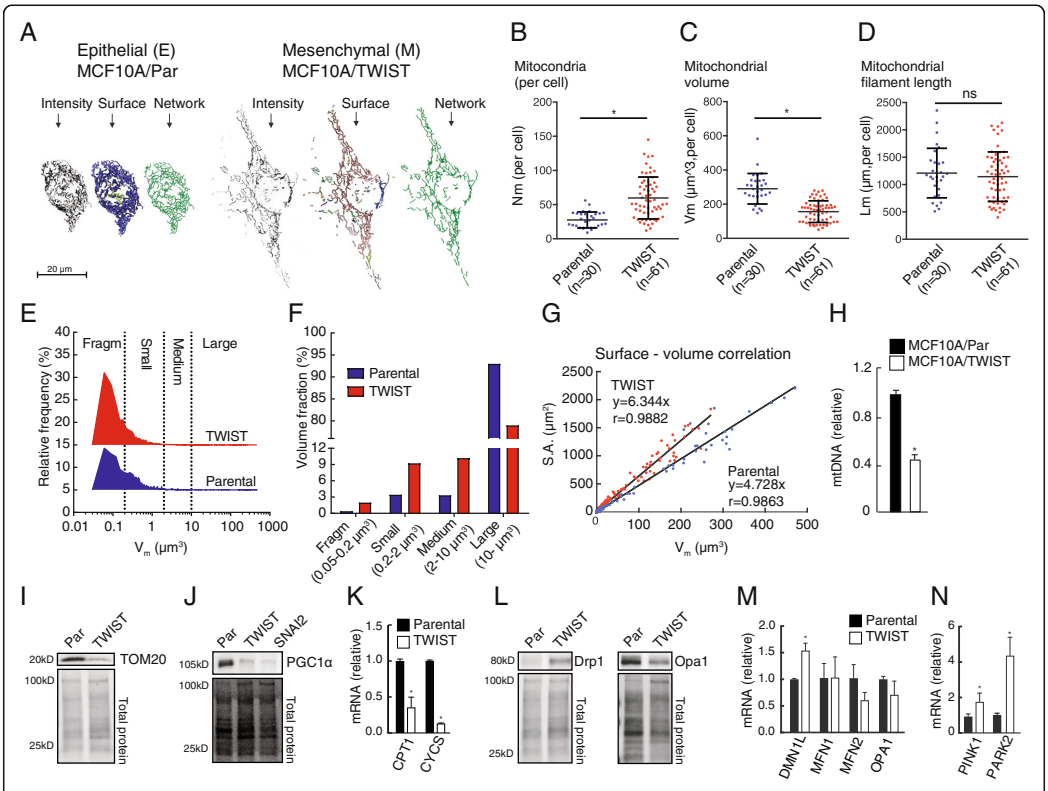

Fig. 6 Mitochondrial mass and morphology. Mitochondrial mass and morphology were compared in MCF10A (parental, epithelial) and MFC10A/TWIST (mesenchymal) cells. **a**–**g** Confocal microscopy and quantitative image analysis of immune-stained mitochondria (TOM20 + ATPB). **a** Based on confocal z-stacks, 3D-models of mitochondrial volume and filament structure were generated, as indicated from left to right in the two image panels. **b** Mean number of mitochondria per cell (N_m). **c** Mean mitochondrial total volume per cell ($V_{m,cell}$). **d** Mean mitochondrial total tubule length per cell ($L_{m,cell}$). **e** Size (volume) frequency distribution comparing mitochondria in MCF10A (parental) versus MCF10A/TWIST cells. **f** Volume fraction analysis of mitochondrial subclasses (size). **g** Surface area (S.A.) to volume (V_m) regression analysis of individual mitochondria in MCF10A (parental) and MCF10A/TWIST cells. The analysis comprised (parental/TWIST) 937/3643 mitochondria with total volume 9020/9554 µm^3, in 30/61 cells (n). **h**–**n** Effects of TWIST overexpression on mtDNA and gene expression of mitochondrial proteins. **h** Amount of mtDNA in MCF10A/TWIST relative to parental MCF10A. **i** Protein expression (WB) of TOM20. **j** Protein expression of PGC1α, including MCF10A/SNAI2 cells. **k** mRNA expression of *CPT1* and *CYCS*. **l** Protein expression (WB) of Drp1 (*DMN1L*) and Opa1. **m** mRNA expression of *DMNL1* (Drp1), *OPA1*, *MFN1*, and *MFN2*. **n** mRNA expression of *PINK1* and *PARK2*. Student's *t* test was used for statistical analysis. Data are shown as mean ± SD. *$p < 0.01$

mitochondrial volume and a morphological change from a compact mitochondrial reticulum to a more dispersed and fragmented network of thinner tubules. Congruent with reduced mitochondrial biomass, the MCF10A/TWIST cells had reduced amounts of mitochondrial DNA (mtDNA), TOM20 protein, the transcriptional co-activator and key regulator of mitochondrial biogenesis PGC1α, and mRNA levels of the mitochondrial proteins carnitine palmitoyl transferase 1 (*CPT1A*) and cytochrome *c* (*CYCS*) (Fig. 6h–k). Further supporting the observed changes in mitochondrial dynamics, the mitochondrial fission-related Drp1 protein was found to be upregulated, whereas the mitochondrial fusion protein OPA1 was downregulated (Fig. 6l). Additional mRNA expression analyses confirmed the upregulation of *DMN1L* (DRP1) and indicated a trend for the downregulation of *OPA1* and *MFN2* but not for *MFN1*, in the MCF10A/TWIST cells compared to MCF10A/Par (Fig. 6m). Further, we observed significantly higher *PINK1* and *PARK2* expression in MCF10A/TWIST cells (Fig. 6n). These data supports that EMT involves loss of mitochondrial biomass and more fragmented organelle structure, consistent with reduced respiratory rates.

Potential links between SDH regulation and EMT activation

Finally, to investigate if the four SDH subunits may have specific impacts on tumor metabolism, mitochondrial dynamics and antioxidant systems related to EMT, we performed correlation analysis including panels of marker genes on the Affymetrix breast cancer cohort. A heat map of the correlation coefficients (Spearman *Rho*) comparing associations between specific genes of interest relative to the SDH subunits and EMT markers is shown in Fig. 7 (the dataset is provided in Additional file 1: Table S2). To clarify, since we aimed to identify potential links between attenuated SDH and EMT activation, we were looking for genes demonstrating an opposite relationship towards SDH compared to EMT (i.e., *Rho* value with opposite signs). In general, *SDHA*, *SDHB*, and *SDHC*, demonstrated similar patterns of association with this panel of genes, in contrast to *SDHD* that showed some divergence compared to the other SDH subunits. This association analysis did not suggest that expression of the EMT315 signature, *TWIST1*, and *SNAI2* was consistently linked to HIF-1 target genes associated with glycolysis, apart from *GLUT3* (Fig. 7a). The expression of *SDHA*, *SDAB*, and *SDHC* tended to be positively associated with the metabolic HIF-1 target genes. Moreover, western blot analysis of HIF-1α revealed no signs of increased protein stabilization in MCF10A overexpressing TWIST, or MCF7 *SDHC/D*$^{+/+}$ and MCF7 *SDHD*$^{+/-}$ cells (Additional file 2: Figure S4). Hence, although our findings do not directly support that SDH suppression promotes a HIF-1-regulated shift towards increased glycolysis in these tumors, it still remains a possibility. HIF1-regulated genes involved in EMT and invasion demonstrated a clear tendency of inverse regulation relative to *SDHA*, *SDHB*, and *SDHC*, while positively linked to EMT markers. Moreover, the increasing expression of the SDH subunits was associated with increasing expression of markers of mitochondrial biomass (Fig. 7b). These markers generally showed weak inverse relationships with EMT-linked gene expression. SDH subunit expression was also associated with genes involved in both mitochondrial fission and fusion, probably reflecting a parallel regulation of genes encoding mitochondrial proteins. Further, a tendency of positive association with autophagy genes such as *BECN1* and *BNIP3* suggests that SDH downregulation is related to modulation of autophagy, and an inverse association with *PARK2* may suggest that mitochondrial quality control is activated under such conditions. Downregulation of SDH subunits tended to be associated with downregulation of antioxidant systems (i.e., positive associations), apart from *GPX2* and *GPX5* showing inverse relationships with all SDH subunits (Fig. 7c). The effects of such changes may be complex, and these data do not reveal if potential changes in tumor redox state due to reduced SDH subunit expression may be associated with EMT. Although some antioxidant enzymes appeared to linked to EMT, such as *GPX7* and *GPX8*, we did not find clear reciprocal relationships with reduced expression of *SDHC* or the other SDH subunits. Finally, analysis of three anticipated target genes did not indicate that AMPK was coherently activated in the context of SDH suppression but rather showed that these genes were individually regulated, with *CPT2* showing a clear positive relationship with expression of *SDHA*, *SDHB*, and *SDHC* (Fig. 7d).

Discussion

This study support that attenuation of SDH represents an inherent element and driver mechanism of the EMT program and especially points to SDHC as a contributing factor in the context of breast cancer. Through comprehensive cellular analyses, we characterized regulatory and functional aspects of the relationship between EMT and SDH, and further found the EMT program to involve distinct changes in mitochondrial function and morphology.

Based on previous reports suggesting that mitochondrial dysfunction and *SDHB* mutations promote EMT [4, 37], we hypothesized that altered enzyme function of SDH may be a determining factor and possibly an integral part of EMT in human tumors, which could be linked to an overarching shift in mitochondrial function and dynamics. Thorough analyses in breast cancer patient cohorts revealed a relatively consistent inverse association between EMT and reduced expression of the *SDHC* subunit. Upon molecular and histological classification of the

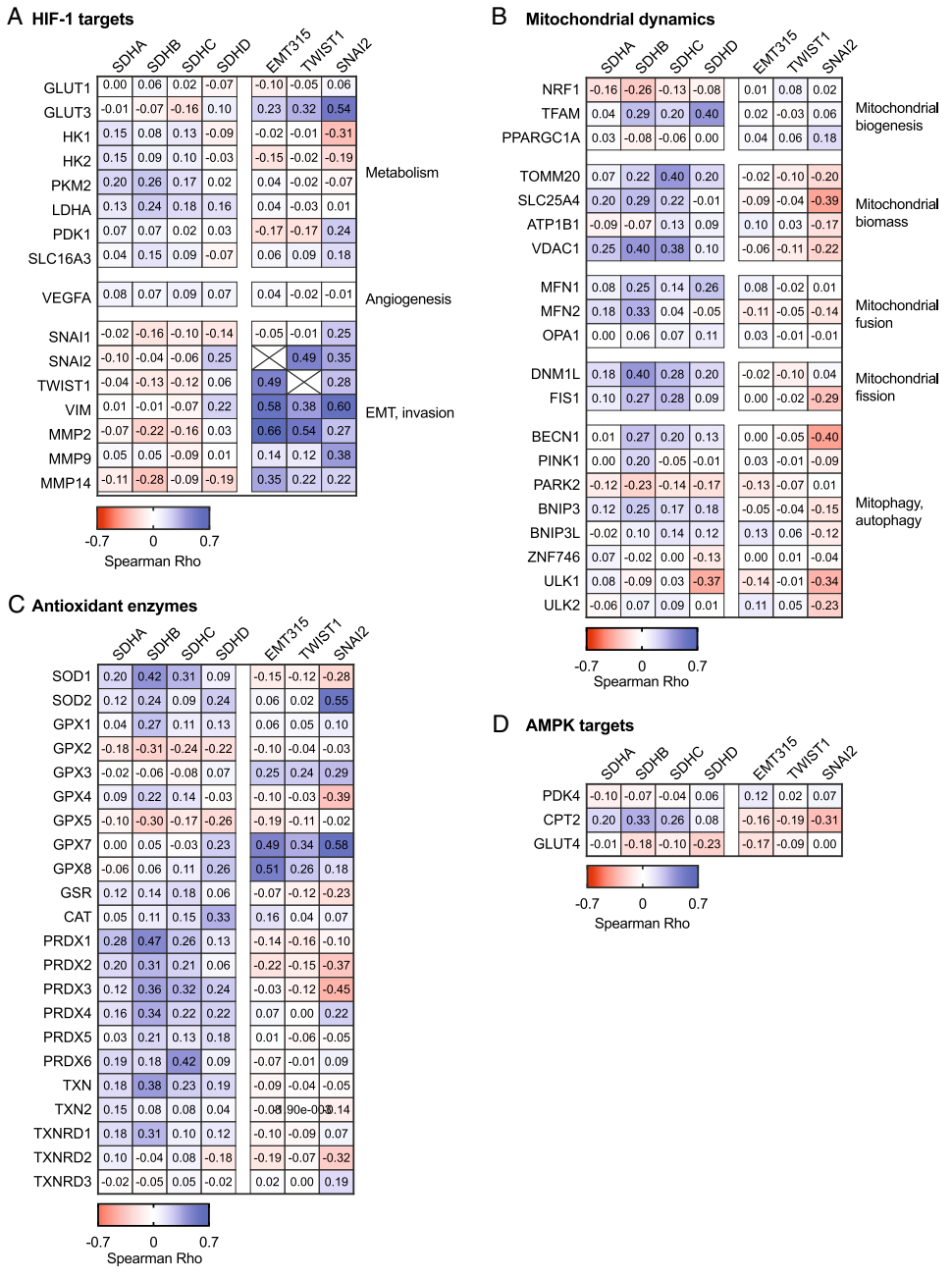

Fig. 7 (See legend on next page.)

(See figure on previous page.)
Fig. 7 Gene expression analysis of potential links between SDH suppression and EMT activation. Gene expression (mRNA) analysis correlating (Spearman) SDH subunits, EMT signature, TWIST1, and SNAI2 to panels of genes focusing on specific processes, based on data from the Affymetrix breast cancer patient meta cohort ($n = 3992$). The heat map panels reflect the directions and strength (*Rho* value) of the associations. The panels of genes included **a** HIF-1 targets, **b** factors involved in mitochondrial dynamic, **c** antioxidant enzymes, and **d** AMPK targets

breast cancer cohorts, we found that the relationship between *SDHC* and EMT was stronger in the basal-like subgroup compared to the non-basal-like subgroup. Interestingly, when looking at overall survival, low *SDHC* level was associated with a worse outcome in basal-like breast carcinoma. This finding can imply that suppressed activity of SDH-linked mitochondrial pathways is associated with a worse prognosis in basal-like breast carcinomas. As mitochondrial function is challenging to assess in frozen and paraffin-embedded samples, there is an urgent need for indicative markers reflecting mitochondrial abnormalities. Our results suggest that *SDHC* expression could serve as a potential prognostic marker to enable further discrimination in the basal-like breast carcinoma subgroup. Furthermore, upon histological classification of the $n = 204$ breast cancer cohort, we found the inverse association between SDHC and EMT to be more pronounced in the ductal subgroup, compared to the lobular, but we did not see an impact on the overall survival.

The relationship between SDHC and EMT was supported in subsequent studies revealing that EMT is induced by CRISPR/Cas9-mediated knockdown of *SDHC*, or SDH enzyme inhibition with malonate in respective cell models. Under these conditions, EMT clearly involved inhibition of SDH enzyme activity, as the ability to utilize succinate as respiratory fuel was significantly reduced. These findings extend the potential impact of SDH attenuation on malignant mechanisms beyond the role as tumor suppressor, as they suggest that transcriptional suppression, not only genetic SDH defects, may promote EMT.

Overexpression of EMT-linked transcription factors (TWIST and SNAI2) caused SDH suppression, reduced mitochondrial respiration, decreased amount of mitochondrial biomass (mtDNA and organelle volume), downregulated mitochondrial biogenesis (including PGC1α), and altered organelle structure. Noteworthy, context-dependent changes of mitochondrial functional state are also often accompanied by accordant effects on organelle structure and amount (i.e., mitochondrial dynamics) [38]. Our findings provide mechanistic insights for previous reports elucidating context-dependent links between SDH inhibition, mitochondrial dysfunction, and EMT [4, 13, 22, 39]. The results are also in agreement with findings suggesting that SNAI1 modulates cell metabolism by decreasing respiratory activity via reduced SDH activity [40]. The EMT-linked mechanisms involving reduced SDH activity may share similarities with the action of other mitochondrial tumor suppressors, such as fumarate dehydrogenase, fumarate hydratase, and isocitrate dehydrogenase, as well as OXPHOS defects that contribute to tumor development [18, 41, 42]. According to our findings, it can be speculated that an increased population of smaller mitochondrial organelles may facilitate cellular plasticity accompanying EMT and that this is associated with processes of mitochondrial quality control, as suggested by increased expression of *PINK1* and *PARK2*. This aspect is emphasized by findings in stem cells where mitochondrial quality is supported through asymmetric organelle sorting during cell division [43] and the role of mitochondrial dynamics during embryogenesis [44].

Interestingly, we found a clear relationship between the cells' ability to form spheroids, wound healing capacity, and EMT state, related to downregulation of *SDHC*. This observation constitutes a convincing example of how metabolic rewiring may represent an integral part of cellular plasticity. It may also incorporate established paradigms of tumor metabolism where suppressed mitochondrial energetics supports biomolecule synthesis or antioxidant defense [45]. Moreover, decreased proliferation and reduced dependency on mitochondrial respiration may constitute a protective adaptation mediating tolerance for a harsh microenvironment, including hypoxia, nutrient deprivation, and therapeutic pressures [46]. This may, however, also open for targeted therapeutic strategies. For instance, RCC tumors with *SDHB* mutations has been shown to be highly dependent on an increased influx of glucose, and glucose interfering drugs have already been proposed as possible therapeutic strategies [47]. Also, it has been shown that mutations in SDH establishes a hypermethylated phenotype in PGL/PCC, possible through the accumulation of succinate [48]. Interestingly, *KRT19*, one of the genes showing the strongest evidence for epigenetic silencing in hypermethylated PGL/PCCs, is closely associated with EMT. This may explain the particularly invasive phenotype of *SDHB*-related tumors.

Gene expression analysis on the Affymetrix breast cancer cohort confirmed that downregulation of *SDHA*, *SDHB*, *SDHC*, and/or *SDHD* is associated with increased expression of EMT and invasion/migration markers and pointed to specific genes that may link to accompanying effects on energy metabolism, mitochondrial quality control, and antioxidant systems to the induction of EMT (Fig. 7). Although HIF-1 and AMPK may be involved in these processes, it appears likely that some of

their anticipated target genes may also be regulated by other mechanisms. Moreover, interactions of SDH and other components of the respiratory chain may affect EMT through effects on reactive oxygen species (ROS) generation and scavenging. Such mechanisms likely depend on cellular origin and phenotype, and probably the state of EMT. Our investigations primarily focused on long-term effects associated with EMT. Whether ROS play a role in the induction of EMT, or transition between different states of EMT, would be an interesting aspect for further studies, provided the metabolic links revealed in the presented work.

As EMT is recognized as a driver mechanism of metastasis, therapy resistance, and immune evasion, our findings provide mechanistic support for further investigations of mitochondrial features as potential therapeutic targets. To this end, mitochondria-targeted drugs such as resveratrol and metformin have been reported to inhibit EMT [49], and metformin has a preventive effect on cancer incidence [50]. The presented findings pointing to SDH suppression as an integral part of the EMT process may therefore open for new strategies to prevent and treat malignancies.

Additional files

Additional file 1: Supplemental methods (PDF 26 kb)

Additional file 2: Figure S1. Gene expression correlation analysis extended. **Figure S2.** DNA sequence verification of *SDHC* and *SDHD* CRIPSR/Cas9 modifications. **Figure S3.** Characterization of EMT in MCF10A cells overexpressing TWIST or SNAI2. **Figure S4.** Western blot analysis of HIF-1α in MCF7 and MCF10A cells. **Table S1.** Gene expression correlation analysis, in cell lines. **Table S2.** Gene expression correlation analysis towards specific gene panels. Table S3. Lists of probes, antibodies, and dyes. (PDF 7335 kb)

Abbreviations

EMT: Epithelial to mesenchymal transition; ER: Estrogen receptor; FH: Fumarate hydratase; GEA: Gene expression analysis; GIST: Gastrointestinal stromal tumor; IDH1: Isocitrate dehydrogenase 1; mtDNA: Mitochondrial DNA; OCR: Oxygen consumption rate; PGL/PCC: Paraganglioma-pheochromocytoma syndrome; qPCR: Quantitative polymerase chain reaction; RCC: Renal cell carcinomas; SDH: Succinate dehydrogenase; TCA cycle: Tricarboxylic acid cycle; TCGA: The cancer genome atlas (https://cancergenome.nih.gov/)

Acknowledgments

We are grateful to Sissel Vik Berge, Ingrid Gavlen, Marianne Enger, Brith Bergum, and Hege A. Dale for their excellent technical assistance and to Nils Halberg for insightful comments to the manuscript. Confocal microscopy and quantitative image analysis were performed using the infrastructure of the Molecular Imaging Center, Department of Biomedicine, University of Bergen. Cell sorting was performed using the infrastructure of the flow cytometry core facility at the Faculty of Medicine, University of Bergen.

Funding

The work was funded by the Norwegian Research Council together with the University of Bergen (214187/F20, Tronstad) and Helse Vest (912148, Røsland).

Availability of data and materials

The datasets supporting the patient-related conclusions of this article are described in [7, 30]. Further details regarding these datasets are available upon request.

Authors' contributions

GVR, SED, DT, JBL, and KJT designed the study. GVR, SED, DT, MKL, ChK, RH, and INP performed cell culture experiments and biochemical analyses. KJ, HJD, and AJA developed and characterized EMT cell models. GVR, FH, and KJT performed confocal microscopy and quantitative image analysis of the mitochondria. SK, PEL, AB, CaK, TZT, and JPT performed GEA in the patients. GVR, SED, DT, JBL, and KJT wrote the manuscript, in dialog with all of the authors. All authors read and approved the final manuscript.

Ethics approval and consent to participate

Patients gave their written informed consent under institutional review board-approved protocols (Rek Vest project #19297 and #13025 and 273/96-82.96).

Consent for publication

All authors have agreed to publish this manuscript.

Competing interests

The authors declare that they have no competing interests.

Publisher's Note

Author details

[1]Department of Biomedicine, University of Bergen, Bergen, Norway. [2]Department of Clinical Science, University of Bergen, Bergen, Norway. [3]Faculty of Science, Ain Shams University, Cairo, Egypt. [4]Cancer Science Institute of Singapore, National University of Singapore, Singapore, Singapore. [5]Department of Pathology, Haukeland University Hospital, Bergen, Norway. [6]Department of Gynecology and Obstetrics, Haukeland University Hospital, Bergen, Norway. [7]Department of Molecular Medicine, University of Southern Denmark, Odense, Denmark. [8]Biomedical Center, University of Iceland, Reykjavík, Iceland. [9]Centre for Cancer Biomarkers (CCBIO), Department of Clinical Medicine, Faculty of Medicine and Dentistry, The University of Bergen, Bergen, Norway. [10]Department of Oncology, Odense University Hospital, 5000 Odense, Denmark. [11]Department of Oncology, Haukeland University Hospital, Bergen, Norway. [12]Biomedical Department of Biochemistry, Yong Loo Lin School of Medicine, National University of Singapore, Singapore, Singapore. [13]Inserm Unit 1186 Comprehensive Cancer Center Institut Gustave Roussy, Villejuif, France. [14]Institute of Molecular and Cell Biology, A-STAR, Singapore, Singapore.

Received: 11 December 2018 Accepted: 4 April 2019
Published online: 01 June 2019

References

1. Nieto MA, Huang Ruby Y-J, Jackson Rebecca A, Thiery Jean P. EMT: 2016. Cell. 2016;166:21–45.
2. Varga J, Greten FR. Cell plasticity in epithelial homeostasis and tumorigenesis. Nat Cell Biol. 2017;19:1133–41.
3. Ye X, Weinberg RA. Epithelial–mesenchymal plasticity: a central regulator of cancer progression. Trends Cell Biol. 2015;25:675–86.
4. Sciacovelli M, Frezza C. Metabolic reprogramming and epithelial-to-mesenchymal transition in cancer. FEBS J. 2017;284:3132–44.
5. Thiery JP, Acloque H, Huang RY, Nieto MA. Epithelial-mesenchymal transitions in development and disease. Cell. 2009;139:871–90.
6. Zheng X, Carstens JL, Kim J, Scheible M, Kaye J, Sugimoto H, Wu C-C, LeBleu VS, Kalluri R. EMT program is dispensable for metastasis but induces chemoresistance in pancreatic cancer. Nature. 2015;527:525–30.
7. Tan TZ, Miow QH, Miki Y, Noda T, Mori S, Huang RY-J, Thiery JP Epithelial-mesenchymal transition spectrum quantification and its efficacy in deciphering survival and drug responses of cancer patients. EMBO Molecular Medicine 2014, 6:1279–1293.

8. Dang L, White DW, Gross S, Bennett BD, Bittinger MA, Driggers EM, Fantin VR, Jang HG, Jin S, Keenan MC, et al. Cancer-associated IDH1 mutations produce 2-hydroxyglutarate. Nature. 2009;462:739–44.
9. Gaude E, Frezza C. Defects in mitochondrial metabolism and cancer. Cancer Metabolism. 2014;2:10.
10. Valcarcel-Jimenez L, Gaude E, Torrano V, Frezza C, Carracedo A. Mitochondrial metabolism: yin and yang for tumor progression. Trends Endocrinol Metab. 2017;28:748–57.
11. Janin M, Esteller M. Oncometabolite accumulation and epithelial-to-mesenchymal transition: the turn of fumarate. Cell Metab. 2016;24:529–30.
12. Tomlinson IP, Alam NA, Rowan AJ, Barclay E, Jaeger EE, Kelsell D, Leigh I, Gorman P, Lamlum H, Rahman S, et al. Germline mutations in FH predispose to dominantly inherited uterine fibroids, skin leiomyomata and papillary renal cell cancer. Nat Genet. 2002;30:406–10.
13. Loriot C, Burnichon N, Gadessaud N, Vescovo L, Amar L, Libé R, Bertherat J, Plouin P-F, Jeunemaitre X, Gimenez-Roqueplo A-P, Favier J. Epithelial to mesenchymal transition is activated in metastatic pheochromocytomas and paragangliomas caused by SDHB gene mutations. J Clin Endocrinol Metab. 2012;97:E954–62.
14. Janeway KA, Kim SY, Lodish M, Nosé V, Rustin P, Gaal J, Dahia PLM, Liegl B, Ball ER, Raygada M, et al. Defects in succinate dehydrogenase in gastrointestinal stromal tumors lacking KIT and PDGFRA mutations. Proc Natl Acad Sci U S A. 2011;108:314–8.
15. Saxena N, Maio N, Crooks DR, Ricketts CJ, Yang Y, Wei MH, Fan TW, Lane AN, Sourbier C, Singh A, et al. SDHB-deficient cancers: the role of mutations that impair Iron sulfur cluster delivery. J Natl Cancer Inst. 2016;108. https://doi.org/10.1093/jnci/djv287.
16. Ricketts CJ, Forman JR, Rattenberry E, Bradshaw N, Lalloo F, Izatt L, Cole TR, Armstrong R, Kumar VK, Morrison PJ, et al. Tumor risks and genotype-phenotype-proteotype analysis in 358 patients with germline mutations in SDHB and SDHD. Hum Mutat. 2010;31:41–51.
17. Astuti D, Latif F, Dallol A, Dahia PL, Douglas F, George E, Skoldberg F, Husebye ES, Eng C, Maher ER. Gene mutations in the succinate dehydrogenase subunit SDHB cause susceptibility to familial pheochromocytoma and to familial paraganglioma. Am J Hum Genet. 2001;69:49–54.
18. Gottlieb E, Tomlinson IP. Mitochondrial tumour suppressors: a genetic and biochemical update. Nat Rev Cancer. 2005;5:857–66.
19. Ghezzi D, Goffrini P, Uziel G, Horvath R, Klopstock T, Lochmuller H, D'Adamo P, Gasparini P, Strom TM, Prokisch H, et al. SDHAF1, encoding a LYR complex-II specific assembly factor, is mutated in SDH-defective infantile leukoencephalopathy. Nat Genet. 2009;41:654–6.
20. Wang H, Chen Y, Wu G. SDHB deficiency promotes TGFβ-mediated invasion and metastasis of colorectal cancer through transcriptional repression complex SNAIL1-SMAD3/4. Transl Oncol. 2016;9:512–20.
21. Loriot C, Domingues M, Berger A, Menara M, Ruel M, Morin A, Castro-Vega L-J, Letouzé É, Martinelli C, Bemelmans A-P, et al. Deciphering the molecular basis of invasiveness in Sdhb-deficient cells. Oncotarget. 2015;6:32955–65.
22. Aspuria P-JP, Lunt SY, Väremo L, Vergnes L, Gozo M, Beach JA, Salumbides B, Reue K, Wiedemeyer WR, Nielsen J, et al. Succinate dehydrogenase inhibition leads to epithelial-mesenchymal transition and reprogrammed carbon metabolism. Cancer Metabolism. 2014;2:21.
23. Kim S, Kim DH, Jung W-H, Koo JS. Succinate dehydrogenase expression in breast cancer. SpringerPlus. 2013;2:299.
24. Ito K, Ito K. Metabolism and the control of cell fate decisions and stem cell renewal. Annu Rev Cell Dev Biol. 2016;32:399–409.
25. Lopez-Otin C, Galluzzi L, Freije JM, Madeo F, Kroemer G. Metabolic control of longevity. Cell. 2016;166:802–21.
26. Colvin H, Nishida N, Konno M, Haraguchi N, Takahashi H, Nishimura J, Hata T, Kawamoto K, Asai A, Tsunekuni K, et al. Oncometabolite D-2-hydroxyglurate directly induces epithelial-mesenchymal transition and is associated with distant metastasis in colorectal cancer. Sci Rep. 2016;6:36289.
27. Hirschey MD, DeBerardinis RJ, Diehl AME, Drew JE, Frezza C, Green MF, Jones LW, Ko YH, Le A, Lea MA, et al. Dysregulated metabolism contributes to oncogenesis. Semin Cancer Biol. 2015;35 Suppl:S129–50.
28. Guha M, Srinivasan S, Ruthel G, Kashina AK, Carstens RP, Mendoza A, Khanna C, Van Winkle T, Avadhani NG. Mitochondrial retrograde signaling induces epithelial–mesenchymal transition and generates breast cancer stem cells. Oncogene. 2013;33:5238.
29. Grassian AR, Lin F, Barrett R, Liu Y, Jiang W, Korpal M, Astley H, Gitterman D, Henley T, Howes R, et al. Isocitrate dehydrogenase (IDH) mutations promote a reversible ZEB1/MicroRNA (miR)-200-dependent epithelial-mesenchymal transition (EMT). J Biol Chem. 2012;287:42180–94.
30. Chrisanthar R, Knappskog S, Løkkevik E, Anker G, Østenstad B, Lundgren S, Risberg T, Mjaaland I, Skjønsberg G, Aas T, et al. Predictive and prognostic impact of TP53 mutations and MDM2 promoter genotype in primary breast cancer patients treated with epirubicin or paclitaxel. PLoS One. 2011;6:e19249.
31. Wik E, Raeder MB, Krakstad C, Trovik J, Birkeland E, Hoivik EA, Mjos S, Werner HM, Mannelqvist M, Stefansson IM, et al. Lack of estrogen receptor-alpha is associated with epithelial-mesenchymal transition and PI3K alterations in endometrial carcinoma. Clin Cancer Res. 2013;19:1094–105.
32. Hodneland Nilsson LI, Nitschke Pettersen IK, Nikolaisen J, Micklem D, Avsnes Dale H, Vatne Røsland G, Lorens J, Tronstad KJ. A new live-cell reporter strategy to simultaneously monitor mitochondrial biogenesis and morphology. Sci Rep. 2015;5:17217.
33. Gjerdrum C, Tiron C, Høiby T, Stefansson I, Haugen H, Sandal T, Collett K, Li S, McCormack E, Gjertsen BT, et al. Axl is an essential epithelial-to-mesenchymal transition-induced regulator of breast cancer metastasis and patient survival. Proc Natl Acad Sci. 2010;107:1124–9.
34. Slaymaker IM, Gao L, Zetsche B, Scott DA, Yan WX, Zhang F. Rationally engineered Cas9 nucleases with improved specificity. Science (New York, NY). 2016;351:84–8.
35. VanLinden MR, Dölle C, Pettersen IKN, Kulikova VA, Niere M, Agrimi G, Dyrstad SE, Palmieri F, Nikiforov AA, Tronstad KJ, Ziegler M. Subcellular distribution of NAD+ between cytosol and mitochondria determines the metabolic profile of human cells. J Biol Chem. 2015;290:27644–59.
36. Nikolaisen J, Nilsson LIH, Pettersen IKN, Willems PHGM, Lorens JB, Koopman WJH, Tronstad KJ. Automated quantification and integrative analysis of 2D and 3D mitochondrial shape and network properties. PLoS One. 2014;9:e101365.
37. Guerra F, Guaragnella N, Arbini AA, Bucci C, Giannattasio S, Moro L. Mitochondrial dysfunction: a novel potential driver of epithelial-to-mesenchymal transition in cancer. Front Oncol. 2017;7:295.
38. Tronstad KJ, Nooteboom M, Nilsson LIH, Nikolaisen J, Sokolewicz M, Grefte S, Pettersen IKN, Dyrstad S, Hoel F, Willems PHGM, Koopman WJH. Regulation and quantification of cellular mitochondrial morphology and content. Curr Pharm Des. 2014;20:5634–52.
39. King A, Selak MA, Gottlieb E. Succinate dehydrogenase and fumarate hydratase: linking mitochondrial dysfunction and cancer. Oncogene. 2006;25:4675–82.
40. Haraguchi M, Indo HP, Iwasaki Y, Iwashita Y, Fukushige T, Majima HJ, Izumo K, Horiuchi M, Kanekura T, Furukawa T, Ozawa M. Snail modulates cell metabolism in MDCK cells. Biochem Biophys Res Commun. 2013;432:618–25.
41. Chandra D, Singh KK. Genetic insights into OXPHOS defect and its role in cancer. Biochim Biophys Acta. 2011;1807:620–5.
42. Sciacovelli M, Gonçalves E, Johnson TI, Zecchini VR, da Costa ASH, Gaude E, Drubbel AV, Theobald SJ, Abbo SR, Tran MGB, et al. Fumarate is an epigenetic modifier that elicits epithelial-to-mesenchymal transition. Nature. 2016;537:544.
43. Katajisto P, Dohla J, Chaffer CL, Pentinmikko N, Marjanovic N, Iqbal S, Zoncu R, Chen W, Weinberg RA, Sabatini DM. Stem cells. Asymmetric apportioning of aged mitochondria between daughter cells is required for stemness. Science. 2015;348:340–3.
44. Chen H, Detmer SA, Ewald AJ, Griffin EE, Fraser SE, Chan DC. Mitofusins Mfn1 and Mfn2 coordinately regulate mitochondrial fusion and are essential for embryonic development. J Cell Biol. 2003;160:189–200.
45. Vander Heiden MG, Cantley LC, Thompson CB. Understanding the Warburg effect: the metabolic requirements of cell proliferation. Science. 2009;324:1029–33.
46. Mohyeldin A, Garzon-Muvdi T, Quinones-Hinojosa A. Oxygen in stem cell biology: a critical component of the stem cell niche. Cell Stem Cell. 2010;7:150–61.
47. Msaouel P, Malouf GG, Tannir NM. Metabolic derangements in succinate dehydrogenase B–mutated renal-cell carcinomas: more than meets the eye? JCO Precision Oncol. 2017;1:1–4.

48. Letouzé E, Martinelli C, Loriot C, Burnichon N, Abermil N, Ottolenghi C, Janin M, Menara M, Nguyen An T, Benit P, et al. SDH mutations establish a hypermethylator phenotype in paraganglioma. Cancer Cell. 2013;23:739–52.
49. Li W, Ma J, Ma Q, Li B, Han L, Liu J, Xu Q, Duan W, Yu S, Wang F, Wu E. Resveratrol inhibits the epithelial-mesenchymal transition of pancreatic cancer cells via suppression of the PI-3K/Akt/NFB pathway. Curr Med Chem. 2013;20:4185–94.
50. Kasznicki J, Sliwinska A, Drzewoski J. Metformin in cancer prevention and therapy. Ann Transl Med. 2014;2:57.

Figure S1

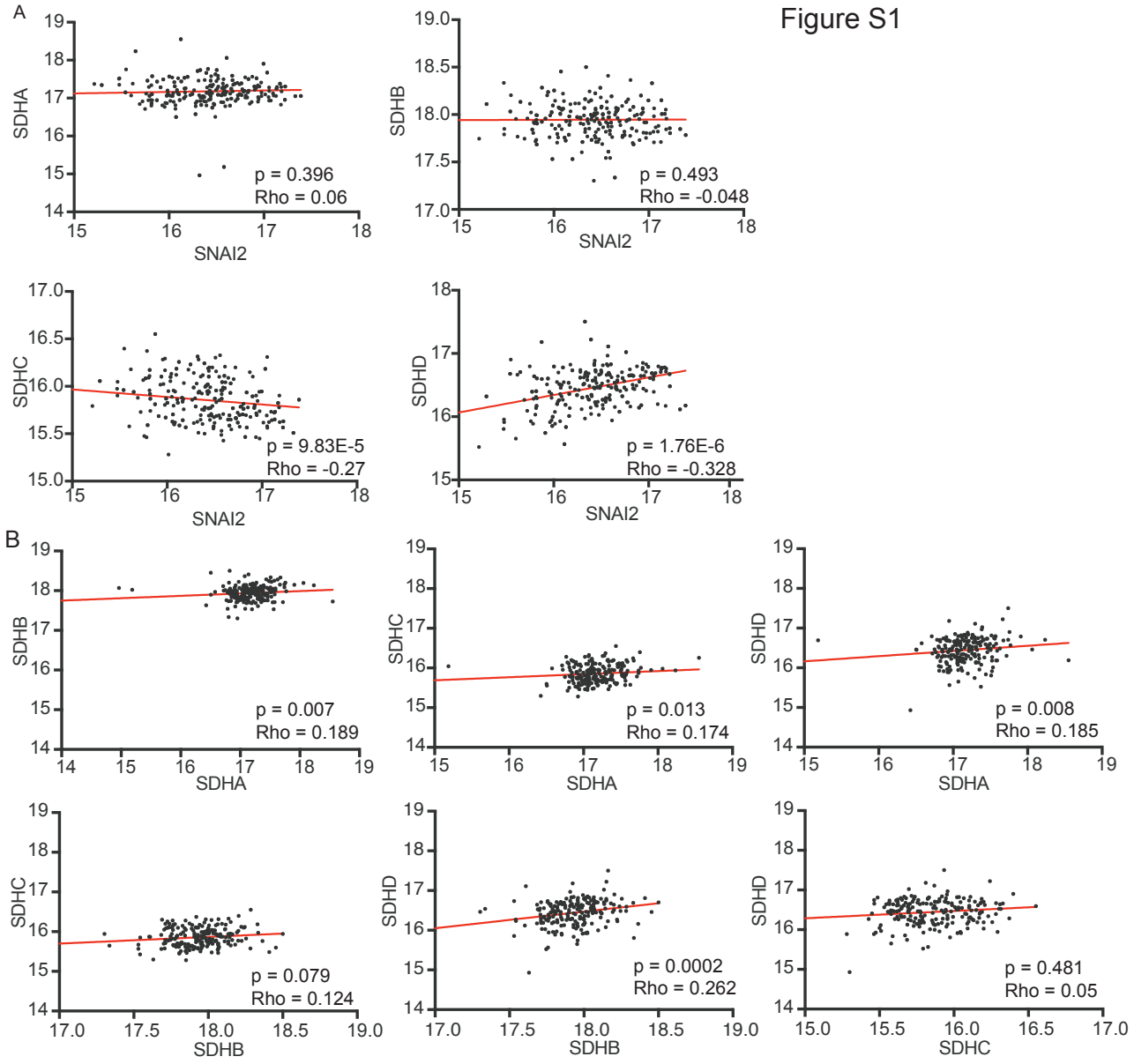

Figure S1: (A) Correlation analysis (Spearman) between the expression of the four SDH subunits relative to SNAI2 in the n=204 breast cancer cohort. (B) Correlation analysis (Spearman) between the individual SDH subunits in the n=204 breast cancer cohort.

Figure S2

A

Homo sapiens chromosome 1, GRCh38.p7 Primary Assembly

Sequence ID: NC_000001.11 Length: 248956422 Number of Matches: 1

Range 1: 161328241 to 161328620 GenBank Graphics Next Match Previous Match

Score	Expect	Identities	Gaps	Strand
614 bits(332)	8e-173	366/380(96%)	11/380(2%)	Plus/Plus

Features: succinate dehydrogenase cytochrome b560 subunit, mitochon...
succinate dehydrogenase cytochrome b560 subunit, mitochon...

```
Query  546        attcgcccttctcggcctcccaaagagctgagattacaggcctgagcaaccatgcctggc  605
Sbjct  161328241  ATCCGCCCGCCTCGGCCTCCCAAAGAGCTGAGATTACAGGCCTGAGCAACCATGCCTGGC  161328300

Query  606        TTGGTATTGCAAAATATTGACTTAATAAAACGTTATGCAAAATATTAAACCAAGTTTACT  665
Sbjct  161328301  TTGGTATTGCAAAATATTGACTTAATAAAACGTTATGCAAAATATTAAACCAAGTTTACT  161328360

Query  666        TTTAGTTATTTTCAAACGGTCTGGTTTTATTTTAGTGCTGTTCCTTTGGGAACCACGGCC  725
Sbjct  161328361  TTTAGTTATTTTCAAACGGTCTGGTTTTATTTTAGTGCTGTTCCTTTGGGAACCACGGCC  161328420

Query  726        AAAGAAGAGATGGAGCGGTTCTGGAATAAGAATATAGGTTCAAACCGTCCTCT-------  778
Sbjct  161328421  AAAGAAGAGATGGAGCGGTTCTGGAATAAGAATATAGGTTCAAACCGTCCTCTGTCTCCC  161328480

Query  779        ----TTACTATCTACAGGTAAGGAAGGATTCTGGAGCCAGAGAATCTAGAGGTAGTGGGT  834
Sbjct  161328481  CACATTACTATCTACAGGTAAGGAAGGATTCTGGAGCCAGAGAATCTAGAGGTAGTGGGT  161328540

Query  835        GAAAGTTCTGAAGGTTGATCTTTAGCCTACTTGATACTTCCCTCACTTTTACTCAACCAA  894
Sbjct  161328541  GAAAGTTCTGAAGGTTGATCTTTAGCCTACTTGATACTTCCCTCACTTTTACTCAACCAA  161328600

Query  895        AATACTGCTATGTAGATGAG  914
Sbjct  161328601  AATACTGCTATGTAGATGAG  161328620
```

B

Homo sapiens chromosome 11, alternate assembly CHM1_1.1

Sequence ID: NC_018922.2 Length: 134889443 Number of Matches: 1

Range 1: 111840691 to 111841012 GenBank Graphics Next Match Previous Match

Score	Expect	Identities	Gaps	Strand
468 bits(518)	5e-129	292/322(91%)	29/322(9%)	Plus/Plus

Features: succinate dehydrogenase [ubiquinone] cytochrome b small s...
succinate dehydrogenase [ubiquinone] cytochrome b small s...

```
Query  64         CTCTCGACTTCCGGTTCACCCAGCATTTCCACTTCCCTGTTTTCTTTCGTCGTCGTGGGT  123
Sbjct  111840691  CTCTCGACTTCCGGTTCACCCAGCATTTCCTCTTCCCTGTTTTCTTTCGTCGTCGTGGGT  111840750

Query  124        GGGAATTGTCGCCTAAGTGGTTCCGGGTTGGTGGATGACCTTGAGCCCTCAGGAACGAGA  183
Sbjct  111840751  GGGAATTGTCGCCTAAGTGGTTCCGGGTTGGTGGATGACCTTGAGCCCTCAGGAACGAGA  111840810

Query  184        TGGCGGTTCTCTGGAGGCTGAGTGCCGTTTGCGGTGCCCTAG----------------  225
Sbjct  111840811  TGGCGGTTCTCTGGAGGCTGAGTGCCGTTTGCGGTGCCCTAGGAGGCCGAGGTGAGGGGT  111840870

Query  226        ----------GAGGTGCTTAGCGTAGCCTCCAGCCAGGGAAGGGGATGGAAGTGAGGAC  274
Sbjct  111840871  CTTCCCACCCTGAGGTGCTTAGCGTAGCCTCCAGCCAGGGAAGGGGATGGAAGTGAGGAC  111840930

Query  275        TCATCTGCCGGGTGGGAGATCTCTTGAGGAGAAGAAAATACCGAAATCACAGCAATGACC  334
Sbjct  111840931  TCATCTGCCGGGTGGGAGATCTCTTGAGGAGAAGAAAATACCGAAATCACAGCAATGACC  111840990

Query  335        ACTGTAGTCTAGGGGTCCAGAT  356
Sbjct  111840991  ACTGTAGTCTAGGGGTCCAGAT  111841012
```

C

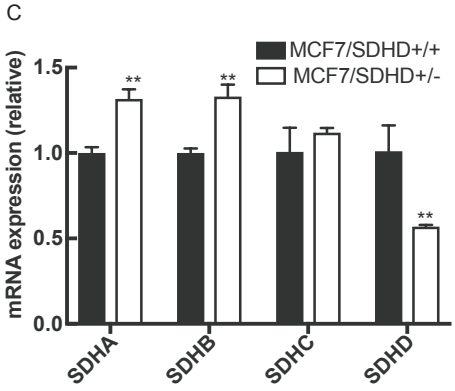

Figure S2: (A) Sequence alignment of the SDHC gene in CRIPSR/ Cas9- modified MCF7 cells and the SDHC wild-type gene, revealing an 11bp frameshift deletion. (B)Sequence alignment of the SDHD gene in CRIPSR/Cas9-modified MCF7 cells and the SDHD wild-type gene, revealing an 29bp frameshift deletion. (C) qPCR analysis of SDHA-D in MCF7 SDHD +/- cells.

Figure S3

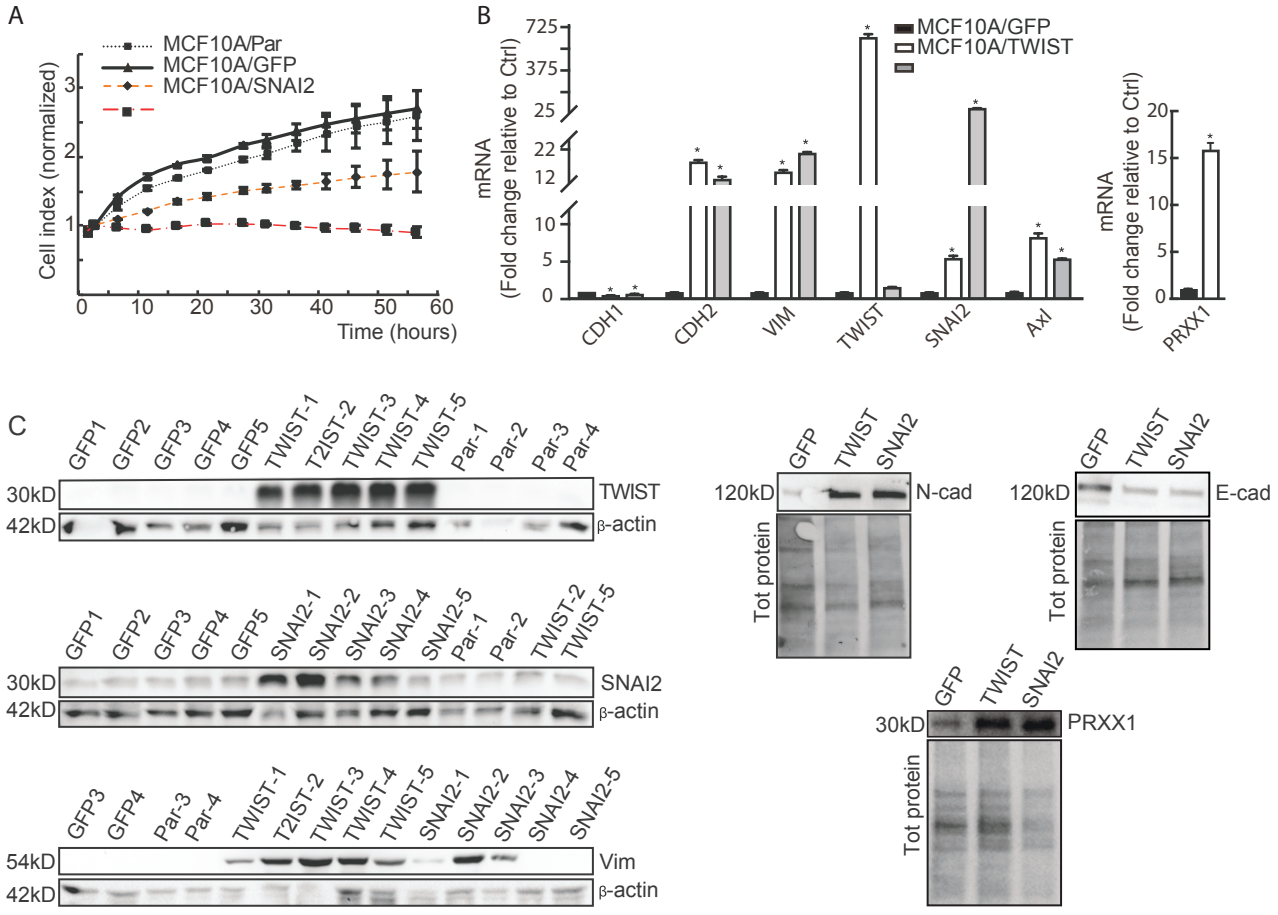

Figure S3: Characterization of the EMT process in MCF10A cells upon overexpression of TWIST and SNAI2 (Slug). (A) Cell proliferation was measured by the use of the xCelligence RTCA DP instrument (ACEA Bioscience, San Diego, CA), which measures cellular impedance (expressed as “Cell index”). The cells (MCF10A, MCF10A/GFP, MCF10A/TWIST, MCF10A/SNAI2) were seeded at a density of 10 000 cells/well. (B) mRNA and (C) protein expression of TWIST and SNAI2, and epithelial (E-cadherin (CDH1)) and mesenchymal (N-cadherin (CDH2), Vimentin (VIM), Twist, SNAI2, Axl and PRXX1) markers. The numbers at the end of the sample name in the western blots refer to passage number after transduction.

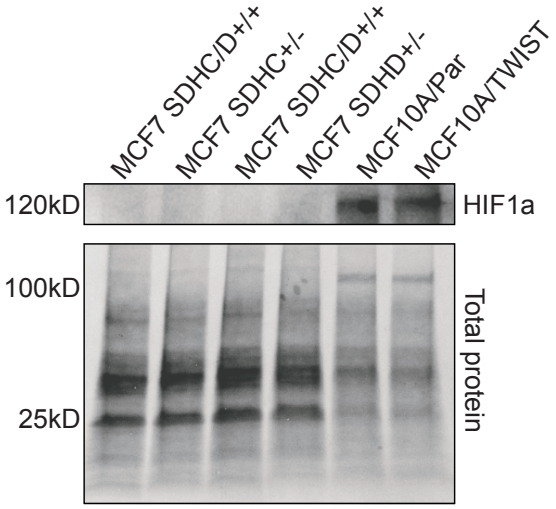

Figure S4: Western blot analysis of HIF1α in MCF7 SDHC/D+/+, MCF7 SDHC+/-, and MCF7 SDHD+/- cells, and in MCF10A/Par and MCF10A/TWIST cells.

Table S1

A

Category	SDHAvsEMT	SDHAvsEMT	SDHBvsEMT	SDHBvsEMT	SDHCvsEMT	SDHCvsEMT	SDHDvsEMT	SDHDvsEMT
	Spear.Rho	Spear.pv	Spear.Rho	Spear.pv	Spear.Rho	Spear.pv	Spear.Rho	Spear.pv
Breast cancer cell	´-0.1578	0.2686	0.0957	0.504	´-0.5174	0.0001	-0.0353	0.8060

B

Disease	SDHAvsEMT	SDHAvsEMT	SDHBvsEMT	SDHBvsEMT	SDHCvsEMT	SDHCvsEMT	SDHDvsEMT	SDHDvsEMT
	Spear.Rho	Spear.pv	Spear.Rho	Spear.pv	Spear.Rho	Spear.pv	Spear.Rho	Spear.pv
Breast invasive carcinoma	´-0.0777	0.0068	´-0.0611	0.0335	´-0.3373	1.2E-33	0.3676	4.51E-40
(BRCA)								

Table S1: Spearman correlation analysis was applied to assess associations between SDH subunit gene expression and EMT315 score on (A) Encyclopedia breast cancer cell line collection (56 cell lines) and for (B)TCGA RNA-seq extracted from GDAC version 2018_01_28 from breast cancer carcinoma cohort (7).

Table S2

	SDHA	SDHA	SDHB	SDHB	SDHC	SDHC	SDHD	SDHD	SNAI2	SNAI2	TWIST1	TWIST1	EMT	EMT
Gene	Rho	pv	Rho	pv	Rho	pv	Rho	pv	Rho	pv	Rho	pv	Rho	pv
SLC2A1	0,002	9,0E-01	0,063	6,7E-05	0,023	1,43E-01	-0,068	1,70E-05	-0,0953	1,45E-09	-0,048	2,22E-03	0,060	1,31E-04
SLC2A3 (Gl	-0,012	4,4E-01	-0,070	8,8E-06	-0,160	1,84E-24	0,102	9,68E-11	0,2313	6,79E-50	0,324	1,28E-98	0,540	3,5E-302
HK1	0,151	6,5E-22	0,084	1,1E-07	0,127	6,01E-16	-0,091	7,16E-09	-0,0236	1,35E-01	-0,013	0,423948	-0,308	4,59E-89
HK2	0,147	6,4E-21	0,087	4,0E-08	0,098	5,17E-10	-0,031	4,80E-02	-0,1503	1,01E-21	-0,024	0,125805	-0,192	9,43E-35
PKM2	0,203	1,2E-38	0,260	4,0E-63	0,166	3,69E-26	0,018	2,46E-01	0,0434	0,00596	-0,020	2,13E-01	-0,066	2,86E-05
LDHA	0,126	1,2E-15	0,237	1,7E-52	0,181	7,85E-31	0,162	4,05E-25	0,0413	8,83E-03	-0,029	6,61E-02	0,008	6,14E-01
PDK1	0,069	1,1E-05	0,071	7,6E-06	0,020	1,95E-01	0,027	0,084600	-0,1724	3,87E-28	-0,170	2,00E-27	0,244	1,92E-55
SLC16A3	0,041	9,7E-03	0,145	2,0E-20	0,089	1,56E-08	-0,071	6,08E-06	0,0590	0,00018	0,088	2,74E-08	0,183	1,64E-31
SLC16A4	-0,151	7,5E-22	-0,051	1,2E-03	0,043	6,41E-03	0,151	8,85E-22	0,2441	1,61E-55	0,128	4,64E-16	-0,025	1,13E-01
VEGFA	0,076	1,2E-06	0,067	2,1E-05	0,093	4,00E-09	0,074	3,11E-06	0,0412	0,00910	-0,016	3,26E-01	-0,006	6,83E-01
SNAI1	-0,023	1,4E-01	-0,156	3,6E-23	-0,099	3,23E-10	-0,138	1,71E-18	-0,0459	3,64E-03	-0,005	7,65E-01	0,252	2,84E-59
SNAI2	-0,095	1,6E-09	-0,045	4,7E-03	-0,062	9,56E-05	0,250	2,97E-58	1,0000	0	0,487	8,1E-238	0,351	5,7E-117
TWIST1	-0,043	6,3E-03	-0,126	9,3E-16	-0,123	5,09E-15	0,059	0,000205	0,4867	8,1E-238	1,000	0,0E+00	0,280	3,00E-73
VIM	0,009	5,5E-01	-0,007	6,6E-01	-0,066	2,51E-05	0,215	2,29E-43	0,5766	0	0,377	1,5E-135	0,600	0,0E+00
MMP2	-0,066	3,2E-05	-0,224	6,5E-47	-0,158	7,90E-24	0,030	0,060545	0,6638	0,0E+00	0,540	1,9E-302	0,273	1,14E-69
MMP9	0,045	4,2E-03	0,055	5,2E-04	-0,088	2,01E-08	0,007	6,69E-01	0,1367	3,30E-18	0,117	1,25E-13	0,384	1,8E-141
MMP14	-0,112	1,2E-12	-0,281	6,9E-74	-0,086	5,20E-08	-0,193	4,87E-35	0,3520	2,1E-117	0,217	4,69E-44	0,220	4,71E-45
PDK4	-0,099	2,7E-10	-0,075	2,0E-06	-0,039	1,25E-02	0,056	0,000389	0,1151	2,60E-13	0,019	2,29E-01	0,069	1,19E-05
PPARGC1A	0,027	8,4E-02	-0,083	1,2E-07	-0,058	2,50E-04	0,001	0,943557	0,0402	1,08E-02	0,056	3,60E-04	0,181	9,54E-31
CPT2	0,201	1,0E-37	0,330	2E-102	0,263	2,16E-64	0,082	2,33E-07	-0,1565	2,03E-23	-0,187	5,82E-33	-0,306	8,03E-88
SLC2A4 (Gl	-0,013	4,1E-01	-0,183	1,1E-31	-0,105	2,60E-11	-0,234	7,59E-51	-0,1735	1,73E-28	-0,087	3,37E-08	-0,001	9,32E-01
NRF1	-0,164	1,1E-25	-0,260	3,9E-63	-0,130	1,45E-16	-0,083	1,46E-07	0,0070	0,65835	0,078	6,43E-07	0,020	1,97E-01
TFAM	0,037	2,0E-02	0,286	2,7E-76	0,200	1,70E-37	0,398	3,3E-152	0,0176	0,26405	-0,031	0,04850	0,058	2,12E-04
PPARGC1A	0,027	8,4E-02	-0,083	1,2E-07	-0,058	0,00025	0,001	9,44E-01	0,0402	1,08E-02	0,056	0,00036	0,181	9,54E-31
TOMM20	0,071	6,1E-06	0,215	2,8E-43	0,396	9,6E-151	0,195	1,00E-35	-0,0208	0,187073	-0,104	3,44E-11	-0,196	5,17E-36
SLC25A4	0,204	4,7E-39	0,291	5,7E-79	0,220	3,44E-45	-0,011	0,503160	-0,0858	5,14E-08	-0,037	2,04E-02	-0,388	2,2E-144
ATP1B1	-0,087	3,8E-08	-0,074	2,6E-06	0,131	7,50E-17	0,085	5,83E-08	0,0984	4,21E-10	0,033	0,035276	-0,167	1,44E-26
VDAC1	0,253	8,2E-60	0,400	4E-154	0,378	9,4E-137	0,100	2,45E-10	-0,0576	2,59E-04	-0,108	6,18E-12	-0,222	4,70E-46
MFN1	0,085	6,9E-08	0,248	3,9E-57	0,139	9,36E-19	0,261	1,66E-63	0,0828	1,51E-07	-0,020	2,10E-01	0,009	0,560201
MFN2	0,176	2,7E-29	0,327	6E-101	0,043	5,91E-03	-0,047	3,19E-03	-0,1123	9,79E-13	-0,052	0,00096	-0,145	3,07E-20
OPA1	-0,003	8,7E-01	0,060	1,3E-04	0,071	6,84E-06	0,108	5,92E-12	0,0323	4,10E-02	-0,007	6,40E-01	-0,014	0,35938
DNM1L	0,177	1,0E-29	0,400	3E-154	0,283	1,01E-74	0,197	2,79E-36	-0,0233	0,139847	-0,098	5,10E-10	0,039	1,28E-02
FIS1	0,103	5,8E-11	0,268	5,5E-67	0,280	5,60E-73	0,087	3,93E-08	0,0045	0,774329	-0,016	3,12E-01	-0,290	1,03E-78
SOD1	0,199	3,6E-37	0,417	5E-169	0,313	8,70E-92	0,091	6,86E-09	-0,1501	1,17E-21	-0,119	3,09E-14	-0,281	1,29E-73
SOD2	0,123	4,8E-15	0,242	1,9E-54	0,089	1,82E-08	0,241	4,45E-54	0,0572	2,87E-04	0,018	2,64E-01	0,553	0,0E+00
GPX1	0,038	1,7E-02	0,272	2,9E-69	0,108	8,49E-12	0,133	2,85E-17	0,0596	0,000160	0,052	0,00092	0,104	4,10E-11
GPX2	-0,176	3,5E-29	-0,309	2,7E-89	-0,242	1,55E-54	-0,219	7,78E-45	-0,1002	2,00E-10	-0,038	1,64E-02	-0,035	2,75E-02
GPX3	-0,017	2,7E-01	-0,057	2,7E-04	-0,082	2,29E-07	0,073	3,97E-06	0,2459	2,44E-56	0,242	1,25E-54	0,294	8,09E-81
GPX4	0,093	3,8E-09	0,217	8,3E-44	0,139	7,20E-19	-0,033	3,88E-02	-0,0999	2,29E-10	-0,034	0,02971	-0,386	1,0E-142
GPX5	-0,100	2,4E-10	-0,303	2,8E-86	-0,172	5,36E-28	-0,258	4,25E-62	-0,1871	6,11E-33	-0,109	4,77E-12	-0,017	0,277220
GPX7	0,002	9,1E-01	0,049	2,1E-03	-0,026	0,096863	0,232	2,76E-50	0,4882	1,5E-239	0,336	2,6E-106	0,580	0,0E+00
GPX8	-0,060	2,7E-02	0,063	2,1E-02	0,109	6,49E-05	0,262	1,72E-22	0,5077	5,11E-89	0,258	6,23E-22	0,178	4,44E-11
GSR	0,125	2,3E-15	0,138	1,5E-18	0,184	6,16E-32	0,057	0,000328	-0,0721	4,86E-06	-0,123	6,46E-15	-0,230	1,61E-49
CAT	0,048	2,5E-03	0,109	3,9E-12	0,151	7,93E-22	0,326	5,6E-100	0,1630	2,67E-25	0,045	4,66E-03	0,075	2,01E-06
PRDX1	0,277	9,2E-72	0,467	2E-216	0,258	7,05E-62	0,126	1,16E-15	-0,1448	2,93E-20	-0,159	3,39E-24	-0,096	1,21E-09
PRDX2	0,198	9,7E-37	0,313	3,3E-92	0,213	3,26E-42	0,057	0,000297	-0,2172	4,72E-44	-0,148	4,82E-21	-0,366	1,3E-127
PRDX3	0,124	3,9E-15	0,356	4E-120	0,318	7,43E-95	0,244	1,14E-55	-0,0337	0,032918	-0,121	1,85E-14	-0,453	5,0E-202
PRDX4	0,164	1,1E-25	0,342	2E-110	0,218	2,72E-44	0,223	1,55E-46	0,0677	1,76E-05	0,001	9,63E-01	0,224	6,93E-47
PRDX5	0,033	2,3E-01	0,205	2,7E-14	0,125	4,21E-06	0,176	7,37E-11	0,0055	0,840649	-0,060	0,027751	-0,053	0,05155
PRDX6	0,192	1,0E-34	0,183	1,3E-31	0,422	1,1E-172	0,087	3,73E-08	-0,0669	2,23E-05	-0,015	0,353144	0,088	1,96E-08
TXN	0,182	3,7E-31	0,384	2E-141	0,229	5,45E-49	0,192	1,69E-34	-0,0946	1,92E-09	-0,038	1,52E-02	-0,047	2,72E-03
TXN2	0,150	1,4E-21	0,083	1,6E-07	0,085	7,32E-08	0,042	7,36E-03	-0,0806	3,16E-07	-0,002	9,04E-01	-0,143	7,91E-20
TXNRD1	0,176	2,2E-29	0,308	4,6E-89	0,100	2,14E-10	0,124	3,52E-15	-0,1007	1,63E-10	-0,087	3,76E-08	0,071	7,50E-06
TXNRD2	0,104	4,9E-11	-0,040	1,1E-02	0,076	1,30E-06	-0,178	8,42E-30	-0,1949	1,20E-35	-0,075	2,13E-06	-0,324	6,37E-99
TXNRD3	-0,023	1,4E-01	-0,054	6,8E-04	0,049	0,00183	-0,022	1,55E-01	0,0214	1,75E-01	0,003	8,70E-01	0,186	1,09E-32
BECN1	0,008	6,0E-01	0,269	1,0E-67	0,205	2,50E-39	0,129	2,64E-16	-0,0048	0,76329	-0,053	7,50E-04	-0,404	1,9E-157
PINK1	0,001	9,4E-01	0,205	3,3E-39	-0,050	0,001571	-0,011	0,468433	0,0259	0,10085	-0,011	5,00E-01	-0,094	2,82E-09
PARK2	-0,120	2,4E-14	-0,225	3,0E-47	-0,144	4,02E-20	-0,173	1,96E-28	-0,1276	4,88E-16	-0,071	6,20E-06	0,005	7,42E-01
BNIP3	0,125	1,9E-15	0,245	4,4E-56	0,174	9,31E-29	0,178	5,42E-30	-0,0546	5,34E-04	-0,043	6,67E-03	-0,154	7,39E-23
BNIP3L	-0,022	1,6E-01	0,102	1,1E-10	0,142	1,32E-19	0,123	5,36E-15	0,1308	9,02E-17	0,062	7,57E-05	-0,124	3,36E-15
ZNF746	0,075	6,2E-03	-0,017	5,3E-01	-0,003	0,902185	-0,125	4,02E-06	-0,0014	0,959629	0,010	0,72092	-0,040	0,14585
ULK1	0,081	2,9E-07	-0,088	2,8E-08	0,029	7,06E-02	-0,366	9,3E-128	-0,1373	2,40E-18	-0,007	0,63843	-0,341	5,2E-110
ULK2	-0,057	2,8E-04	0,073	3,2E-06	0,091	7,23E-09	0,012	0,456505	0,1150	2,73E-13	0,048	2,36E-03	-0,231	1,28E-49

Table S2: Gene expression (mRNA) correlation analysis (Spearman) between SDH subunits and listed genes in the Affymetrix breast cancer patient meta cohort (n=3,992)

A

Probes all from applied biosystems

Gene name	Gene	Catalog number
AXL receptor tyrosine kinase	AXL	hs01064444
Carnitine palmitoyltransferase 1A	CPT1A	hs00912671
Cytochrome c	CYCS	hs01588974
Dynamin 1 like	DNM1L	hs01552605
E-cadherin	CHD1	hs01023894
Eukaryotic 18S rRNA Endogenous Control	18S	4310893E
Mitochondrially encoded NADH dehydrogenase 1	MT-ND1	hs02596873
Mitofusin 1	MFN1	hs00966851
Mitofusin 2	MFN2	hs00208382
N-cadherin	CDH2	hs00983056
OPA1, mitochondrial dynamin like GTPase	OPA1	hs01047018
Parkin RBR E3 ubiquitin protein ligase	PARK2	hs01038325
PTEN induced putative kinase 1	PINK1	hs00260868
Snail family zinc finger 2	SNAI2	hs00950344
Succinate dehydrogenase complex, subunit A, flavoprotein (Fp)	SDHA	hs00417200
Succinate dehydrogenase complex, subunit B, iron sulfur (Ip)	SDHB	hs01042482
Succinate dehydrogenase complex, subunit C, integral membrane protein	SDHC	hs01698067
Succinate dehydrogenase complex subunit D	SDHD	hs00829723
Vimentin	VIM	hs00185584

B Table S3

Antibody	Catalog number	Company
Anti-DRP1 antibody	ab56788	Abcam
Anti-N Cadherin antibody	ab18203	Abcam
Anti-SDHC antibody	ab155999	Abcam
Anti-SDHA antibody	ab14715	Abcam
Anti-SDHB antibody	ab14714	Abcam
Anti-Vimentin antibody	ab8978	Abcam
Anti-Vimentin antibody	ab92547	Abcam
E-Cadherin	3195	Cell Signaling
E-Cadherin	ab40772	Abcam
E-Cadherin	14472	Cell Signaling
Goat anti-Mouse IgG (H+L) Cross-Adsorbed Secondary Antibody, Alexa Fluor 594	a11005	Thermo Fisher
Goat anti-Rabbit IgG (H+L) Cross-Adsorbed Secondary Antibody, Alexa Fluor 647	a21244	Thermo Fisher
PGC1 alpha	sc-13067	Santa Cruz
Purified Mouse Anti-OPA1	612606	BD Transduction Laboratories ™
Tom20 Antibody (FL-145)	sc-11415	Santa Cruz Biotech,
HIF1a Antibody	#3716	Cell Signaling

C

Dye	Catalog number	Company
Alexa Fluor™ 555 Phalloidin	A34055	Thermo Fisher
Hoechst	33342	Thermo Fisher
ProLong™ Diamond Antifade Mountant with DAPI	P36962	Thermo Fisher
Pyronin Y	213519	Sigma

Table S3: (A) Probes used in experiments presented. (B) Antibodies used in experiments presented. (C) Probes and dyes used in experiments presented.

SUPPLEMENTAL METHODS

Gene expression analysis (GEA) of human breast cancer samples

Breast cancer samples were from a HUS-cohort of 204 patients diagnosed with locally advanced disease and randomized to neoadjuvant epirubicin or paclitaxel monotherapy in a prospective study aiming at identifying predictive factors (termed the n=204 cohort). These patients have been described in detail previously [1]. The breast cancer meta-cohort (*n*=3992) [2] was previously curated from 26 Affymetrix U133A or U133 Plus2 gene expression cohorts publicly available on GEO. Briefly, the 26 cohorts were RMA-normalized, and subsequently standardized using ComBat [3]. An EMT signature score (here called EMT8 score) was calculated as previously reported, including the EMT related genes *CDH1, CTNNA2, CTNNB1, CDH2* and *CDH3* [4, 5] in addition to *TWIST, SNAI2* and *KRT19* expression. The sum of the downregulated genes (*CDH1, CTNNB1, CTNNA2* and *KRT19*) were subtracted from the sum of the upregulated genes (*CDH2*, *CDH3, SNAI2* and *TWIST*). A second score (here called EMT315 score) is based on the two-sample Kolmogorov-Smirnov test, and estimates the difference in cumulative distribution between consensus epithelial and mesenchymal genes (315 genes in total) derived from 6 carcinoma types [2]. For both EMT signature scores the expression values were mean normalized and scaled to the same standard deviation (SD). Analysis was performed using the statistical software SPSS (Statistical Package of Social Science) version 22.0. Spearman correlation coefficient analyses were applied to assess correlation between SDHs gene expression and EMT315 score. The breast cancer subtypes were classified based on the molecular subgroups published by Perou CM, et al in 2000 [6]. When relevant, the tumors were analyzed as estrogen receptor negative *vs* positive (ER-/+), or as basal like *vs* non-basal like. Additional histological subclassification into ductal and luminal carcinoma was available for the n=204 cohort.

Cell culture

The breast epithelial cells MCF10A (ATCC, Manassas, VA) were grown in DMEM/F12 (Dulbecco's Modified Eagle's Medium/Nutrient F-12 Ham, Sigma) containing 50 µg/mL penicillin/streptomycin (P-0781, Sigma), 5 % horse serum (B15021, PAA/GE Healthcare, Little Chalfont, UK), 20 ng/ml EGF (E9644, Sigma), 10 µg/ml insulin (I1882, Sigma), 0.5 µg/ml hydrocortisone (H0888, Sigma) and 100 ng/ml cholera toxin (C8052, Sigma). The MCF7 breast cancer cell line (ATCC) was cultured in EMEM (BL12-125F, ATCC) which was supplemented with 10 % heat-inactivated fetal bovine serum (FBS, SH30079.03, GE Healthcare Hyclone), 1 % L-glutamine (G7513, Sigma) and 50 µg/mL penicillin/streptomycin. All cells were routinely incubated in 5 % CO_2 at 37ºC. Cells subjected to gene editing by CRISPR/Cas9 were STR-profiled before and after editing. The GlobalFiler™ PCR Amplification Kit and GeneScan 600 LIZ dye size standard (Life technologies), was used according to the manufacturer's instructions. Results were assessed by the GeneMapper®ID-X software (v.1.4) and observed alleles were compared to the theoretical alleles available at (www.atcc.org). The experiments were performed with cultures passaged less than 10 times from thawing.

Mitochondrial respiration analysis

Oxygen consumption rate (OCR) was measured using the Seahorse XFe96 Analyzer (Agilent, Santa Clara, CA), according to the manufacturers protocols and previous description [7, 8]. All materials were from Sigma-Aldrich (St. Louis, MO) unless otherwise stated. Cell number and concentrations of compounds were optimized for each cell type. The cells were transferred to the analysis plate the day before measurement, and incubated overnight. For analysis of SDH-linked activity, the cells were permeabilized to facilitate cellular uptake of succinate and ADP, by adding the Seahorse XF plasma membrane permeabilizer (PMP) (Agilent; MCF10A, 1.5 nM; MCF7, 1 nM) immediately before or under the analysis, as indicated. The cell plate was

transferred to the instrument after replacing the culture medium with the mitochondrial assay solution (MAS), containing mannitol (229 mM), sucrose (70 mM), KH_2PO_4 (10 mM), $MgCl_2$ (5 mM), HEPES (2 mM), EGTA (1 mM) and 0.2 % fatty acid free BSA. Succinate (10 mM), ADP (4 mM), oligomycin (3 µM), antimycin A (10 µM) and rotenone (10 µM) were added as indicated in the figures. For studies of mitochondrial respiration in intact cells, OCR was recorded after successive administrations of oligomycin (3 µM), CCCP (MCF10A, 1.5 µM; MCF7, 0.75µM), rotenone (1 µM) and antimycin A (1 µM). These studies were performed in cell culture medium (D5030) supplemented with glucose (10 mM), pyruvate (2 mM) and glutamine (4 mM) as the major substrates; or in MAS medium without BSA, supplemented with pyruvate (2 mM), glutamine (4 mM) or succinate (10 mM). All data were normalized to cell number using Hoechst 33342 (Thermo Fisher Scientific), or protein content, measured using the Pierce® BCA Protein Assay Kit (Thermo Fisher Scientific, Waltham, MA).

Confocal microscopy and quantitative image analysis of mitochondria

Cells were plated at a density of 50000 cells/well on coverslips placed in 24-well cell culture plates. Following over night incubation, the cells were fixed in 4 % PFA for 15 min and permeabilized with 0.5 % Triton X-100 for 4 min. After washing and blocking in TBS-T/5%BSA the cells were incubated with a mixture of primary antibodies (1:100 TOM20, FL145 Santa Cruz Biotech, Dallas, Texas; 1:500 ATPB, AB5452 Abcam, Cambridge, UK) in the blocking solution for 1 h at room temperature, and then over night at 4 ^{o}C. After washing and blocking, the cells were incubated with secondary antibodies (Alexa 546 anti-rabbit and Alexa 647 anti-mouse, (Molecular Probes, Eugene, OR) for 1 h at room temperature. The coverslips were mounted in Prolong Diamond antifade with DAPI (Thermo Fisher Scientific, Waltham, MA).

Confocal z-stacks were acquired on a confocal Leica TCS S5 microscope (Leica microsystems, Wetzlar, Germany), using a Lambda 63x 1.4 NA oil objective. Image pixel size

was 0.0944 µm (x and y) and bit depth 12, z-spacing 0.34 µm. Image processing and quantitative analysis were performed using the Image-Pro Plus software (version 7.0) (Media Cybernetics, Inc., Washington, USA), as described previously [9]. The acquired 12 bit z-stacks were background corrected (fixed level within each experiment) and processed by 3D blind deconvolution. Single cells were manually segmented to enable analysis of individual cells. The single cell z-stacks were loaded into the 3D module of the software and analyzed. The surface level was fixed for the experiments in this study. Structures larger than 0.05 μm^3 were accounted as mitochondrial objects. Mitochondrial network analysis was performed as previously described [7, 9].

REFERENCES

1. Chrisanthar R, Knappskog S, Løkkevik E, Anker G, Østenstad B, Lundgren S, Risberg T, Mjaaland I, Skjønsberg G, Aas T, et al: **Predictive and Prognostic Impact of TP53 Mutations and MDM2 Promoter Genotype in Primary Breast Cancer Patients Treated with Epirubicin or Paclitaxel.** *PLoS ONE* 2011, **6:**e19249.
2. Tan TZ, Miow QH, Miki Y, Noda T, Mori S, Huang RY-J, Thiery JP: **Epithelial-mesenchymal transition spectrum quantification and its efficacy in deciphering survival and drug responses of cancer patients.** *EMBO Molecular Medicine* 2014, **6:**1279-1293.
3. Johnson WE, Li C, Rabinovic A: **Adjusting batch effects in microarray expression data using empirical Bayes methods.** *Biostatistics* 2007, **8:**118-127.
4. Wik E, Raeder MB, Krakstad C, Trovik J, Birkeland E, Hoivik EA, Mjos S, Werner HM, Mannelqvist M, Stefansson IM, et al: **Lack of estrogen receptor-alpha is associated with epithelial-mesenchymal transition and PI3K alterations in endometrial carcinoma.** *Clin Cancer Res* 2013, **19:**1094-1105.
5. Salvesen HB, Carter SL, Mannelqvist M, Dutt A, Getz G, Stefansson IM, Raeder MB, Sos ML, Engelsen IB, Trovik J, et al: **Integrated genomic profiling of endometrial carcinoma associates aggressive tumors with indicators of PI3 kinase activation.** *Proc Natl Acad Sci U S A* 2009, **106:**4834-4839.
6. Perou CM, Sørlie T, Eisen MB, van de Rijn M, Jeffrey SS, Rees CA, Pollack JR, Ross DT, Johnsen H, Akslen LA, et al: **Molecular portraits of human breast tumours.** *Nature* 2000, **406:**747.
7. Hodneland Nilsson LI, Nitschke Pettersen IK, Nikolaisen J, Micklem D, Avsnes Dale H, Vatne Røsland G, Lorens J, Tronstad KJ: **A new live-cell reporter strategy to simultaneously monitor mitochondrial biogenesis and morphology.** *Scientific Reports* 2015, **5:**17217.
8. VanLinden MR, Dölle C, Pettersen IKN, Kulikova VA, Niere M, Agrimi G, Dyrstad SE, Palmieri F, Nikiforov AA, Tronstad KJ, Ziegler M: **Subcellular Distribution of NAD+ between Cytosol and Mitochondria Determines the Metabolic Profile of Human Cells.** *Journal of Biological Chemistry* 2015, **290:**27644-27659.

9. Nikolaisen J, Nilsson LIH, Pettersen IKN, Willems PHGM, Lorens JB, Koopman WJH, Tronstad KJ: **Automated Quantification and Integrative Analysis of 2D and 3D Mitochondrial Shape and Network Properties.** *PLoS ONE* 2014, **9:**e101365.

II

Mitochondrion 49 (2019) 97–110

Contents lists available at ScienceDirect

Mitochondrion

journal homepage: www.elsevier.com/locate/mito

Original Research Article

Upregulated PDK4 expression is a sensitive marker of increased fatty acid oxidation

Ina Katrine Nitschke Pettersen[a,1], Deusdedit Tusubira[a,1], Hanan Ashrafi[a], Sissel Elisabeth Dyrstad[a], Lena Hansen[a,b], Xiao-Zheng Liu[a], Linn Iren Hodneland Nilsson[a], Nils Gunnar Løvsletten[c], Kjetil Berge[d], Hege Wergedahl[e], Bodil Bjørndal[f], Øystein Fluge[b], Ove Bruland[g], Arild Christian Rustan[c], Nils Halberg[a], Gro Vatne Røsland[a,b], Rolf Kristian Berge[f,h], Karl Johan Tronstad[a,*]

[a] Department of Biomedicine, University of Bergen, Norway
[b] Department of Oncology and Medical Physics, Haukeland University Hospital, Bergen, Norway
[c] Department of Pharmacy, University of Oslo, Norway
[d] Skretting AS, Stavanger, Norway
[e] Department of Sport, Food and Natural Sciences, Western Norway University of Applied Sciences, Bergen, Norway
[f] Department of Clinical Science, University of Bergen, Norway
[g] Department of Medical Genetics and Molecular Medicine, Haukeland University Hospital, Bergen, Norway
[h] Department of Heart Disease, Haukeland University Hospital, Bergen, Norway

ARTICLE INFO

Keywords:
Metabolic regulation
Metabolic flexibility
Fatty acid oxidation
Mitochondria
Cell metabolism
Biomarker
Pyruvate dehydrogenase kinase
Peroxisome proliferator-activated receptor (PPAR)

ABSTRACT

Fatty acid oxidation is a central fueling pathway for mitochondrial ATP production. Regulation occurs through multiple nutrient- and energy-sensitive molecular mechanisms. We explored if upregulated mRNA expression of the mitochondrial enzyme pyruvate dehydrogenase kinase 4 (PDK4) may be used as a surrogate marker of increased mitochondrial fatty acid oxidation, by indicating an overall shift from glucose to fatty acids as the preferred oxidation fuel. The association between fatty acid oxidation and PDK4 expression was studied in different contexts of metabolic adaption. In rats treated with the modified fatty acid tetradecylthioacetic acid (TTA), *Pdk4* was upregulated simultaneously with fatty acid oxidation genes in liver and heart, whereas muscle and white adipose tissue remained unaffected. In MDA-MB-231 cells, fatty acid oxidation increased nearly three-fold upon peroxisome proliferator-activated receptor α (PPARα, *PPARA*) overexpression, and four-fold upon TTA-treatment. *PDK4* expression was highly increased under these conditions. Further, overexpression of *PDK4* caused increased fatty acid oxidation in these cells. Pharmacological activators of PPARα and AMPK had minor effects, while the mTOR inhibitor rapamycin potentiated the effect of TTA. There were minor changes in mitochondrial respiration, glycolytic function, and mitochondrial biogenesis under conditions of increased fatty acid oxidation. TTA was found to act as a mild uncoupler, which is likely to contribute to the metabolic effects. Repeated experiments with HeLa cells supported these findings. In summary, PDK4 upregulation implies an overarching metabolic shift towards increased utilization of fatty acids as energy fuel, and thus constitutes a sensitive marker of enhanced fatty acid oxidation.

Abbreviations: ACC, acetyl-CoA carboxylase; ACOX, acyl-CoA oxidase 1; AICAR, 5-aminoimidazole-4-carboxamide ribonucleotide; AMPK, AMP-dependent protein kinase; CCCP, carbonyl cyanide 3-chlorophenylhydrazone; COX4I1, cytochrome *c* oxidase subunit IV; CPT, carnitine palmitoyltransferase; ECAR, extracellular acidification rate; GFP, green fluorescence protein; ME-1, malic enzyme 1; mTOR, mammalian target of rapamycin; NRF1, nuclear respiratory factor 1; OCR, oxygen consumption rate; PA, palmitic acid; PDH, pyruvate dehydrogenase; PDK, pyruvate dehydrogenase kinase; PPAR, peroxisome proliferator-activated receptor; TFAM, mitochondrial transcription factor A; TTA, tetradecylthioacetic acid; WAT, white adipose tissue; WY 14,643, 4-Chloro-6-(2,3-xylidino)-2-pyrimidinylthioacetic acid

* Corresponding author at: Department of Biomedicine, University of Bergen, Jonas Lies vei 91, N-5009 Bergen, Norway.
E-mail address: karl.tronstad@uib.no (K.J. Tronstad).

[1] Equal contribution.

https://doi.org/10.1016/j.mito.2019.07.009
Received 12 April 2019; Received in revised form 1 July 2019; Accepted 24 July 2019
Available online 25 July 2019

1. Introduction

Mitochondrial fatty acid oxidation is a crucial and highly regulated fueling pathway for aerobic ATP production in mammalian organisms. Abnormalities of mitochondrial fatty acid oxidation affects diverse cellular and systemic functions, and have been linked to conditions such as diabetes, metabolic syndrome, cancer, cancer cachexia, neurodegeneration and ME/CFS (Naviaux et al., 2016; Germain et al., 2017; Rohlenova et al., 2018; Adeva-Andany et al., 2018; Fukawa et al., 2016). Functional analysis of mitochondrial fatty acid oxidation in conventional biopsies are difficult, partly since it requires viable cells or non-frozen tissue samples. Identification of sensitive and effective surrogate markers of mitochondrial fatty acid oxidation may thus provide new opportunities to assess (patho)physiological effects on metabolism. Fatty acid catabolism is co-regulated with other pathways of cell metabolism to support homeostasis when the energy supply or demand change. There is a well-established concept of reciprocal regulation between fatty acid and glucose oxidation for energy purposes. Different types of metabolic adaptations may occur to accommodate (patho) physiological changes (Sugden and Holness, 1994; Trexler et al., 2014; Jose et al., 2013). The pyruvate dehydrogenase (PDH) complex and the carnitine palmitoyltransferase (CPT) system are important in this context. PDH converts pyruvate from glycolysis to acetyl-CoA and CO_2 through oxidative decarboxylation, whereas the CPT system transports fatty acids into mitochondria, a rate-limiting process for acetyl-CoA production by mitochondrial fatty acid oxidation. PDH and the CPT system are both regulated in response to changing energy conditions, partly through contextual nutrient-gene and nutrient-protein interactions that leads to metabolic adaptations. Increased rates of fatty acid oxidation, e.g. due to starvation or insulin-deficient diabetes, is associated with suppression of PDH activity (reviewed in (Holness and Sugden, 2003)). This is important for conserving 3-carbon precursors for glucose synthesis when glucose is scarce. Such long-term adaptive effect on PDH activity status can partly be explained by altered expression of PDH kinases (PDKs), which phosphorylate and inhibit the PDH complex (Holness and Sugden, 2003). There are four PDK isoenzymes, PDK1–4, all expressed in a tissue-specific manner (reviewed in (Jeong et al., 2012)). As suggested by Holness and Sugden, the PDKs may be considered to act as tissue homeostats supporting adequate context-dependent regulation of energy fueling pathways (Holness and Sugden, 2003). In particular, changed PDK4 expression appears to play an important role in lipid-related metabolic adaptations in various tissues (reviewed in (Holness and Sugden, 2003; Sugden, 2003; Roche and Hiromasa, 2007)). Increased level of PDK4, e.g. due to starvation (Wu et al., 2000), favors inactivation of PDH in oxidative tissues, and thereby implements an influential metabolic shift from glucose to fatty acid oxidation. Furthermore, under such conditions, reduced production of malonyl-CoA, an important inhibitor of mitochondrial fatty acid uptake and oxidation (the CPT system), will support increased rates of fatty acid oxidation.

Fatty acid oxidation is also controlled by nutrient- and energy-sensitive factors, such as AMP-dependent protein kinase (AMPK), the family of peroxisome proliferator-activated receptor transcription factors (PPARs) and the mammalian target of rapamycin (mTOR) (recently reviewed in (Desvergne et al., 2006; Lin and Hardie, 2018; Saxton and Sabatini, 2017)). The PPAR family consists of three main isoforms (PPARα, PPARδ, PPARγ), among which PPARα is a central regulator of context-dependent changes in fatty acid oxidation (Desvergne et al., 2006). AMPK is activated by a low cellular energy state, which commonly leads to increased mitochondrial biogenesis and stimulated oxidation rates (Hodneland Nilsson et al., 2015; Tronstad et al., 2014). AMPK also inactivates acetyl-CoA carboxylase (ACC), which is an enzyme producing malonyl-CoA (Winder et al., 1997; O'Neill et al., 2014). Pharmacological activation of AMPK with 5-aminoimidazole-4-carboxamide ribonucleotide (AICAR) causes increased fatty acid oxidation in rat muscle (Merrill et al., 1997). In contrast to PPARα and AMPK, the activity of mTOR primarily supports biosynthesis rather than catabolism. Hence, in an energy-limited context, e.g. glucose deprivation, increased rates of mitochondrial fatty acid oxidation may be supported by multiple regulatory events, including PPARα and/or AMPK activation, and mTOR inhibition. The contextual effects depend on both the type of trigger as well as cell-specific properties regarding the contributing signaling factors and their downstream mediators, such as PDKs. These mechanisms regulate both the activity balance between glucose and fatty acid oxidation, and the ability to switch between these fueling pathways, a trait often referred to as metabolic flexibility (Galgani et al., 2008).

PDK4 is normally highly expressed in tissues with high energy demand, including heart, skeletal muscle, liver, kidney, pancreatic islet and lactating mammary gland (Holness and Sugden, 2003; Wu et al., 2000). In these tissues, PDK4 expression is typically induced when the blood free fatty acid level increases, such as during starvation; and this is mediated partly through PPARα, but also by other mechanisms (Jeong et al., 2012; Sugden et al., 2001). PPARα-agonists, such as WY-14,643, have been found to significantly induce PDK4 expression in rat muscle (Wu et al., 1999), and PDK4 upregulation through PPARα may be involved in cancer cachexia (Pin et al., 2019). Further, PDK4 was reported to be highly upregulated upon cardiac-restricted overexpression of PPARα in mice, and this was associated with increased myocardial fatty acid oxidation rates (Finck et al., 2002). Upregulation of PDK4 was also found in adipocytes after treatment with the PPARγ-selective activator rosiglitazone, but not liver and muscle (Cadoudal et al., 2008). In muscle cells, PPARδ was found to mediate contextual upregulation of PDK4 (Badin et al., 2012; Feng et al., 2014). Although AMPK and mTOR are known to respond to low energy conditions, there are few reports on how these factors may affect the relationship between PDK4 and fatty acid oxidation e.g. upon starvation. Combined activation of AMPK and PPARδ caused increased *Pdk4* expression in mouse muscle, and this was associated with increased fat oxidation during prolonged exercise (Manio et al., 2016). The hypolipidemic modified fatty acid tetradecylthioacetic acid (TTA) is known to act through multiple mechanisms to induce mitochondrial fatty acid oxidation in cells and animals, both dependent and independent of PPARs (Berge et al., 2005; Rost et al., 2009; Grav et al., 2003; Wensaas et al., 2009). Potential effects of TTA on PDK4 expression have not yet been reported.

Based on current knowledge, increased PDK4 expression appears to imply a coordinated metabolic shift from glucose to fatty acids as major energy fuel. The present study was undertaken to solidify the relationship between PDK4 expression and fatty acid oxidation, by pursuing in vivo findings through extensive investigations of context-dependent metabolic functions in living cells.

2. Materials and methods

2.1. Rat model

The rat study was part of a larger study previously reported (Vigerust et al., 2012). The protocol was approved by the Norwegian State Board of Biological Experiments with Living Animals. Ten weeks old male Wistar rats (200–250 g) were obtained from Taconic Europe. After one week of acclimatization, the control group was fed on high fat diet (23% lard + 2% soybean oil), and treatment group was given the same diet supplemented with TTA (0.375%) for 50 weeks. The diets were isocaloric (energetic value 4900 Kcal). Animals were anaesthetized and sacrificed under non-fasting condition. Blood was drawn by cardiac puncture. All tissues were stored in liquid nitrogen before analysis. Further information is provided in (Vigerust et al., 2012).

2.2. Cell culture

All cell cultures were incubated at 37 °C (5% CO_2 in air).

Compounds and materials were from Sigma-Aldrich (St. Louis, MO, US), and catalogue numbers refers to products from this company, unless otherwise stated. MDA-MB-231 and HeLa cells were cultured in DMEM (4.5 g/l glucose, #D5671) supplemented with 10% heat-inactivated fetal bovine serum (FBS, #SH30079.03, GE Healthcare Hyclone), 50 µg/ml penicillin/streptomycin (#P-0781) and 2 mM L-glutamine.

2.3. Overexpression of PPARA and PDK4

For the overexpression of *PPARA*, a double-stranded DNA fragment (g-Block) encoding human *PPARA* and containing BamHI and *Sal*I restriction enzymes cutting sites was synthesized by Integrated DNA Technologies (IDT, Coralville, IA, US). The g-block fragment was then subcloned into the pBABE-puro (Addgene, plasmid 1764) retroviral vector with a puromycin resistance gene. An empty pBABE-puro vector was used as a control. HEK293T packaging cells were transfected with the retroviral vector and packaging vectors by Lipofectamine-2000 transfection (#11668–019, Thermo Fisher Scientific, Waltham, MA, US), following the manufacturer's instructions. At 5 h post-transfection, the medium was replaced with 10 ml fresh DMEM supplemented with 10% FBS. Virus were harvested after 24 h post-transfection. For retroviral infection, MDA-MB-231 cells were seeded in a 10-cm dish and infected with virus in the presence of polybrene (8 µg/ml). Cells were selected by puromycin (2 µg/ml) 48 h post infection.

For the overexpression of *PDK4*, A MMLV retrovirus gene expression vector containing *PDK4* cDNA (NM_002612) and *Bsd*, the blasticidine resistance gene (Kimura et al., 1994) was acquired from VectorBuilder (VectorBuilder Inc. 150 Pine Forest Drive, Suite 803, Shenandoah, TX 77384). HEK293 derived Phoenix-AMPHO (ATCC® CRL-3213™) packaging cells were transfected with the retroviral vector by Lipofectamine-2000 transfection, following the manufacturer's instructions. Stably transfected virus producing packaging cells were selected in DMEM medium containing 10 µg/ml blasticidin (#ant-bl-05, InvivoGen, 5, rue Jean Rodier F-31400 Toulouse, France), as described by others (Pear et al., 1993). For retroviral infection, MDA-MB-231 cells were seeded in 6-well plates and infected with virus in the presence of protamine sulfate (5 µg/ml). Cells were selected by blasticidin (10 µg/ml) 72 h post infection.

2.4. Cell culture treatment conditions

To investigate long-term effects (6 days) of metabolic modulators, 250,000 cells were plated in T75 flasks and incubated overnight to allow proper attachment. Final concentrations of 5-aminoimidazole-4-carboxamide 1-β-D-ribofuranoside (AICAR, 0.5 mM, Toronto Research Chemicals Inc., North York, ON, Canada), rapamycin (50 nM), tetradecylthioacetic acid (TTA, 30 µM and 60 µM, Synthetica AS, Oslo, Norway), 4-Chloro-6-(2,3-xylidino)-2-pyrimidinylthioacetic acid (WY 14,643, 10 µM) and vehicle (DMSO, 60 µM) were added to respective flasks. On day 3, the medium was replaced, and treatment continued. On day 5, the cells were re-plated at optimized cell densities for subsequent analyses the next day (day 6).

2.5. Extracellular flux analysis to study cell metabolism

Extracellular flux analysis was performed with the Seahorse XF^{e}96 Analyzer (Agilent, Santa Clara, CA, US). This simultaneously measures the oxygen consumption rate (OCR) and extracellular acidification rate (ECAR) in the medium directly above adherent cells. The experiments were performed according to standard protocols, and cell number and compound concentrations were optimized for each cell type. Cells were seeded in 96-well assay plates (Hela; 20,000, MDA-MB-231; 30,000 cells/80 µl/well) and let adhere overnight (5% CO_2 in air, 37 °C). The next day, growth medium was replaced with assay medium (un-buffered, phenol red-free DMEM, #D5030) supplemented for mitochondrial respiration assay with 10 mM glucose, 2 mM sodium pyruvate, 4 mM L-glutamine, pH 7.4, and for glycolysis assay with 4 mM glutamine, pH 7.4. After 1 h incubation in the Prep Station (37 °C, CO_2-free, Agilent) the plate was placed in the Seahorse XF^{e}96 Analyzer. Chemical modulators were injected sequentially to obtain metabolic flux profiles. For the mitochondrial respiration assay the final concentration of the modulators were 3 µM oligomycin, 1 µM CCCP, 1 µM rotenone and 1 µM antimycin A. For the glycolysis assay, final concentrations of 10 mM glucose, 3 µM oligomycin and 100 mM 2-deoxyglucose were added.

To study acute effects of palmitic acid (PA) and its modified analogue TTA, the cells (untreated) were seeded according to standard protocol (described above). The fatty acids (dissolved in DMSO) were added at specified concentrations (final concentrations: 30, 60, 100 and 200 µM) to the mitochondrial respiration assay medium immediately before inserting the plate into the Seahorse XF^{e}96 Analyzer.

When relevant, data were normalized to protein content, measured using the Pierce® BCA Protein Assay Kit (Thermo Fisher Scientific, Waltham, MA, US).

2.6. Substrate oxidation assay by $^{14}CO_2$-trapping

Substrate oxidation was assessed by providing the radiolabeled (^{14}C) substrate of interest to the cells, accompanied by trapping of the released $^{14}CO_2$; a technique previously described in (Wensaas et al., 2007). Cells were seeded in 96-well CellBind® microplates (MDA-MB-231; 45,000, HeLa; 40,000 cells/well) in DMEM and incubated overnight to allow proper attachment. The radiolabeled substrate of interest, either [1-^{14}C]pyruvic acid (0.25 µCi/ml), D-[^{14}C(U)]glucose (2 µCi/ml for MDA-MB-231, 4 µCi/ml for HeLa) or [1-^{14}C]palmitic acid (1 µCi/ml), all from PerkinElmer (Waltham, MA, US), was given in DPBS (with $MgCl_2$ and $CaCl_2$, #D8662) supplemented with 10 mM HEPES and 10 µM BSA. L-carnitine (1 mM) and glucose (0.5 mM) were included in the assay medium for palmitic acid oxidation. Respective amounts of non-radiolabeled substrate were added to obtain final concentrations of sodium pyruvate (0.2 mM or 2 mM), glucose (5 mM) and BSA-conjugated palmitic acid (100 µM), as indicated in the figures. For uncoupled substrate oxidation, the optimized concentration of CCCP (1 µM for pyruvate and glucose oxidation, 3 µM for palmitic acid oxidation) was added to the medium. The optimal CCCP concentration was higher for palmitic acid oxidation compared to the others due to the increased amount of BSA, which binds hydrophobic molecules. Etomoxir (40 µM) was added to selected wells during palmitic acid oxidation, to monitor the contribution of non-mitochondrial CO_2 production, which usually was 10–20% of basal activity (data not shown). The $^{14}CO_2$ trapping was performed as described (Wensaas et al., 2007). In brief, an inverted UniFilter®-96w GF/B microplate (PerkinElmer), activated for CO_2 capture with 1 M NaOH, was sealed to the top of the 96-well CellBind® cell culture microplate, and incubated for the indicated period of time at 37 °C. Subsequently, scintillation liquid (30 µl, Ultima Gold XR or MicroScint PS PerkinElmer) was added to the filters and the filterplate sealed with a TopSealA (PerkinElmer). Radioactivity was measured using a microplate scintillation counter (TopCount NXT, Packard, Meriden, CT, US or the MicroBeta^2 Microplate Counter, PerkinElmer). Protein measurement was performed for data normalization. The cells were washed twice with PBS, lysed (0.1 M NaOH), and measured using Pierce® BCA Protein Assay Kit (Thermo Fisher Scientific).

2.7. Gene expression by qPCR assays

Gene expression analysis in animal tissues was done as previously reported (Vigerust et al., 2012; Lindquist et al., 2017; Dyrstad et al., 2018). RNA was isolated from frozen tissues stored at −80 °C. In cell culture experiments, the cells were washed with PBS, pelleted and stored at −80 °C. Cellular RNA was extracted using the RNeasy mini kit including DNase digestion (RNase-Free DNase) (QIAGEN, Venlo,

Netherlands). Total RNA (50 ng/μl) was estimated by the use of a Nanodrop ND-1000 Spectrophotometer (NanoDrop Technologies, Boston, MA, US) and reversely transcribed using the Applied Biosystem's High Capacity cDNA Reverse Transcription Kit (Thermo Fisher Scientific) according to manufacturer instructions. All probes were obtained from Applied Biosystems unless otherwise stated. Probes used were: Acyl-CoA oxidase 1, (*ACOX* Human: Hs01074241, *Acox* Rat: Rn01460628), Cytochrome c oxidase subunit IV *(COX4I1* Human: Hs00971639), Carnitine palmitoyltransferase 1A *(Cpt1a* Rat: Rn00580702, *CPT1A* Human: Hs00912671), Carnitine palmitoyltransferase 1B (*Cpt1b* Rat: Rn00682395), Carnitine palmitoyltransferase 2 (*Cpt2* Rat: Rn00563995), Pyruvate dehydrogenase kinase 4 (*Pdk4* Rat: Rn00585577_m1, PDK4 Human: Hs01037712), Peroxisome proliferator activated receptor α (*PPARA* Human: Hs00947536), Malic enzyme-1 (*Me-1* Rat: Rn00561502_m1, *ME-1* Human: Hs00159110), Mitochondrial transcription factor A (*Tfam* Rat: Rn00580051_m1, *TFAM* Human: Hs01082775) and Nuclear respiratory factor (*Nrf* Rat: Rn01455960_m1). The reaction mixtures were loaded into a LightCycler® 480 Multiwell Plate 384 (Roche, Basel, Germany) by the Mosquito HV® low volume pipetting instrument (TTP Labtech Ltd., UK) (Dyrstad et al., 2018). The qPCR was run in a LightCycler 480 system (Roche, Basel, Germany) with the "Dual Color Hydrolysis probe – UPL Probe 384-11" instrument template-program. The expression level of each gene was calculated as fold change based on the delta delta Ct method (Livak and Schmittgen, 2001) and was normalized against 18S rRNA (Rat: RT-CKFT-18S from Eurogentec, Seraing, Belgium, Human: Eukaryotic 18S rRNA Endogenous Control, 4310893E).

2.8. Protein expression by western blotting

The cell pellets were lysed in RIPA lysis buffer (#sc24948, Santa Cruz Biotechnology, Dallas, TX) following the manufactures instructions. Pierce® BCA Protein Assay Kit (Thermo Fisher Scientific) was used to measure protein concentration in the lysates. The protein lysate mixed together with XT Sample Buffer (#1610791, Bio-Rad) were heated at 95 °C for 5 min, before 10–12 mg protein was loaded per well. The electrophoresis was done using Mini-PROTEAN® TGX™ Protein Gels, 4–20% gradient, running buffer (#1610772, Bio-Rad) and Bio-Rad Mini Protean 3 cell system (90 V for 15 min, 110 V for 1 h). The BioradTurbo Transfer System (2.5A, 25 V, 7 min) was used to transfer (transfer buffer, #1610734, Bio-Rad) the proteins onto the activated (30 s in metanol) polyvinylidene fluoride (PVDF) membrane (Trans-Blot® Turbo™ Mini-size LF PVDF). The membranes were blocked, for 1 h in room temperature, in Odyssey Blocking Buffer (TBS) (LI-COR Biosciences) before labeled with anti-PDK4 antibody (#ab11033, mouse monoclonal [1C2BG5], Abcam) diluted 1:500 in blocking buffer overnight at 4 °C. Anti-GAPDH antibody (#60004–1, mouse monoclonal, Proteintech) at a dilution of 1:1000 was used as loading control. After washing in TBS-T buffer the membranes were incubated for 2 h in IRDye® 800CW Goat anti-Mouse IgG secondary antibody (1:20000) (#P/N 926–32,210, LI-COR Bioscience). The protein bands were visualized using the 800 nm IRlong channel in the Amersham Typhoon Gel and Blot Imaging Systems (GE healthcare). Amersham™ Imager 600 software was used to view and analyze the blot images together with ImageJ software.

2.9. Live-cell reporter strategy to monitor mitochondrial biogenesis

Mitochondrial biogenesis was measured using a GFP-based live-cell reporter strategy previously described in (Hodneland Nilsson et al., 2015). Briefly, a reporter construct (NRF1mitoGFP) with mitoGFP under the control of a promoter with NRF-1 responsive element was inserted into HeLa (HeLaNRF1/c4) and MDA-MB-231 (MDA-MB-231/NRF1) cells. Following the treatment, the cellular expression of mitoGFP (fluorescence intensity) was measured as a readout of mitochondrial biogenesis. The cells were treated as indicated for 6 days, before they were trypsinized, washed with PBS and kept on ice until analyzed by flow cytometry (AccuriTM C6, BD Accuri Cytometers Inc., Ann Arbor, MI, US). The data were analyzed by FlowJo software.

2.10. Plasma lactate and glucose measurements

Biosen C-Line GP+ (EKF Diagnostics, Cardiff, UK) was used to measure glucose and lactate concentrations in rat plasma, according to manufacturer's instructions.

2.11. Statistical analysis

All data were analyzed using Graphpad Prism 8 software (GraphPad Software; San Diego, CA, US). Results are shown as mean ± SD. ANOVA and student's *t*-test were used to evaluate statistical differences between the interventions and control. Pearson's correlation coefficients were used when comparing two independent variables. $P < .05$ was considered statistically significant.

3. Results

3.1. Pdk4 expression is a sensitive indicator of mitochondrial fatty acid oxidation in rat tissues

Increased hepatic fatty acid oxidation is established as an important mechanism behind the hypolipidemic effects of the modified fatty acid TTA in rats (Berge et al., 2005). In multiple studies, upregulated fatty acid oxidation has been demonstrated, both based on gene expression and enzymatic activity, most extensively in liver, but also in heart (Berge et al., 2005; Vigerust et al., 2012; Oie et al., 2013; Turell, 1989). In the present study, we used TTA-treatment as a model to evaluate the relationship between *Pdk4* mRNA expression and fatty acid oxidation *in vivo*. Gene expression was measured in tissue samples from a previous experiment in rats, where rats were treated with TTA for 50 weeks (Vigerust et al., 2012). *Pdk4* expression was compared with the expression of genes related to fatty acid oxidation in liver, heart, skeletal muscle and white adipose tissue (Fig. 1A, and Supplementary Fig. S1). In the liver of TTA-treated rats, the level of *Pdk4* mRNA increased 18-fold (18.0 ± 2.6), compared to control rats. This was associated with increased hepatic expression of *Cpt1a* (liver isoform, 2.4 ± 0.8), *Cpt2* (5.1 ± 1.2), and the classical PPARα target gene *Acox* (10.1 ± 2.8), supporting previous findings (Vigerust et al., 2012). Interestingly, TTA-treatment caused a potent increase in the expression of the muscle isoform *Cpt1b* in liver (487.1 ± 195.4), which has not previously been reported. The hepatic expression of *Tfam* was increased (2.4 ± 1.1) suggesting that elements of mitochondrial biogenesis may be involved, although *Nrf1* was not affected. We also analyzed the expression of cytosolic malic enzyme *Me-1* due to its interactions in pyruvate metabolism, as well as fatty acid oxidation by mediating TCA anaplerotism (Gibala et al., 2000; Carley et al., 2015). TTA-treated rats presented significantly increased expression of *Me-1* in liver (58.0 ± 21.9). In heart, a moderate induction of *Pdk4* (2.5 ± 0.7) was accompanied by relatively small, but statistically significant, increases in *Cpt1b* (1.2 ± 0.1), *Acox* (1.7 ± 0.3) and *Me-1* (1.5 ± 0.3) mRNA levels, and a small reduction in *Tfam* (0.8 ± 0.04), whereas the other transcripts remained unchanged. None of these genes were significantly affected in skeletal muscle or white adipose tissue in TTA-treated rats compared to controls. Plasma glucose and lactate levels were measured to evaluate how this long-term adaptation of oxidative metabolism affected systemic glucose homeostasis (Fig. 1B-C). While no effect was found for plasma lactate, the plasma glucose levels tended to be slightly lower in TTA-treated rats compared to controls, although this effect did not reach statistical significance. In summary, TTA-treated rats presented regulatory effects on fatty acid oxidation genes in agreement with a significant induction in liver and a moderate induction in heart, supporting previous measurements (Berge et al., 2005; Oie et al., 2013).

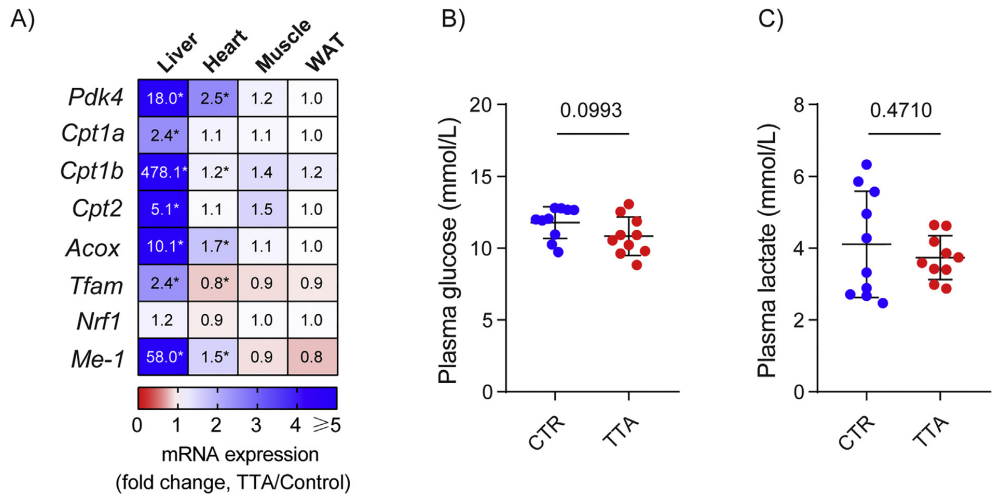

Fig. 1. *Pdk4* expression and metabolic adaptation in TTA-treated rats.
Rats were administered control (CTR) or TTA-supplemented diet for 50 weeks (Vigerust et al., 2012). (A) Gene expression in liver, heart, skeletal muscle and white adipose tissue (WAT) was measured using real time quantitative PCR. The heat map indicates mean expression level relative to control (ddCT method, detailed data in Supplementary Fig. S1). (B) Glucose and (C) lactate concentrations in plasma from the CTR and TTA fed rats. Each dot represent one animal and group mean ± SD (n = 8–10) is indicated. Statistical analysis was performed by t-test. *$p < .05$, p-values are shown in (B) and (C). TTA, tetradecylthioacetic acid.

Importantly, upregulation of fatty acid oxidation was accompanied by increased *Pdk4* expression, generally to a higher magnitude compared to other genes commonly used as indicators of mitochondrial fatty acid oxidation.

3.2. Fatty acid oxidation and PDK4 expression are strongly induced by PPARA-overexpression

As a proof of principle cell model where upregulation of fatty acid oxidation is expected, we investigated *PDK4* mRNA expression in MDA-MB-231 cells modified to overexpress *PPARA* (MDA-MB-231/PPARA, Fig. 2). Based on our previous experience with various cell models, the MDA-MB-231 line was chosen as the primary model due to its active oxidative metabolism, and the observation that these cells present a significant increase in fatty acid oxidation under relevant conditions. Several of the experiments were also repeated with HeLa cells, which we commonly find to display similar metabolic effects as MDA-MB-231, albeit often less pronounced.

The mRNA level of *PPARA* was 82.3 ± 14.4-fold higher in the MDA-MB-231/PPARA cells, compared to the parental cells. Noteworthy, this caused a 24.9 ± 1.8-fold increase in *PDK4* mRNA level, and upregulation of genes involved in fatty acid catabolism such as *ACOX* (51.0 ± 12.5), *CPT1A* (2.3 ± 0.1), *COX4I1* (1.9 ± 0.05) and *ME-1* (2.0 ± 0.03) (Fig. 2A). The expression of the mitochondrial transcription factor *TFAM* was slightly reduced (0.7 ± 0.04) in the MDA-MB-231/PPARA cells, suggesting that the increased expression of these mitochondrial enzymes was not linked to increased mitochondrial biogenesis.

To investigate if *PPARA* overexpression caused a metabolic fuel change, we measured glucose and fatty acid oxidation by trapping $^{14}CO_2$ produced under incubation with the respective radiolabeled substrates. Fatty acid oxidation was increased nearly three-fold in the MDA-MB-231/PPARA cells compared to the parental cells (Fig. 2B). In the same cells, glucose oxidation was reduced by 20%, when glucose was provided as the major substrate (Fig. 2C). These data support the notion that *PDK4* expression and fatty acid oxidation are co-regulated by PPARα, leading to an overall metabolic shift towards increased oxidation of fatty acid instead of glucose.

3.3. PDK4 overexpression leads to increased fatty acid oxidation

The increase in *PDK4* expression may occur as a parallel effect besides the stimulated fatty acid oxidation, or it may be a causative factor of the metabolic shift. To address this question, we investigated the effects of *PDK4* overexpression in MDA-MB-231 cells (i.e. MDA-MB-231/PDK4 cells). The levels of PDK4 mRNA and protein were low in the parental cells, and the increased amounts in the modified cells confirmed successful overexpression (Fig. 3A-B). Although the PDK4 antibody gave weak band intensity, the immunoblot showed increased level in PDK4-overexpressing cells (Fig. 3B). We then investigated if this leads to reduced pyruvate oxidation, which would be the expected consequence of PDK4-mediated inhibition of the PDH complex. Following incubation in high glucose environment (25 mM), pyruvate oxidation was 32% reduced in the MDA-MB-231/PDK4 cells (borderline statistical significance), compared to the parental cells (Fig. 3C). This activity was stimulated in both cell types when grown in low glucose compared to high glucose medium, but pyruvate oxidation remained lower in the MDA-MB-231/PDK4 compared to the parental cells. Noteworthy, fatty acid oxidation was 74% increased in *PDK4* overexpressing cells compared to parental cells when grown in 25 mM glucose, but the difference disappeared following growth in 1 mM glucose, primarily due to a significant increase in the parental cells (Fig. 3D). These data strongly support that there is a tight causative relationship between PDK4 and fatty acid oxidation. Apparently, *PDK4* overexpression lead to a shift towards fasting-type energy metabolism even in a high glucose environment. Hence, the differences between parental and *PDK4* overexpressing cells were smaller following growth in a low glucose environment, since this significantly enhanced fatty acid oxidation in the parental cells but not to the same extent in *PDK4*-overexpressing cells.

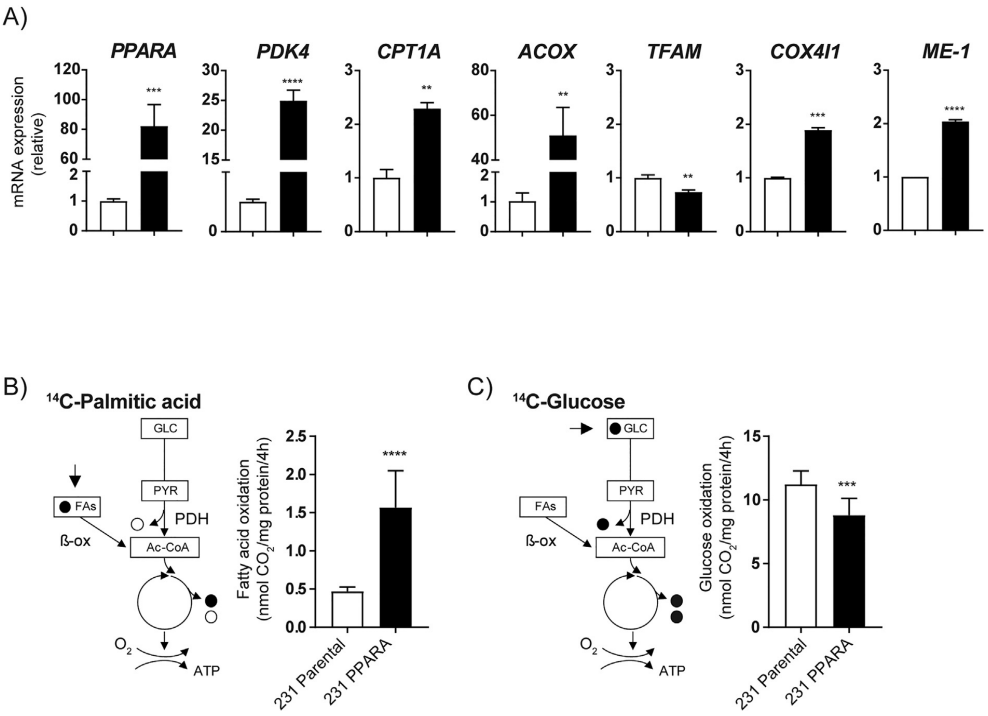

Fig. 2. Effect of *PPARA* overexpression on *PDK4* expression and fuel oxidation.
The effects of increased *PPARA* expression were investigated in MDA-MB-231 cells. The figure compares the unmodified (231 Parental) and *PPARA* overexpressing (231 PPARA) cells. (A) Expression of *PPARA*, *PDK4, CPT1A, ACOX, TFAM, COX4I1* and *ME-1*, measured using real time quantitative PCR. The diagrams show mRNA expression relative to the CTR group (ddCT method), as mean ± SD of triplicate measurements. (B) Fatty acid oxidation; $^{14}CO_2$-production during 4 h incubation with [1-^{14}C]palmitic acid (1 μCi/ml, 100 μM), in presence of L-carnitine (1 mM) and glucose (0.5 mM). (C) Glucose oxidation; $^{14}CO_2$-production during 4 h incubation with D-[^{14}C(U)]glucose (2 μCi/ml, 5 mM). The oxidation data are normalized to cell protein content (mg), and are displayed as mean ± SD of 4–8 replicates. The pathway illustrations show the carbon flux fueled by the ^{14}C-labeled substrates. The filled and open circles represent radiolabeled (filled, ^{14}C) and non-labeled (open) carbons, released as CO_2 under the respective conditions. The shown experiments are representative for three separate experiments. Statistical analysis was performed by *t*-test. **p* < .05, ***p* < .01, ****p* < .001, *****p* < .0001.

3.4. Increased PDK4 expression reflects upregulated fatty acid oxidation under conditions of metabolic adaptation

In order to investigate the relationship between fatty acid oxidation and *PDK4* expression in different contexts of metabolic adaptation, we studied the effects of long-term (6 days) treatment with TTA and selective activators of AMPK (AICAR) and PPARα (WY 14,643) in MDA-MB-231 cells. The mRNA level of *CPT1A*, which often is used as an indicator of mitochondrial fatty acid oxidation, was lower after treatments with AICAR and WY 14,643, compared to control, but increased approximately two-fold in cultures treated with 30 μM or 60 μM TTA (Fig. 4A). The effect of TTA on *PDK4* expression was of significantly higher magnitude (7.3 ± 0.3 at 30 μM TTA, 12.2 ± 1.2 at 60 μM TTA) compared to *CPT1A*. AICAR treatment caused reduced *PDK4* expression, whereas WY 14,643 had no effect. None of the agents were found to induce the mRNA expression of the classical PPARα-target *ACOX* in these cells. Only AICAR induced the expression of *TFAM* (2.7 ± 0.1), suggesting that this treatment, in contrast to the others, causes activation of mitochondrial biogenesis. Replication of this experiment with Hela cells supported that TTA, but not AICAR and WY 14,643, caused moderate upregulation of *CPT1A* simultaneous with a strong induction of *PDK4* (Supplementary Fig. S2). HeLa cells tended to have a mild upregulation of *TFAM* and *ACOX* expression for all the treatments except for 60 μM TTA.

The highest concentration of TTA (60 μM) caused a 4-fold increase in basal fatty acid oxidation in MDA-MB-231 cells, and the effect was slightly less with the lower concentration (30 μM) (Fig. 4B). In our experience, functional changes of this magnitude in cell metabolism are rarely observed in living cell cultures. AICAR and WY 14,643 did not affect fatty acid oxidation in these cells. Additional measurements in presence of the mitochondrial uncoupler carbonyl cyanide 3-chlorophenylhydrazone (CCCP) showed that the maximal fatty acid oxidation capacity was approximately two-fold increased in the TTA-treated cells (for both TTA concentrations). Enhanced fatty acid oxidation in TTA-treated cells was not found to be accompanied by a reciprocal reduction in basal glucose oxidation, yet there was a moderate decrease in AICAR-treated cells (Fig. 4C). We then measured pyruvate oxidation in order to obtain a more direct assessment of mitochondrial oxidation, disconnected from the potential rate-limiting influence of glycolysis. Basal pyruvate oxidation tended to be reduced after treatment with 60 μM TTA, with as significant 30% reduction under uncoupling conditions (Fig. 4D). Similar effects were seen in HeLa cells after treatment with AICAR, WY 14,643 or TTA (Supplementary Fig. S2). In summary, metabolic adaptation involving induced fatty acid oxidation was accompanied by strongly increased *PDK4* mRNA expression in these cell models. This effect was observed after treatment with TTA known to regulate multiple energy-sensitive mechanisms, but not with selective activators of AMPK (AICAR) or PPARα (WY 14,643), under these

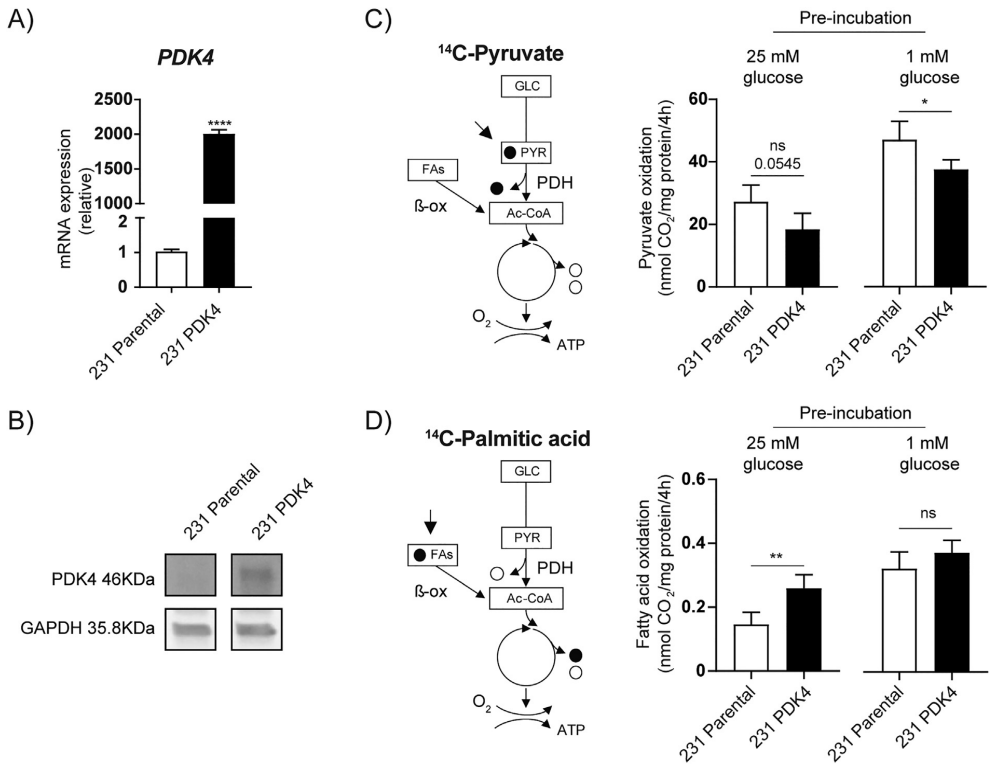

Fig. 3. Effect of *PDK4* overexpression in pyruvate and fatty acid oxidation.
The effects of *PDK4* overexpression were investigated in MDA-MB-231 cells. The figure compares the unmodified (231 Parental) and *PDK4* overexpressing (231 PDK4) cells. (A) Confirming overexpression of *PDK4* using real time quantitative PCR. The mRNA expression level is displayed relative to the 231 Parental cells (ddCT method) as mean ± SD of triplicate measurements, and is representative for two separate experiments. (B) Increased PDK4 protein expression was confirmed by Western blot analysis. (C-D) Pyruvate and fatty acid (palmitic acid) oxidation was measured following overnight pre-incubation in medium with 1 mM or 25 mM glucose. (C) Pyruvate oxidation; $^{14}CO_2$-production during 4 h incubation with [1-^{14}C]pyruvic acid (0.25 μCi/ml, 0.2 mM), in presence of glucose (0.5 mM). (D) Fatty acid oxidation; with [1-^{14}C]palmitic acid (1 μCi/ml, 100 μM), in presence of L-carnitine (1 mM) and glucose (0.5 mM). The oxidation data are normalized to cell protein content (mg) and are displayed as mean ± SD of 4–8 replicates, from one representative of three separate experiments. The pathway illustrations show carbon flux fueled by the ^{14}C-labeled substrates. The filled and open circles represent radiolabeled (filled, ^{14}C) and non-labeled (open) carbons released as CO_2 under the respective conditions. Statistical analysis was performed by *t*-test. *$p < .05$, **$p < .01$, ***$p < .001$, ****$p < .0001$.

experimental conditions.

A previously established genetic reporter strategy was utilized to further evaluate the potential role of mitochondrial biogenesis under these conditions (Hodneland Nilsson et al., 2015). The reporter construct consists of a gene for mitochondrial GFP under the control of a responsive element of NRF1, which is a central nuclear transcription factor controlling expression of mitochondrial proteins. Single cell analysis was performed by flow cytometry in HeLa and MDA-MB-231 cells containing the reporter construct, following treatments with AICAR, WY 14,643 or TTA (Fig. 4E). Only AICAR was found to have a significant effect on mitochondrial biogenesis in HeLa cells, and this agreed with the findings in MDA-MB-231 cells (borderline statistical significance). This effect of AICAR was also previously observed in HeLa cells (Hodneland Nilsson et al., 2015). Both the genetic reporter results and the *TFAM* expression data indicated that the fuel shift from glucose to fatty acids occurs without simultaneous induction of mitochondrial biogenesis in these cell types. Western blot analysis supported that PDK4 protein abundance was increased following treatment with TTA, but not WY 14,643, in HeLa cells (Fig. 4F).

3.5. Effects of metabolic adaptation on mitochondrial respiration and glycolysis

To investigate if increased fatty acid oxidation was associated with changes in mitochondrial respiration, we measured oxygen consumption rate (OCR) in MDA-MB-231 cells after long-term (6 days) treatment with AICAR, WY 14,643 or TTA, and upon overexpression of *PPARA* (Fig. 5). Following measurement of the basal respiratory rate, we assessed descriptors of mitochondrial function through sequential additions of pharmacological modulators. Leak respiration rate was obtained after addition of oligomycin (ATP synthase inhibitor), and subsequently CCCP was administered to measure uncoupled respiratory capacity. Rotenone (respiratory complex I inhibitor) was then added, followed by antimycin A (respiratory complex III inhibitor) to assess non-mitochondrial activity (residual oxygen consumption, background activity). Interestingly, the basal respiratory rates were similar among the different conditions of metabolic adaptation (AICAR, WY 14,643, TTA and *PPARA* overexpression), and compared to respective controls (untreated and DMSO (vehicle)), with a minor increase in cultures treated with WY 14,643 and 60 μM TTA. Leak respiration was increased 2–3-fold in the TTA treated cultures compared to control (DMSO),

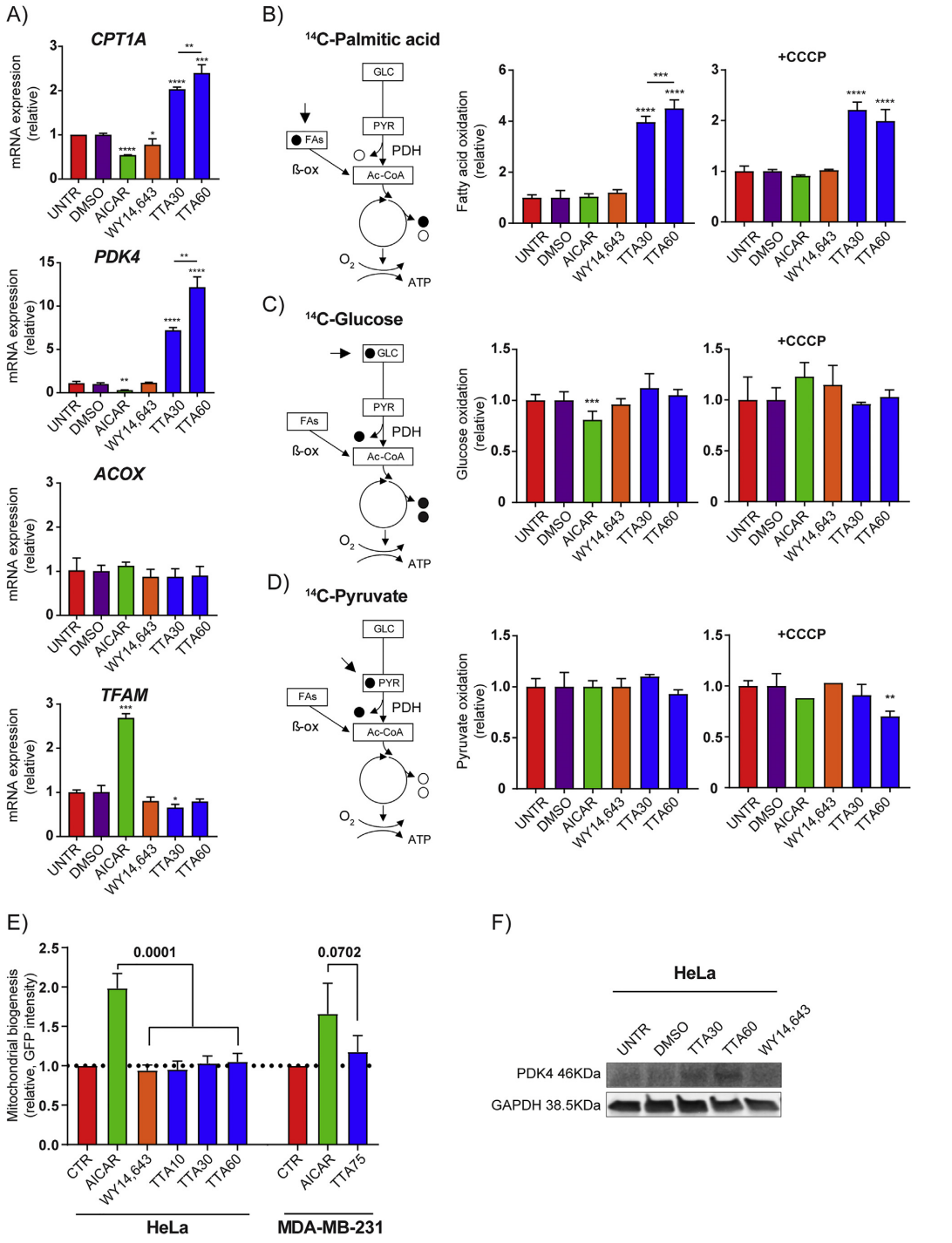

(caption on next page)

Fig. 4. *PDK4* expression and fatty acid oxidation in contexts of metabolic adaptation.
MDA-MB-231 were treated for 6 days with AICAR (0.5 mM), WY 14,643 (10 μM) or TTA (30 μM or 60 μM). Control cultures were untreated (UNTR, for AICAR) or DMSO-treated (DMSO, for WY 14,643 and TTA). (A) Real time quantitative PCR analysis of *TFAM*, *ACOX*, *CPT1A* and *PDK4*. The diagrams show mRNA expression relative to the control group (ddCT method), as mean ± SD of triplicate measurements. (B-D) Substrate oxidation was assessed by measuring $^{14}CO_2$-production during 4 h incubation with the respective radiolabeled substrate, in the absence and presence of an uncoupler (CCCP). (B) Fatty acid oxidation; with [1-^{14}C]palmitic acid (1 μCi/ml, 100 μM), in presence of L-carnitine (1 mM) and glucose (0.5 mM). (C) Glucose oxidation; with D-[^{14}C(U)]glucose (2 μCi/ml, 5 mM). (D) Pyruvate oxidation; with [1-^{14}C]pyruvic acid (0.25 μCi/ml, 2 mM). CCCP concentrations were 1 μM for glucose and pyruvate oxidation, and 3 μM for palmitic acid oxidation (higher due to the increased BSA concentration). The oxidation data are normalized to cell protein content (mg) and shown as mean ± SD of 4–8 replicates. The pathway illustrations show the carbon flux fueled by the ^{14}C-labeled substrates. The filled and open circles represent radiolabeled (filled, ^{14}C) and non-labeled (open) carbons, released as CO_2 under the respective conditions. (E) Measurement of mitochondrial biogenesis using a GFP-based reporter construct in HeLa and MDA-MB-231 cells. The reporter cells were treated before mitoGFP was detected by flow cytometry (10,000 cells per sample). (F) Western blot analysis of PDK4 in HeLa cells treated for 6 days with TTA (30 μM or 60 μM) or WY 14,643 (10 μM). All diagrams display representative data as, mean ± SD, for three separate experiments. Statistical analysis was performed by *t*-test. *$p < .05$, **$p < .01$, ***$p < .001$, ****$p < .0001$.

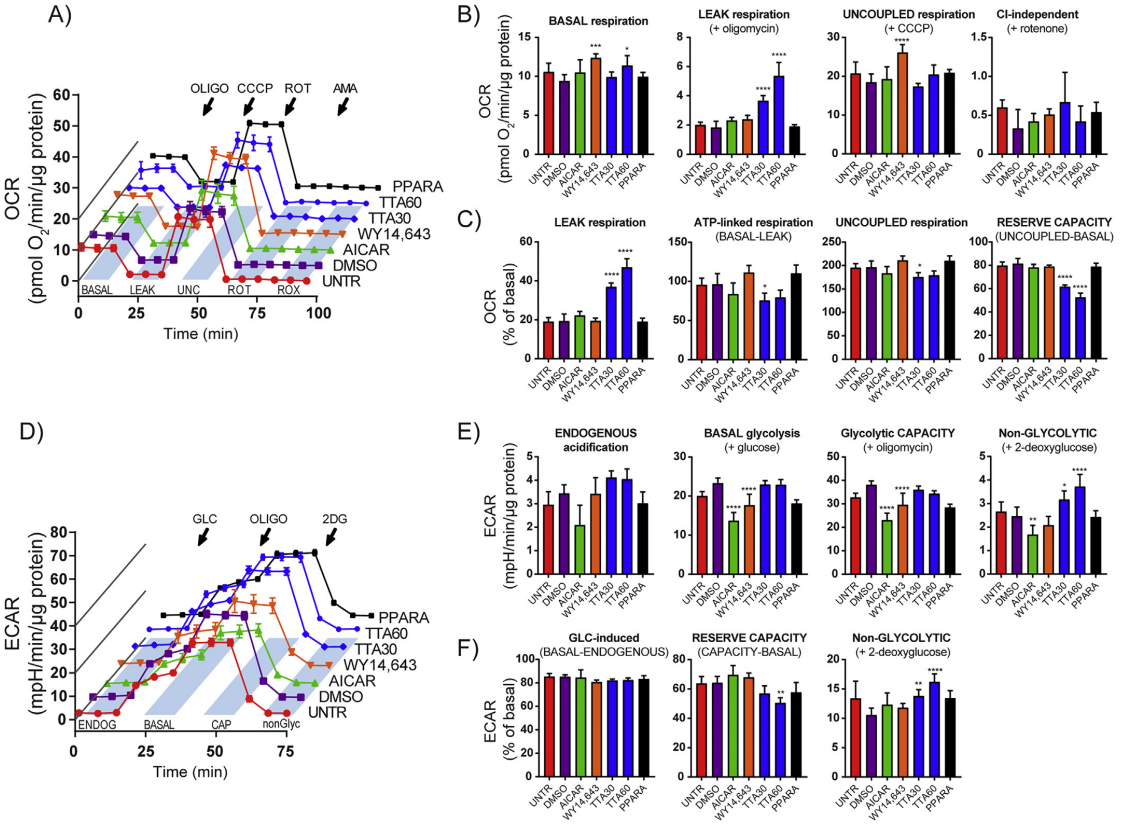

Fig. 5. Analysis of mitochondrial respiration and glycolysis.
Oxygen consumption rate (OCR) and extracellular acidification rates (ECAR) were measured in MDA-MB-231 cells after 6 days treatment with AICAR (0.5 mM), WY 14,643 (10 μM) and TTA (30 μM or 60 μM), and in cells overexpressing *PPARA*. Control cultures were untreated (UNTR, for AICAR and PPARA) or DMSO-treated (DMSO, for WY 14,643 and TTA) cells. (A) Representative traces of OCR (pmol O_2/min/μg protein). Following measurement of basal respiration (BASAL), specific modulators were added as indicated: 3 μM oligomycin to obtain leak respiration (LEAK), 1 μM CCCP to access uncoupled respiration (UNC), 1 μM rotenone to measure rotenone-resistant respiration (ROT) and 1 μM antimycin A to measure residual oxygen consumption (ROX). (B) Data extracted from the analyses in A, after subtraction of non-mitochondrial activity (ROX). (C) Analysis of functional integrity of mitochondria. Rates of interest calculated as % of basal OCR. (D) Representative traces of ECAR (mpH/min/μg protein). The specific modulators were added following measurement of endogenous activity (ENDOG), as indicated: 10 mM glucose (GLC) to obtain basal glycolysis (BASAL), 3 μM oligomycin to assess glycolytic capacity (CAP) and 100 mM 2-deoxyglucose (2DG) to measure non-glycolytic activity (non-Glyc). (E) Data extracted from the analyses in D. (F) Analysis of glycolytic function. Rates of interest calculated as % of basal ECAR. Data are displayed as mean ± SD of 6–8 replicates, from one representative of three separate experiments Statistical analysis was performed by ANOVA. *$p < .05$, **$p < .01$, ***$p < .001$, ****$p < .0001$.

apparently in a concentration-dependent manner. The uncoupled respiratory capacity was not significantly affected by AICAR, TTA or *PPARA*-overexpression, however, WY 14,643 caused approximately 20% increase compared to the control (DMSO) (Fig. 5B). Calculating these data as percentage of the basal respiratory rate (Fig. 5C) revealed that TTA significantly increased the fraction of oxygen consumption associated with leak respiration, and therefore caused a congruent decrease in ATP-linked respiration. The effects of the treatments on the relative respiratory capacity (uncoupled) were generally negligible, while TTA significantly reduced the reserve capacity. The findings were reproduced in HeLa cells (Supplementary Fig. S3). In summary, the highly increased fatty acid oxidation rate observed after treatment with TTA and upon overexpression of *PPARA* was not associated with major changes in basal mitochondrial respiration. However, TTA led to effects consistent with mild uncoupling, which may represent an additional mechanism contributing to metabolic adaptations.

Analysis of glycolytic function was performed by monitoring extracellular acidification rate (ECAR) following sequential additions of glucose to obtain basal respiratory rate, oligomycin to measure glycolytic capacity, and 2-deoxyglucose to determine non-glycolytic activity (Fig. 5D). There was a general reduction in normalized ECAR after treatment with AICAR and WY 14,643 in MDA-MB-231 cells (Fig. 5E), but upon additions of glucose and upon addition of oligomycin, the relative rates were similar to control (Fig. 5F), suggesting that glycolysis was modulated as normal under these conditions. No change in glycolytic activity was found in *PPARA*-overexpressing cells, compared to control cells. TTA-treated cells were also similar to control, but had a relatively high non-glycolytic acidifying component, displayed both before addition of glucose and after addition of 2-deoxyglucose. The TTA-treated cells tended to have slightly reduced reserve glycolytic capacity, and this was statistically significant in the cultures treated with 60 μM TTA (Fig. 5F). Similar findings were obtained in HeLa cell cultures, where TTA also caused a statistically significant increase in normalized basal glycolysis (Supplementary Fig. S3). In summary, the effects of metabolic modulators on glycolysis did not demonstrate a strong correlation with the changes in fatty acid oxidation under these conditions.

3.6. Mild uncoupling may contribute to increased fatty acid oxidation upon TTA-treatment

Based on the obtained data suggesting an uncoupling effect of TTA on mitochondrial respiration, we designed an experiment to investigate if TTA may mediate such effects through an acute mechanism. TTA was compared with palmitic acid, a normal saturated fatty acid, when added at different concentrations to MDA-MB-231 cells immediately before OCR analysis (Fig. 6A-B). Acute uncoupling activity could then be detected as an increase in leak respiration after addition of oligomycin. The data clearly demonstrated that TTA, but not palmitic acid, caused a concentration-dependent increase in leak respiration (Fig. 6C). Both TTA and palmitic acid caused a minor concentration-dependent decrease in uncoupled respiration after addition of CCCP (Fig. 6D). The uncoupling property of TTA was found to be relatively mild, as the highest concentration of 200 μM, which exceeds the normally tolerable concentration for cell survival, caused approximately 30% uncoupling compared to full uncoupling mediated by 1 μM CCCP (Fig. 6E). These findings were also reproduced in HeLa cells (Supplementary Fig. S4). Our data suggest mild uncoupling as a new mechanism of TTA, which induces an additional energy stress likely to influence and accentuate effects on nutrient-sensitive fueling pathways to support energy homeostasis. Such a mechanism may explain the effects related to the changed energy state previously observed in rat liver (Grav et al., 2003).

3.7. PDK4 expression reports synergistic effects of TTA and rapamycin on fatty acid oxidation

Rapamycin, an inhibitor of mTOR, has previously been found to increase fatty acid oxidation (Sipula et al., 2006). Further, studies in rat hepatocytes have linked the effects of TTA to regulation of mTOR (Hagland et al., 2013). To investigate if mTOR inhibition influences TTA-mediated metabolic adaptation, we treated MDA-MB-231 with TTA and rapamycin, separately and in combination. Rapamycin alone did not affect mRNA expression of *CPT1A* and *PDK4*. In combination with TTA, however, the levels of both these mRNAs were significantly higher than in cells treated with TTA alone (Fig. 7A-B). Exactly the same pattern was seen on rates of fatty acid oxidation, both under basal and uncoupled conditions (CCCP) (Fig. 7C). Further, we performed correlation analysis of *PDK4* and *CPT1A* expression relative to fatty acid oxidation, with data from different conditions of metabolic adaptation (Fig. 7D). Expression of *PDK4* and *CPT1A* was found to correlate strongly with each other, and with fatty acid oxidation activity. These data support a tight regulatory and functional relationship between *PDK4* expression and fatty acid oxidation in different metabolic contexts. An advantage of using *PDK4*, above *CPT1A*, as an indicator of fatty acid oxidation would be the significantly higher magnitude of induction, and therefore a larger dynamic range and higher sensitivity.

4. Discussion

This study shows that upregulated *PDK4* mRNA expression is strongly associated with increased activity of mitochondrial fatty acid oxidation in metabolically adapted cells and rat tissues. Overall, we found good correlation between the relative magnitude of *PDK4* upregulation and the accompanying increase in fatty acid oxidation. Based on these findings, we suggest that *PDK4* mRNA expression may be used as a sensitive surrogate marker for changes in mitochondrial fatty acid oxidation when investigating (pato)physiological adaptations of energy metabolism.

The activity of mitochondrial fatty acid oxidation is influenced by many factors, including diet, physical activity, toxic exposure, epigenetics and mutations. An unhealthy impact on fatty acid oxidation could lead to suboptimal energy balance, energy deficiency, excessive lipid storage and metabolic stresses, which ultimately contribute to pathogenesis both at an organ and systemic level (Adeva-Andany et al., 2018). On the other hand, metabolic adaptations may have positive impact, for instance in response to endurance training which increases the capacity of mitochondrial fatty acid oxidation to accommodate the elevated demands of energy (ATP) (Booth et al., 2015). In the laboratory, mitochondrial fatty acid oxidation may be assessed by measuring the products formed when radiolabeled fatty acid substrates are provided to intact cells or fresh preparations (extracts, homogenates) of cell cultures or tissues (e.g. (Wensaas et al., 2007)). However, such methods are often inaccessible, or incompatible with regards to the available sample material. Measurement of surrogate markers, such as mRNA expression of relevant genes, may therefore represent an attractive strategy to study regulatory effects on fatty acid oxidation. As far as we know, there is no consensus to which gene targets that are optimal for serving as expression reporters of a metabolic shift involving increase in fatty acid oxidation. As for enzymes of the fatty acid oxidation machinery, the changes in mRNA expression are often found subtle and with complex cell-type specific regulation. Therefore, we investigated *PDK4* expression as a possible candidate for such purpose, under conditions of metabolic adaptation driven by different regulatory programs involving AMPK, PPARs and mTOR, which are relevant for mechanisms of exercise, starving, obesity and contexts of defective metabolism.

In rats that were treated with TTA for 50 weeks, we found significantly increased expression of *Pdk4* particularly in liver, and to some extent in heart, but not in skeletal muscle and white adipose tissue

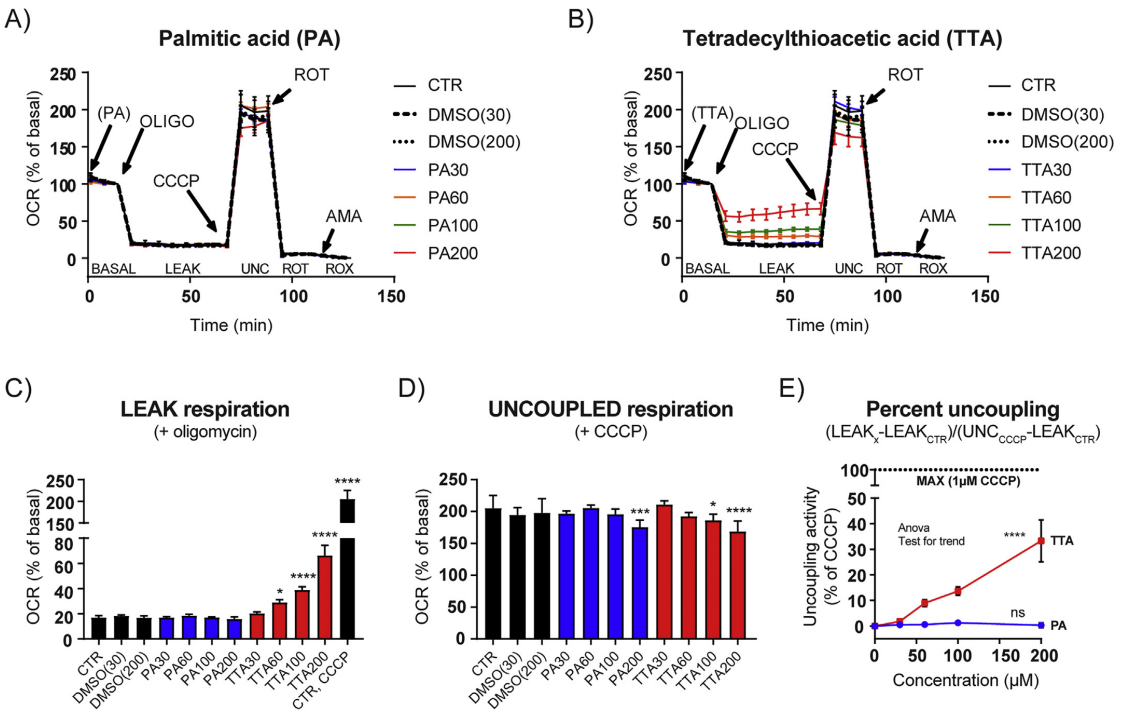

Fig. 6. TTA exerts mild uncoupling activity.

Oxygen consumption rate (OCR) was measured in MDA-MB-231 cells immediately after administration palmitic acid (PA) or tetradecylthioacetic acid (TTA), at concentrations of 30–200 μM. (A-B) Representative traces of OCR as % of initial rate (BASAL), in presence of PA or TTA. Specific modulators were added as indicated: 3 μM oligomycin to obtain leak respiration (LEAK), 1 μM CCCP to access uncoupled respiration (UNC), 1 μM rotenone to measure rotenone-resistant respiration (ROT) and 1 μM antimycin A to measure residual oxygen consumption (ROX). (C) LEAK respiration and (D) UNCOUPLED respiration shown as % of basal OCR. (E) Uncoupling activity mediated by PA and TTA, compared to complete uncoupler, CCCP (100%). The agent-induced LEAK rate (i.e. $LEAK_X$ - $LEAK_{CTR}$) was calculated relative to the CCCP-induced LEAK rate (i.e. UNC_{CCCP}-$LEAK_{CTR}$). Data are displayed as mean ± SD of 6–8 replicates, from one representative of three separate experiments. Statistical analysis was performed by ANOVA. $*p < .05$, $**p < .01$, $***p < .001$, $****p < .0001$.

(WAT). This parallels well with increased rates of mitochondrial fatty acid oxidation especially in liver, and also in heart tissue, of TTA-treated rats (Berge et al., 2005; Oie et al., 2013). In addition, we found a pronounced increase in the muscle isoform *Cpt1b* in liver, yet only a minor increase in heart, and no detectable effect in muscle and WAT. TTA also caused significantly increased *Me-1* expression in rat liver, supporting that strengthened TCA anaplerotism contributes to the adaptation of high mitochondrial fatty acid oxidation rates (Gibala et al., 2000; Carley et al., 2015). These data underscore the importance of context- and tissue-specific influences on gene regulation associated with the fatty acid oxidation machinery. Interestingly, PDK4 upregulation was consistently presented under conditions of increased fatty acid oxidation in our studies, both in vivo and in vitro.

In cultured MDA-MB-231 cells, we found highly increased *PDK4* expression accompanying enhanced mitochondrial fatty acid oxidation upon *PPARA*-overexpression and after long-term treatment with TTA. Congruently, *PDK4*-overexpression caused reduced pyruvate oxidation simultaneously with increased fatty acid oxidation when the cells were grown in high glucose. When transferred to low glucose conditions, fatty acid oxidation in the parental cells increased to the same level as the *PDK4*-overexpressing cells. This supports the theory that increased *PDK4* expression contributes to fasting/starving-type metabolism with stimulated fatty acid oxidation (Wu et al., 2000), and our findings suggest that this program is constitutively active in the *PDK4*–overexpressing cells. Hence, there is strong evidence for a tight regulatory and functional relationship between *PDK4* and the fatty acid oxidation pathway. Direct activation of PPARα with WY-14,643 had no effect on fatty acid oxidation in MDA-MB-231 cells, possibly due to a low endogenous amount of this transcription factor, since overexpression caused classical effects on cellular gene expression and metabolism. The AMPK activator AICAR induced *TFAM* expression, suggestive of increased mitochondrial biogenesis as previously observed in HeLa cells (Hodneland Nilsson et al., 2015); however, there was no effect on mitochondrial fatty acid oxidation. On the contrary, AICAR had a suppressive effect on *CPT1A* and *PDK4* expression. This is compatible with previous findings in rat adipose tissue (Wan et al., 2010), but not in skeletal muscle (Merrill et al., 1997). Interestingly, in addition to the known function as panPPAR activator, TTA was found to act directly as a mild mitochondrial uncoupler, which may contribute to the changed energy state previously observed in rat liver (Grav et al., 2003). In that study, reduced mitochondrial membrane potential was found in rat liver after treatment with TTA, however, it remained unclear if this could be a direct or indirect mechanism. Due to the acute effects in our present cell culture study, it seems likely that TTA has a direct uncoupling effect on the mitochondrial inner membrane.

Inhibition of mTOR by rapamycin did not induce fatty acid oxidation or *PDK4* expression in MDA-MB-231 cells, but it accentuated the effects of TTA, suggesting that mTOR can act together with other pathways of metabolic adaptation in a context-dependent manner. In support, mTOR has been found to be regulated by the level of PDK4 in

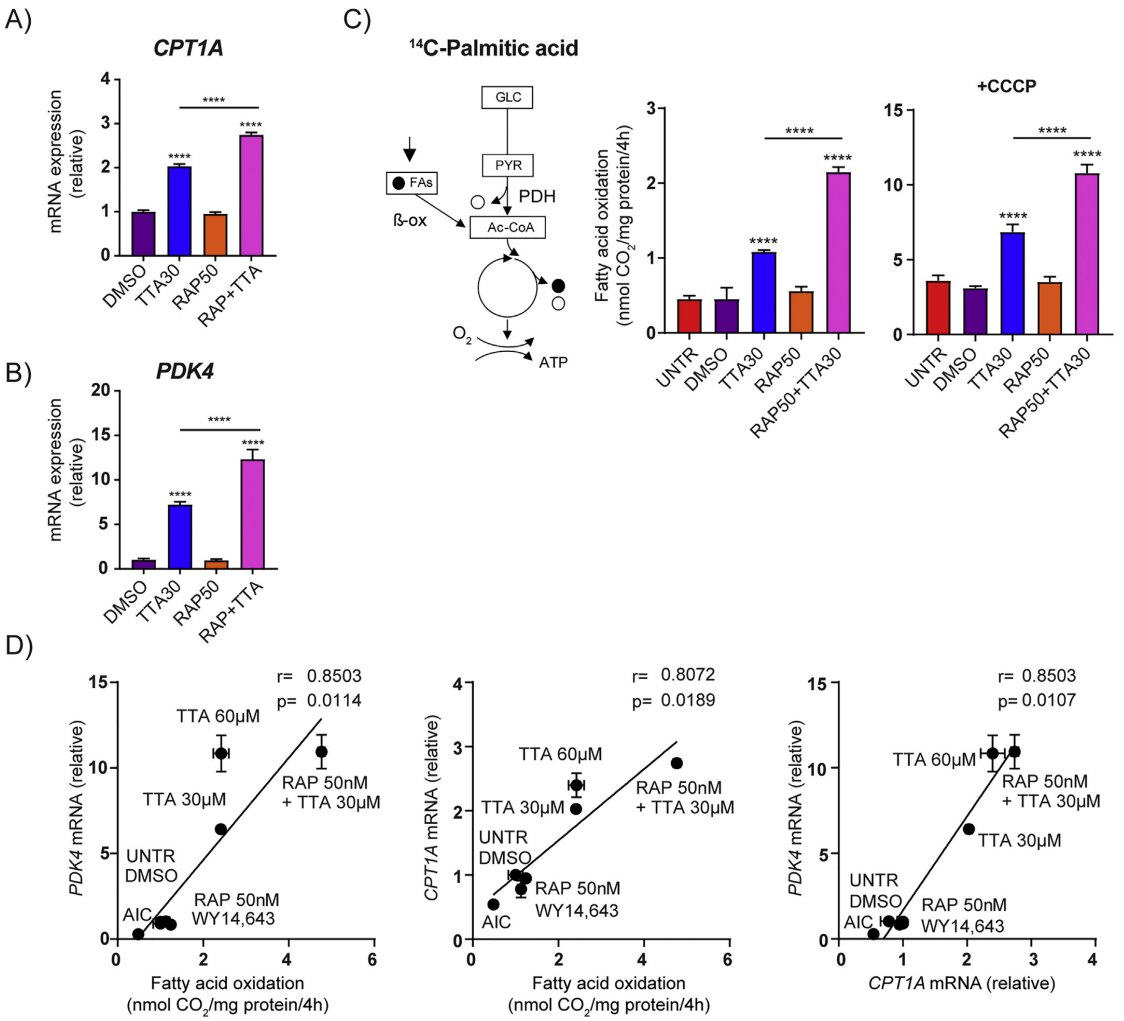

Fig. 7. Synergistic effects of TTA and rapamycin on fatty acid oxidation.
MDA-MB-231 were treated for 6 days with TTA (30 µM) or rapamycin (50 nM, RAP), separately and in combination. (A) *CPT1A* and (B) *PDK4* expression was measured using real time quantitative PCR as mean ± SD of triplicate measurements. (C) Fatty acid oxidation was assessed by measuring $^{14}CO_2$-production during 4 h incubation with [1-^{14}C]palmitic acid (1 µCi/ml, 100 µM) in presence of L-carnitine (1 mM) and glucose (0.5 mM), with and without an uncoupler (3 µM CCCP). The oxidation data are normalized to cell protein content (mg). The pathway illustrations show the carbon flux fueled by the ^{14}C-labeled palmitic acid. The filled and open circles represent radiolabeled (filled, ^{14}C) and non-labeled (open) carbons, released as CO_2 under the respective conditions. (D) Correlation analysis (Spearman) of data obtained from multiple conditions of metabolic adaptation. *PDK4* mRNA expression was analyzed relative to fatty acid oxidation and *CPT1A* expression. The oxidation data are shown as mean ± SD of 4–8 replicates, from one representative for three separate experiments. Statistical comparisons was performed by ANOVA. *p < .05, **p < .01, ***p < .001, ****p < .0001.

cultured cells (Liu et al., 2014). In separate experiments, we found the effects in HeLa cells to be similar to the observations in MDA-MB-231 cells.

A rather striking observation was the minor changes regarding mitochondrial respiration and lactate production under basal cell culture assay conditions, despite the pronounced changes in metabolic fuel utilization indicated by increased fatty acid oxidation. This suggests that the increase in fatty acid oxidation did not change the activity balance between mitochondrial respiration and glycolysis, but rather a change in substrate preference serving to maintain the supply of acetyl-CoA for the TCA cycle. This type of cellular metabolic adaptation is likely to affect properties of metabolic flexibility and associated stress mechanisms, and therefore the susceptibility for changes in nutrient supply. The present study primarily investigated metabolic effects under standard cell culture conditions, which includes high glucose concentration (normally 25 mM in DMEM), and favorable effects on glycolysis are expected to occur under such conditions. The dependency on mitochondrial oxidative metabolism following relevant adaptations of fuel utilization may be addressed further e.g. by reducing the amount of glucose, or replacing glucose with galactose in the culture medium (Arroyo et al., 2016).

Systemic and cellular nutrient-sensitive mechanisms in the body

interact to mediate adaptations to changed metabolic needs or conditions (e.g. due to activity or diet). For instance, increased release of free fatty acids from adipose tissue under fasting would be expected to influence metabolism in relevant tissues, partly through ligand activation of PPARs. The effects of such events will vary depending on tissue and cell type. Therefore, it was interesting to find that increased *PDK4* expression was a rather consistent sign of increased fatty acid oxidation throughout this study. Measuring *PDK4* may be relevant in clinical investigations, as exemplified by the finding that upregulated *PDK4* expression in blood cells was associated with impaired PDH function in ME/CFS patients (Fluge et al., 2016), which may involve adaptations of fatty acid oxidation (Naviaux et al., 2016; Germain et al., 2017). Furthermore, diurnal variation in *PDK4* expression in blood cells was recently reported to be associated with plasma free fatty acid levels, supporting that this mirrors an important aspect of metabolic fuel switching (Yamaguchi et al., 2018). Hence, based on these findings, and supported by the current literature, upregulated *PDK4* expression appears as a sensitive marker for metabolic adaptations involving increased rates of mitochondrial fatty acid oxidation.

Acknowledgements

We are grateful to Sissel Vik Berge and Endre Stigen for their excellent technical assistance, and to Stein-Rune Lindhom for the custom made equipment for $^{14}CO_2$-trapping. Flow cytometry was performed using the infrastructure of The Bergen Flow Cytometry Core Facility, Department of Clinical Science, University of Bergen, Norway. The work was funded by grants from the Research Council of Norway (272680), and the Kavli Trust, Norway.

Declaration of Competing Interest

The authors declare that they have no conflicts of interest with the contents of this article.

Appendix A. Supplementary data

Supplementary data to this article can be found online at https://doi.org/10.1016/j.mito.2019.07.009.

References

Adeva-Andany, M.M., Carneiro-Freire, N., Seco-Filgueira, M., Fernandez-Fernandez, C., Mourino-Bayolo, D., 2019. Mitochondrial beta-oxidation of saturated fatty acids in humans. Mitochondrion 46, 73–90.

Arroyo, J.D., Jourdain, A.A., Calvo, S.E., Ballarano, C.A., Doench, J.G., Root, D.E., Mootha, V.K., 2016. A genome-wide CRISPR death screen identifies genes essential for oxidative phosphorylation. Cell Metab. 24, 875–885.

Badin, P.M., Loubiere, C., Coonen, M., Louche, K., Tavernier, G., Bourlier, V., Mairal, A., Rustan, A.C., Smith, S.R., Langin, D., Moro, C., 2012. Regulation of skeletal muscle lipolysis and oxidative metabolism by the co-lipase CGI-58. J. Lipid Res. 53, 839–848.

Berge, R.K., Tronstad, K.J., Berge, K., Rost, T.H., Wergedahl, H., Gudbrandsen, O.A., Skorve, J., 2005. The metabolic syndrome and the hepatic fatty acid drainage hypothesis. Biochimie 87, 15–20.

Booth, F.W., Ruegsegger, G.N., Toedebusch, R.G., Yan, Z., 2015. Endurance exercise and the regulation of skeletal muscle metabolism. Prog. Mol. Biol. Transl. Sci. 135, 129–151.

Cadoudal, T., Distel, E., Durant, S., Fouque, F., Blouin, J.M., Collinet, M., Bortoli, S., Forest, C., Benelli, C., 2008. Pyruvate dehydrogenase kinase 4: regulation by thiazolidinediones and implication in glyceroneogenesis in adipose tissue. Diabetes 57, 2272–2279.

Carley, A.N., Taglieri, D.M., Bi, J., Solaro, R.J., Lewandowski, E.D., 2015. Metabolic efficiency promotes protection from pressure overload in hearts expressing slow skeletal troponin I. Circ. Heart Fail. 8, 119–127.

Desvergne, B., Michalik, L., Wahli, W., 2006. Transcriptional regulation of metabolism. Physiol. Rev. 86, 465–514.

Dyrstad, S.E., Tusubira, D., Knappskog, S., Tronstad, K.J., Rosland, G.V., 2018. Introducing nano-scale quantitative polymerase chain reaction. Biochem. Biophys. Res. Commun. 506, 923–926.

Feng, Y.Z., Nikolic, N., Bakke, S.S., Boekschoten, M.V., Kersten, S., Kase, E.T., Rustan, A.C., Thoresen, G.H., 2014. PPARdelta activation in human myotubes increases mitochondrial fatty acid oxidative capacity and reduces glucose utilization by a switch in substrate preference. Arch. Physiol. Biochem. 120, 12–21.

Finck, B.N., Lehman, J.J., Leone, T.C., Welch, M.J., Bennett, M.J., Kovacs, A., Han, X., Gross, R.W., Kozak, R., Lopaschuk, G.D., Kelly, D.P., 2002. The cardiac phenotype induced by PPARalpha overexpression mimics that caused by diabetes mellitus. J. Clin. Invest. 109, 121–130.

Fluge, O., Mella, O., Bruland, O., Risa, K., Dyrstad, S.E., Alme, K., Rekeland, I.G., Sapkota, D., Rosland, G.V., Fossa, A., Ktoridou-Valen, I., Lunde, S., Sorland, K., Lien, K., Herder, I., Thurmer, H., Gotaas, M.E., Baranowska, K.A., Bohnen, L.M., Schafer, C., McCann, A., Sommerfelt, K., Helgeland, L., Ueland, P.M., Dahl, O., Tronstad, K.J., 2016. Metabolic profiling indicates impaired pyruvate dehydrogenase function in myalgic encephalopathy/chronic fatigue syndrome. JCI Insight 1, e89376.

Fukawa, T., Yan-Jiang, B.C., Min-Wen, J.C., Jun-Hao, E.T., Huang, D., Qian, C.N., Ong, P., Li, Z., Chen, S., Mak, S.Y., Lim, W.J., Kanayama, H.O., Mohan, R.E., Wang, R.R., Lai, J.H., Chua, C., Ong, H.S., Tan, K.K., Ho, Y.S., Tan, I.B., Teh, B.T., Shyh-Chang, N., 2016. Excessive fatty acid oxidation induces muscle atrophy in cancer cachexia. Nat. Med. 22, 666–671.

Galgani, J.E., Moro, C., Ravussin, E., 2008. Metabolic flexibility and insulin resistance. Am. J. Physiol. Endocrinol. Metab. 295, E1009–E1017.

Germain, A., Ruppert, D., Levine, S.M., Hanson, M.R., 2017. Metabolic profiling of a myalgic encephalomyelitis/chronic fatigue syndrome discovery cohort reveals disturbances in fatty acid and lipid metabolism. Mol. BioSyst. 13, 371–379.

Gibala, M.J., Young, M.E., Taegtmeyer, H., 2000. Anaplerosis of the citric acid cycle: role in energy metabolism of heart and skeletal muscle. Acta Physiol. Scand. 168, 657–665.

Grav, H.J., Tronstad, K.J., Gudbrandsen, O.A., Berge, K., Fladmark, K.E., Martinsen, T.C., Waldum, H., Wergedahl, H., Berge, R.K., 2003. Changed energy state and increased mitochondrial beta-oxidation rate in liver of rats associated with lowered proton electrochemical potential and stimulated uncoupling protein 2 (UCP-2) expression: evidence for peroxisome proliferator-activated receptor-alpha independent induction of UCP-2 expression. J. Biol. Chem. 278, 30525–30533.

Hagland, H.R., Nilsson, L.I., Burri, L., Nikolaisen, J., Berge, R.K., Tronstad, K.J., 2013. Induction of mitochondrial biogenesis and respiration is associated with mTOR regulation in hepatocytes of rats treated with the pan-PPAR activator tetradecylthioacetic acid (TTA). Biochem. Biophys. Res. Commun. 430, 573–578.

Hodneland Nilsson, L.I., Nitschke Pettersen, I.K., Nikolaisen, J., Micklem, D., Avsnes Dale, H., Vatne Rosland, G., Lorens, J., Tronstad, K.J., 2015. A new live-cell reporter strategy to simultaneously monitor mitochondrial biogenesis and morphology. Sci. Rep. 5, 17217.

Holness, M.J., Sugden, M.C., 2003. Regulation of pyruvate dehydrogenase complex activity by reversible phosphorylation. Biochem. Soc. Trans. 31, 1143–1151.

Jeong, J.Y., Jeoung, N.H., Park, K.G., Lee, I.K., 2012. Transcriptional regulation of pyruvate dehydrogenase kinase. Diabetes Metab. J. 36, 328–335.

Jose, C., Melser, S., Benard, G., Rossignol, R., 2013. Mitoplasticity: adaptation biology of the mitochondrion to the cellular redox state in physiology and carcinogenesis. Antioxid. Redox Signal. 18, 808–849.

Kimura, M., Takatsuki, A., Yamaguchi, I., 1994. Blasticidin S deaminase gene from Aspergillus terreus (BSD): a new drug resistance gene for transfection of mammalian cells. Biochim. Biophys. Acta 1219, 653–659.

Lin, S.C., Hardie, D.G., 2018. AMPK: sensing glucose as well as cellular energy status. Cell Metab. 27, 299–313.

Lindquist, C., Bjorndal, B., Rossmann, C.R., Tusubira, D., Svardal, A., Rosland, G.V., Tronstad, K.J., Hallstrom, S., Berge, R.K., 2017. Increased hepatic mitochondrial FA oxidation reduces plasma and liver TG levels and is associated with regulation of UCPs and APOC-III in rats. J. Lipid Res. 58, 1362–1373.

Liu, Z., Chen, X., Wang, Y., Peng, H., Wang, Y., Jing, Y., Zhang, H., 2014. PDK4 protein promotes tumorigenesis through activation of cAMP-response element-binding protein (CREB)-Ras homolog enriched in brain (RHEB)-mTORC1 signaling cascade. J. Biol. Chem. 289, 29739–29749.

Livak, K.J., Schmittgen, T.D., 2001. Analysis of relative gene expression data using real-time quantitative PCR and the 2(−Delta Delta C(T)) method. Methods 25, 402–408.

Manio, M.C., Inoue, K., Fujitani, M., Matsumura, S., Fushiki, T., 2016. Combined pharmacological activation of AMPK and PPARdelta potentiates the effects of exercise in trained mice. Physiol. Rep. 4.

Merrill, G.F., Kurth, E.J., Hardie, D.G., Winder, W.W., 1997. AICA riboside increases AMP-activated protein kinase, fatty acid oxidation, and glucose uptake in rat muscle. Am. J. Phys. 273, E1107–E1112.

Naviaux, R.K., Naviaux, J.C., Li, K., Bright, A.T., Alaynick, W.A., Wang, L., Baxter, A., Nathan, N., Anderson, W., Gordon, E., 2016. Metabolic features of chronic fatigue syndrome. Proc. Natl. Acad. Sci. U. S. A. 113, E5472–E5480.

Oie, E., Berge, R.K., Ueland, T., Dahl, C.P., Edvardsen, T., Beitnes, J.O., Bohov, P., Aukrust, P., Yndestad, A., 2013. Tetradecylthioacetic acid increases fat metabolism and improves cardiac function in experimental heart failure. Lipids 48, 139–154.

O'Neill, H.M., Lally, J.S., Galic, S., Thomas, M., Azizi, P.D., Fullerton, M.D., Smith, B.K., Pulinilkunnil, T., Chen, Z., Samaan, M.C., Jorgensen, S.B., Dyck, J.R., Holloway, G.P., Hawke, T.J., van Denderen, B.J., Kemp, B.E., Steinberg, G.R., 2014. AMPK phosphorylation of ACC2 is required for skeletal muscle fatty acid oxidation and insulin sensitivity in mice. Diabetologia 57, 1693–1702.

Pear, W.S., Nolan, G.P., Scott, M.L., Baltimore, D., 1993. Production of high-titer helper-free retroviruses by transient transfection. Proc. Natl. Acad. Sci. U. S. A. 90, 8392–8396.

Pin, F., Novinger, L.J., Huot, J.R., Harris, R.A., Couch, M.E., O'Connell, T.M., Bonetto, A., 2019. PDK4 drives metabolic alterations and muscle atrophy in cancer cachexia. FASEB J. 33, 7778–7790.

Roche, T.E., Hiromasa, Y., 2007. Pyruvate dehydrogenase kinase regulatory mechanisms and inhibition in treating diabetes, heart ischemia, and cancer. Cell. Mol. Life Sci. 64, 830–849.

Rohlenova, K., Veys, K., Miranda-Santos, I., De Bock, K., Carmeliet, P., 2018. Endothelial

cell metabolism in health and disease. Trends Cell Biol. 28, 224–236.
Rost, T.H., Haugan Moi, L.L., Berge, K., Staels, B., Mellgren, G., Berge, R.K., 2009. A pan-PPAR ligand induces hepatic fatty acid oxidation in PPARalpha−/− mice possibly through PGC-1 mediated PPARdelta coactivation. Biochim. Biophys. Acta 1791, 1076–1083.
Saxton, R.A., Sabatini, D.M., 2017. mTOR signaling in growth, metabolism, and disease. Cell 168, 960–976.
Sipula, I.J., Brown, N.F., Perdomo, G., 2006. Rapamycin-mediated inhibition of mammalian target of rapamycin in skeletal muscle cells reduces glucose utilization and increases fatty acid oxidation. Metabolism 55, 1637–1644.
Sugden, M.C., 2003. PDK4: a factor in fatness? Obes. Res. 11, 167–169.
Sugden, M.C., Holness, M.J., 1994. Interactive regulation of the pyruvate dehydrogenase complex and the carnitine palmitoyltransferase system. FASEB J. 8, 54–61.
Sugden, M.C., Bulmer, K., Gibbons, G.F., Holness, M.J., 2001. Role of peroxisome proliferator-activated receptor-alpha in the mechanism underlying changes in renal pyruvate dehydrogenase kinase isoform 4 protein expression in starvation and after refeeding. Arch. Biochem. Biophys. 395, 246–252.
Trexler, E.T., Smith-Ryan, A.E., Norton, L.E., 2014. Metabolic adaptation to weight loss: implications for the athlete. J. Int. Soc. Sports Nutr. 11, 7.
Tronstad, K.J., Nooteboom, M., Nilsson, L.I., Nikolaisen, J., Sokolewicz, M., Grefte, S., Pettersen, I.K., Dyrstad, S., Hoel, F., Willems, P.H., Koopman, W.J., 2014. Regulation and quantification of cellular mitochondrial morphology and content. Curr. Pharm. Des. 20, 5634–5652.
Turell, M.J., 1989. Effect of environmental temperature on the vector competence of Aedes fowleri for Rift Valley fever virus. Res. Virol. 140, 147–154.
Vigerust, N.F., Cacabelos, D., Burri, L., Berge, K., Wergedahl, H., Christensen, B., Portero-Otin, M., Viste, A., Pamplona, R., Berge, R.K., Bjorndal, B., 2012. Fish oil and 3-thia fatty acid have additive effects on lipid metabolism but antagonistic effects on oxidative damage when fed to rats for 50 weeks. J. Nutr. Biochem. 23, 1384–1393.
Wan, Z., Thrush, A.B., Legare, M., Frier, B.C., Sutherland, L.N., Williams, D.B., Wright, D.C., 2010. Epinephrine-mediated regulation of PDK4 mRNA in rat adipose tissue. Am. J. Physiol. Cell Physiol. 299, C1162–C1170.
Wensaas, A.J., Rustan, A.C., Lovstedt, K., Kull, B., Wikstrom, S., Drevon, C.A., Hallen, S., 2007. Cell-based multiwell assays for the detection of substrate accumulation and oxidation. J. Lipid Res. 48, 961–967.
Wensaas, A.J., Rustan, A.C., Just, M., Berge, R.K., Drevon, C.A., Gaster, M., 2009. Fatty acid incubation of myotubes from humans with type 2 diabetes leads to enhanced release of beta-oxidation products because of impaired fatty acid oxidation: effects of tetradecylthioacetic acid and eicosapentaenoic acid. Diabetes 58, 527–535.
Winder, W.W., Wilson, H.A., Hardie, D.G., Rasmussen, B.B., Hutber, C.A., Call, G.B., Clayton, R.D., Conley, L.M., Yoon, S., Zhou, B., 1997. Phosphorylation of rat muscle acetyl-CoA carboxylase by AMP-activated protein kinase and protein kinase a. J. Appl. Physiol. (1985) 82, 219–225.
Wu, P., Inskeep, K., Bowker-Kinley, M.M., Popov, K.M., Harris, R.A., 1999. Mechanism responsible for inactivation of skeletal muscle pyruvate dehydrogenase complex in starvation and diabetes. Diabetes 48, 1593–1599.
Wu, P., Blair, P.V., Sato, J., Jaskiewicz, J., Popov, K.M., Harris, R.A., 2000. Starvation increases the amount of pyruvate dehydrogenase kinase in several mammalian tissues. Arch. Biochem. Biophys. 381, 1–7.
Yamaguchi, S., Moseley, A.C., Almeda-Valdes, P., Stromsdorfer, K.L., Franczyk, M.P., Okunade, A.L., Patterson, B.W., Klein, S., Yoshino, J., 2018. Diurnal variation in PDK4 expression is associated with plasma free fatty acid availability in people. J. Clin. Endocrinol. Metab. 103, 1068–1076.

Supplementary information

Upregulated PDK4 expression is a sensitive marker of increased fatty acid oxidation

Ina Katrine Nitschke Pettersen[a#], Deusdedit Tusubira[a#], Hanan Ashrafi[a], Sissel Elisabeth Dyrstad[a], Lena Hansen[a,b], Xiao-Zheng Liu[a], Linn Iren Hodneland Nilsson[a], Nils Gunnar Løvsletten[c], Kjetil Berge[d], Hege Wergedahl[e], Bodil Bjørndal[f], Øystein Fluge[b], Ove Bruland[g], Arild Christian Rustan[c], Nils Halberg[a], Gro Vatne Røsland[a,b], Rolf Kristian Berge[f,h], Karl Johan Tronstad[a*]

[a]Department of Biomedicine, University of Bergen, Norway, [b]Department of Oncology and Medical Physics, Haukeland University Hospital, Bergen, Norway, [c]Department of Pharmacy, University of Oslo, Norway, [d]Skretting AS, Stavanger, Norway, [e]Department of Sport, Food and Natural Sciences, Western Norway University of Applied Sciences, Bergen, Norway, [f]Department of Clinical Science, University of Bergen, Norway, [g]Department of Medical Genetics and Molecular Medicine, Haukeland University Hospital, Bergen, Norway, [h]Department of Heart Disease, Haukeland University Hospital, Bergen, Norway. [#] Equal contribution

Content

Gene	Liver	Heart	Muscle	WA T
Pdk4	18.0 0 ± 2.58*	2.48 ± 0.75 *	1.16 ± 0.93	1.02 ± 0.60
Cpt1a	2.42 ± 0.80*	1.12 ± 0.19	1.07 ± 0.31	1.00 ± 0.40
Cpt1b	478.09 ± 195. 43*	1.19 ± 0.10 *	1.40 ± 0.52	1.22 ± 0.57
Cpt2	5.15 ± 1.22*	1.06 ± 0.14	1.52 ± 0.60	1.01 ± 0.19
Acox	10.1 3 ± 2.84*	1.71 ± 0.27 *	1.11 ± 0.27	1.01 ± 0.17
Tfam	2.36 ± 1.13*	0.83 ± 0.04 *	0 .89 ± 0.1 6	0.93 ± 0.13
Nrf1	1.16 ± 0.30	0.94 ± 0.11	1.04 ± 0.12	1.03 ± 0.19
Me-1	57.9 7 ± 21.93 *	1 .52 ± 0.28*	0.90 ± 0.24	0.79 ± 0.41

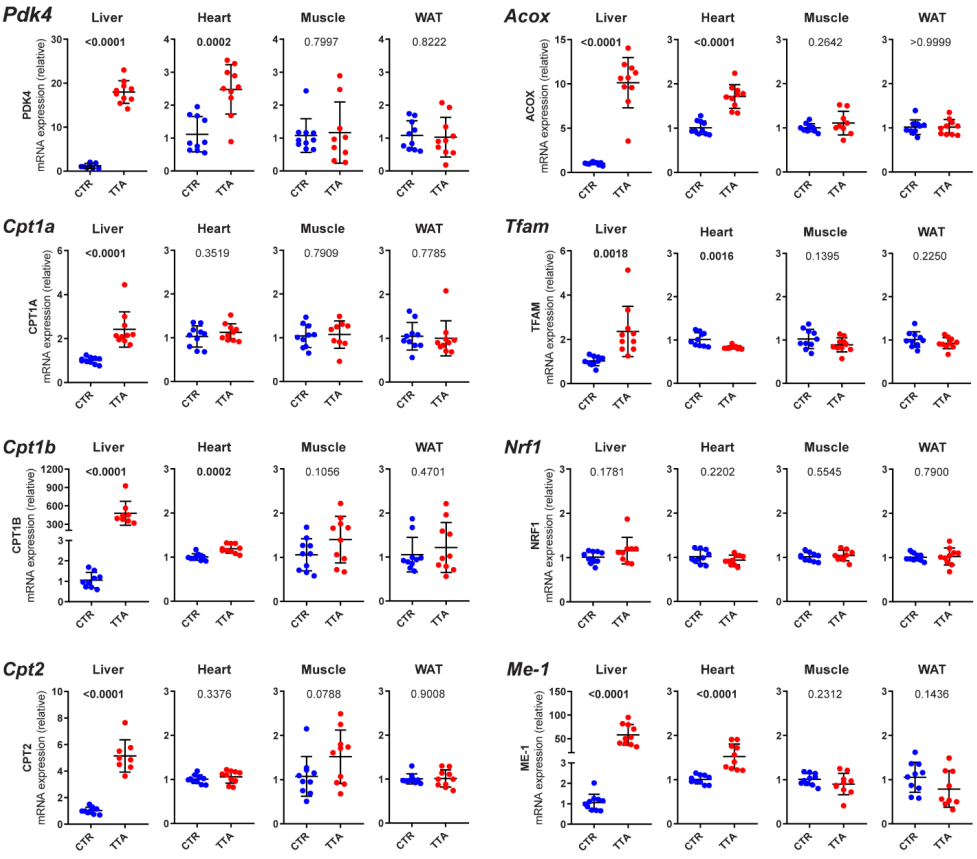

Supplementary Fig. S1. Gene expression associated with fatty acid oxidation in TTA-treated rats.
Gene expression was analyzed in liver, heart, skeletal muscle and white adipose tissue (WAT) from rats administered control (CTR) or TTA-supplemented diet for 50 weeks (Vigerust et al, 2012, J Nutr Biochem 23, 1384-1393), using real time quantitative PCR. The data are shown as mRNA expression relative to the CTR group (ddCT method).Data are shown as mean ± SD (n = 8-10). Statistical analysis was performed by t-test. *p< .01

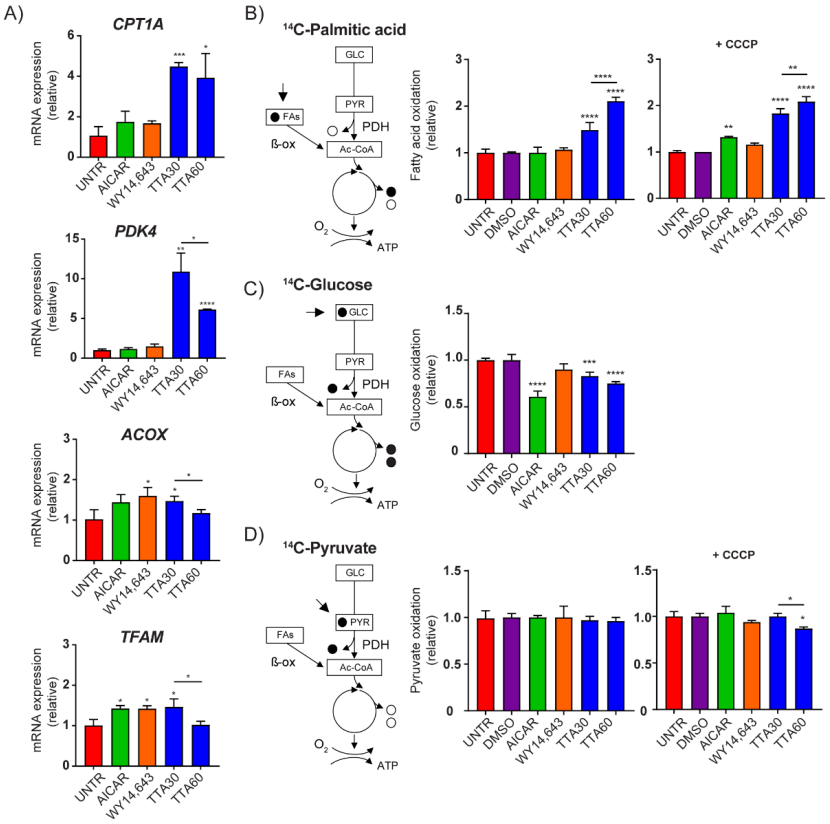

Supplementary Fig. S2. *PDK4* expression and fatty acid oxidation in contexts of metabolic adaptation**.**
HeLa were treated for 6 days with AICAR (0.5 mM), WY 14,643 (10 µM) or TTA (30 µM or 60 µM). Control cultures were untreated (UNTR, for AICAR) or DMSO-treated (DMSO, for WY 14,643 and TTA). (A) Real time quantitative PCR analysis of *TFAM*, *ACOX*, *CPT1A* and *PDK4*. The diagrams show mRNA expression relative to the control group (ddCT method), as mean ± SD of triplicate measurements. (B-D) Substrate oxidation was assessed by measuring $^{14}CO_2$-production during 2h incubation with the respective radiolabeled substrate, in the presence and absence of uncoupler (CCCP). (B) Fatty acid oxidation; with [1-^{14}C]palmitic acid (1 µCi/ml, 100 µM) in presence of L-carnitine (1 mM) and glucose (0.5 mM). (C) Glucose oxidation; with D-[^{14}C(U)]glucose (4 µCi/ml, 5 mM). (D) Pyruvate oxidation; with [1-^{14}C]pyruvic acid (0.25 µCi/ml, 2 mM). CCCP concentrations were 1 µM for glucose and pyruvate, and 3 µM for palmitic acid oxidation. The oxidation data are normalized to cell protein content (mg), calculated relative to the respective control, and shown as mean ± SD of 4-8 replicates. The pathway illustrations show the carbon flux fueled by the ^{14}C-labeled substrates. The filled and open circles represent radiolabeled (filled, ^{14}C) and non-labeled (open) carbons, released as CO_2 under the respective conditions. All figures display representative data as, mean ± SD, from one representative of three separate experiments. Statistical analysis was performed by t-test. *p< .05, **p< .01, ***p< .001, ****p< .0001

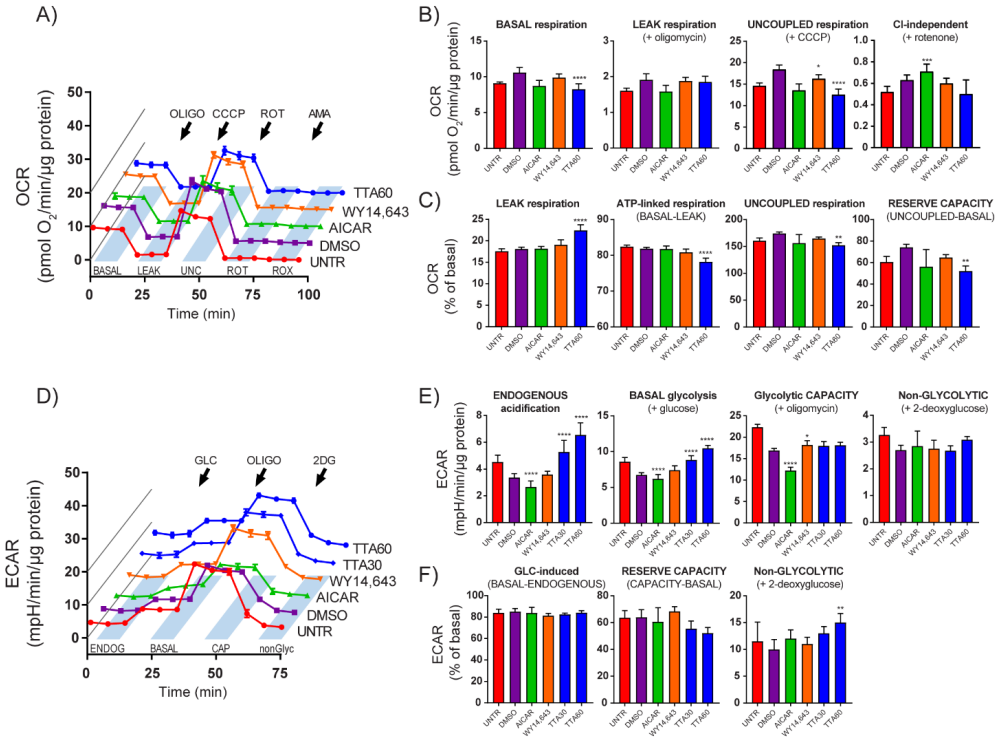

Supplementary Fig. S3. Analysis of mitochondrial respiration and glycolysis.
Oxygen consumption rate (OCR) and extracellular acidification rates (ECAR) were measured in HeLa cells after 6 days treatment with AICAR (0.5 mM), WY 14,643 (10 µM) and TTA (30 µM or 60 µM). Control cultures were untreated (UNTR, for AICAR) or DMSO-treated (DMSO, for WY 14,643 and TTA) cells. (A) Representative traces of OCR (pmol O_2/min/µg protein). Following measurement of basal respiration (BASAL), specific modulators were added as indicated: 3 µM oligomycin to obtain leak respiration (LEAK), 1 µM CCCP to access uncoupled respiration (UNC), 1 µM rotenone to measure rotenone-resistant respiration (ROT) and 1 µM antimycin A to measure residual oxygen consumption (ROX). (B) Data extracted from the analyses in A, after subtraction of non-mitochondrial activity (ROX). (C) Analysis of functional integrity of mitochondria. Rates of interest calculated as % of basal OCR. (D) Representative traces of ECAR (mpH/min/µg protein). The specific modulators were added following measurement of endogenous activity (ENDOG), as indicated: 10 mM glucose (GLC) to obtain basal glycolysis (BASAL), 3 µM oligomycin to assess glycolytic capacity (CAP) and 100 mM 2-deoxyglucose (2DG) to measure non-glycolytic activity (non-Glyc). (E) Data extracted from the analyses in D. (F) Analysis of glycolytic function. Rates of interest calculated as % of basal ECAR. Data are displayed as mean ± SD of 6-8 replicates, from one representative of three separate experiments. Statistical analysis was performed by ANOVA. *p< .05, **p< .01, ***p< .001, ****p< .0001

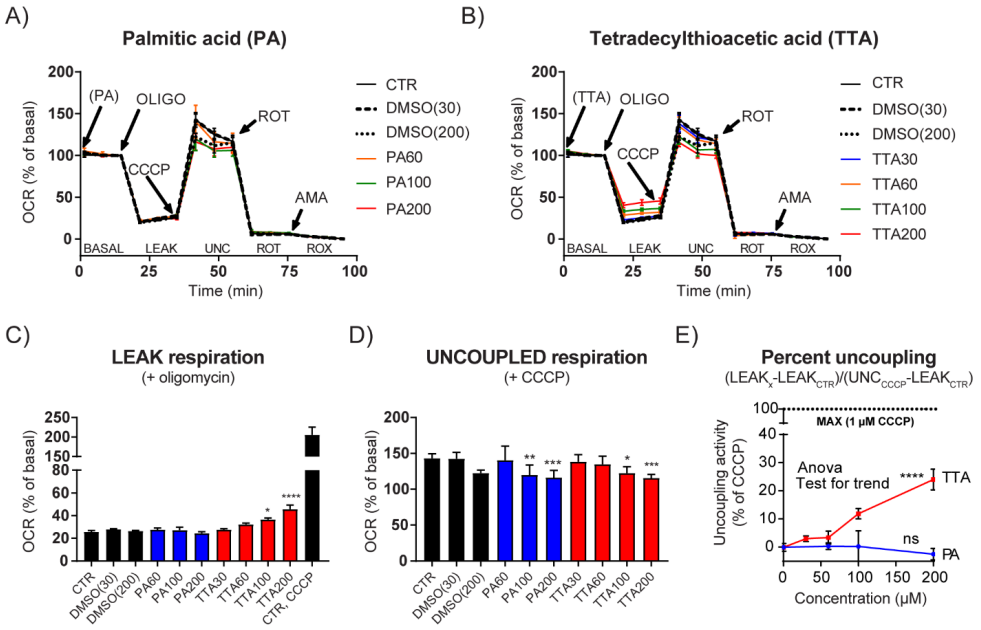

Supplementary Fig. S4. TTA exerts mild uncoupling activity.
Oxygen consumption rate (OCR) was measured in MDA-MB-231 cells immediately after administration palmitic acid (PA) or tetradecylthioacetic acid (TTA), at concentrations of 30 -200 µM. (A-B) Representative traces of OCR as % of initial rate (BASAL), in presence of PA or TTA. Specific modulators were added as indicated: 3 µM oligomycin to obtain leak respiration (LEAK), 1 µM CCCP to access uncoupled respiration (UNC), 1 µM rotenone to measure rotenone-resistant respiration (ROT) and 1 µM antimycin A to measure residual oxygen consumption (ROX). (C) LEAK respiration and (D) UNCOUPLED respiration shown as % of basal OCR. (E) Uncoupling activity mediated by PA and TTA, compared to complete uncoupler, CCCP (100 %). The agent-induced LEAK rate (i.e. $LEAK_X$ - $LEAK_{CTR}$) was calculated relative to the CCCP-induced LEAK rate (i.e. UNC_{CCCP}-$LEAK_{CTR}$). Data are displayed as mean ± SD of 6-8 replicates, from one representative of three separate experiments. Statistical analysis was performed by ANOVA. *p< .05, **p< .01, ***p< .001, ****p< .0001

Graphic design: Communication Division, UiB / Print: Skipnes Kommunikasjon AS

uib.no

ISBN: 9788230869673 (print)
9788230864746 (PDF)